Assessing Miniaturized Sensor Performance using Supervised Learning, with Application to Drug and Explosive Detection

Alstrøm, Tommy Sonne

Publication date:
2013

Document Version
Publisher's PDF, also known as Version of record

Assessing Miniaturized Sensor Performance using Supervised Learning, with Application to Drug and Explosive Detection

Tommy Sonne Alstrøm

Kongens Lyngby 2012
IMM-PhD-2012-292

Technical University of Denmark
Informatics and Mathematical Modelling
Building 321, DK-2800 Kongens Lyngby, Denmark
Phone +45 45253351, Fax +45 45882673
reception@imm.dtu.dk
www.imm.dtu.dk IMM-PhD-2012-292

Summary (English)

This Ph.D. thesis titled "Assessing Miniaturized Sensor Performance using Supervised Learning, with Application to Drug and Explosive Detection" is a part of the strategic research project "Miniaturized sensors for explosives detection in air" funded by the Danish Agency for Science and Technology's, Program Commission on Nanoscience Biotechnology and IT (NABIIT), case number: 2106-07-0031. The project, baptized "Xsense" was led by professor Anja Boisen, DTU Nanotech. DTU Informatics participate in the project as data analysis partner.

This thesis presents advances in the area of detection of vapor emanated by explosives and drugs, similar to an electronic nose. To evaluate sensor responses a data processing and evaluation pipeline is required. The work presented herein focuses on the feature extraction, feature representation and sensor accuracy. Thus the primary aim of this thesis is twofold; firstly, present methods suitable for assessing sensor accuracy, and secondly improve sensor performance by enhancing the preprocessing and feature extraction.

Five different miniaturized sensors are presented. Naturally, each sensor require its own special preprocessing and feature extraction techniques before the sensor responses can be applied to supervised learning algorithms. The technologies used for sensing consist of Calorimetry, Cantilevers, Chemoselective compounds, Quartz Crystal Microbalance and Surface Enhanced Raman Scattering. Each of the sensors have their own strength and weaknesses. The reasoning for using multiple sensors was the desire to investigate the feasibility for an integrated multisensor solution. A unique setup of multiple independent detectors is able to vastly enhance accuracy compared to what a single sensor can deliver.

As we are detecting hazardous compounds this enables the need for sensors to deliver not only decisions but also certainty about decisions. This requirement is handled by introducing classifiers that offer posterior probabilities and not only decisions. The three probabilistic classification models utilized are Artificial Neural Networks, Logistic Regression and Gaussian Processes. Often, there is no tradition for using these methods in the communities of the prescribed sensors. Here, a method of too much complexity is often undesired so it is a balance when to utilize more sophisticated methods. For this reason, an array of methods that only discriminate between samples are used as baseline. The methods used vary from sensor to sensor, as these methods serve as baseline performance when introducing new methods.

The most widely used baseline method in this thesis is the k-nearest-neighbor algorithm. This method is of particular interest in the application of sensors, as the sensors are designed to provide robust and reliable measurements. That means, the sensors are designed to have repeated measurement clusters.

Sensor fusion is presented for the sensor based on chemoselective compounds. An array of color changing compounds are handled and in unity they make up an colorimetric sensor array. In this setting it is valuable to qualify which compounds in the colorimetric sensor array are important. That knowledge enables the ability to either reduce the size of the sensor or replace less sensitive and unimportant compounds with more selective and responsive compounds. A framework based on forward selection Gaussian Process classification is demonstrated to successfully identify a set of important compounds.

Summary (Danish)

Ph.D.-projektet "Assessing Miniaturized Sensor Performance using Supervised Learning, with Application to Drug and Explosive Detection" er et led i det strategiske forskningsprojekt "Miniaturized sensors for explosives detection in air", som er af Det Strategiske Forskningsråds Programkomite for Nanovidenskab og -teknologi, Bioteknologi og IT (NABIIT), bevilling 2106-07-0031. Projektet er blevet døbt "Xsense" og blev ledet af professor Anja Boisen, DTU Nanotech. DTU Informatik deltager i projektet som data analyse partner.

Formålet med projektet har været at udvikle nano-sensorer med henblik på at skabe grundlaget for en elektronisk næse, som kan detektere farlige stoffer f.eks. sprængstoffer. En sådan næse ville kunne bruges i lufthavne, hos anti-terror korps, i afsøgningen af vejsidebomber, m.v. og dermed kraftigt reducere den menneskelige risiko.

Forskningsarbejdet har haft to primære mål. For det første at præsentere metoder, som var i stand til at vurdere sensorernes nøjagtighed. For det andet at forbedre sensorernes ydeevne gennem optimeret signalbehandling og datamodellering. Ved identifikation af farlige stoffer, er der behov for en sensor som kan detektere med høj nøjagtighed, men også behov for vurdering af hvor pålidelighed denne er.

Arbejdet har involveret fem forskellige kemiske nano-sensorer og fokuseret på udvikling, optimering og evaluering af metoder og modeller til databehandling. Sensorne viser sig i stand til at detektere sprængstoffer som ofte bliver benyttet af terrorister såvel som stoffer i forbindelse narkotika bekæmpelse. Nøjagtigheden kan forbedres hvis systemet indeholder flere sensorer. Fordele

ved en integreret enhed er undersøgt og de er indikationer at nøjagtigheden kan forbedres i et multisensor system.

Preface

This thesis was prepared at the Department of Informatics and Mathematical Modeling, Technical University of Denmark, in partial fulfillment of the requirements for acquiring the Ph.D. degree in engineering. The Ph.D. project was a part of the strategic research project named "Xsense - Miniaturized sensors for explosives detection in air", led by Professor Anja Boisen, DTU Nanotech, and funded by the Danish Agency for Science and Technology's, Program Commission on Nanoscience Biotechnology and IT (NABIIT).

The Xsense project worked towards the development of four individual sensor technologies for detection of explosives. All of the sensor technologies can potentially be incorporated into a single miniaturized device. The main hypothesis of the project is that sufficient reliability can only be ensured by merging several independent measuring principles.

The main idea behind this Ph.D. project was to develop the signal processing pipeline for each sensor and then perform sensor fusion. This objective however turned out to be a little too optimistic. A complete device was never built and the work herein is exclusively about the processing of data obtained using the individual sensors and the application of machine learning methods to assess the performance of the sensors. Fortunately the work conducted in Xsense has spurred a new project named MUSE, which in many ways is a continuation of Xsense. The application area is different, but the sensor technologies are similar and there is a greater focus on sensor integration. There is also a continuity of personnel. Several of the researchers in MUSE participated in Xsense, and now these people have more experience and know-how.

In Xsense, each sensor technology was developed and refined by people at DTU

Nanotech and Department of Chemistry, Syddansk University respectively. All data was collected by researchers at DTU Nanotech though. Due to the data flow in Xsense, my project turned out to be provider of data analysis knowledge for the researchers developing the sensors. My research has therefore been very much about handling the data produced by these sensors, assessing the sensor performance and then handing the results to the scientists at DTU Nanotech. Thus, whenever data has been handled, the overall goal was always to assess and possibly improve the sensor performance.

The starting point was to use existing techniques, and if the sensor was able to deliver flawless performance using these techniques, no refinement in the signal processing was made. For this very reason, the research conducted has not at all been equally balanced among the sensors. Some of the sensing principles were mature and there was already a lot of work published on those, whereas others were rather new and here there was often more room for improvement.

Also a lot of traditional statistical hypothesis testing and design of experiments have been carried out. Not all experiments used an experimental design as it turned out that most "sensor people" are not aware of the issues solved by the application of a proper experimental design. So this Ph.D. project has been educational not just for me but also for the people at DTU Nanotech. Two different worlds have meet and we have all come out richer.

In the early days of the project, no data was produced as the sensors were under development. Fortunately I was able to get hold of data similar to the data that would be produced within Xsense, but with the application of ecstacy detection. The thesis contains a chapter about detection of ecstasy using quartz microbalance sensors. This sensor was also developed at DTU Nanotech in another project called Nanonose.

The thesis consists of a summary report and a collection of six research papers written during the period 2008–2012. Four of the papers have been published elsewhere whereas the remaining two still have to be published. One is still in draft (paper F) while the other has been submitted. A total of 15 research papers have been co–authored in the period, but only the papers that contained contributions in the signal processing of sensor data have been included in the thesis.

The introductory chapter will explain chemical sensing and the need for new devices for explosives detection. Knowledge about chemical detection is not assumed. Readers knowledgeable in the area on explosives detection can go directly to the end of the chapter. There, an outline of the thesis is given as well as a list of the main contributions contained herein. The list of contributions is best read in order to know where the thesis advances current methods.

Chapter 2 will then explain how machine learning in the context of sensors can be employed. Readers with knowledge in machine learning can skim this chapter, however attention should be given to section 2.3. Here I explain specifically how the models were applied for the sensors, as well as which performance measures were used. Further, the implementation details for each model are given although not explained. If the implementation of the model was not done by either me or my collaborators, I will give references to the software that was used. Interested readers can find in-depth explanations in the referred material. Likewise it is also my aim to publish the majority of the code used to create the results presented throughout this thesis so others can reproduce the results.

Chapter 3 and 4 extract and present the main advances in the area of signal processing and how specifically the models explained in chapter 2 were applied. Advances have been made mostly on the sensors based on quartz microbalance crystals and chemoselective colorimetric compounds and the two chapters are based on the papers B-F. These papers are provided mostly as supporting information to chapter 3 and 4.

The material covered in paper A is only covered briefly in the main part of the thesis (chapter 1 and 5). The paper shows proof-of-concept measurements made on the four sensors in the Xsense project and justify the application of a multisensor approach. The paper can be read as stand-alone. With these words, I wish you happy reading and I hope you will have an informative ride.

Lyngby, 31-December-2012

Tommy Sonne Alstrøm

List of Publications made during the PhD

Submitted Journal Papers

[A] Tommy S. Alstrøm, Natalie V. Kostesha, Filippo G. Bosco, Michael S. Schmidt, Jesper K. Olsen, Michael Bache, Jan Larsen, Mogens H. Jakobsen, and Anja Boisen. Miniaturized multisensory approach for the highly sensitive and selective detection of explosives. *Submitted to Journal of Materials Chemistry*, 2013.

- Sanjukta Bose, Stephan S. Keller, Tommy S. Alstrøm, Anja Boisen, and Kristoffer Almdal. Design of Experiments for Process Optimization of Spray Coated Polymer Films. *Submitted to Langmuir*, 2013.

Published Conference Papers

[B] Tommy S. Alstrøm, Jan Larsen, Claus H. Nielsen, and Niels B. Larsen. Data-driven modeling of nano-nose gas sensor arrays. In Ivan Kadar, editor, *Proceedings of SPIE*, volume 7697, pages 76970U–76970U–12. SPIE, 2010. doi: 10.1117/12.850314.

- Michael S. Schmidt, Natalie Kostesha, Filippo Bosco, Jesper K. Olsen, Carsten Johnsen, Kent a. Nielsen, Jan O. Jeppesen, Tommy S. Alstrøm, Jan Larsen, Mogens H. Jakobsen, Thomas Thundat, and Anja Boisen.

Xsense: using nanotechnology to combine detection methods for high sensitivity handheld explosives detectors. In *Proceedings of SPIE*, volume 7664, pages 76641H–76641H–6, 2010. doi: 10.1117/12.850219.

- Natalie V. Kostesha, Tommy S. Alstrøm, Carsten Johnsen, Kent A. Nielsen, Jan O. Jeppesen, Jan Larsen, Mogens H. Jakobsen, and Anja Boisen. Development of the colorimetric sensor array for detection of explosives and volatile organic compounds in air. In *Proceedings of SPIE*, volume 7673, pages 76730I–76730I–9, April 2010. doi: 10.1117/12.850310.

- Natalie V. Kostesha, Michael S. Schmidt, Filippo G. Bosco, Jesper K. Olsen, Carsten Johnsen, Kent A. Nielsen, Jan O. Jeppesen, Tommy S. Alstrøm, Jan Larsen, Thomas Thundat, Mogens H. Jakobsen, and Anja Boisen. The Xsense project: The application of an intelligent sensor array for high sensitivity handheld explosives detectors. In *Sensors Applications Symposium (SAS), 2011 IEEE*, pages 7–11, 2011. doi: 10.1109/SAS.2011.5739782.

- Michael S. Schmidt, Natalie V. Kostesha, Filippo G. Bosco, Jesper K. Olsen, Carsten Johnsen, Kent A. Nielsen, Jan O. Jeppesen, Tommy S. Alstrøm, Jan Larsen, Thomas Thundat, Mogens H. Jacobsen, and Anja Boisen. Xsense - a miniaturised multi-sensor platform for explosives detection. In *Proceedings of SPIE*, volume 8031, pages 803123–803123–7, 2011. doi: 10.1117/12.884050.

- Natalie V. Kostesha, Tommy S. Alstrøm, Carsten Johnsen, Kent A. Nielsen, Jan O. Jeppesen, Jan Larsen, Anja Boisen, and Mogens H. Jakobsen. Multi-colorimetric sensor array for detection of explosives in gas and liquid phase. In *Proceedings of SPIE*, volume 8018, pages 80181H–80181H–12, 2011a. doi: 10.1117/12.883895.

[C] Tommy S. Alstrøm, Jan Larsen, Natalie V. Kostesha, Mogens H. Jakobsen, and Anja Boisen. Data representation and feature selection for colorimetric sensor arrays used as explosives detectors. In *IEEE International Workshop on Machine Learning for Signal Processing (MLSP)*, pages 1–6, 2011. doi: 10.1109/MLSP.2011.6064615.

[D] Tommy S. Alstrøm, Raviv Raich, Natalie V. Kostesha, and Jan Larsen. Feature extraction using distribution representation for colorimetric sensor arrays used as explosives detectors. In *IEEE International Conference on Acoustics, Speech, and Signal Processing (ICASSP)*, pages 2125–2128, 2012. doi: 10.1109/ICASSP.2012.6288331.

[E] Tommy S. Alstrøm, Bjørn S. Jensen, Mikkel N. Schmidt, Natalie V. Kostesha, and Jan Larsen. Hausdorff and Hellinger for Colorimetric Sensor Array Classification. In *IEEE International Workshop on Machine Learning*

for Signal Processing (MLSP), pages 1–6, 2012. doi: 10.1109/MLSP.2012.6349724.

- Natalie V. Kostesha, Tommy S. Alstrøm, Jan Larsen, Anja Boisen, and Mogens H. Jakobsen. Multi-Colorimetric Sensor Array for Detection of Illegal Materials. In *IEEE Sensors*, number 09, 2012.

Under preparation

- Colorimetric sensor array data processing toolbox. 2013. URL http://www.imm.dtu.dk/pubdb/p.php?6498.

- Tommy S. Alstrøm and Jan Larsen. Feature Extraction and Signal Representation for Colorimetric Sensor Arrays. Technical report, DTU Informatics, 2010-2012. URL http://www.imm.dtu.dk/pubdb/p.php?5845.

[F] Natalie V. Kostesha, Tommy S. Alstrøm, Olga V. Mednova, Carsten Johnsen, Kent A. Nielsen, Jan O. Jeppesen, Mogens H. Jakobsen, Jan Larsen, and Anja Boisen. Advanced detection of explosives using multi-colorimetric sensor array. *Will be submitted to Journal of American Chemical Society (JACS)*, 2013.

- Tommy S. Alstrøm, Ryota Tomioka, Bjørn S. Jensen, Mikkel N. Schmidt, Natalie V. Kostesha, and Jan Larsen. Robust Feature Extraction for Colorimetric Sensor Arrays. *Will be submitted to IEEE Transactions on Signal Processing*, 2013.

- Jaeyoung Yang, Mirkó Palla, Filippo G. Bosco, Michael S. Schmidt, Tomas Rindzevicius, Tommy S. Alstrøm, Milan N. Stojanovic, Anja Boisen, Jingyue Ju, and Qiao Lin Utilizing large area mapping of uniform SERS substrates for ultra sensitive and specific detection of biomolecules. *To be submitted to ACS Nano*, 2013.

Acknowledgements

In the writing of this thesis I also had the chance to look back on the past four years of my life. It turned out that quite a lot of people have contributed in making this thesis possible.

First, I'd like to thank my supervisor, associate professor Jan Larsen for choosing me to be the person that could carry out this work, to inspire discussions and to teach me the style and etiquette of academia.

Anja Boisen, professor at DTU Nanotech has also been an inspiration and I would like to thank her for the support and encouragement she has given me throughout the project, and for taking time to help me improve my work and understanding in nanotechnology. The same gratitude is extended to Mogens H. Jakobsen whom offered financial support and invited me to his group for three months to improve the work on the colorimetric sensor array.

I would like to thank all the people of the cognitive systems section and in particular professor Lars K. Hansen and associate professor Ole Winther whom have been of great help and inspiration. Your insight in machine learning runs deep and thank you for taking the time to explain theories to me. Both of you have always been helpful when I came knocking on your door. I would like to extend the same gratitude to associate professor Morten Mørup who has always been helpful when I had questions to ask.

I also wish to thank Dr. Morten Angren for helping me to understand the L1 and L2 regularization and the connection to Gaussian/Laplacian priors. The understanding had eluded me many times before you took the time to explain

it to me.

This thesis has been made a lot more readable due to the help from several proofreaders. I am sure that readers are also happy that the language has been improved and is more smooth on the eye now than earlier editions. Proofreaders of this theses are (in alphabetic order): Carsten Stahlhut, Dylan O'Donnell, Gitte S. Alstrøm, Mikkel N. Schmidt, Natalie V. Kostesha, and Scott Mileham. Thanks to you all.

The work presented in this thesis would never have be possible without the help from my close collaborator. Their contributions have in so many ways improved my research for which I am very grateful. Their contributions are written here, in alphabetic order:

Collaborator	Contributions
Bjørn S. Jensen	Implemented the distance kernel specified in (4.32) and the multiple kernel covariance function specified in (4.33). Without these implementations, it is unlikely that the sensor fusion for colorimetric arrays would be carried out within this project. I'm very grateful that Bjørn took time to do this even though he didn't really had time to do it. Having a keen understanding of Gaussian Process classification, he also assisted me in writing section 2.5.4, and should be considered a main contributor to this section.
Claus H. Nielsen	Conducted all experiments with the quartz crystal microbalance sensors. Claus also spend time to help me understand the ideas behind of polymer-based sensors.
Filippo Bosco	Conducted all experiments with the cantilever sensor and has participated in many fruitful discussions in Xsense.
Gabriela Blagoi	Was involved in the early stages of the colorimetric sensor array and help me understand the technology.
Jesper K. Olsen	Conducted all experiments on the calorimetric sensor. Even after Jesper got a full-time job in the industry he took time to answer questions by email.

Michael S. Schmidt	Conducted all experiments with the surface enhanced Raman scattering sensor. Michael has on numerous occasions patiently explained the idea behind Raman scattering, and when I think I finally understood I always had to ask for more clarifications.
Mikkel N. Schmidt	Suggested the idea of using Hausdorff for colorimetric sensor arrays. Mikkel has also taken time to explain a great deal of machine learning methods to me in my time here.
Natalie V. Kosteha	Carried out experiments with the colorimetric sensor array. Assisted in categorize the chemicals and described their possible application areas. As such, Natalie should be considered as the main author of appendix G. Natalie also managed to proof read the entire thesis and correct my chemistry mistakes where it was needed.
Raviv Raich	Brought the idea of histogram methods for colorimetric sensor arrays to the table. This idea has been crucial in going forward with the work with colorimetric sensor arrays.
Ryota Tomioka	Has patiently helped me to understand multiple kernel learning and inspired the idea to utilize the method for colorimetric sensor arrays.

I want to express my gratitude to my parents and my parents in law. Conducting a Ph.D. study with small kids is never easy but thankfully you have all extended a helping hand in the time of need.

Finally, I want to express my deepest gratitude to my loving wife, Gitte S. Alstrøm. Her support and encouragement has been crucial for me during the past four years and without her support I would never have been where I am today and finish my Ph.D study. I am forever thankful.

Nomenclature

Terms

Term	Meaning
Analyte	A chemical constituent or substance that is exposed to a sensor and undergo analysis.
Antipersonnel mine	Landmine is specifically designed to harm humans.
Chemoselective	Selective compound that reacts with just one functional group in the presence of others.
Deflagrate	A substance that is suddenly and violently ignited, i.e. an explosive.
Density estimation	Estimation of the concentration of a detected vapor.
Difference map	A graphical representation of the response of a colorimetric sensor array.
Dot	Refers to a circular dot on a colorimetric sensor array. The dot consist of a dye that has been spotted on a piece of silica gel and then dried.
Dye	Refers to a given chemo-selective compound employed in a colorimetric sensor array. One dye corresponds to one sensor.
False alarm	A positive detection that turned out to be false.
Precursor	A substance that participates in the chemical reaction that produces another substance.
Solvent	Substance that are used to dissolve compounds.
Trace detection	Detection of small amount of analyte vapor in air.

Treatment	In terms of classical analysis of experiments, the treatment is the act of exposing the object of interest to the factors that is under investigation. In the context of sensors, a treatment refers to the act if exposing the sensor to a control or a target compound.

Abbreviations

Term	Meaning
i.i.d.	Independent and identically distributed
1-NN	1-nearest-neighbor
ANN	Artificial Neural Network
AXO	Abandoned explosive ordnance
CDF	Cumulative distribution function
DPI	Dots per inch
DTA	Differential Thermal Analysis
DTA	Differential Thermal Analysis
EP	Expectation Propagation
ERW	Explosive Remnants of War
GP	Gaussian Process
GPR	Gaussian Process Regression
GTD	Global Terrorism Database
GTI	Global Terrorism Index
HCA	Hierarchical Cluster Analysis
HCL	Hierarchical Cluster Analysis
ICBL	International Campaign to Band Landmines
IED	Improvised Explosives Device
k-NN	k-nearest-neighbor
LHS	Left hand side
LOOCV	Leave-One-Out Cross Validation
LR	Linear regression
MAE	Mean Absolute Error
NMF	Non-negative Matrix Factorization
PC	Principal Components
PCA	Principal Component Analysis
PCR	Principal Component Regression
ppm	parts-per-million
QCM	Quartz Crystal Microbalance

RCBD	Randomized Complete Block Design
RGB	Red-green-blue color model
RHS	Right hand side
RMAE	Relative Mean Absolute Error
RT	Room Temperature
RT	Room Temperature
SERS	Surface Enhanced Raman Scattering
SLR	Sparse Logistic Regression
SotA	State of the Art
SVD	Singular Value Decomposition
UXO	Unexploded ordnance

Notation

Symbol	Meaning
D	The dimensionality of the data being treated.
$\mathcal{D}$	Denotes the dataset $\mathcal{D} = \{\mathbf{x}_i, y_i\}_{i=1}^N$
$\mathbb{E}[f]$	Expectation of f.
ε	A normal distributed random variable used to add noise to models.
$E(\cdot)$	The error function.
$E_D(\cdot)$	The data dependent part of the error function.
$E_{\mathbf{w}}(\cdot)$	The data independent part of the error function.
$\mathbb{E}_h[f]$	The expectation with respect to the distribution measure h, $\mathbb{E}_h[f] = \int f(\mathbf{x})h(\mathbf{x})d\mathbf{x}$
$h(\cdot)$	Denotes the activation function used in a neural network.
$\mathbf{I}^k_{(i,j)}$	An image matrix for channel k where the channels are RGB.
$\mathbf{I}_{\text{bef}}$	The image of a colorimetric sensor array before exposure.
$\mathbf{I}_{\text{aft}}$	The image of a colorimetric sensor array that has been exposed.
$\mathbf{I}_{\text{dif}}$	The difference image of a colorimetric sensor array.
$k - CV$	k fold cross validation, k can be a number.
$k(\mathbf{x}, \mathbf{x}')$	A kernel function or the covariance function.
K	The number of classes in a data set.
$m(\mathbf{x})$	The mean function prior of a Gaussian Process.
M	The dimensionality of a reduced subspace based on $\mathbf{X}$.
N_{err}	The total number of missclassified points in a classification problem.
N^k	The total number of measurements in a given dataset with class label k.
N	The total number of measurements in a given dataset.

N_{tr}^k	The number of training points for class k.
$\mathbb{R}$	The set of real numbers.
$\mathbb{R}_{0+}$	The set of non-negative real numbers, $\mathbb{R}_{0+} = \{x \mid 0 \leq x < \infty\}$
$\mathbf{x}$	A vector of dimensionality D that contains a measurement.
$x_{m,n}$	Corresponds to element $\mathbf{X}_{(m,n)}$.
$\mathbf{X}$	A $D \times N$ data matrix.
$\mathbf{X}_{(m,n)}$	The element on the mth row and nth column in the matrix $\mathbf{X}$.
y_i	The label that is associated with measurement x_i.
$\boldsymbol{\theta}$	Vector that contains hyperparameters.

Contents

Chapter 1

Introduction

This Ph.D. project concerns the detection of explosives and drugs in air and is a part of "Xsense". The Xsense project has worked towards the development of four individual sensor technologies for detection of explosives. The sensor development has primarily been driven by two aims; to provide new tools for the fight against terrorism and to provide cost efficient yet reliable sensors that can be applied in the area of demining.

To meet either of these goals, a sensor platform that can detect explosives is required. Detection of explosives is complicated due to the existence of a vast array of explosive substances. The list of explosives employed by terrorists is long and the detection is further complicated by terrorists often producing their own explosives, usually referred to as an *improvised explosives device* (IED) [Wernick and Von Glinow, 2012, Rollings and Wyler, 2012].

The situation of landmines is likewise complex as there exist an estimated 650 different types of *antipersonnel* mines around the world [Habib, 2007]. Antipersonnel landmines are specifically designed to harm humans and is typically dug into soil. Landmines are mostly an issue in developing countries where the local inhabitants are often forced to cultivate minefields or they will starve [Landmine Monitor, 2012].

The detection of drugs is closely related to the fight against terrorism[1]. The funding of terror cells is often (in part) achieved by the manufacturing and distribution of illicit drugs [Costa et al., 2010]. Hence, it is a natural step to investigate how well sensors can detect drugs.

Nevertheless, the primarily objective of the Xsense project was to develop a miniaturized sensor platform for the detection of explosives so we will start there. Due to the complexity of the detection of explosives, the playing field had to be narrowed down and the sensors were tested on a few selected compounds which will be detailed later. Furthermore, the sensors has been deployed exclusively in a laboratory setting where numerous proof-of-concept measurements has been made. The issue of mixed compounds (IEDs) is not handled explicitly in the project, but instead several substances that is used to manufacture explosives are measured standalone.

Measurements have also been performed on an array of non-explosive substances that served as control. A list that details all of the applied substances and their possible application can be found in appendix G. Finally, the task of getting the explosives to the sensor in a real world setting is not handled within the Xsense project. It is basically assumed that this is handled by an external device called a preconcentrator that will collect samples in sufficient amounts.

Today vapors emanating from explosives are mainly detected by canines, electronic nose and sniffing probes [Furton and Lawrence, 2001, Singh, 2007, Yinon, 2003]. The electronic nose is the device that combines chemical-sensing and pattern-recognition systems; in nature it could be the sensing organ of an animal like the nose of a bomb-sniffing dog or rat as illustrated on figure 1.1. The sensor can recognize specific molecules and can be applied in many areas of research, such as food quality analysis, medical diagnostics, explosives, toxins detection, and environmental. Further, the sensor has shown high capability for detecting substances, such as ammonium nitrate and mineral explosives (salts) in low concentrations [Gui et al., 2009]. Nevertheless, the traditionally applied electronic nose technique has limitations due to the detection problems at low analyte concentrations, as well as at high or low temperature and humidity.

The minimization of false alarms is identified as a priority in sensing devices [Yinon, 2003, Gui et al., 2009]. Currently, the screening and identification of suspicious substances is often done by canine units or specialized teams which employ sophisticated methods e.g. terahertz pulsed spectroscopic imaging [Fitch et al., 2007, Barber et al., 2005], gas chromatography, mass spectroscopy [Barshick and Griest, 1998] or long-range Raman spectrometry [Carter et al., 2005]. The

[1] In this work we are only concerned with the detection of illicit drugs and explosives. Legal substances such as medicine or fireworks are not what is in focus here.


Figure 1.1: The two state of the art explosives detection units at work. Image of the dog is courtesy of [Danminar, 2012] and the rat is courtesy of [APOPO, 2012].

screening is characterized by a high assignment of personnel and high costs [Shea and Morgan, 2007]. Furthermore, in relation to the requested volume the methods are often slow. Airport screening requires systems to handle up to 10 passengers per minute [Shea and Morgan, 2007]. Canine units work swiftly but require breaks, have significant upkeep cost and can only be applied by expert handlers [Shea and Morgan, 2007].

Todays market shows a demand for portable multisensor instruments [Air, 2012, Rki, 2012, Ins, 2012]. These instruments are sensitive enough to detect low concentrations of analytes and can within a few seconds identify common volatile compounds. For example, in the product "GDA 2" by AirSense Analytics, a combination of different sensors is applied. The product comprises an ion mobility spectrometer, a photo ionization detector, two semiconductor gas sensors and an electrochemical cell. Other detecting combinations like an array of chemical sensors [Stetter et al., 2000, Suslick et al., 2004a, Kostesha et al., 2010] or a surface modified with different sensing layers can also be called a multisensor approach.

The use of detection systems based on multisensor approaches could tremendously help in the fast identification of explosives, reduce false alarms and provide new opportunities for the real-time analysis of explosives [Xsense, 2012]. A simultaneous application of a variety of sensor techniques, which are based on different physical principles, will enhance the collection of data where erroneous detections are statistically independent. This improves the possibility to reliably detect presence of explosives molecules with a high confidence [Stetter et al., 2000, Raman et al., 2009].

The application of multisensor detection technologies has a great perspective in the identification of different analytes. In the cases of demining, a minimum

acceptable clearance rate of 99.6% has been set by United Nations [Kimberg, 1996]. Obtaining this rate is almost impossible using a single detection technique. Trained dogs are by many considered the best known explosives detector, but they require excessive training and are greatly obstructed by the environment. In severe cases their accuracy may be as low as 50% [Habib, 2007].

The sensors within this thesis measure responses based on chemical reduction-oxidation reactions, molecular interactions, etc. so there is a need for some introductory remarks about the nomenclature of trace detection.

1.1 Chemical sensing

All of the sensors presented in this theses are chemical sensors that is used for vapor detection emanating by explosives (or drugs), also denoted as trace detection. Trace detection is the detection of a small amount of molecules in air. While the sensor manufacturing is very different all of them still rely on the evaporation of the chemical target denoted *analyte*. An analyte is the substance or chemical constituent that is undergoing analysis, either *classification* or *density estimation*. Classification is the act of identifying which compound is reacting with the sensor whereas density estimation is the task of estimating how much of the compound is present.

Often, the target analyte is dissolved into some kind of carrier liquid or carrier gas. This carrier is denoted a *solvent*. Solvents are widely used in the production of chemical constituents, whether these are cosmetics, explosives or something else. Whenever one of our sensors is utilized it is always designed with the detection of a specific compound in mind. An experiment is then conducted with the target analyte and some alternative analytes could for example be solvents that are used to create explosives as well as other compounds. As such, solvents serve as potential false alarms for the compound that we really want to detect. If solvents were not included in the experiment, the experimenter really does not know if the sensor is detecting the solvent or the target molecule, unless of course it can be argued by other means that the sensor made a positive detection.

1.2 Antiterrorism

Over the past decade, explosives have been a preferred tool for terrorists [Wernick and Von Glinow, 2012, Rollings and Wyler, 2012]. The organization of

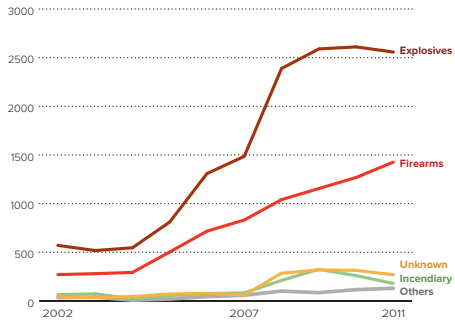

Figure 1.2: Types of weapons used in terrorist attacks in the period 2002-2011. The most common choice is explosives followed by firearms. Figure courtesy of [Global Terrorism Index, 2012].

Compound	Incidents	Fatalities	Injuries
Ammonium Nitrate (AN)	94	139	328
Royal Demolition Explosive (RDX)	22	121	437
Triacetone Triperoxide (TATP)	3	17	26
Trinitrotoluene (TNT)	1272	1695	6177

Table 1.1: Confirmed instances where the listed compounds were used to perform an attack [Global Terrorism Database, Dec, 2012].

Global Terrorism Index (GTI) has compiled figures of all recorded attacks in 2002-2011 and here explosives clearly shows to be the weapon of choice, which is shown on figure 1.2.

The issue of terrorism is a global concern and almost every country in the world is affected by the threat posed by terrorism. GTI has computed the threat posed by terrorism according to a heuristic on the scale 0-10 for 158 countries, and inspection of the results geographically shown in figure 1.3 reveals that terrorism is indeed a worldwide concern. The figure also shows that the density of terrorist attacks is highest in Columbia, the Middle-east, India, Pakistan and the Philippines.

In the scope of Xsense we have measured four compounds commonly applied by terrorists. These are the three explosives RDX, TATP and TNT and the salt ammonium nitrate (widely found in fertilizers). The compounds and the recorded number of incidents are listed in table 1.1. RDX and TNT are military class compounds whereas TATP is a recently applied compound utilized in IEDs that is easily manufactured using ordinary house-hold chemicals.

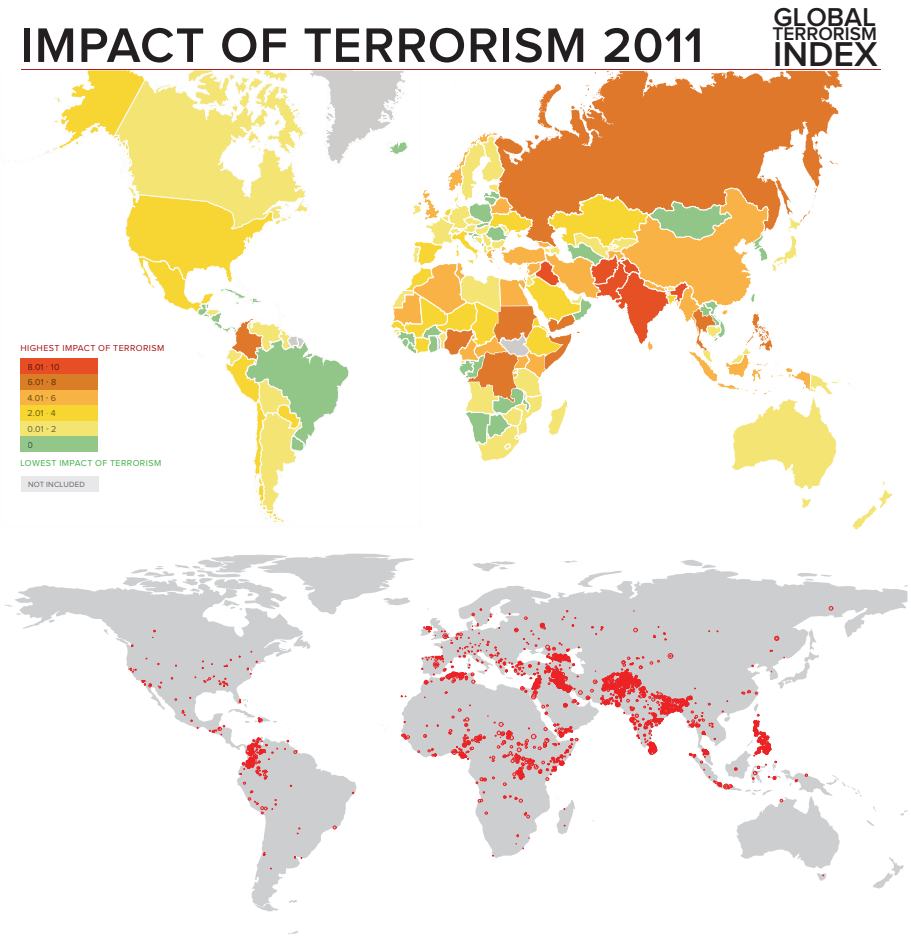

Figure 1.3: The top map illustrates the worldwide threat calculated according to the global terrorism index. The red dots on the bottom map marks geographical locations of attacks. Figures courtesy of [Global Terrorism Index, 2012].

It should be noted that table 1.1 only enumerates the number of confirmed instances. Often the compound cannot be identified precisely, e.g. in the well-known Oklahoma bombing where 168 fatalities and 650 injured were listed, the explosive type is listed as unknown, even though it is the general notion that ammonium nitrate was used it cannot be established beyond reasonable doubt [Hoffman, 1998]. The perhaps most well-known recent example happened in Norway, 2011, where a terrorist attacked the prime minister's office building located in Oslo using a lethal bomb based on ammonium nitrate [Pol, 2011a].

The explosive TATP is not widely used but is well known in Denmark. Here, we had two recent incidents (2007 and 2010) of failed terrorist attacks where the police made arrests before the attacks were completed [Pol, 2011b, 2008].

Two more compounds where measured and although not often utilized (no records where found in the GTD) by terrorists they are still highly relevant. The first one is HMX (Octogen) which is closely related to RDX as the two compounds are chemically close and in the production of RDX up to 10% of the produced RDX turns out to be HMX (see appendix F). HMX is also often mixed with TNT and thus it is possible that HMX has already been applied by terrorists but merely it could not be detected post-blast.

The other compound measured was 2,4-dinitrotoluene (DNT). DNT is a byproduct of TNT as TNT decomposed into DNT in time so an indirect method of detecting TNT is to detect DNT. DNT has higher vapor pressure than TNT and is therefore easier to collect and detect compared to TNT.

As a final note, the fatalities/injuries in table 1.1 is the minimum as only confirmed numbers are included. A total of of 50,098 incidents that included explosives are recorded. If the incidents[2] that resulted in more that 100 victims are extracted, a total of 396 incidents are recorded with a total of 19,353 fatalities and 59,106 injuries [STA].

1.3 Demining

Antipersonnel mines were first applied on a wide scale in World War II and has been widely used since then [ICBL, 2012]. Originally a military weapon, landmines has evolved to become an issue for civilian life as well. This is due to mine fields remaining intact in former battle areas after ended conflicts. In the year 2011 the portion of civilian casualties was at 72% out of all recorded casualties.

In the mission of demining the International Campaign to Band Landmines (ICBL) is a significant organization on the goal of worldwide demining and most of the information contained in this section is based on the reports made by the Landmine and Cluster Munition Monitor research by ICBL[3].

[2] excluding incidents within legitimate warfare.

[3] Landmine and Cluster Munition Monitor is the research and monitoring initiative of the International Campaign to Ban Landmines (ICBL) and the Cluster Munition Coalition (CMC) and has provided civil-society reporting on landmines, cluster munitions and other explosive remnants of war since 1999. The ICBL is the author of the reports. Human Rights Watch is the publisher of reports from 1999-2004 and Mines Action Canada is the publisher of reports

Demining took place in 1997 with the creation of the "Ottawa treaty". The Ottawa treaty is a framework for putting a total ban of landmines into place. Countries that have signed the treaty also commits to clearance of minefields and assisting affected communities. ICBL calls for a total ban on usage of antipersonnel mines, as well as clearance of emplaced landmines and *explosive remnants of war* (ERW). ERW refers to ordnance left behind after an ended conflict such as explosive devices that failed to detonate (UXO) or equipment that has been abandoned (AXO). Both UXO and AXO pose a significant threat to local communities. Removal of ERW is also related to antiterrorism, since military groups recover ERW and use them to manufacture their own explosives devices (IEDs). Landmines are almost a worldwide problem, with presence of minefields in Asia, Africa, South America and Europe (see figure 1.4). Fortunately the creation of new minefields has almost come to a stop. In 2011–2012 only two governments applied new antipersonnel mines, Myanmar and Syria. The list of countries containing new minefields is a bit wider though, as non-state armed groups also deploy antipersonnel mines. This has been recorded to happen in Afghanistan, Colombia, Myanmar, Pakistan, Thailand, and Yemen.

It is mostly in developing countries that minefields are a problem. The list of countries that have most casualties due to landmines are dominated by developing countries located in Africa and the Middle-east. The number of casualties in 2011 on countries with over 100 casualties, with the number of casualties in parentheses was: Afghanistan(812), Pakistan(569), Colombia(538), Myanmar(381), Cambodia(211), South Sudan(206), Libya(184), Somalia(146), Iraq(141), and Sudan(122).

In recent years the number of casualties is declining. The number of registered casualties since the year 2000 is displayed in figure 1.5. The numbers are anticipated to be more precise in the latter years as more countries have developed registration procedures as the years went by, e.g. in year 2000 it was estimated that the total number of casualties was about 20,000 even though the recorded number is just 8,000. A total of 4,286 casualties by ERW was registered in the year of 2011, a significant decrease since the year 2000. The amount of casualties in year 2011 among children was 42% and in some countries the percentage was as high as 61%, so ERW are mostly hurting children. According to [Landmine Monitor, 2012] the appearance of minefields is decreasing and "Worldwide, an area covering some $3,000\text{km}^2$ remains to be cleared of antipersonnel mines".

Current demining techniques are expensive compared to laying new mines. In 2007, [Habib, 2007] reported that the production cost of an antipersonnel mine was about 3-30US$ whereas the cost of clearing one mine was ranging between 300-1,000US$. One of the major reasons is that minefields must be cleared using

from 2004 onward.

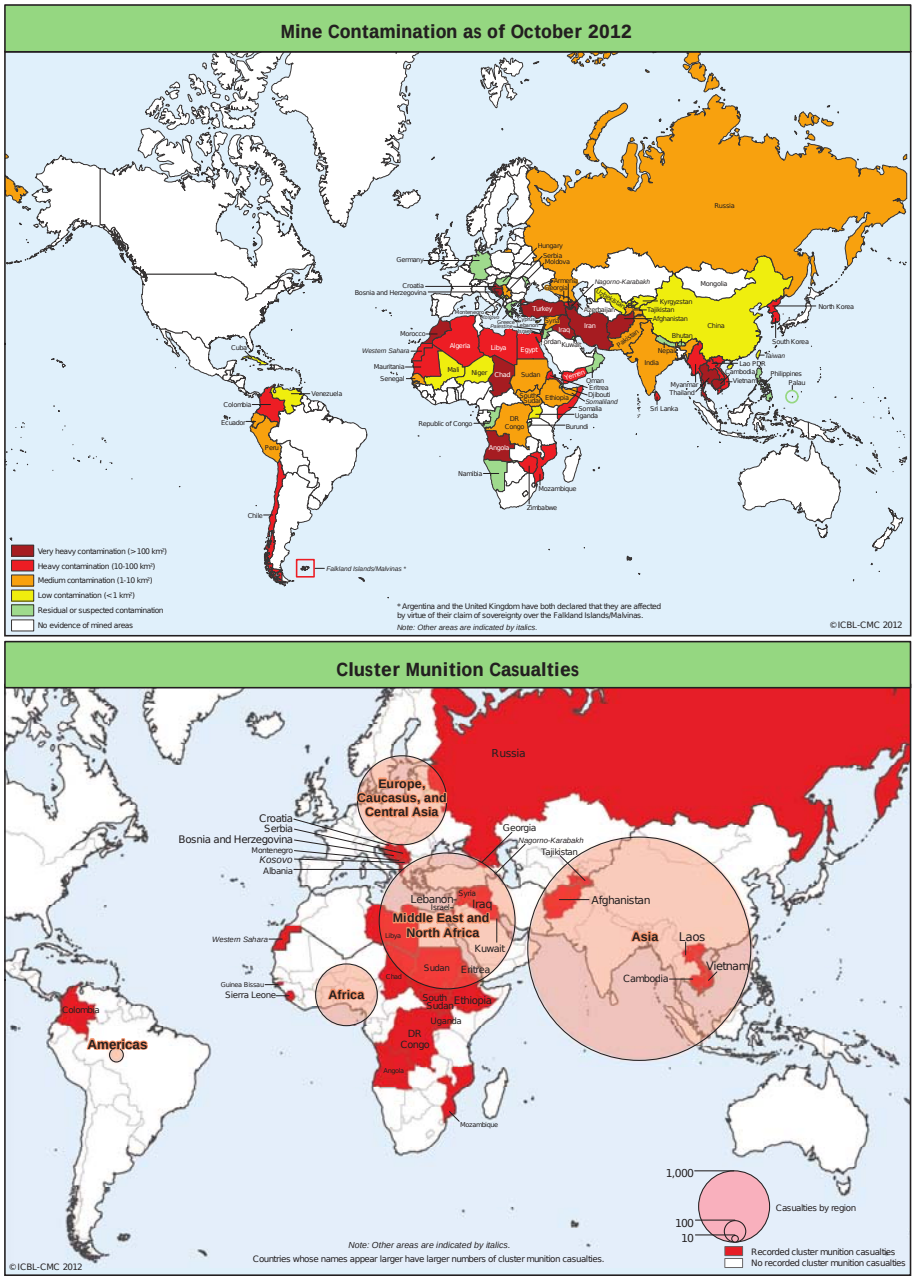

Figure 1.4: Figures courtesy of [Landmine Monitor, 2012].

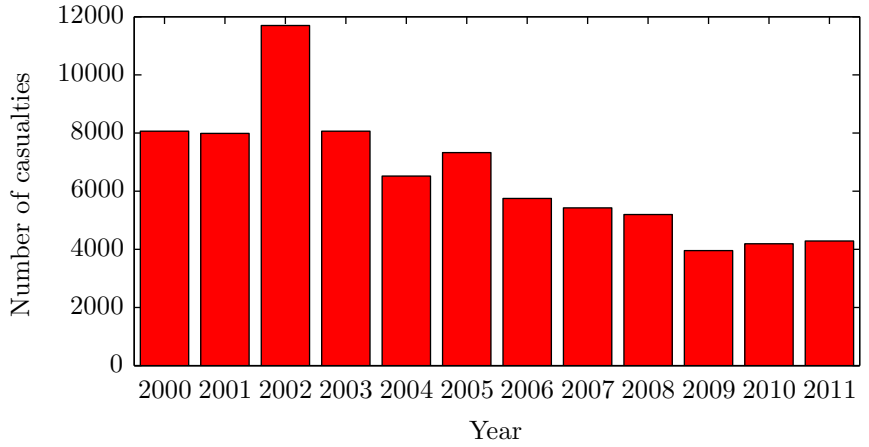

Figure 1.5: The number of casualties per year from explosive remnants of war. Although the number of casualties rise on a few instances the number of casualties is generally decreasing. The graph is based on numbers from [Landmine Monitor, 2012].

multiple techniques, otherwise the required minimum acceptable clearance rate of 99.6% cannot be achieved. This situation calls for the development of efficient methods.

Despite the need for new reliable detection devices there is yet to be developed a satisfactory mobile and portable solution. Sensors must not only easily detect a variety of hidden explosives but they must also be able to detect illegal chemicals and products of the explosives industry. A further requirement is that the sensing device should be portable, rapid, highly sensitive, specific (minimize false alarms), and inexpensive [Schmidt et al., 2011a].

1.4 Explosive detection using a multisensor approach

The main hypothesis in the Xsense project is that sufficient reliability can only be ensured by merging several independent and sensitive measuring principles. The basic scientific goal of the Xsense project was on the development and refinement of miniaturized sensors in order to achieve a detection limit towards explosives in the parts-per-billion range. DNT and TNT were the major test molecules as TNT is commonly found in landmines, and DNT is a byproduct of

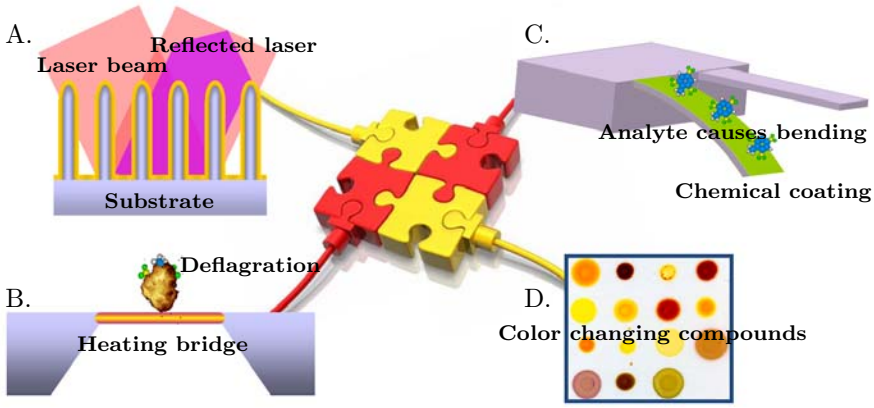

Figure 1.6: Illustration of the four sensing techniques used in Xsense: A. Surface enhanced Raman scattering sensor; sensor; B. Calorimetric sensor; C. Cantilever sensor; D. Colorimetric sensor.

TNT. DNT that leaks to the surrounding soil is generally easier to detect than TNT thus TNT is located by detecting DNT.

The proposed multisensor system is based on four miniaturized sensors: calorimeter, cantilever, colorimetric array, and surface enhanced Raman scattering (SERS). The four utilized sensors are shown on figure 1.6.

SERS is increasingly used as a versatile analytical tool for both chemical and biochemical sensors in liquid and gas phase. In fact, single molecule detection with SERS has been demonstrated [Kneipp et al., 1997]. SERS-based sensors rely on increasing the number of inelastically scattered photons from an analyte adsorbed on a so-called SERS substrate. A new class of SERS substrates has been developed at DTU Nanotech using standard clean-room silicon processing techniques [Talian et al., 2009]. This class of substrates demonstrates a signal enhancement factor of up to $7.8 \cdot 10^6$ due to plasmonic effects from a nanostructured and silver coated surface.

Calorimetry is widely applied to investigate thermal properties of various sample analytes. The micro-calorimetric sensing device used in Xsense is based on differential thermal analysis (DTA) where the temperature difference between two highly sensitive temperature sensors is measured [Yi et al., 2008a, b, Senesac et al., 2009, Greve et al., 2010]. One sensor is loaded with a sample analyte and the other is left blank. Using integrated heating elements both sensors are heated at a constant rate while the differential temperature is continuously measured. At certain temperatures the sample will sublimate, melt, evaporate or deflagrate

which results in a change in differential temperature.

The cantilever based sensor is an established micro- and nano-mechanical sensing tool for trace detection of biochemical compounds [Raiteri et al., 2001, Fritz, 2008, Boisen et al., 2011]. The response of cantilever-based sensors can be measured by monitoring change in resonance frequency of the cantilevers. A negative frequency shift is generated through mass added to the surface of the cantilevers [Fritz et al., 2000, Sushko et al., 2008]. Generally, the larger the resonance frequency change, the higher the amount of a given analyte is present in the sample. The change in resonance frequency of each cantilever is measured. The surface of the cantilever is functionalized with receptor molecules designed to specifically bind target analytes [Gimzewski et al., 1994].

Colorimetric sensing is a technique which can be useful in both detection and identification of volatile organic compounds in air and liquids [Kostesha et al., 2011, Zhang and Suslick, 2005, Nielsen et al., 2008]. Chemoselective compounds are capable of changing colors when exposed to analytes or analyte mixtures. The colorimetric sensor array technique showed great potential for real-time[4] monitoring of analytes such as DNT, acids, alcohols and arenas with sensitivity below the parts-per-million (ppm) range [Kostesha et al., 2010]. Chemoselective compounds are capable of recognizing specific analytes; this recognition is a function of intermolecular interactions, basically weak, non-covalent interactions or donor-acceptor interactions.

As mentioned in the introduction, multisensor devices are emerging such as the GDA 2. But, while the "GDA 2" is a handheld device it has a weight of 4.2 kg. The methods proposed in Xsense enables use of micro- and nano sized sensors and these sensors can facilitate a even lighter handheld device that can contain a multitude of sensors. This is a great strength in the goal of developing high accuracy sensors. Suppose that the sensor measuring techniques in Xsense are completely independent and that each sensor have an accuracy of just 75%. A multisensor approach would under these assumptions have an accuracy of 99.6%. The *main* hypothesis of the Xsense project is exactly that; to investigate to what extent the sensors are independent, and what accuracy can be obtained by a combined solution as opposed to each of the sensor individually.

1.5 Sensor evaluation framework

The development of a multisensor system begins with the development of the individual sensor technologies. Some of the technologies in Xsense are rather

[4] 2 minutes of analyte exposure is needed for the current sensor.

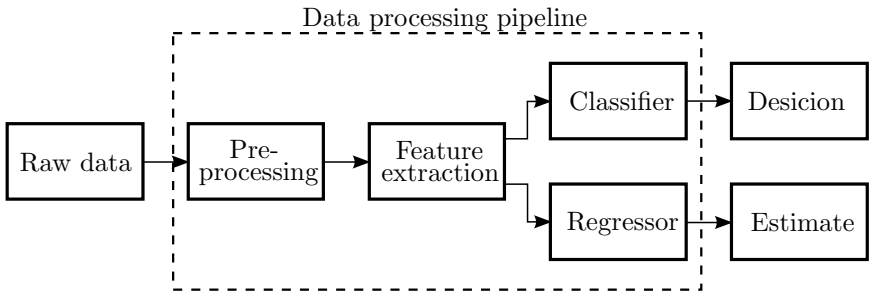

Figure 1.7: Data processing pipeline used throughout this thesis.

new and here we hypothesize that the accuracy of these sensors can be improved if more specifically designed methods are developed. The work carried out herein is about handling data produced by these sensors and how the sensor performance can be assessed.

The generic framework that is repeated throughout the thesis is, 1) collection of sensor data, 2) preprocessing and feature extraction, 3) assessment of the sensor performance using machine learning. The procedure is illustrated in figure 1.7.

Some requirements were put on the machine learning methods. The current state of the art (SotA) machine learning method for the given sensor field is included as baseline. But as we are detecting hazardous compounds we require that the classifier offers posterior probabilities and not only classifications.

When working with sensors the quality and accuracy of the sensor have to be assessed. In our measurement setup we often work both in the *two-class* setting and the *multiclass* setting. In the two-class setting, we are looking to identify the analyte as either an explosives or non–explosives. In the multiclass setting we are working in a more precise setting where either the exact name of the analyte is used (e.g. DNT) or the chemical family of the analyte (e.g. DNT is an explosive substance). When working in the multiclass setting, the goal is to understand the strength of the sensor better and often the results are illustrated using a *confusion matrix*. A confusion matrix illustrates the amount measurements that was not classified correctly and where the sensor has weaknesses.

When comparing classifiers, often they are compared using the McNemar significance test [McNemar, 1947]. The McNemar is a paired test which uses the number of cases where two classifiers disagree about a decision. One p–value is calculated for each comparison. In the cases of multiple hypothesis testing, the framework proposed by Storey [Storey, 2002] is applied. Based on the p–values an expected positive false discovery rate (E[pFDR]) is calculated. This rate is

used to calculate the expected quantity of wrongly significant results relative to all significant results.

1.6 Outline

The remainder of the thesis is structured as follows; Chapter 2 gives a brief review of the origins of machine learning and describes the machine learning methods that is applied in subsequent chapters. The focus of the chapter is on the models and how they are applied and not so much how exactly the training is handled. Often the training involves the minimization of a cost function. Where appropriate the cost function will be described as well, but concerning the numerical optimizations that is carried out, readers are referred to reference material.

Chapter 3 shows some advanced made to quartz microbalance crystal (QCM) sensor detection and estimation of concentration levels. QCM based sensors are highly linear, yet sophisticated non-linear methods have often been applied and in particular artificial neural networks. A data set is presented and analyzed using both linear and non–linear methods, and a recommendation on the handling of data based on QCM sensors is summarized.

Chapter 4 includes several advances made to the colorimetric sensor array data processing. First, the preprocessing of images is described and then the tradition feature extraction process is detailed. Next follows some advances made on visualization of colorimetric sensor arrays and the issues with current feature selection methods are highlighted. Then follows advanced in the handling and modeling of colorimetric sensor array data. Finally a generic framework based on Gaussian process classification is introduced and used to identify important chemoselective compounds.

Chapter 5 introduces the multisensor approach that formed the backbone of the Xsense project. The chapter extracts the main results that is more elaborately presented in appendix A. A dataset inspired by a post-blast[5] car bomb scenario was created. The analytes are measured on all four sensors under identical conditions. Based on the findings it is rendered probably that a multisensor approach comprising the aforementioned sensors will improve the overall prediction accuracy.

Chapter 6 summarizes the thesis, highlights the innovations and put them into

[5]The situation after a detonation have occurred and forensics collect samples in order to identify the explosives that was used

perspective.

Papers B-F are in most part covered in chapter 3 and 4 and serve as supporting information. Finally, appendix G enumerates the analytes that has been applied in the work presented in this thesis.

Contributions

Here follows a condensed list of scientific contributions contained in this thesis:

- Improved performance of density estimation on quartz microbalance crystal based sensors by applying Gaussian process regression [chapter 3, paper B].
- Improved the visualization and interpretation of data collected from colorimetric sensor arrays by application of the cumulative density function [chapter 4].
- Developed a unified approach to perform both sensor selection and analyte classification for colorimetric sensor arrays. This is achieved by use of sparse logistic regression [paper C].
- Improved accuracy in prediction performance for colorimetric sensor arrays by improving the feature extraction. The color representation is carried out using distribution methods and the Hausdorff distance [chapter 4, paper D, E].
- Developed a sensor selection and sensor fusion scheme that based on Gaussian process classification for colorimetric sensor arrays. The sensor selection effectively identifies sensors that will improve prediction performance when sensor fusion is performed [chapter 4, paper E].
- Improved classification accuracy by applying 1-nearest-neighbor majority voting for SERS-based sensors [paper A].
- Improved signal visualization of responses from calorimetric sensors by conducting noise reduction using Gaussian process regression [paper A].

Chapter 2

Learning Theory in the context of sensors

Modern day machine learning concerns the processing and handling of data. Data is typically divided into two groups: labeled or unlabeled, and which machine learning method should be applied depends on the data. Labeled data is for example data gathered for prediction tasks, e.g. prediction of explosives or prediction of the amount of explosives. Here, the experimenter will collect data simultaneously with labeling each measurement appropriately. On the contrary unlabeled data is data gathered without labels, but where the experimenter has collected data without labels and e.g. would like to discover structures in the data in order to gain insight. Discovering these structures can be used to label the data and thus create a labeled dataset. To reflect the distinction between labeled and unlabeled data, machine learning methods are traditionally divided into three categories:

- **Unsupervised learning** concerns unlabeled data. Typical usage is to discover structure in data in an objective manner, i.e. the algorithm has no knowledge of labels. In the context of sensors, unsupervised learning is often applied to visualize the data.

- **Supervised learning** concerns the handing of labeled data. The goal is to construct an algorithm that is able to predict labels. When handing

sensor data, the algorithm is used to determine what the sensor measured and possibly also quantify how much is measured.

- **Reinforcement learning** which is closely related to supervised learning although here the data labels are not explicit. In reinforcement learning the computer algorithm has the ability to learn from a delayed reward, e.g. in a game of checkers.

Handling of sensor data is mostly in the supervised learning domain. As such the majority of this chapter is about supervised learning.

Before delving into the world of machine learning some opening remarks on notation are in order. When measuring the sensor responses are digitalized using a sensor dependent system. The response is either a scalar response or a multivariate response. A multivariate response is a readout that consists of more than one scalar, e.g. a spectrum or multiple quantities measured simultaneously. In case of a scalar response, the response is denoted x. If the response is multivariate the scalars are stacked into a vector $\mathbf{x} = (x_1, \ldots, x_D)$. The variable D denotes the number of scalars that are measured each time a sensor readout is performed. This number D is referred to as the *dimensionality* of the data which naturally emerges when data is represented using the *vector space* model. In this model each observation corresponds to a column in the data matrix $\mathbf{X} = [\mathbf{x}_1\ \mathbf{x}_2\ \cdots\ \mathbf{x}_N]$ where N denotes the total number of measurements (or data points). Throughout this thesis we assume that $\mathbf{X} \in \mathbb{R}^{D \times N}$.

The remainder of this chapter will first give a brief overview of the history of machine learning and formally define machine learning. This is followed by a overview of the methods that is applied in later chapters. No attempt to explain the models exhaustively and derive how algorithms learn the models has been made. Such derivations is found in referred material listed for each method as they are explained.

2.1 A brief history of machine learning

The concept of learning was put in a machine learning context in the late 1940's. One of the pioneers of machine learning was Claude E. Shannon. Although Shannon is often proclaimed as the "father of the information age" he also made significant contributions which helped spur the development of machine learning. In 1949 he wrote a paper[6] discussing how a computer could be programmed

[6]To my best knowledge this is the oldest reference to the concept of a learning machine. Alan M. Turing published a famous paper in 1936 describing the "Turing Machine". While the

to play chess [Shannon, 1950a]. Although Shannon did not specifically use the term "machine learning" or "artificial intelligence" he did discuss possible future evolvements from the theoretical framework presented in the paper. Considering the importance of modern machine learning, it is quite humorous that Shannon, in his introduction, tones down the importance of such application by writing "Although perhaps of no practical importance, the question is of theoretical interest" [Shannon, 1950a]. The items he enumerated include numerous areas that have been solved successfully since then:

> "(1)Machines for designing filters, equalizers, etc.
> (2)Machines for designing relay and switching circuits.
> (3)Machines which will handle routing of telephone calls based on the individual circumstances rather than by fixed patterns.
> (4)Machines for performing symbolic (non-numerical) mathematical operations.
> (5)Machines capable of translating from one language to another.
> (6)Machines for making strategic decisions in simplified military operations.
> (7)Machines capable of orchestrating a melody.
> (8)Machines capable of logical deduction."
>
> Shannon (1950a)

In the following year Shannon managed to build a machine which was possibly the very first example of machine learning. The example is manifested in an electrically controlled mouse named Theseus [Shannon, 1950b]. Figure 2.1 displays the machine built by Shannon and Theseus at work. The mouse is set loose in a 5×5 maze and expected to locate a predefined tile. By exploring, the mouse learns the layout of the maze remembering the position of walls. Once the maze has been fully explored the mouse is able to navigate through the maze flawlessly. The maze can be altered on the fly and the mouse will adapt and relearn the new layout. AT&T Inc. has put a video online where Shannon is presenting the machine [Shannon, 1950b]. The video is an example of the brilliance of one of the great pioneers of information theory.

Other important developments happened in the year of 1950. In this year Alan M. Turing published the famous paper titled "Computing Machinery and Intelligence" where he considers the question "Can machines think?" [Turing, 1950]. Turing even refers to the concept of a "learning machine" – a mechanical machine with the ability to learn from experience. However it was not until a few

Turing Machine is a learning machine as such, his paper described more on how an algorithm could be implemented in machinery and not so much on the topic of how a machine could be programed to learn from experience.

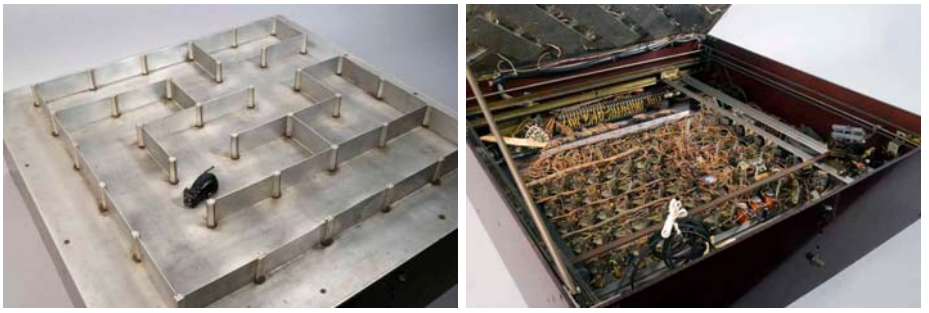

Figure 2.1: Image of Theseus at work (left) and the controlling electronics under the hood (right). Courtesy of [MIT Museum].

years later John McCarthy coined the term "artificial intelligence". In 1955 McCarthy wrote a proposal for support for the "Dartmouth Artificial Intelligence Conference" held in 1956 where he defined the term. In an interview given by McCarthy he explained:

> Interviewer: "You're credited with coining the term "artificial intelligence" just in time for the 1956 conference. Were you just putting a name to existing ideas, or was it something new that was in the air at that time?"
>
> McCarthy: "Well, I came up with the name when I had to write the proposal to get research support for the conference from the Rockefeller Foundation. And to tell you the truth, the reason for the name is, I was thinking about the participants rather than the funder."
>
> "Claude Shannon and I had done this book called "Automata Studies," and I had felt that not enough of the papers that were submitted to it were about artificial intelligence, so I thought I would try to think of some name that would nail the flag to the mast. "
>
> Skillings (2006)

A few years later, in 1959, the term "machine learning" was used by Arthur L. Samuel – perhaps for the first time. In his paper "Some Studies in Machine Learning Using the Game of Checkers" Samuel discussed how he had created a computer program that was able to learn how to play a better game of checkers than himself. Samuel, Shannon and others often described machine learning as a computer algorithm with the ability to learn from experience. McCarthy proposed a more concise definition in a publication from 2007:

> "It [AI] is the science and engineering of making intelligent machines, especially intelligent computer programs. It is related to the similar task of using computers to understand human intelligence, but AI does not have to confine itself to methods that are biologically observable."
>
> McCarthy (2007)

Machine learning is often thought of as a branch of artificial intelligence as the two disciplines have very similar goals. How the two fields are different can be learned by looking at a definition given by Tom M. Mitchell:

> "The field of machine learning is concerned with the question of how to construct computer programs that automatically improve with experience."
>
> Mitchell (1997)

That is, machine learning concerns construction of computer programs whereas artificial intelligence is broader. Further Mitchell formally defines what a machine learning program exactly is:

> "A computer program is said to **learn** from experience E with respect to some class of tasks T and performance measure P, if its performance at tasks in T, as measured by P, improves with experience E."
>
> Mitchell (1997)

To achieve the above mentioned goals, modern machine learning relies heavily on statistics. In fact, modern machine learning and statistics are so closely knit together that often one cannot tell when a practitioner is doing machine learning or statistics. The distinction is discussed by Neil D. Lawrence in a recent lecture titled "What is machine learning?" [Lawrence, 2010]. Lawrence refers to a conversation in particular between Zoubin Ghahramani and Tony O'Hagan. They discussed whether machine learning is indeed just statistics or not. Based on the discussion Lawrence states that statistics and machine learning is not the same, because the two fields have ultimately different goals. Lawrence explains

> "Statistics and machine learning are fundamentally different. Statistics aims to provide a human with the tools to analyze data. Machine learning wants to replace the human in the processing of data."
>
> Lawrence (2010)

To summarize, both disciplines are engaged about the handling of data, they use similar tools, often the same tools, but the end goal for machine learning research is ultimately different than statistical research.

2.2 Unsupervised learning

Visualizing the data in $\mathbf{X}$ can sometimes be challenging especially if D is higher than three or four. In this thesis unsupervised learning is used both for visualizing the data matrix $\mathbf{X}$ and for performing dimensionality reduction. The main idea behind the methods presented in this section is that there exists some latent structure in the data that is more suitable for representing the data. If such a structure exists then the potential for dimensionality reduction of data is there. Further, possibilities for making meaningful visualizations using just a few dimensions also exists.

2.2.1 Principal component analysis

Principal Component Analysis (PCA) was originally proposed by Karl Pearson in 1901 [Pearson, 1901]. The concept of the procedure is to transform the data stored in $\mathbf{X}$ to a new coordinate system that is more suitable to represent the data (to reiterate, $\mathbf{X}$ is a representation of the data in Euclidean space of dimension D). This is achieved by a linear transformation of $\mathbf{X}$. Then PCA will identify a new set of basis vectors, *principal components* (PCs). The first PC identified is the direction which contains the most variance, hence the main assumption of PCA is that this is the direction that will best capture the structure of the data.The second direction is now identified as the direction of second-most variance with the constraint that it has to be orthogonal to the previous basis vector(s) and so forth. The idea is illustrated in figure 2.2 in the two dimensional case. The two variables in question are quite strongly correlated. The line of worst fit which is orthogonal to the line of best fit is mostly projecting noise and is thus not needed. PCA works very well for high dimensional data provided that the signal-to-noise ratio is sufficiently high. Otherwise the identified basis vectors will mostly display noise.

Various algorithms exist to compute PCA [Eldén, 2007, Shlens, 2009], but the most commonly used is singular value decomposition[7] (SVD). SVD is the

[7]SVD is used due to computational advantages. When SVD is used to perform PCA, the matrix $\mathbf{X}$ is centered by subtracting the mean off each measurement type (i.e. each row) before calculating the factorization.

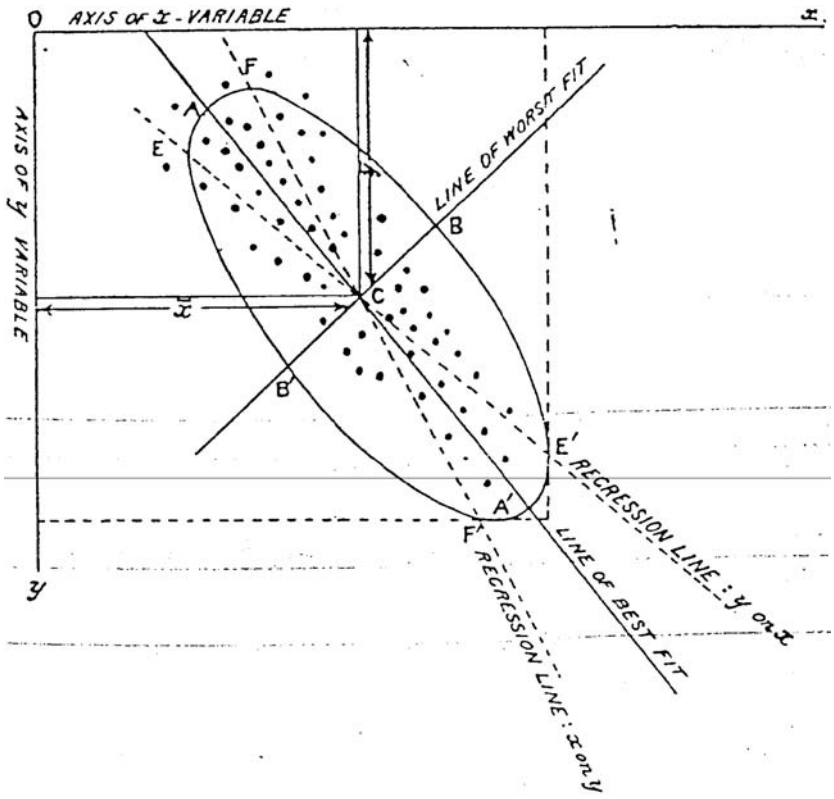

Figure 2.2: PCA as illustrated by the inventor Karl Pearson [Pearson, 1901]. In the example there is just one variable which is a latent structure that is a linear combination of the two variables x and y. In modern day machine learning the y-axis is denoted as x_2 as this is the second observed variable. The letter y is usually used for labels in supervised learning. Permission granted by Taylor & Francis group, copyright 1901.

following matrix factorization

$$\mathbf{X} = \mathbf{S}\mathbf{\Sigma}\mathbf{V}^\top \tag{2.1}$$

where $\mathbf{S} \in \mathbb{R}^{D\times M}$ and $\mathbf{V} \in \mathbb{R}^{M\times N}$ are orthogonal, that is $\mathbf{S}^\top\mathbf{S} = \mathbf{I}$ and $\mathbf{V}^\top\mathbf{V} = \mathbf{I}$. The matrix $\mathbf{\Sigma} \in \mathbb{R}_{0+}^{M\times M}$ is a diagonal matrix with elements $\mathbf{\Sigma} = \text{diag}(\sigma_1, \sigma_2, \cdots, \sigma_M)$ and is ordered such that $\sigma_1 \geq \sigma_2 \geq \cdots \geq \sigma_M \geq 0$. The value of M will be the minimum of $M = \min(D, N)$. The parameter M can also be chosen to be smaller in which case the above equation no longer holds and the factorization becomes an approximation using the first M principal components. This corresponds to dimensionality reduction.

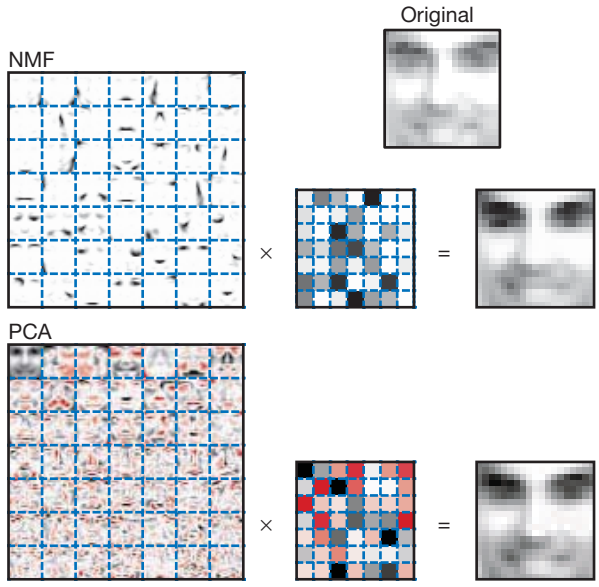

Figure 2.3: Non–negative matrix factorization as introduced by Lee and Seung. The matrices to the left graphically illustrate the identified basis vectors. Colors on gray scale represent positive values, white corresponds to zero and colors containing red represent negative values. The middle matrices are the loadings matrices. Adapted by permission from Macmillan Publishers Ltd: Nature [Lee and Seung, 1999], copyright 1999.

Of final note the amount of variance explained by the mth PC is often calculated and displayed when making PCA plots or conducting dimensionality reduction. The amount of variance explained by the mth PC is calculated as

$$\text{Var}(\text{PC}_m) = \frac{\sigma_m}{\sum_i \sigma_i} \tag{2.2}$$

A strategy for dimensionality reduction is to choose M such that the new subspace explains 95% or 99% of the variance in the data.

2.2.2 Non-negative matrix factorization

Non–negative Matrix Factorization (NMF) is a linear vector–space projection method much like PCA, but with different considerations and assumptions. The

method is applicable provided that the data contains no negative values[8], that is $\mathbf{X} \in \mathbb{R}_{0+}^{D\times N}$. In this case NMF will identify basis vectors and loadings that have no negative values as well. This should increase the interpretability of both the basis vectors and the loadings. The NMF model is

$$\mathbf{X} \approx \mathbf{AS} \tag{2.3}$$

where $\mathbf{A} \in \mathbb{R}_{0+}^{D\times M}$ and $\mathbf{S} \in \mathbb{R}_{0+}^{M\times N}$. The method is also known as Positive Matrix Factorization [Paatero and Tapper, 1994] but is largely credited to Daniel D. Lee and H. Sebastian Seung [Lee and Seung, 1999] due to their proposal of a computationally simple procedure to estimate $\mathbf{A}$ and $\mathbf{S}$.

NMF will often identify more sparse basis vectors which are easier to interpret, see figure 2.3. The NMF basis vectors identified comprise various recognizable facial features and then the loading matrix displays how much of each feature is needed to construct a face. PCA identifies a drastically different solution where most basis vectors are hard to interpret. Interestingly, even though the PCA identifies a much more complex basis and loadings matrix, the face constructed using PCA is of similar quality to the naked eye.

2.3 Supervised learning

In supervised learning the data is accompanied with a label so data is measured as a pair $(\mathbf{x}, y)$. The label y is either a univariate continuous variable or a discrete variable. Handling of continuous data is regression. Handling of discrete variable is classification. There exists a few variations of classification problems depending on the nature of the discrete variable. Suppose that observations have to be identified to belong to one of K distinct classes. In this case the data is called nominal. If $K = 2$ the classification problem is called binary, and for $K > 2$ the classification problem is multinomial (or multiclass). The last type of data, which is not handled is this thesis, is ordinal data. Here the K distinct classes can be ordered according to some scale.

As in the unsupervised case the data is stored in a design matrix $\mathbf{X}$ and the labels in a vector $\mathbf{y}$. Typically supervised learning problems are formulated as the problem of learning a function $f(\cdot)$ that maps observations to labels

$$y_i = f(\mathbf{x}_i) \tag{2.4}$$

where $\mathbf{x}_i$ is the ith measurement and y_i is the corresponding label. The function $f(\cdot)$ is manifested in the form of a mathematical model. Supervised learning

[8] Or all negative values are set to zero.

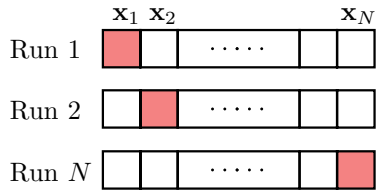

Figure 2.4: Leave-one-out cross validation illustrated. In each run exactly one test point is used (the colored) and $N-1$ points are used to train the classifier. Each point is used as test point exactly once

concerns how one identifies the model that "best" maps the observations to labels. The handling of labeled data leaves open questions such as how should the outcome of $f(\cdot)$ be handled, how do we choose between multiple inferred models and how is the quality of a model assessed. These issues will be discussed in this section as well as how supervised learning is employed in the framework of sensors.

The subject of model evaluation, model selection and decision theory is rather large thus in this section only the theory applied in this thesis is explained. Further information can be found in the books [Berger, 1985, Bishop, 2006, Hastie et al., 2008, Chen et al., 2010].

2.3.1 Model evaluation

In supervised learning, the data stored in $\mathbf{X}$ is divided into two separate matrices: the training set matrix, $\mathbf{X}_{tr}$ and the test set matrix, $\mathbf{X}_*$. The model used to approximate the function $f(\cdot)$ is decided based on the data in $\mathbf{X}_{tr}$. Further the model is also inferred based on $\mathbf{X}_{tr}$. This stage is often called the *inference stage*. The performance of the model is now evaluated on the test set $\mathbf{X}_*$ in the *decision stage*.

The purpose of dividing the data into two portions is to be able to estimate the *generalization error*. The generalization error is a measure of how well a sensor performs on unknown data. This corresponds to real world scenarios where a sensor is always measuring unknown data. Obviously the true generalization error can never be known and must be estimated from data. A realistic estimate thus requires a very rich data set that encompass a broad range of classes. In the case of having limited number of measurements, the generalization error can be estimated using the method of *leave-one-out* cross validation (LOO-CV) [Hansen and Larsen, 1996]. The leave-one-out cross validation scheme is illustrated in figure 2.4. A rather significant disadvantage of LOO-CV, is that

LOO-CV requires the training of N models which quickly becomes infeasible due to computational cost. In this case, precision on the generalization error estimate can be sacrificed by dividing the data into equally sized portions thus reducing the amount of needed models. This concept is called K-fold cross validation (K-CV).

2.3.2 Model selection

The supervised methods explained throughout this chapter all have tuneable parameters that will have influence on the performance. The topic of model selection handles how the parameters are chosen to best represent the observed data. However, the caveat is that we want the model that performs best on unknown test data and not on the training data. In order to meet this goal the parameterization of $f(\mathbf{x})$ is changed to include the model parameters. The function then is $f(\mathbf{x}, \mathbf{w})$ where $\mathbf{w}$ denotes model parameters. Two methods are employed depending on the type of parameters. The first method is again cross validation. Here, the cross validation is performed over the training set, and then the model that performs with the best generalization error is being used. This model is trained anew on the entire training set, before prediction on the test set is performed.

The second method that is employed to estimate the model parameters is the method of *maximum likelihood*. Here, the model parameters are formulated in the context of a prior probability function $p(\mathbf{w})$. The effect of the observed data, $\mathcal{D} = \{\mathbf{x}_i, y_i\}_{i=1}^N$, is likewise expressed through a probability function $p(\mathcal{D}|\mathbf{w})$. Now, given Bayes' rule [Bishop, 2006, Laplace, 1812, MacKay, 1992a] the posterior $p(\mathbf{w}|\mathcal{D})$ takes the form

$$p(\mathbf{w}|\mathcal{D}) = \frac{p(\mathcal{D}|\mathbf{w})p(\mathbf{w})}{p(\mathcal{D})} \tag{2.5}$$

The equation is often put in words:

$$\text{posterior} = \frac{\text{likelihood} \times \text{prior}}{\text{evidence}} \tag{2.6}$$

In the case where we have no knowledge about the prior $p(\mathbf{w})$, i.e. all model parameters are equally likely before observing data such that $p(\mathbf{w})$ is a uniform distribution, the posterior is proportional to the likelihood

$$p(\mathbf{w}|\mathcal{D}) \propto p(\mathcal{D}|\mathbf{w}) \tag{2.7}$$

In maximum likelihood, one looks at the probability $p(\mathcal{D}|\mathbf{w})$ as a function of $\mathbf{w}$ and then maximizes this function in respect to $\mathbf{w}$. As equation (2.7) shows, this

corresponds to choosing the value of $\mathbf{w}$ that maximizes the posterior probability of $\mathbf{w}$.

In some models, the prior $p(\mathbf{w})$ is not chosen to be uniform but is governed by some other distribution. In this case, the prior for $\mathbf{w}$ is written as $p(\mathbf{w}|\boldsymbol{\theta})$ where $\boldsymbol{\theta}$ is a vector that contains the hyperparameters. Hyperparameters are quantities that control the distribution of the model parameters. Given hyperparameters, the posterior now takes the form

$$p(\mathbf{w}|\mathcal{D}, \boldsymbol{\theta}) = \frac{p(\mathcal{D}|\mathbf{w}, \boldsymbol{\theta})p(\mathbf{w}|\boldsymbol{\theta})}{p(\mathcal{D}|\boldsymbol{\theta})} \tag{2.8}$$

Hence, the likelihood function must now be optimized both in terms of $\mathbf{w}$ and $\boldsymbol{\theta}$. However, the hyperparameters are optimized in the evidence function (again, the evidence distribution is interpreted as a function of $\boldsymbol{\theta}$)

$$p(\mathcal{D}|\boldsymbol{\theta}) = \int p(\mathcal{D}|\mathbf{w})p(\mathbf{w}|\boldsymbol{\theta})d\mathbf{w} \tag{2.9}$$

that is, *all* model parameters $\mathbf{w}$ are considered by integrating over $\mathbf{w}$. This approach is called *marginalization* over $\mathbf{w}$, and for this reason equation (2.9) is often referred to as *marginal likelihood*.

2.3.3 Performance measures

Performance measures are different depending on the type of data being handled. We begin with classification, where each measurement is mapped to one of K classes. Generally the number of classes in a data set is denoted K, and has nothing to do with the K in "K-fold cross validation".

First we consider a *discriminant function* which is a model that directly maps an observation to a label. The way the performance of classifiers is measured in this thesis is by the accuracy, defined as

$$\text{Accuracy} = \frac{\text{Number of correctly classified measurements}}{\text{Total number of measurements}} \tag{2.10}$$

From the Accuracy measure follows another measure that is also often reported, which is the "classification error rate" defined as 1 - Accuracy.

When measuring highly dangerous chemicals such as explosives, classifiers must not only be able to classify explosives, they must also be able to measure the certainty of the classifier regarding the decision. One way to achieve this is to model the posterior probability

$$p(\mathcal{C}_k|\mathbf{x}) = f(\mathbf{x}) \tag{2.11}$$

Models that model the posterior probability directly are called *discriminative models*. Prediction is carried out by mapping $\mathbf{x}$ to the label that has the highest posterior probability. This approach obtains the highest accuracy which also seem rather intuitive [Bishop, 2006].

For continuous data the performance measure must reflect the ability to predict a scalar. The most simple measure one might think of is the mean absolute error defined as

$$\text{MAE} = \frac{1}{N}\sum_{n=1}^{N}|y_n - \hat{y}_n| \tag{2.12}$$

In essence the MAE measures how much a prediction is off the mark on average. This measure is often inappropriate in the context of sensors, because sensors often operate over a large range of values, and prediction accuracy is important for values in both the lower and higher range. This issue is fixed by the mean relative absolute error

$$\text{RMAE} = \frac{1}{N}\sum_{n=1}^{N}\left|\frac{y_n - \hat{y}_n}{y_n}\right| \tag{2.13}$$

This measure calculates how much an error is off the mark on average in percentage! Thus prediction errors in the entire range are equally important.

2.4 Regression

Handling continuous data is done using a regression model however there are numerous ways to model continuous data. Overall we distinguish between linear and non-linear models. Linear models are suited for data that can be modeled linearly, either by directly applying the data to the model or by introducing non-linear features based on the original data.

Four different models are discussed, first the classic linear regression model. This model has issues in the case where the dimensionality of the data is greater than the number of measurements $D > N$. This deficiency can be handled in a number of ways. Two strategies are introduced, one being the concept of *regularization* and the other being that of dimensionality reduction. Finally two non-linear methods are introduced, one being artificial neural network regression which is a classic well-known model. The other Gaussian process regression (GPR) which has advantages compared to the other models but also dis-advantages. The main advantage of GPR when working with sensors is that

Gaussian process models (GP) also inherently model prediction uncertainty[9]. The regression models introduced in this section are almost the same that are used for classification, only the models are changed to handle nominal data.

2.4.1 Linear regression

Linear regression was most likely proposed by Gauss [Stigler, 1981] and uses the model

$$y = w_0 + \mathbf{w}^\top \mathbf{x} \tag{2.14}$$

where $\mathbf{w}$ is usually called the *weight* vector or the *loadings* vector. From the equation it is seen that $\mathbf{w}$ is of length D, and in this thesis we further require all numbers to be real numbers i.e. $\mathbf{w} \in \mathbb{R}^D$. Inspection of the equation reveals that one would require $D + 1$ equations to uniquely solve the set of equations. Having more equations (observations) will results in an overdetermined system[10] where there are too many equalities to be met. In this case one can estimate the vector $\mathbf{w}$ using the method of *least squares*.

The idea is to find the solution that comes as close as possible to solving the equations by solving the minimization problem

$$\mathbf{X}_0 = [\mathbf{x}_0 \; \mathbf{x}_1 \; \cdots \; \mathbf{x}_n] \tag{2.15}$$

where $\mathbf{x}_0$ is a vector of length D containing ones. Using the above design matrix the least squares estimate of $\mathbf{w}$ is

$$\mathbf{w} = (\mathbf{X}_0 \mathbf{X}_0^\top)^{-1} \mathbf{X}_0^\top \mathbf{y} \tag{2.16}$$

The set of equations generated by the above expressions is usually referred to as the *normal* equations. It can be shown that given the measurements follow a linear model and are contaminated by Gaussian distributed noise this is the optimal estimate of $\mathbf{w}$ [Bishop, 2006]. The model described here forms the basis of both prediction models applied later.

Applying least square regression corresponds to minimizing the function

$$E_D(\mathbf{w}) = \frac{1}{2} \sum_{i=1}^{n} (y_i - \hat{y}_i)^2 \tag{2.17}$$

[9] Although one has to remember that the uncertainty predicted is under the assumption that the model is correct, as the uncertainty is modeled within the model.

[10] Unless some observations are linearly determined by others.

That is, least square minimizes the sum of the squared error. The concept of an error function is important in supervised learning. In linear regression the solution is found in closed form, but in other instances the model is learned by some minimization of an error function, often derived by maximum likelihood.

The case arises if one has an under-determined system. In this scenario there are too few equations to estimate $\mathbf{w}$ uniquely, i.e. an ill-posed problem[11]. Further constraints must be put on $\mathbf{w}$ in order to make the solution unique and tractable. We use the approach of *regularization*. The basic idea behind regularization is imposing penalties for large values in $\mathbf{w}$. The system will now have a unique solution and often be converted to a well-posed problem thus avoiding over-fitting. The error function is separated into a data dependent part $E_D(\mathbf{w})$ and a data independent part $E_{\mathbf{w}}(\mathbf{w}, \boldsymbol{\lambda})$

$$E(\mathbf{w}) = E_D(\mathbf{w}) + E_{\mathbf{w}}(\mathbf{w}, \boldsymbol{\lambda}) \tag{2.18}$$

There are various choices of $E_{\mathbf{w}}(\mathbf{w}, \boldsymbol{\lambda})$ which will be introduced as they are applied.

2.4.2 Principal component regression

Principal component regression (PCR) is an alternative strategy to handle the issue of under-determined systems. Principal component regression is a linear regression method that is related to regularized least squares regression and partial least squares regression [Eldén, 2007, Bishop, 2006]. It is essentially a combination of linear regression and PCA. The parameters to be chosen when using principal component regression are which principal components to include in the regression. We include principal components in the model ordered by their variance choosing the highest variance component. The new set of variables generated is used as input to a linear regression model.

2.4.3 Artificial neural network regression

The artificial neural network model is originally inspired by a mathematical formulation on the processes happening in the brain, introduced by [McCulloch and Pitts, 1943]. However, much credit is given to Rosenblatt [Rosenblatt, 1962] for his *perceptron* model which is illustrated on figure 2.5. The network is a *feed-forward* network where data flows through the network in order to reach

[11] The problem might have been ill-posed anyway as well-posed problems also require stability in the solution of $\mathbf{w}$.

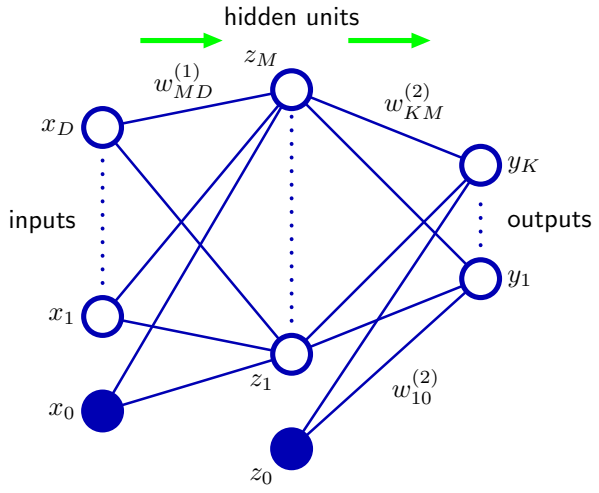

Figure 2.5: Figure by courtesy of Christopher M. Bishop [Bishop, 2006]

a prediction. For each dimension in $\mathbf{x}$ a corresponding input node is given and for each output an output node is given. What makes the network special is the hidden layer consisting of M nodes z_j. Essentially each hidden node has its own linear model associated. Following the principle of neurons, the hidden nodes can be either active or inactive. This is formally achieved by wrapping each linear model with an activation function $h(\cdot)$. In this work we use the tangent hyperbolic sigmoidal function $z_j = \tanh(a_j), h : \mathbb{R} \to [-1; 1]$. The output node thus becomes a linear combination of M activation functions. Formally the model for node y_k can be written as

$$y_k(\mathbf{x}, \mathbf{w}) = \sum_{j=0}^{M} w^{(2)}_{kj} h \left(\sum_{i=0}^{D} w^{(1)}_{ji} x_j \right) \tag{2.19}$$

The equation specified corresponds to the network displayed in figure 2.5.

Training neural networks is generally a non-convex problem however the rewards for such a complex model is the gain of a very general approximation possibility. Therefore neural networks with one hidden layer are said to be *universal approximators*. This knowledge is largely due to [Hornik et al., 1989, Hornik, 1991, 1993] who published a series of papers investigating which type of functions could be approximated. Using the tangent hyperbolic sigmoidal function as activation function, almost any function can be approximated, provided the network has a sufficiently large number of hidden units.

Unfortunately, introduction of each hidden node results in $D + K$ additional parameters that must be estimated. Thus the big issue when using ANN is not

the flexibility in approximation capability, but to find the best solution. A great deal of research has gone into how to estimate the weights.

The training used throughout this thesis is based on an implementation by [Sigurdsson et al., 2004]. This is a two-layer feed-forward network with tangent hyperbolic sigmoidal function as activation function. When used for regression there is only one output unit, thus the k subscript vanishes.

Here the number of hidden units is assumed to be found by other means, e.g. by CV whereas the model parameters $\mathbf{w}$ are governed by a zero mean Gaussian prior (see section 2.3.2). Stacking all weights into one vector $\mathbf{w}$ the prior is

$$p(\mathbf{w}|\alpha) = \mathcal{N}(\mathbf{w}|\mathbf{0}, \alpha^{-1}\mathbf{I}) \tag{2.20}$$

and the corresponding error function becomes

$$E(\mathbf{w}) = E_D(\mathbf{w}) + \frac{\alpha}{2}\|\mathbf{w}\|_2^2 \tag{2.21}$$

The value α is optimized by marginal likelihood as described in section 2.3.2. The network training is performed by iteratively optimizing the error function for a given α and then performing evidence optimization on α. The initial value for α is always $\alpha = 1/D$.

2.4.4 Gaussian process regression

The theory behind Gaussian process regression goes back as far as 1880 [Lauritzen, 1981], but was put into a machine learning context by [Williams and Rasmussen, 1996]. A Gaussian process (GP) is completely specified by its mean function and covariance function. Gaussian process is defined as [Rasmussen and Williams, 2006a], "A Gaussian process is a collection of random variables, any finite number of which have a joint Gaussian distribution."

Suppose that the function $f(\cdot)$, that maps observations to labels, is taken to be a real random process. Two new functions are defined, the mean function $m(\mathbf{x})$ and the covariance function $k(\mathbf{x}, \mathbf{x}')$ of the process:

$$m(\mathbf{x}) = \mathbb{E}\left[f(\mathbf{x})\right] \tag{2.22}$$

$$k(\mathbf{x}, \mathbf{x}') = \mathbb{E}\left[\left(f(\mathbf{x}) - m(\mathbf{x})\right)\left(f(\mathbf{x}') - m(\mathbf{x}')\right)\right] \tag{2.23}$$

The formal Gaussian process is written as

$$f(\mathbf{x}) \sim \mathcal{GP}\left(m(\mathbf{x}), k(\mathbf{x}, \mathbf{x}')\right) \tag{2.24}$$

where $m(\mathbf{x})$ is the mean function of the real process $k(\mathbf{x}, \mathbf{x}')$

Sensor measurements are (almost) always noisy, however when we build a model of a sensor response, what we would really like to model is the sensor and not the noise. As such, a natural model to assume is

$$y = f(\mathbf{x}) + \varepsilon \tag{2.25}$$

Prediction is in this case

$$f(\mathbf{x}_*) = \sum_{i=1}^{N} \alpha_i k(\mathbf{x}_i, \mathbf{x}_*) \tag{2.26}$$

To summarize, the covariance function is the heart of prediction using GP, and it is paramount to choose a suitable covariance function. Of popular choice is the squared exponential kernel

$$k(\mathbf{x}, \mathbf{x}') = \exp\left(-\frac{\|\mathbf{x} - \mathbf{x}'\|_2^2}{2\ell^2}\right) \tag{2.27}$$

The specific choice of covariance function is introduced as the GPR framework is applied. Generally we use the implementation made by [Rasmussen and Nickisch, 2010].

2.5 Classification

Classification is closely related to the regression models, as classification is a special case of regression where the prediction variable is constrained to be discrete. There are essentially three families of classification methods: cluster based classifiers, linear classifiers and nonlinear classifiers. They have different assumptions, e.g. cluster based classifiers assume that the data points measured are clustered. In turn, that means cluster based methods might extrapolate poorly depending on the type of sensor response, e.g. if theoretical insight about the sensor reveals a linear dependence between the measured variables and the responses linear classifiers are better suited. Non-linear methods assume that a non-linear effect may exist. All three types of classifiers have been used and will be explained in this section. The explanations are typically shorter compared to the regression section, and only the differences when moving from regression to classification are highlighted.

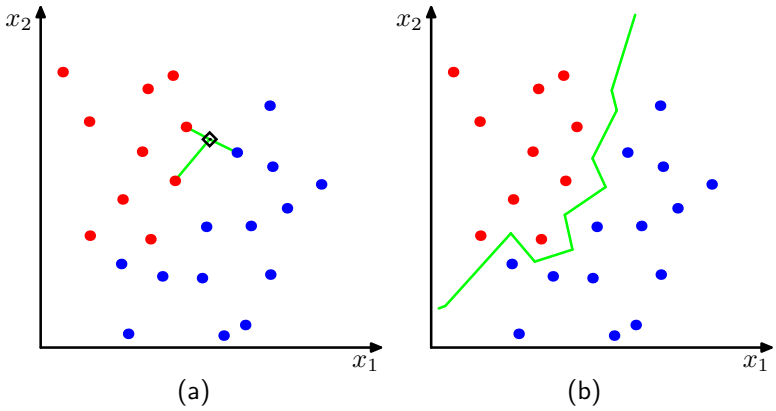

Figure 2.6: A. Black diamond refers to a new test point that is going to be classified. The k-nn classifier in this case identifies the three closest points. B. The green line represents the decision place in case only the closest point (1-nn) is being used to classify unknown points. Figures courtesy of [Bishop, 2006].

2.5.1 *k*-nearest-neighbor

The k-nearest-neighbor (k-NN) is an effective classification technique that has the general assumption that points belonging to the same class should cluster together. As such it can be characterized as a cluster based classification algorithm. The basic idea is illustrated in figure 2.6.

When testing an unknown data point, the Euclidean distances for all known points are calculated. The classes of the closest k points are then identified and the unknown point is classified using majority voting of these known points. In the event of a tie, the algorithm uses the nearest neighbor among the tied classes to break the tie selecting the closest point as the class.

2.5.2 Vector-space classification

In vector-space classification, the data is represented in a subspace of lower dimensionality than the original space. Training consists of finding a suitable subspace as representative for each class. When classifying an unknown data point, the data point is projected into each subspace. The subspace that represents the data point best (calculated as residuals) is chosen as the correct class.

This is done as follows; the training points stored in $\mathbf{X}$ is factorized using either NMF or PCA. Using CV the optimal dimensionality of the subspaces are found where the subspaces are required to be of the same dimensionality. After training we have one matrix per class. When classifying test points, the data points are projected into each of the subspaces. Classification is made by identifying the unknown class as the subspace that represents the data point best.

2.5.3 Sparse logistic regression

The logistic regression model is an extension of the linear regression model. Although the name implies regression the logistic regression model is a classification model. The idea is to use the output of a linear regression model and then "squash" it using the *logistic sigmoid* function

$$\sigma(y) = \frac{1}{1 + \exp(-y)} \tag{2.28}$$

The sigmoid function has a domain $y \in \mathbb{R}$ and a range of $\sigma(y) = [0, 1]$, thus it maps the real space into a number that can be interpreted as a probability. Binary logistic regression is now defined by the model

$$p(\mathcal{C}_1|\mathbf{x}) = \sigma(\mathbf{w}^\top \mathbf{x}) \tag{2.29}$$

with $p(\mathcal{C}_2|\mathbf{x}) = 1 - p(\mathcal{C}_1|\mathbf{x})$. The model is extended to a multiclass model by using the *normalized exponential* (also called softmax)

$$p(\mathcal{C}_k|\mathbf{x}) = \frac{\exp(\mathbf{w}_k^\top \mathbf{x})}{\sum_j \exp(\mathbf{w}_j^\top \mathbf{x})} \tag{2.30}$$

For the logistic regression model a closed form solution of $\mathbf{w}$ no longer exists and one must be estimated using iterative techniques.

To promote a sparse solution and to handle over-fit, we use L1 regularization. This is achieved by adding the term to the error function where λ is the model selection parameter.

$$E_{\mathbf{w}}(\mathbf{w}) = \lambda \|\mathbf{w}\|_1 \tag{2.31}$$

The error function is minimized using the *Projection L1* method described by Schmidt *et al.* [Schmidt et al., 2007].

2.5.4 Gaussian process classification

Gaussian process classification comes naturally now that Gaussian Process regression has been explained. As in the case with GPR the framework is imple-

mented using [Rasmussen and Nickisch, 2010]. The model choice of covariance function is still the same, as is the choice of a mean function, but having discrete variables the modeling changes.

Here we consider the binary case so the labels are now $y = +1$ for the target class and $y = -1$ for all other classes. The cumulative Gaussian[12] is considered

$$p\left(y_i|f\left(\mathbf{x}_i\right)\right) = \int_{-\infty}^{y_i \cdot f(\mathbf{x}_i)} \mathcal{N}\left(t|0,1\right) dt = \Phi\left(y_i \cdot f\left(\boldsymbol{x}_i\right)\right) \tag{2.32}$$

which is parameterized by a given function value, $f(\mathbf{x}_i)$. Hence, the model, or free parameter is the function value, $f(\mathbf{x}_i)$, and by taking a Bayesian approach, we can directly consider the posterior over the function defined by the finite set of random variables, $\mathbf{f} = [f(\mathbf{x}_1), f(\mathbf{x}_2), ..., f(\mathbf{x}_N)]^\top$, i.e.,

$$p\left(\mathbf{f}|\mathbf{y},\mathbf{X}\right) = \frac{p\left(\mathbf{y}|\mathbf{f}\right)p\left(\mathbf{f}|\mathbf{X}\right)}{\int p\left(\mathbf{y}|\mathbf{f}\right)p\left(\mathbf{f}|\mathbf{X}\right)d\mathbf{f}} = \frac{p\left(\mathbf{y}|\mathbf{f}\right)p\left(\mathbf{f}|\mathbf{X}\right)}{p\left(\mathbf{y}|\mathbf{X}\right)} \tag{2.33}$$

The prior for $f(\mathbf{x})$ is then a Gaussian process as specified in (2.24).

Given the probit likelihood model, the posterior over $p\left(\mathbf{f}|\mathbf{y},\mathbf{X}\right)$ needs to be approximated and here the Expectation Propagation (EP) which provides a Gaussian approximation to the posterior is used [Rasmussen and Williams, 2006a].

The prediction for a new input $\mathbf{x}_*$ is obtained by first computing the predictive distribution, $p(f_*|\mathbf{y},\mathbf{X},\mathbf{x}_*)$, which is Gaussian due to the EP approximation ($f_* = f(\mathbf{x}_*)$). The probability of a given class $\mathcal{C}_1$ is computed by

$$p\left(\mathcal{C}_1|\mathbf{y},\mathbf{X},\mathbf{x}_*\right) = \int p\left(y = +1|f^*\right)p(f^*|\mathbf{y},\mathbf{X},\mathbf{x}_*)df^* \tag{2.34}$$

and $p\left(\mathcal{C}_2|\mathbf{y},\mathbf{X},\mathbf{x}_*\right) = 1 - p\left(\mathcal{C}_1|\mathbf{y},\mathbf{X},\mathbf{x}_*\right)$.

2.5.5 Artificial neural network classification

The neural network framework used for classification is largely identical to the framework presented in the regression case with two differences which are highlighted in this section. Again the implementation provided by [Sigurdsson et al., 2004] is used.

[12] Also known as the probit model

First, number of output nodes is increased to $K-1$, i.e. the number of classes in the dataset minus one, and then the outputs are converted to probabilities by using a modified softmax

$$p(\mathcal{C}_k|\mathbf{x}) = \frac{\exp(y_k(\mathbf{x}))}{1+\sum_{k'=1}^{K-1}\exp(y_{k'}(\mathbf{x}))} \tag{2.35}$$

where the output from each node y_k is defined in (2.19). The probability for class K is then

$$p(\mathcal{C}_K|\mathbf{x}) = 1 - \sum_{k=1}^{K-1} p(\mathcal{C}_k|\mathbf{x}) \tag{2.36}$$

The other difference is the addition of outlier detection. Outlier detection aims to locate random label noise which could lead to wrong decisions. Having outlier detection should improve the networks ability to predict accurately. The outlier probability is introduced in the data dependent part of the model as the hyperparameter β, leading to the error function

$$E(\mathbf{w}) = E_D(\mathbf{w},\beta) + \alpha E_{\mathbf{w}}(\mathbf{w}) \tag{2.37}$$

β is a scaled outlier probability as detailed in [Sigurdsson et al., 2004] with the range $\beta = [0; 1/(K-1)]$.

Chapter 3

Quartz crystal microbalance sensors

Quartz crystal microbalance (QCM) devices, originally proposed by Günter Sauerbrey [Sauerbrey, 1959], are often used as gas sensors. The working principle of a QCM sensor resemble a tuning fork. The resonance frequency response of QCM sensors is close to linear with respect to mass change. The crystal itself is not selective and will change mass whenever some molecule is present on the crystal. To make the sensor selective the crystal is coated with some kind of chemical. The coating is specifically chosen or designed to detect a predetermined type of analyte. Some coatings are chosen as responders to relevant background molecules as well. This is done to strengthen the sensor in an environment which contains a rich amount of molecules.

In this chapter we examine a QCM sensor consisting of eight different coatings. A picture of one of the crystals is shown on figure 3.1. The sensor is used to detect both the type of gas (classification) and the gas density (regression). We investigate current QCM state-of-the-art classification and density estimation techniques. Classification methods previously applied to QCM sensors are principal component analysis [Lu et al., 2009, Rosengren et al., 2009, Si et al., 2007], hierarchical cluster analysis [Ying et al., 2008, Sepcic et al., 2004] and artificial neural networks [Gulbag et al., 2008]. However NMF has never been tried despite the fact that QCM sensor responses are almost always positive. In this chapter we conduct classification using ANN, SVD and NMF.

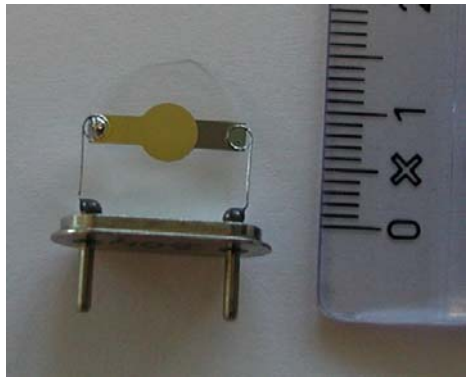

Figure 3.1: Picture of an uncoated QCM device.

For density estimation three different methods are evaluated; Principal component regression, artificial neural network and Gaussian process regression. PCR is a linear method that performs well with a limited amount of training points although it handles non–linearity in data poorly. To overcome this problem, neural networks have usually been applied as the non–linear model [Gulbag et al., 2008, Saraoglu and Kocan, 2010, Mumyakmaz et al., 2008, Özmen et al., 2006]. However, GPR is so far an untried method for QCM data. GPR, a non–linear method like ANN, should be able to perform well with a limited amount of data points.

3.1 Detection of Ecstasy

The dataset is focused on the detection of Ecstasy. The analyte "benzodioxol" is an important precursor for Ecstasy. The other analytes in the dataset are compounds used in the production of Ecstasy but can also be found elsewhere. Hence they serve as a natural background.

The data is measured using eight different coatings thus the dimensionality of the data is $D = 8$. Six different analytes were measured, $K = 6$, which are: acetone, benzodioxol, ethanol, heptane, pentanol and water. Each analyte was measured at six different concentration levels, listed in table 3.1. Each experiment is repeated three times, thus the dataset contains a total of $N = 108$ measurements. Details on the measurement system is found in appendix B.

PCA is used to visualize the entire dataset more effectively, see figure 3.2. The sensor response for each analyte is almost on a linear manifold of its own, hence

Level	Acetone	Benzodioxol	Ethanol	Heptane	Pentanol	Water
1	2125	820	900	628	103	288
2	4250	1640	1800	1526	192	575
3	8500	3280	3600	2512	300	1150
4	18200	6575	7200	5025	416	2300
5	32400	13150	14400	10050	600	4600
6	72800	26300	28800	20100	1400	9200

Table 3.1: List of concentration levels for each of the analytes. All concentration levels are in ppm.

the usage of linear methods is justified and reasonable. Also, it seems that PC1 and PC2 is sufficient to classify benzodioxol and pentanol whereas the other analytes are very close, especially at low concentration levels.

3.1.1 Data partitioning

The data is partitioned into a training set and a test set. Learning curves are produced for each algorithms so the size of the training set will vary. The number of training points per analyte, denoted N_{tr}^k, will have a lower bound at $N_{tr}^k = 3$ and an upper bound of $N_{tr}^k = 12$. The upper bound corresponds to an experimental setup where all concentration levels for each analyte are included twice.

The training set size is increased in roughly the same manner as an experimenter would include more and more experiments. The training set is expanded as follows: each analyte must be represented evenly in the training set - thus the training set size N_{tr} is a multiple of K. Furthermore, each concentration level within each analyte is represented as evenly as possible, e.g. for $N_{tr}^k = 6$ each concentration level is represented exactly once. The data partitioning is graphically illustrated in figure 3.3.

3.1.2 Model evaluation

The two–tiered model described in section 1.5 is adopted where classification and concentration level estimation is carried out separately. Output from the sensor is applied to a classifier. Based on the decision made by the classifier, a given regression model is selected with one regression model per analyte. Altogether, the output from the framework is both an analyte name and a concentration

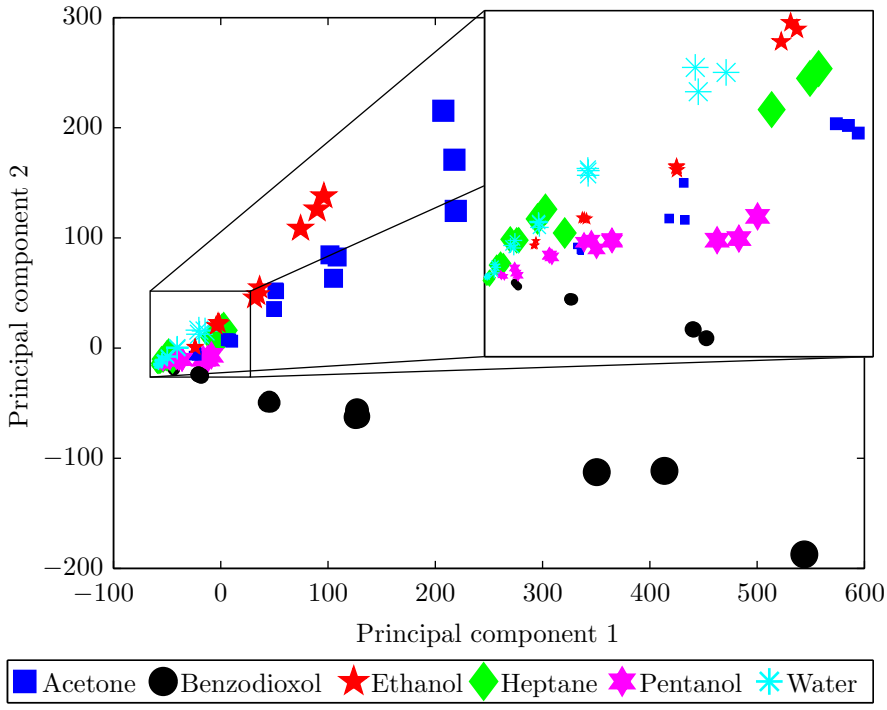

Figure 3.2: The data visualized using PCA. The symbol size represents the concentration level: the higher the concentration the bigger the symbol.

level.

Each data partitioning and subsequent model training and evaluation is performed 100 times. This is done to ensure that we are not comparing the algorithms on a training/test set that turned out to be an exception rather than the norm. The models are evaluated using LOO-CV, hence all numbers reported are the generalization estimate.

3.1.3 Analyte classification

As mentioned in the introduction, the performance of three methods is assessed. Of particular interest is the performance of NMF compared to the two SotA methods in detection using QCM sensors, SVD and ANN. Before the results are displayed some notes on how model selection and model training were performed is given.

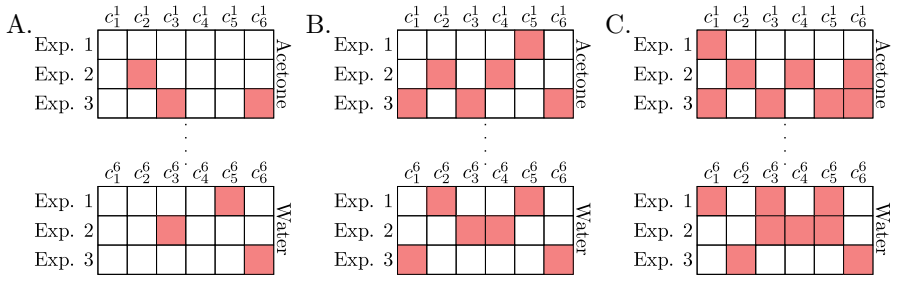

Figure 3.3: Illustration of three different data partitioning scenarios. Each square corresponds to a data point. The collection of blank squares constitute the test set and the collection of colored squares constitute the training set. The c_i^k denotes concentration level i for analyte k. Here acetone corresponds to $k = 1$ and water is $k = 6$. A. $N_{tr}^k = 3$. B. $N_{tr}^k = 6$. C. $N_{tr}^k = 8$.

Model training

The model parameters are in all cases selected based on cross validation. For SVD and NMF will use leave–one–out cross validation (LOO-CV). However, due to computational limitations, model selection for ANN classification is 6–fold cross validation. The each fold will contain one data point per analyte. The performance of the classifiers are evaluated based on the classification error rate, already defined in section 2.3.1, but stated for completeness

$$E_{err} = \frac{N_{err}}{N} \tag{3.1}$$

Training of NMF

NMF assumes that all values in $\mathbf{X}$ is non–negative so all negative values in the dataset are set to zero. Effectively it means pentanol will be classified without using the contribution from HDFD (see appendix B, figure B.3).

To reiterate classification using NMF, the data matrix $\mathbf{X}$ is factorized according to

$$\mathbf{X} \approx \mathbf{AS} \tag{3.2}$$

where $\mathbf{A} \in \mathbb{R}_{0+}^{D \times M}$ and $\mathbf{S} \in \mathbb{R}_{0+}^{M \times N}$. One subspace, $\mathbf{A}^k$, is found as a representation for each analyte. The subspaces are required to be of equal size. The size of the subspaces M is estimated by LOO-CV on the training set. Allowable

subspace size is in the interval $M \in \{2, \ldots, \min(N_{tr}^k - 1, 10)\}$. Note that M must be less than the amount of training points – so if $N_{tr}^k = 3$, the subspace size is automatically chosen to be $M = 2$.

Training of NMF consists of estimating $\mathbf{A}$ and $\mathbf{A}$. Each element of matrices $\mathbf{A}$ and $\mathbf{S}$ is initialized to a value drawn from a uniform distribution in the interval $]0; 1[$. The stopping criterion for the algorithm is either 30 iterations or 10^{-4} as relative error, whatever comes first.

Training of SVD

Classification using SVD is identical to the NMF classification method except for the matrix factorization. The matrix factorization is carried out using SVD instead and basis vectors are included based on their eigenvalues, always choosing the basis vector with the highest eigenvalue. As with NMF the model selection parameter is the subspace size M, which is found using LOO-CV, again constrained to the subspace size for each analyte being identical. For model selection the allowable subspace size is $M \in \{1, \ldots, \min(N_{tr}^k - 1, 7)\}$.

Training of ANN

The neural network has an input layer, a hidden layer and an output layer. The network has eight inputs – one per crystal, and six outputs – one per analyte. The number of hidden units in the network is found using 6-CV. The number of hidden units tested was two to six.

Prior to training the entire dataset is whitened (made zero mean and scaled to unit variance). The error function $E(\boldsymbol{w})$ has two hyper–parameters α and β.

$$E(\boldsymbol{w}) = E_D(\boldsymbol{w}, \beta) + \alpha E_W(\boldsymbol{w}) \tag{3.3}$$

where $E_D(\boldsymbol{w}, \beta)$ is the cross-entropy error function and $E_W(\boldsymbol{w})$ is a regularization term as explained in section 2.4.3. The hyperparameters are initialized to $\alpha = 8$ and $\beta = 0$ and the network weights are initialized using a zero mean Gaussian with variance equal to α. The stopping criterion for the network training is either 100 iterations or if the hyperparameters are updated with a margin lower that 10^{-5}. Each network training cycle is repeated 10 times and the network with the lowest training error $E_D(\boldsymbol{w}, \beta)$ is selected.

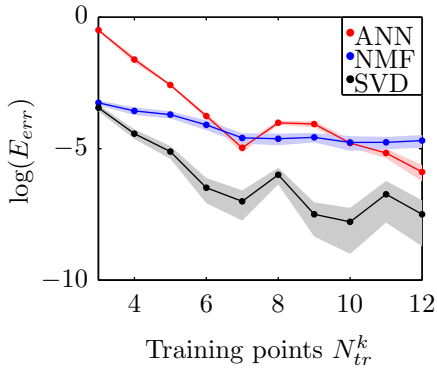

Figure 3.4: Learning curves for the classification algorithms on a test set. The shaded area is the standard error on the mean.

Results

Figure 3.4 shows learning curves for the three algorithms. The SVD classifier is the preferred method regardless of the amount of training points. The performance of SVD classification is superior to both ANN and NMF. Using only 3 training points per analyte we gain remarkable accuracy – only misclassifying 3% of the test points. ANN is quite poor initially but as the amount of training point increases ANN classification catches up. But clearly, given the almost linear responses of QCM sensors, a method such as ANN is hardly justified – at least for this data. A numerical representation of figure 3.4 can be found in appendix B, table B.1.

3.1.4 Concentration estimation

Concentration estimation is conducted using PCR, ANN and GPR. Linear regression could have been, but since we mostly have under-determined systems it would overfit. Instead PCR is included as this is the most typical approach to handle overfitting in QCM sensing. Of special interest is the performance of GPR since no previous work has been done in QCM sensing with this method.

Model training

The model parameters for ANN and PCR are selected based on cross validation. For GPR three different covariance functions are tested. One could argue that

the choice of covariance function is a model parameter, however, we take the view that it's a separate model type. Using this notion, there are no model parameters in GPR.

When performing concentration estimation, only points measured on the same analyte are used. The performance measure used is the mean relative absolute error, already defined in section 2.3.1, but stated for completeness

$$\text{MRAE} = \frac{1}{N_{tr}^k} \sum_{i=1}^{N_{tr}^k} \left| \frac{y_i - \hat{y}_i}{y_i} \right| \tag{3.4}$$

where y_i is the true concentration, $\hat{y}_i$ is the predicted concentration.

Training of PCR

The parameters to be chosen when using principal component regression are which principal components to include in the regression. We include principal components in the model ordered by their variance choosing the highest variance component. The number of allowable components is $M \in \{1, \ldots, \min(N_{tr}^k, 8)\}$.

Training of ANN

Training of neural networks for regression uses the same configuration as for classification. For each analyte, one neural network containing one output neuron is trained, where the output neuron is the concentration level estimate. Alternatively, one could have trained one network with one output neuron per analyte, however, comparing ANN with the other models becomes unjust as the models are no longer trained on the same data. This is the only reason for the choice of one ANN per analyte.

Training of GPR

A Gaussian process is completely specified by its mean function and covariance function, therefore these are the two functions that must be defined when using GPR. A zero mean Gaussian is used, hence to make this prior plausible the empirical mean is subtracted from the data. The empirical mean and empirical variance are calculated using the training set alone and as such the test data is not guaranteed to have either zero mean or unit variance.

Three different covariance functions are used, all based on the squared exponential covariance function

$$k(\mathbf{x}, \mathbf{x}') = \sigma_f^2 \exp\left(-\frac{1}{2}(\mathbf{x} - \mathbf{x}')^\top \mathbf{M}(\mathbf{x} - \mathbf{x}')\right) + \sigma_n^2 \delta_{pq} \tag{3.5}$$

where σ_f^2, σ_n^2 and $\mathbf{M}$ are the *hyper–parameters*. Choosing $\mathbf{M}_{iso} = \ell^{-2}\boldsymbol{I}$ yields the isotropic squared exponential function where ℓ is the length–scale. Choosing $\mathbf{M}_{ard} = \text{diag}(\boldsymbol{\ell})^{-2}\boldsymbol{I}$ yields automatic relevance determination. The two approaches are combined by adding the covariance functions together thus creating the third covariance function. The hyperparameters are found using the marginal likelihood approach as discussed by [Rasmussen and Williams, 2006a]. During optimization up to 1000 function evaluations are allowed. The initial values for hyper–parameters are drawn from a zero–mean Gaussian distribution with unit variance. In order to avoid bad local minima, 10 optimizations are run, and then the hyperparameters that yield the best marginal likelihood are chosen.

Results

Learning curves for concentration level estimation are shown in figure 3.5. ANN is generally worst, probably because there are too few training points to train an adequate neural network solution, or because it is too hard to find a good solution, just as was the case for classification. For a small amount of points, $N_{tr}^k = 3$, the best regressor is PCR. Only for benzodioxol concentration estimation is PCR surpassed, where the GP ARD+ISO combination is the best. At $N_{tr}^k = 4$, GPR generally performs similar to PCR and for $N_{tr}^k \geq 5$ GPR is either the superior method or on par for all choices of analyte. At $N_{train} = 12$ the GPR method offers superior accuracy. There is no significant indication of which of the three covariance functions is the best although the combined covariance function seems slightly better.

3.2 Related work

QCM sensors have been applied in many different scenarios, and also been studied using supervised learning, both to identify analytes and to conduct density/concentration level estimation.

Among the most used classification schemes are principal component analysis, hierarchical cluster analysis (HCL) and artificial neural networks. Both PCA

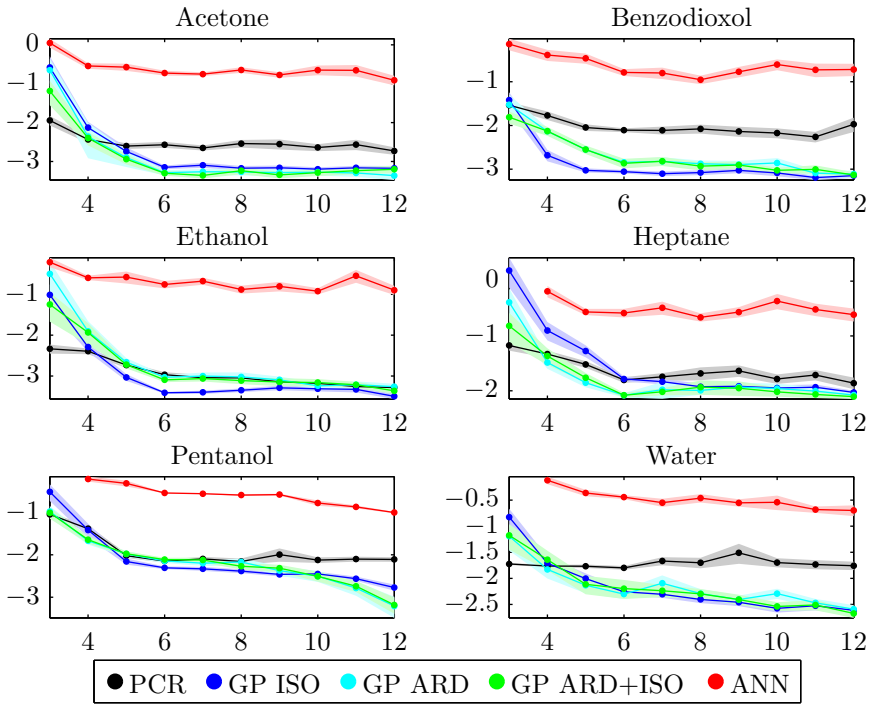

Figure 3.5: Learning curves for the regression algorithms. On the x-axis is the number of training points per analyte, N_{tr}^k. On the y-axis is the log of the mean relative absolute error log(MRAE). The shaded area is 2 times the standard error on the mean. The standard error is multiplied to enhance visibility.

and HCA have been commonly applied to visualize QCM data and to argue that a classifier could easily be built [Lu et al., 2009, Rosengren et al., 2009, Si et al., 2007, Ying et al., 2008, Sepcic et al., 2004]. ANN has been applied as well, recently by Gulbag et al., where an approach using probabilistic neural networks coupled with radial basis functions is applied [Gulbag et al., 2008].

For concentration level estimation, partial least squares (PLS) has been used on QCM sensors with success by Si et al. [Si et al., 2007] to estimate the concentration level of ethanol and toluene. Wang and Shih [Wang and Shih, 2006] used multivariate linear regression to compute the concentrations of methanol and carbon disulfide. Artificial neural networks have been applied as density estimators in a vast range of applications. Saraoglu and Kocan used ANN to estimate the blood glucose value by breath from patients [Saraoglu and Kocan, 2010]. Mumyakmaz et al. applied a model based on two networks where one ANN classifies analytes and the other ANN quantifies the concentration

ratios [Mumyakmaz et al., 2008]. The quantifying ANN handles three different analytes (acetone, chloroform and methanol) simultaneously by having one output neuron per analyte. Ozmen et al. applied ANN to estimate concentration levels in mixtures of analytes. They conducted experiments of three analytes (acetone, ethanol and trichloroethylene) but in their mixtures consisted of two analytes at various concentration levels [Özmen et al., 2006].

3.3 Summary

A two–tiered data analysis framework has successfully classified responses from an eight–dimensional polymer coated QCM sensor. By using linear methods such as SVD and NMF, remarkable high accuracy ($> 96\%$) is obtained, even with as low as 3 training points per analyte. Having one training point per analyte per concentration level ($N_{tr}^k = 6$, SVD has a classification accuracy of 99.8%. NMF does not perform to the level of SVD, but for a limited amount of training points NMF is still better than ANN. This study clearly shows that one should think twice before applying ANN to QCM sensors. The theory behind QCM states that the responses should be linear, and as such there is little reason to introduce a highly non-linear method such as ANN. Furthermore, ANN are notoriously hard to train and requires a lot of computational effort, especially compared to SVD which can be computed in seconds on modern computers.

For concentration level estimation, the Gaussian process regression quickly became better than the linear method, and both methods are significantly better than ANN. The issue with ANN regression being most likely that it is too hard to identify the proper solution.

The best case scenario for GPR is a mean relative error of 3%. However the GPR method does have difficulties when having just three training points per analyte. Likely this is due to the zero mean Gaussian prior and the way data partitioning is performed. For training sets where the lowest and/or highest concentration levels are omitted the GPR will perform poorly. In general the GPR will predict zero concentrations outside the training interval. The performance outside the training interval could probably be improved by adding a growing term to the prior or using a thin–plate spline kernel as covariance function [Wahba, 1990].

Arguably the GPR performs close to the level of an ideal concentration level estimator. The expected error of an ideal estimator is related to the variance of the measurement points [Bishop, 2006]. As the PCA plots show, there is notable variance between measurements of the same concentration level, so it is not possible to create an estimator with zero estimation error.

To sum up, one should use GPR to perform concentration level estimation for QCM instead of PCR or ANN. If there are issues with too many data points, sparse approaches exist [Smola and Bartlett, 2000].

Chapter 4

Colorimetric sensors

A colorimetric sensor array is an ensemble of chemoselective[13] compounds, typically called dyes that will undergo a color change when exposed to molecules in air or a target substance (analyte). Each dye can also be considered as a single sensor so we will also refer to a dye as a "sensor". Hence, a colorimetric sensor array is in essence a multisensor approach where each sensor is based on the same technology.

Measuring with a colorimetric sensor array is considered to be a two-step procedure. Prior exposure to an analyte, each dye is digitally recorded typically using a flatbed scanner or a digital camera. The sensor array is then exposed to the target and the colors are recorded again. Figure 4.1 shows an example of a colorimetric sensor array where RDX have been measured. Each dye is realized as a dot on the material that makes up the sensor array.

This chapter gives an overview of the advances made in the signal processing of colorimetric sensor array. The results presented are largely based on results from the papers in appendix C, D, E and F. Section 4.1 describes how the colorimetric sensor arrays are digitalized and how the dyes are located on the sensor array. The positioning of the dyes is an issue that must be handled due to two factors; First, the arrays are manufactored and digitalized by hand so

[13] Chemoselectivity is when a compound have a preferential reaction over a set of other possible reactions.

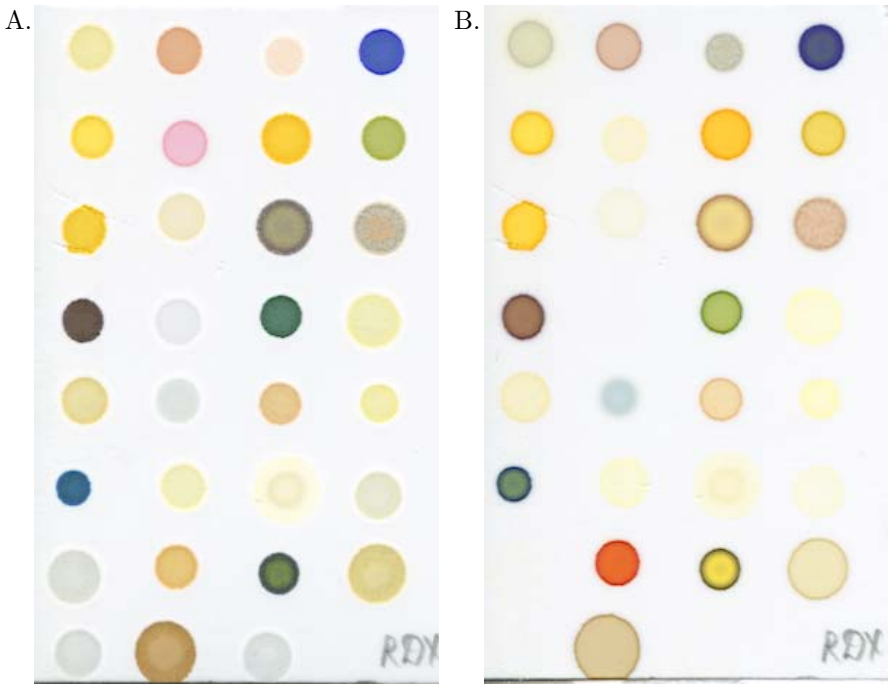

Figure 4.1: Example of a colorimetric sensor array. A. The sensor array before exposed to the target analyte. B. The sensor array exposed to RDX at 100℃. Some sensors change color, some evaporate and finally some remains unchanged.

the exact dye localization changes from array to array. Secondly, some analytes may change the size and geometry of a dye.

In section 4.2 the sensor arrays that have been utilized is described as well as the analytes that was measured.

Section 4.3 gives an overview of the traditional methods of visualizing colorimetric data. The traditional approaches like utilization of difference images have some weaknesses that are often ignored, such as the lack of uniqueness and the inability to visualize repeated measurements in a condensed manner. An alternative visualization technique based on the *cummulative density function* that copes with these weaknesses is introduced. However, the introduced visualization method have other weaknesses, so the technique should be used as complementary to existing techniques.

The next section, section 4.4 handles the presented datasets and give some

results on the sensor accuracies. Traditional feature extraction techniques are employed and we argue that these can be improved. Further, we show the sparse logistic regression model works well in analyzing sensor performance. The method is benchmarked against k-nearest-neighbor classification which is the de-facto standard classier for colorimetric sensor arrays.

In section 4.5 a traditional statistic analysis is performed and is used to improve the colorimetric sensor accuracy. Traditionally, the color change of the sensors is used as the sensor response, but in this section we show that the original color also have an effect on the sensor response.

Finally, in section 4.6 new dye color representation techniques are introduced. These techniques are based on distance measures between the sensor responses and as such they do not fit well into the traditional classifiers that assumes a vector-space representation. To handle this issue while also performing sensor selection, we introduce a forward selection paradigm based on Gaussian process classification.

4.1 Preproccesing of images

Before the colorimetric sensor array are analyzed using computers the sensor response digitalized using an ordinary flatbed scanner (Epson V750-M Pro Perfection scanner). The images are captured immediately[14] after immobilization of dyes and after exposure of analytes. Pictures were obtained at 600 DPI in a lossless format using the red-green-blue (RGB) color scheme with 8 bits per color. An image captured in the RGB color scheme produces a matrix for each of the RGB color channels. Formally the image is written as $\mathbf{I}^k_{(i,j)}$ which corresponds to the value of pixels at row i, column j for color channel k where $k = \{1, 2, 3\}$. The range for i and j varies from image to image as the images are captured by manual labor.

4.1.1 Dye localization

After digitalization the next step is to locate the dyes. All the sensor arrays are fabricated by hand and therefore the exact dye location varies. The algorithm for locating dyes have changed during the research project and different

[14] Due to the manual fabrication process, the dyes that where spotted in the initial part of the process was exposed to the surrounding environment for up to 15 minutes whereas the dyes that were spotted in the latter part was only contaminated for a few seconds.

algorithms have been used in different papers [Alstrøm and Larsen, 2011]. The algorithms has largely been inspired by the approach used in DNA micro-array spot localization explained by [Bemis, 2004]. In this section, the most recent version of the algorithm will be described. This algorithm is based purely on the images before exposure to target analyte. This is because exposing the sensor array to certain analytes will cause the dyes to completely vanish (to the perception of the scanner). Figure 4.1 show examples of dyes that completely vanish when exposed to target analyte. The gray dyes in the lower left corner has become the same color as the background.

Initially the sensor array before exposure, denoted $\mathbf{I}_{\text{bef}}$ is smoothed using a symmetric Gaussian filter. Each weight in Gaussian filter is calculated as

$$h_g(n_1, n_2, \sigma) = \exp\left(-\frac{n_1^2 + n_2^2}{2\sigma^2}\right) \tag{4.1}$$

where the parameters have been chosen as n_1 and n_2 is in the set $\{-2, -1, 0, 1, 2\}$ and $\sigma = 3$. The width and standard deviation has been experimentally chosen with the aim to of remove undesired artifacts from the sensors while at the same time maintaining the size of the dot and keeping the primary color unaffected. The filter is normalized such that the filter sums to one:

$$h(n_1, n_2, \sigma) = \frac{h_g(n_1, n_2, \sigma)}{\sum_{n_1, n_2} h_g(n_1, n_2, \sigma)} \tag{4.2}$$

A circular averaging filter has also been considered and was used in earlier versions of the algorithm. This filter has a similar structure as a Gaussian filter in the sense that it computes an weighted average over an area with larger weights in the center. Realizations of the filters are shown on figure 4.2.

The filter is linearly applied to $\mathbf{I}_{\text{bef}}$ where the corresponding filtered image is denoted as $\tilde{\mathbf{I}}$. An example of the noise reduction properties of the filters is found in figure 4.3. The artifact in the lower left corner of figure 4.3A is particularly troublesome when identifying dots, so it's exactly defects like this we seek to remove. While the circular averaging filter almost manages to completely remove the artifact the Gaussian filter is superior in this regard.

The next step of the algorithm is to separate colors from dyes from the background color. To do this we assume that the majority of the image consists of clean silica gel. Figure 4.4 shows the histograms of the image displayed in figure 4.1A where it is clearly seen that the majority of pixel values are light gray. Having this assumption in mind, the background is removed by first

A.

0.032	0.038	0.040	0.038	0.032
0.038	0.044	0.047	0.044	0.038
0.040	0.047	0.050	0.047	0.040
0.038	0.044	0.047	0.044	0.038
0.032	0.038	0.040	0.038	0.032

B.

0.000	0.017	0.038	0.017	0.000
0.017	0.078	0.080	0.078	0.017
0.038	0.080	0.080	0.080	0.038
0.017	0.078	0.080	0.078	0.017
0.000	0.017	0.038	0.017	0.000

Figure 4.2: A. Gaussian filter will smooth pixels more drastically which in turn will smear out defects that consist of only a few pixels. B. Circular averaging filter that was used in earlier version of the algorithm.

finding the most frequent pixel value for each color channel excluding zeros[15]

$$b_k = \arg\max_{x \neq 0} \left| \left\{ n \mid \tilde{\mathbf{I}}^k_{(i,j)} = x \right\} \right| \qquad \forall i, j \tag{4.3}$$

where $\{\mathbf{b} \in \mathbb{Z}^3 \mid b_k > 0 \wedge b_k < 256\}$. A new matrix is now calculated by subtracting $\mathbf{b}$ from each pixel of the image

$$\mathbf{B}_{(i,j)} = \left\| \mathbf{b} - \widetilde{\mathbf{I}}_{(i,j)} \right\|_2^2 \qquad \forall i, j \tag{4.4}$$

The matrix $\mathbf{B}$ can be visualized as a gray scaled image by coloring elements equal to zero as black and then gradually coloring increasing values increasingly white. Based on the matrix $\mathbf{B}$ a new black–white image is constructed and stored in the matrix $\widetilde{\mathbf{B}}$ such that $\{\widetilde{\mathbf{B}} \in \mathbb{R}^{m \times n} \ : \ \mathbf{B}_{(i,j)} = \mathbf{B}^2_{(i,j)}\}$. The matrix $\widetilde{\mathbf{B}}$ is constructed by choosing the pth quantile as a threshold (initially set to 0.80) for when a value should be set to one. All values below the threshold is set to zero and all values above the threshold is set to one. The matrix is a binary mask for pixels that is considered as a potential dye location. Finally, since the dyes are realized as circular dots all holes are filled. The process is illustrated in figure 4.5.

The next step is to identify possible locations to search for the circular dots that makes up a dye. The mean value of the binary image matrix is calculated for

[15] Zeros may exist in the image due to a rare need to manually rotate the image before the algorithm processes the image. Some of the captured images had the sensor placed askew inside the scanner.

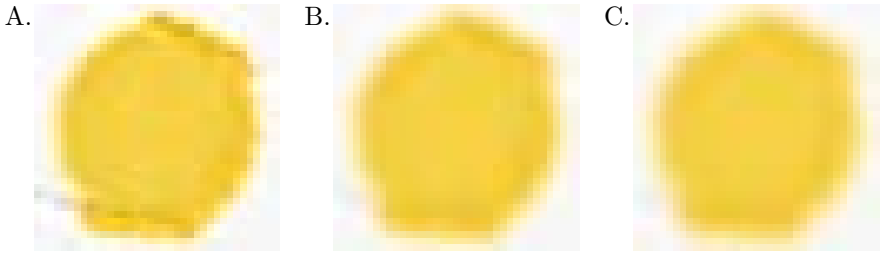

Figure 4.3: A. Raw image of a dot taken from figure 4.1A. B. The dot is smoothed using the circular averaging filter. Some remains of the artifacts in the lower left corner remains. C. The dot is smoothed using the Gaussian filter. The artifacts has almost been completely removed.

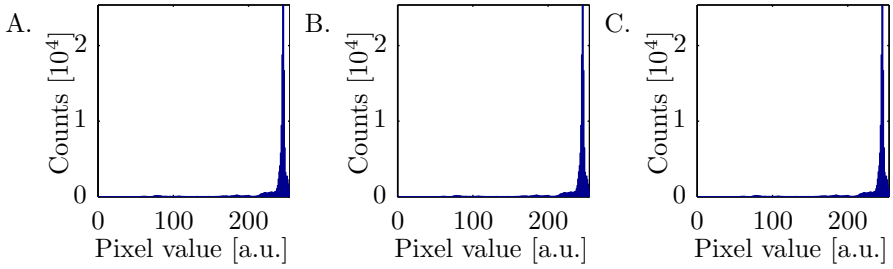

Figure 4.4: A. Histogram of red channel. B. Histogram of green channel. C. Histogram of blue channel.

each row and column producing two vectors $\mathbf{m}_{row}$ and $\mathbf{m}_{column}$

$$m_{row,i} = \frac{1}{n} \sum_{j} \widetilde{\mathbf{B}}_{(i,j)} \qquad \forall i \tag{4.5}$$

$$m_{column,j} = \frac{1}{m} \sum_{i} \widetilde{\mathbf{B}}_{(i,j)} \qquad \forall j \tag{4.6}$$

If these vectors are considered as a graph, the graph will have peaks in the areas where there is much mass of ones (i.e. potential dye pixels). Before identifying peaks the the vectors are smoothed using a 3rd order Savitzky–Golay [Savitzky and Golay, 1964]. The process is illustrated in figure 4.6.

The algorithm requires some manual tuning. The user is required to define the number of dyes that must be localized. Looking and the lower right corner of the images in figure 4.5 there are some remnants of the letters “RDX” that is

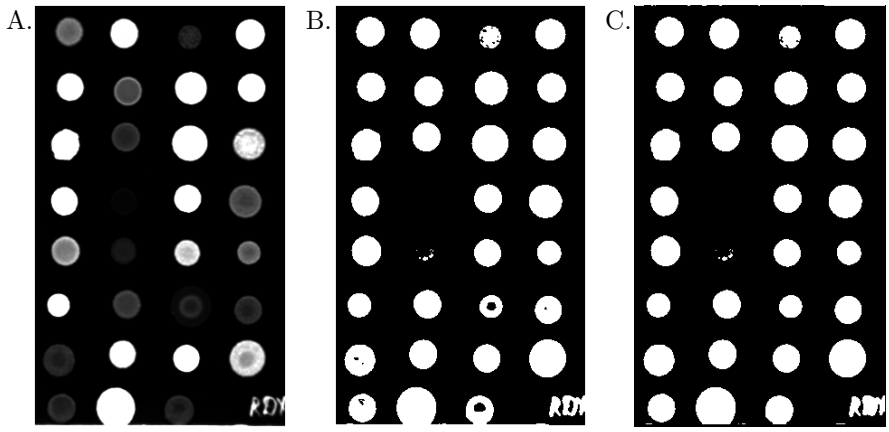

Figure 4.5: A. The enhanced gray scaled image that created based on the background matrix **B** calculated for the measurement displayed on figure 4.1. B. The corresponding black-white image when using the 0.8 quantile. C. The black-white when holes has been filled.

marked as potential dye. The labeling is always made in the lower right corner, so the algorithm starts searching from the upper left corner and then searches row-wise. But once the algorithm has found the prescribed number of dyes the search is terminated. The user is then asked to confirm the dye locations. If the dye locations were not correct, the algorithm restarts lowering the threshold with 0.01 and then the process is repeated.

The user can also manually mark areas with zeros such that these areas will not be searched. This is required for sensor arrays that e.g. have defects on the surface as these defects often have colors different that the background. There exist a number of features of more pragmatic nature which make the dye localization process smoother for the investigator. These are described in a MATLAB toolkit of the dye localization algorithm, found in the published toolkit for colorimetric sensor arrays listed on page xi.

4.1.2 Aligning images

Dye localization on the image after exposure to analyte is carried out differently. This is mainly due to the fact that some dyes completely vanish. Instead, the image pairs that comprise a measurement are aligned. The image $\mathbf{I}_{\text{bef}}$ is used as a reference image and then the image captured of the sensor after exposure,

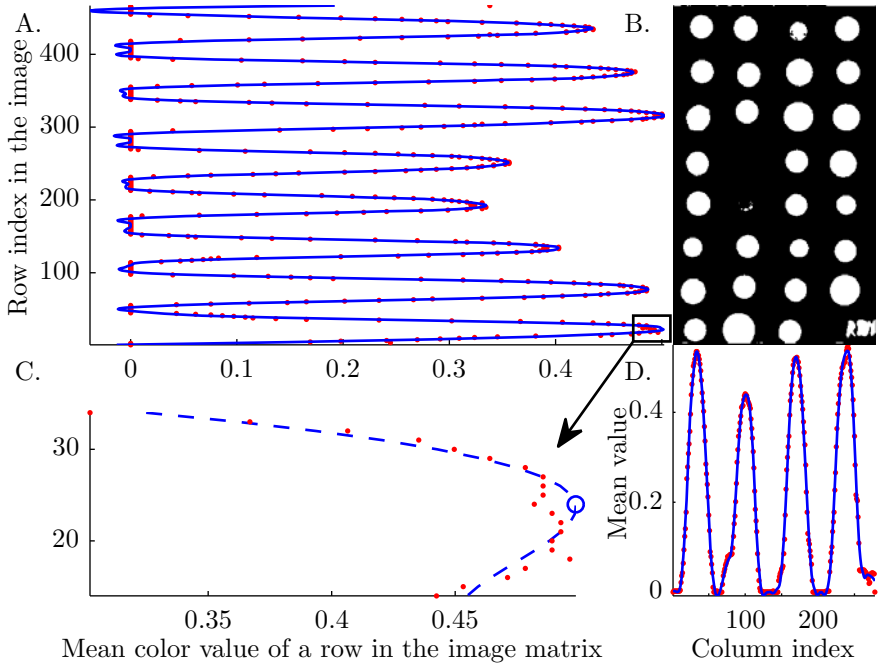

Figure 4.6: Example of how the potential search areas are located. A. Visualization of the row-wide average. B. The binary image. C. Illustration of the smoothing effect of the Savitzky–Golay filter D. Visualization of the column-wide average.

denoted $\mathbf{I}_{\text{aft}}$ is translated and rotated to align with the reference image. The aligning of images are considered as an optimization problem formally put on the form

$$\min_{\boldsymbol{t},\theta} \|\mathbf{I}_{\text{bef}} - g(\mathbf{I}_{\text{aft}}, \boldsymbol{t}, \theta)\|_1/(mn) \tag{4.7}$$

where $\mathbf{t}$ is an (x, y) translation, θ is a rotation and $g(\cdot)$ is the function that implements the transformation: first rotating the images using nearest neighbor interpolation, then translating (x, y)–pixels according to $\boldsymbol{t}$. The parameters $(\boldsymbol{t}, \theta)$ are initialized to zero.

The value of the expression that is minimized can be interpreted as the amount of *color* per pixel where a fully black pixel is fixed at a value of zero. At perfect image alignment, all the background pixels will be black[16] and all dye pixels

[16] Of course this statement is subject to scanner precision and that no defects have occurred

will have the weakest possible color, hence, blackness per pixel should be maximized. The optimization problem is solved using a UCMINF implementation by [Nielsen, 2001], which can be found in a public available toolbox [Nielsen, 2010].

Once the optimization problem has been solved a difference matrix is calculated

$$\mathbf{I}_{\text{dif}} = \mathbf{I}_{\text{bef}} - g(\mathbf{I}_{\text{aft}}, \hat{\boldsymbol{t}}, \hat{\theta}) \tag{4.8}$$

The values in $\mathbf{I}_{\text{dif}}$ can be both positive and negative, so the difference matrix does not represent a real image. On figure 4.8 a subset of the difference matrix is visualized. By taking the absolute value of all the elements in $\mathbf{I}_{\text{dif}}$, visualization is possible as all values now fall into the range of RGB images.

4.1.3 Feature extraction

The final step of colorimetric preprocessing before the data is suitable to machine learning methods is feature extraction. As mentioned in chapter 1, one of the major research topics covered in this thesis is the pursuit of optimal feature extraction/dye representation for colorimetric sensors. In this section, the most typical single feature approach is covered as well as other single feature approaches. A single feature approach is a feature extraction method that reduces the sensor response to a single number, i.e. the mean statistic.

The typical feature extraction methodology of colorimetric sensor arrays consists of extracting the mean color change of each dye for each color channel (RGB). A digitalized dye consist of up to several hundred pixels, therefore summarizing a color change with just one color is quite convenient. However, in order for the mean to be a robust and informative measure of color change, the pixels of a dye have to be normally distributed (or at least have a symmetric distribution with one mode). One of the more extreme examples of a response from a colorimetric sensor is visualized in figure 4.7. The dye color distribution is a bimodal distribution and the color that is calculated as the mean color is rarely found in the color distribution. Clearly, in this case the mean color fails to capture the essential properties of the sensor response.

Other possible single feature approaches could be to use either the median or mode. Just as the case with the mean, the median requires a symmetric distribution with one mode. On the other hand the mode does not require the distribution to be symmetric and could potentially be more robust. However, all

to the background while exposing the sensor array to the target analyte. For the measurement setup used this assumption turned out to be reasonable.

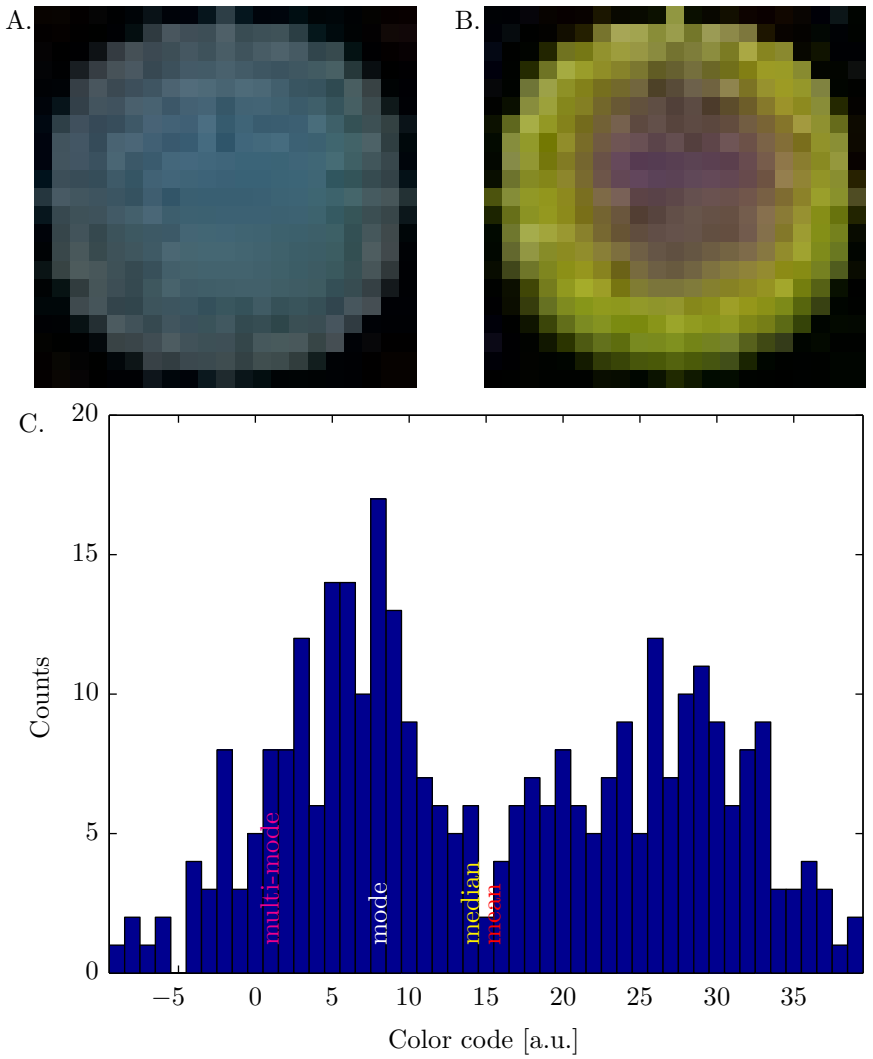

Figure 4.7: An example of a specific dye of colorimetric sensor array exposed to the explosive analyte HMX. A. The sensor before exposure. B: The enhanced (more light is added) difference image. C: Histogram of the difference color of the blue channel.

the aforementioned statistics have the weakness that they consider each channel in the RGB color scheme as independent of each other. A multi-mode statistic

Figure 4.8: Illustration of the coffee stain effect. The images are a magnification of dot 27 from figure 4.1. A. Control image. B. Exposed image. C. Difference image.

does not have this weakness and will find the most occurring color in the dye. These four feature extraction methods will be compared in section 4.4.

There is an additional significant concern that can affect the accuracy of the feature extraction. This is the *coffee stain effect* which is a consequence of the drying of the dye. During spotting[17] the dye is liquid and once the dye is onto the silica gel the dye begin to dry, leaving a dark rim as illustrated on figure 4.8. The color of the outer rim is unreliable as the effect is not reliably reproducible. To accommodate for the coffee stain effect, a smaller area of a dye is used for feature extraction, corresponding to 2/3 of the dye radius, the figure that is traditionally used (see appendix E).

4.2 Datasets

The sensor arrays have been employed on a wide range of compounds. These compounds can basically be divided into five different categories; 2) Target: the target substances which in this chapter is either explosives or drugs. 2) Control: a blank measurement that is used to make sure the sensor did measure "something" (e.g. room temperature on the table). 3) Real world disturber: substances which are commonly found in real world scenarios that may disturb and possible ruin measurements (e.g. aldehydes). 4) Precursor: compound that is used to manufacture target chemical and may also be a part of the target chemical (e.g. ammonium nitrate). 5) Positive false alarm: A compound that is part of the target chemical but also widely used elsewhere (e.g. acetone). It can also be a compound that is known to have affinity with some of the sensors

[17] The process of spotting the dyes onto the silica gel.

Category	N^k	Treatment	N^k
Acid	32	Acetic acid (AA)	10
		Formic acid (FA)	11
		Hydrogen chloride (HCl)	11
Alcohol	20	Ethanol (EtOH)	7
		Methanol (MeOH)	6
		Propanol (PrOH)	7
Aldehyde	12	Nonanal (NA)	6
		Octonal (OA)	6
Arene	10	Toluene (Tol)	10
Environment	12	100℃	6
		Room temperature (RT)	6
Explosive	20	Dinitrotoluene (DNT)	16
		Trinitrotoluene (TNT)	4
Ketone	7	Acetone (Ac)	7
Salt	16	Potassium chloride (KCl)	5
		Ammonium chloride (NH4Cl)	6
		Sodium chloride (NaCL)	5

Table 4.1: The first proof-of-concept dataset collected, named dataset "A". It consists of $N = 129$ measurements in total. The numbers specified by N^k are the number of measurements made per class, depending on the class label being the category or the treatment.

in the array.

Three datasets have been collected with three different sensor arrays. The first sensor array utilized comprised 15 sensors [Kostesha et al., 2010]. The sensor array was employed on 15 different analytes that was divided into 7 class labels based on chemical families. The dataset also contains control measurements conducted at both room temperature and 100℃. This is required as the explosives are heated to 100℃ when measuring,[18] whereas analytes belonging to the other chemical families are measured at room temperature. The dataset is detailed in table 4.1. A detailed explanation follows: most of the chemistry on the sensor array was known to be sensitive to acids hence acids are included as

[18]The explosives have low vapor pressure so at room temperature there is almost no vapor present. The explosives are then heated in order to decrease the time required to perform measurements.

Category	N^k	Treatment	N^k
Drug	6	Isosafrole (IA)	2
		Lysergic acid diethylamide (LSD)	2
		Phenylacetone (PhA)	2
Environment	8	100℃	4
		Room temperature (RT)	4
Explosive	8	Dinitrotoluene (DNT)	2
		Octogen (HMX)	2
		Cyclotrimethylenetrinitramine (RDX)	2
		Triacetone Triperoxide (TATP)	2

Table 4.2: The second dataset collected, named dataset "B" consists of $N = 22$ measurements in total. The numbers specified by N^k are the number of measurements made per class, depending on the class label being the category or the treatment.

possible false alarm [Nielsen, 2012]. The alcohols are also possible false alarm since alcohols are commonly used as solvents when manufacturing explosives. The aldehydes included are real world disturber as aldehydes are secrete from commonly found bugs. Arenes, and in particular Toluene is used to produce TNT and is included as a precursor. Acetone is a widely used solvent that is a possible disturber. The salts included are chosen based on two different conditions; KCl and NH4CL are present in air in maritime climate (e.g. Denmark) as these evaporate from the ocean. And finally, NaCl is widely found but can also be used to produce explosives.

The second dataset collected was measured using the same sensors as in the previous sensor array with one added sensor [Kostesha et al., 2011]. The scope here was to measure illicit drugs and other types of explosives. The chemicals categorized as drugs were: Isosafrole, a precursor for an array of drugs such as Ecstacy and Metamphetamine; LSD, a commonly known hallucination drug; Phenylacetone, a precursor for an array of drugs such as Ampethamine and Metamphetamine. The drugs have sufficiently high vapor pressure to be measured at room temperature. The new explosives included were HMX, RDX and TATP, which have already been described in chapter 1. These explosive are measured at 100℃.

The final dataset consists of 31 sensors, 16 old and 15 new. The dataset is collected using a randomized complete block design (RCBD) which is detailed in appendix F, page 222. The list of analytes and measurements are shown

Category	N^k	Treatment	N^k
Acid	45	Acetic acid (AA)	15
		Formic acid (FA)	15
		Hydrogen chloride (HCl)	15
Alcohol	27	Ethanol (EtOH)	13
		Methanol (MeOH)	14
Amine	42	Ethylendiamine (EDA)	14
		Propylamine (PA)	14
		Triethanolamine (TEA)	14
Arene	14	Toluene (Tol)	14
Environment	28	100℃	14
		Room temperature (RT)	14
Explosive	56	Dinitrotoluene (DNT)	14
		Octogen (HMX)	14
		Cyclotrimethylenetrinitramine (RDX)	14
		Triacetone Triperoxide (TATP)	14
Ketone	13	Acetone (Ac)	13
Salt	14	Potassium nitrate (KNO3)	14
Thiol	14	Mercaptoethanol (ME)	14

Table 4.3: The last dataset collected, named dataset "C". It consists of $N = 253$ measurements in total. The numbers specified by N^k are the number of measurements made per class, depending on the class label being the category or the treatment.

in table 4.3. Amines were included in this dataset as they are also widely used solvents. The salt included are the kind that can be used to produce homemade explosives, but is also widely used in fertilizers. The sulfur analogue of alcohols, thiols are used to measure food freshness and was mostly included in the experiment in order to investigate new areas of application, but thiols can also be considered common real-world disturbers.

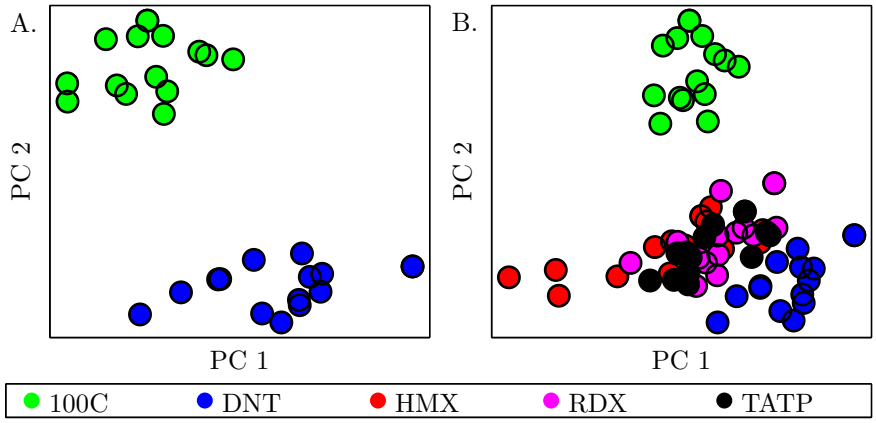

Figure 4.9: Visualization using principal component analysis of the data presented in section 4.5. A. PCA using 100℃ and DNT. B. More explosives added to the plot; HMX, RDX and TATP. Note, PC 1 and PC 2 changes as new data are added.

4.3 Visualization of colorimetric data

Data from colorimetric sensors is often visualized using principal component analysis. If the sensor signal is strong as is often the case with colorimetric sensor array experiments, PCA will successfully display class dispersion. Visualization examples are shown in figure 4.9. Here the data is nicely visualized in the case of two classes, however when three more explosives are added, the class dispersion lessens and it is no longer clear to what extend the sensor is able to distinguish between classes. Furthermore, added new data will change the principal component which will also change the plots in figure 4.9. So, one disadvantage of plots made using PCA is that adding new points will change the plot as whole.

Another major trend in colorimetric sensing is visualization using *difference maps* (or analogously, difference images). A difference map is calculated as follows; 1) extract the mean color difference for each sensor array, 2) for each analyte, calculate the mean response, 3) convert the mean values to integers by rounding off, then take the absolute value 4) enhance the final results by linearly expanding a predefined color range to span the entire RGB range. Figure 4.10 shows two difference maps calculated using the prescribed procedure. The procedure can be modified in a number of ways e.g. by using another statistic than the mean or by taking the absolute values of $\mathbf{I}_{\text{dif}}$ and displaying the result as an RGB image.

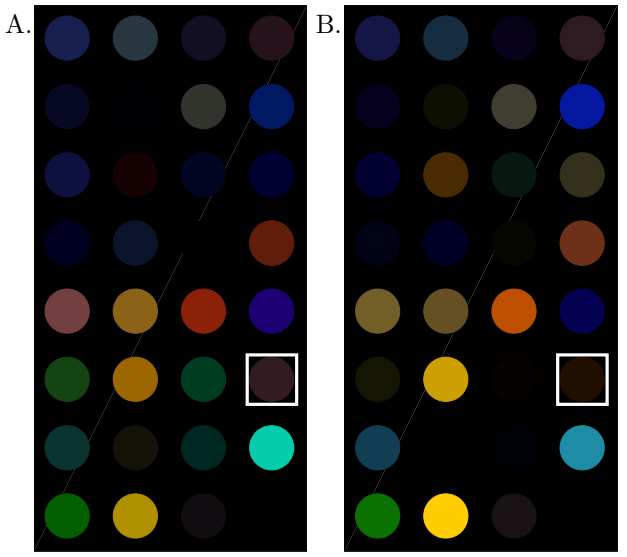

Figure 4.10: Difference maps based on the data presented in section 4.5. Dye #24 is highlighted - this is a very good detector of DNT although it is not easily shown using difference maps. A. Mean difference map of 100℃. B. Mean difference map of DNT.

The above procedure has some clear disadvantages; due the the need of taking absolute values, the corresponding difference map is not unique, i.e. for a given color channel the color change can be in both a negative or positive direction on the RGB color scale, which is two different colors on the exposed image. But in the difference map the color will be the same. Further, a difference map is arbitrary due to the color expanding. So why is difference maps so heavily used? Most likely due to difference maps being easy to interpret but also because the response is visualized in the same domain as the original sensor.

An alternative visualization that complement the difference map well is plot of the empirical cumulative density function (CDF) as shown on figure 4.11. The plot is the empirical CDF function plotted using colors. The CDF plot shows clear and significant differences in the response, even though it may be hard to spot these color differences in the difference map. For dye 24 – red, the situation described earlier is occurring, the control measurement changes color in one direction whereas the explosives change color in another direction. On the CDF plot (figure 4.11), a clear signal separation is visualized whereas on the difference map (figure 4.10) only a vague signal separation is displayed.

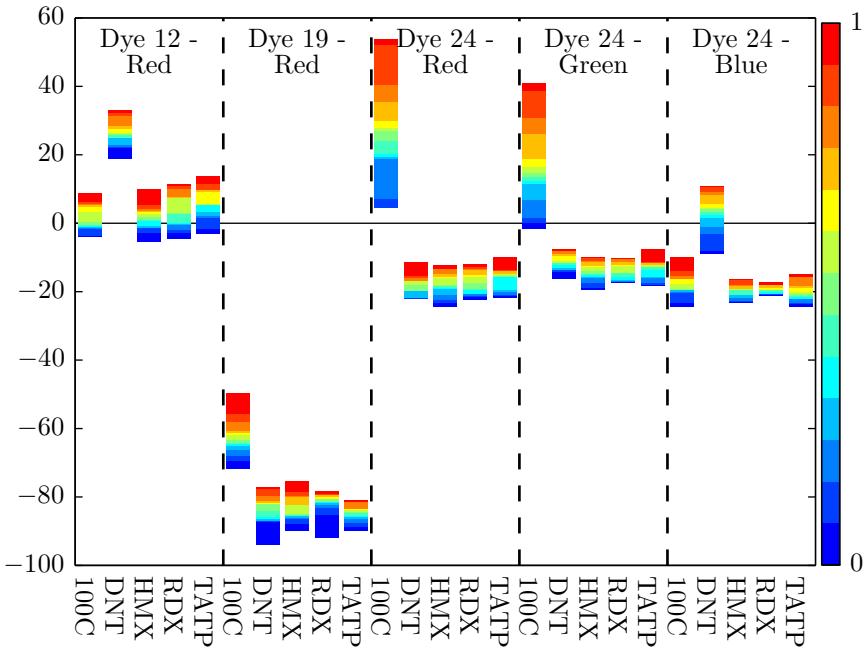

Figure 4.11: CDF plot of selected dyes using the data presented in section 4.5. Dye 12 is a very good DNT detector. Dye 12 is discriminative for DNT whereas dye 19 and 24 are not discriminative for DNT but for explosives in general.

Another advantage of CDF is the ability to visualize signal spread and even raw measurements. If the resolution of the CDF function is chosen to be the same as the number of measurements, the color changes will happen where the measurement are located. The notable disadvantage of CDF plots are that they are harder to interpret and understand for untrained users. Further, displaying the entire dataset will clutter the plot and often a few selected dyes/color combinations must be chosen. However these dyes can easily be identified using e.g. a statistical test such as the Mann–Whitney–Wilcoxon test [Wilcoxon, 1945, Mann and Whitney, 1947]. The dyes presentation here are found using exactly this method, see appendix F for further details.

4.4 Detection using single value statistics on difference colors

In section 4.1.3 the traditional feature extracting for colorimetric sensors was explained. In this section we investigate how well the single value statistics perform. The goal is the establish if one statistic is universally better than the other. It could be that the best statistic depends on both the dataset and the classifier employed. To mitigate this effect the the feature extraction methods are investigated on three different datasets using four different classifiers. The goal is to identify if one of the single feature extraction methods are optimal. The optimal feature extracting method could easily depend on both the classifier and the dataset. By using multiple datasets and multiple classifiers we are in position to make more generic conclusions.

The classifiers used to evaluate the features are: 1–nearest-neighbor (1-NN), k–nearest-neighbor (k–NN), sparse logistic regression (SLR) and artificial neural networks (ANN). The reason for choosing these classifiers are as follows; 1–NN and k–NN are basically the de-facto method when analyzing colorimetric sensor responses (see section 4.7), and these are included to establish a baseline performance. The reason for choosing SLR, is because this is the "simplest" of classifiers that offers two important properties; 1) SLR is a probabilistic classier[19]. 2) We seek to qualify which dyes in the sensor are important. This knowledge enables the ability to either reduce the size of the sensor or replace less sensitive dyes. ANN is mainly included in order to investigate if the usage of a non–linear model improves prediction performance.

Model training

In order to estimate the generalization error the data is partitioned using 10–fold stratified cross validation (CV). The methods perform model selection within each fold, again using 10–fold stratified CV. The performance of the classifiers are evaluated based on the classification error rate, already defined in section 2.3.1, but stated here for completeness

$$E_{err} = \frac{N_{err}}{N} \tag{4.9}$$

where N_{err} is the number if misclassified measurements and N is the total number of measurements.

[19] It is a probabilistic classier in the sense that it models the posterior class probability directly, i.e. a discriminative model.

k–nearest neighbor

For k–NN, the model selection parameter is the number of neighbor that is used to perform classification. All possible values of k is probed during model selection.

Sparse logistic regression

Sparse logistic regression uses L1 regularization in the error function. The error function was specified in equation (2.18), but written for completeness

$$E(\mathbf{w}) = E_D(\mathbf{w}) + \lambda \|\mathbf{w}\|_1 \tag{4.10}$$

where $E_D(\mathbf{w})$ is the data dependent error function for ordinary logistic regression. During training, the weights $\mathbf{w}$ are initialized to zero. Possible regularization values are $\lambda = [0, 10]$.

Training of artificial neural networks

The neural network applied is the usual two-layered feed-forward network with error function specified in equation (2.37), but stated for completeness

$$E(\mathbf{w}) = E_D(\mathbf{w}, \beta) + \alpha E_{\mathbf{w}}(\mathbf{w}) \tag{4.11}$$

The hyper-parameter are initialized to $\alpha = D$ and $\beta = 0$. Each network training cycle is repeated ten times and the network with the lowest error rate on the on training set is selected.

The number of hidden units is the model parameter. To estimate the number of hidden units, we assume that the misclassification error is roughly convex in terms of number of hidden units, that is, we minimize $E_{err}(N_{hu})$. The training begins with two hidden units. Hidden units are iteratively added until $E_{err}(N_{hu})$ stop decreasing. At that point, the "optimal" N_{hu} is identified. Of course, given the noise in the data *and* the fact that ANN training is a non-convex optimization problem, the above scheme will likely identify different values for optimal N_{hu} for each run. Nevertheless this scheme should provide a good estimation for a suitable number of hidden units.

Method	Median	Mode	Multi-mode	Mean	Combined
A-1-NN	5.40	**5.83**	5.27	5.33	5.40
A-K-NN	5.77	**6.20**	5.40	5.15	5.52
A-SLR	5.71	5.52	**6.08**	5.71	5.71
A-ANN	5.52	5.40	5.52	**5.71**	5.64
B-1-NN	1.77	1.77	**2.18**	1.91	1.77
B-K-NN	1.64	1.50	**1.91**	1.64	1.64
B-SLR	1.36	1.36	**1.91**	1.36	1.36
B-ANN	1.36	1.09	**1.50**	1.36	1.36
C-1-NN	6.05	6.12	**6.15**	6.05	6.05
C-K-NN	5.91	6.05	5.94	**6.12**	6.05
C-SLR	**6.79**	6.69	6.65	6.72	**6.79**
C-ANN	6.40	6.37	6.19	**6.47**	NaN
Total	1	2	**6**	3	1

Table 4.4: Summary of how well the features and classifiers perform compared to random guessing i.e. how many times better the classifier is compared to random guessing. The best performers are highlighted. The figures that correspond to flawless prediction are; 8 for dataset A, 3 for dataset B, and 9 for dataset C. A figure of 1 would correspond to random guessing.

4.4.1 Comparing the statistics

Since the sensors have a different amount of classes, we find it better to assess the quality of the classifiers by using the classification rate relative to random guessing as the classification rate alone can be misleading. For example a classification rate of 0.33% for sensor B would only be as good as random guessing while for sensor A and C it would be better than random guessing. The ratio is calculated as $(N_{correct} \cdot N_C)/N$, where N_C is the number of points correctly classified, N is the total number of points and N_C is the number of classes.

Table 4.4 shows the best statistic is the multivariate mode which is the best performer in six out of twelve cases[20]. However, all the other features are also represented at least once as the top performer, so the results indicate that in order to build the most accurate classifier one must extract all of the proposed features from the colorimetric sensor and then let the feature selection be part of the model selection process.

[20] This table is based on the results one presented in table C.2, page 168. During the writing of this thesis, it was discovered that Octonal was wrongly categorized as alcohol so all the numbers for dataset A has been recomputed.

The considered classification methods all perform similarly. As expected the simplest method, 1-NN is the best performer on the smallest dataset B. For dataset A, the k-NN method is the best performer and on dataset C the SLR method is the best performer. The non-linear ANN is performing well. As is the case with ANN, there is a high number of parameters to estimate and the fact that SLR is better than ANN except in one instance where they are equal, implies that linear methods such as SLR is better suited to model data from colorimetric sensor arrays.

Interestingly 1-NN performs better than k-NN on dataset C, indicating that there is high variance in the data, as k-NN should perform at least as good as 1-NN. The situation likely arises because of noise in the dataset and it seems that to obtain a good estimate of model parameters require a finer partitioning than 10–fold cross validation.

The logistic regression method demonstrated equal classification ability compared to k-NN and due to the added perks in terms of sparsity and probabilistic decisions, SLR is preferable to k-NN. The results do not merit the use of a non–linear method such ANN. This is likely because there is not enough training data and since the experimental process of colorimetric sensors is time consuming, methods that work with fewer points are more appealing.

The results about which statistic to are more ambitious. The multi-mode statistic is the overall best choice, but any of the feature extraction statistics are the best choice at least once. What can be concluded though is that it is not given beforehand that the traditional approach of using the mean is the best choice.

4.4.2 Detection of explosives

Two datasets have been collected with the purpose of detection of explosives, dataset A (table 4.1)and dataset C (table 4.3). The first dataset was collected using the 1st generation sensor array which consisted of just 15 sensors. It turned out that the sensor array was not very good at detecting the exact analyte in question, but was able to identify the group of the analyte with greater precision. The sensors in the array consisted exclusively of chemoselective dyes specifically designed to react with explosives. Therefore, it was no surprise to see the array could detect explosives accurately but struggled with other compounds.

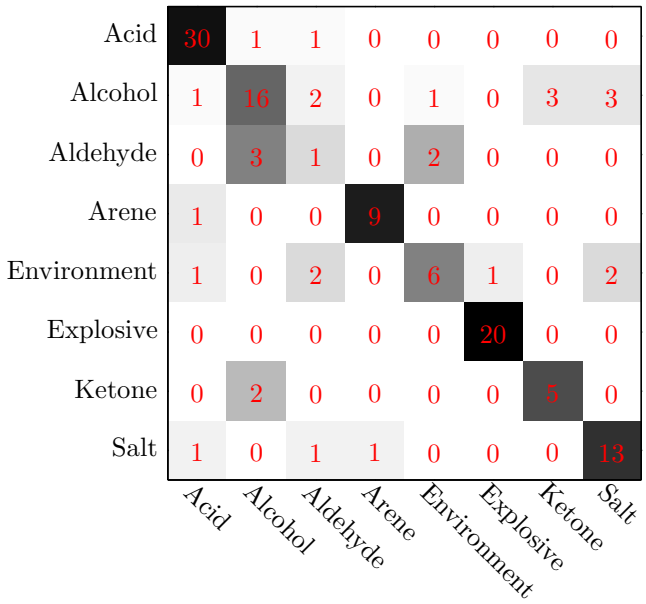

Figure 4.12: Confusion matrix for dataset A computed using the highest performing configuration as indicated in table 4.4.

4.4.3 Detection of drugs

This dataset is the smallest only consisting of $N = 14$ data point. The purpose of the dataset was to establish if the sensor array could be used to detect illicit drugs as well as military class explosives. The confusion matrix computed using the multi-mode 1-NN configuration is shown in figure 4.14. Due to the low number of measurements collected per class, any conclusions drawn from this dataset should be taken with moderation. The sensor is able to distinguish drugs from explosives as all except one of the misclassification are due to false negatives (drugs/explosives classified as environment). However, a PCA plot of the data strongly suggests that the low classification accuracy is mostly due to the limited amount of measurements, and of more measurements were collected a linear classier with higher accuracy could be computed [Kostesha et al., 2011].

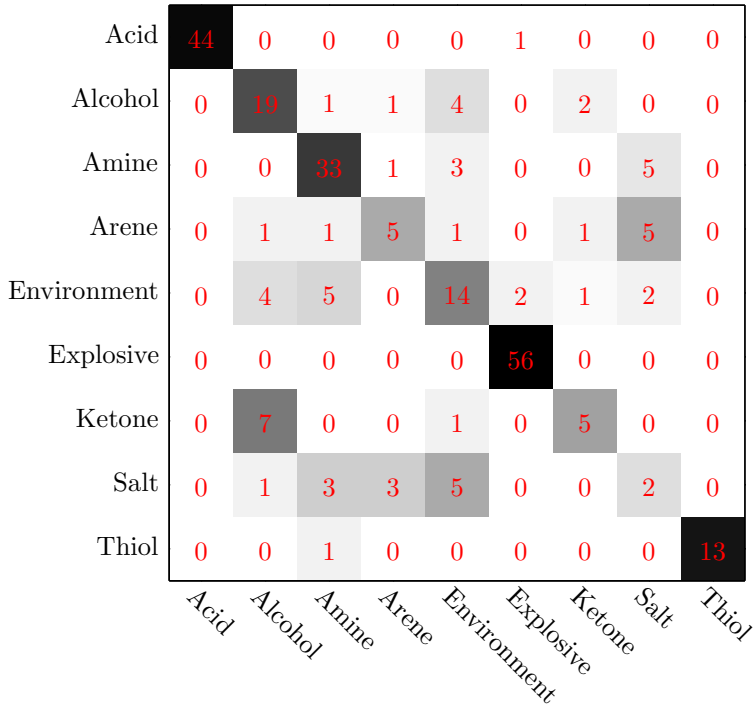

Figure 4.13: Confusion matrix for dataset C computed using the highest performing configuration as indicated in table 4.4.

4.5 Improving detection accuracy by calibrating colors

In section 4.4, the only information used by the classification methods are the class labels. Put in terms of traditional *Design and Analysis of experiments* (DoE) [Montgomery, 2009], the model used is

$$y_{ijkl} = \mu_{ikl} + \varepsilon_{ijkl} \tag{4.12}$$

where y_{ijkl} is the sensor response, μ_{ikl} is the *treatment* effect and ε_{ijkl} is the noise induced at each measurement assumed to be independent and identically distributed (i.i.d.). For the analysis in this section, the mean color difference is used as sensor response as this is the response traditionally used. The *treatment* effect μ_{ikl} is effect of exposing the sensor to a given analyte (i.e. the class label). The i index refers to different *treatments*, $i = \{1, 2, \ldots, N_a\}$. The j index refers to repeated measurements, $j = \{1, 2, \ldots, N\}$. The index k and l are the sensor response index, i.e. we operate with N_s sensors with $L = 3$ channels for each

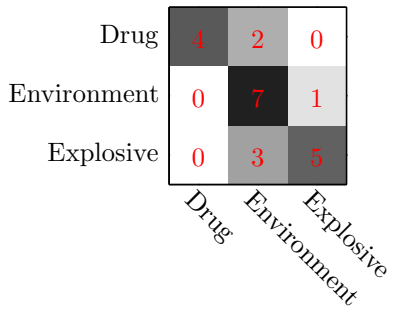

Figure 4.14: Confusion matrix for dataset B computed using the highest performing configuration as indicated in table 4.4.

sensor (RGB); $k = \{1, 2, \ldots, N_s\}$, $l = \{1, 2, 3\}$. Thus we have $N_s L$ systems of equations that must be analyzed as each sensor array yields a total of $N_s L$ readouts per measurement.

The data presented in table 4.3 was collected using the randomized complete blocked design approach (RCBD). In this design, the measurements are grouped into $B = 15$ blocks, and within each block each analyte is exposed to the sensor array exactly once. The exact experimental details can be found in appendix F. The purpose of the design is to enable more precise estimation of effects since the variation from block to block can be removed; hence the RCBD is often referred to as a noise reducing design. Adding the block effect to the model yields

$$y_{ijkl} = \mu_{ikl} + \beta_{jkl} + \varepsilon_{ijkl} \tag{4.13}$$

where β_{jkl} is the effect of the j'th block. As the experiment was designed according to the scheme where each repetition was in a distinct block, j can be replaced as the block index instead of the repetition index j (β_{jkl} instead of i). For each of our $N_s L$ systems there will be B block effect variables. All of these variables must be zero; otherwise there is an effect from the blocking. Thus the null hypothesis that can be applied is

$$\begin{aligned} H_0 &: \beta_{1kl} = \beta_{2kl} = \cdots = \beta_{Bkl} = 0 \\ H_1 &: \beta_{jkl} \neq 0 \quad \text{for at least one } j \end{aligned} \tag{4.14}$$

The equation is augmented further by considering if the difference color contains all the information about color change, i.e. the color of a sensor before exposure might have influence on the color after exposure. This corresponds to conducting analysis of covariance (ANCOVA) originally proposed by [Fisher,

1938]. Formally, the color before exposure to analyte is a possible *covariate* (or *concomitant* variable) of the sensor response:

$$y_{ijkl} = \mu_{ikl} + \beta_{jkl} + \alpha_{ikl}(x_{ijkl} - \bar{x}_{i\cdot kl}) + \varepsilon_{ijkl} \tag{4.15}$$

whereα_{ikl} is a linear regression coefficient. If α_{ikl} is different than zero, then the color response before exposure has influence on sensor response (k, l) for treatment i. The null hypothesis when testing for significant covariates is

$$\begin{aligned} H_0 &: \alpha_{ikl} = 0 \\ H_1 &: \alpha_{ikl} \neq 0 \end{aligned} \tag{4.16}$$

The model specified in equation (4.15) is considered the complete model and is applied to the data. Using that model, adjusted responses that averages out the effects from blocks and covariates is calculated.

The hypothesis tests (4.14) and (4.16) reveals that both blocking effects and the covariate effects are significant. 25 out of the 31 sensors are subject to blocking effects. Significance of the covariate effects depend on the treatment (analyte) and on the sensor as well, but in the case of explosives approximately 2/3 of the responses showed to have a covariate effect. The p-values are shown in appendix F, page 234–239.

4.5.1 Evaluation using k-nearest-neighbor

The impact of the noise reduction model (4.15) is investigated by use of k-nearest-neighbor. The classifier was trained used the double LOOCV scheme, where the inner loop estimates a value for k and the outer loop estimates the generalization error, just as described earlier.

Initially the data is converted to a binary classification in the explosives versus rest problem. Here it turned out that the sensor was very accurate even for the unadjusted values, making three false alarms (non-explosives identified as explosives) and zero false negatives (explosives identified as non-explosives). For the adjusted values however, no errors was made.

To elaborate further, the data is handled as a multiclass problem using the analyte names as class labels. For the unadjusted values a total of 114 measurements are correctly classified corresponding to an accuracy of 45.1%, as shown in figure 4.15. For the adjusted values, a total of 159 measurements are correctly classified corresponding to an improved classification accuracy of 62.8%, as shown in figure 4.16.

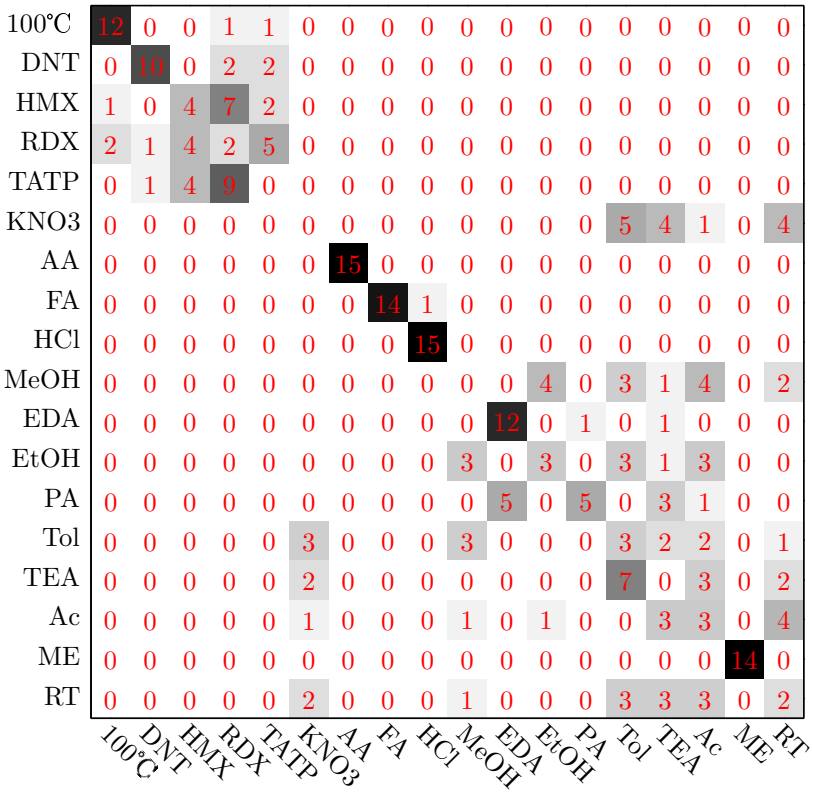

Figure 4.15: Confusion matrix calculated using k-nearest-neighbor on unadjusted values according to model (4.12). The overall accuracy is 45.1%.

In real-world scenarios, it would be difficult to calibrate for colors as the calibration is dependent on the analyte being measured. However, this result can be used as an incentive to refine the production process of colorimetric sensor arrays. If the sensor arrays always have the same color before exposure, no calibrations should be needed, and only the block effect will come into place. The block effect, in real-world scenarios, could be handled by performing a series of control measurements along with the real detection measurement.

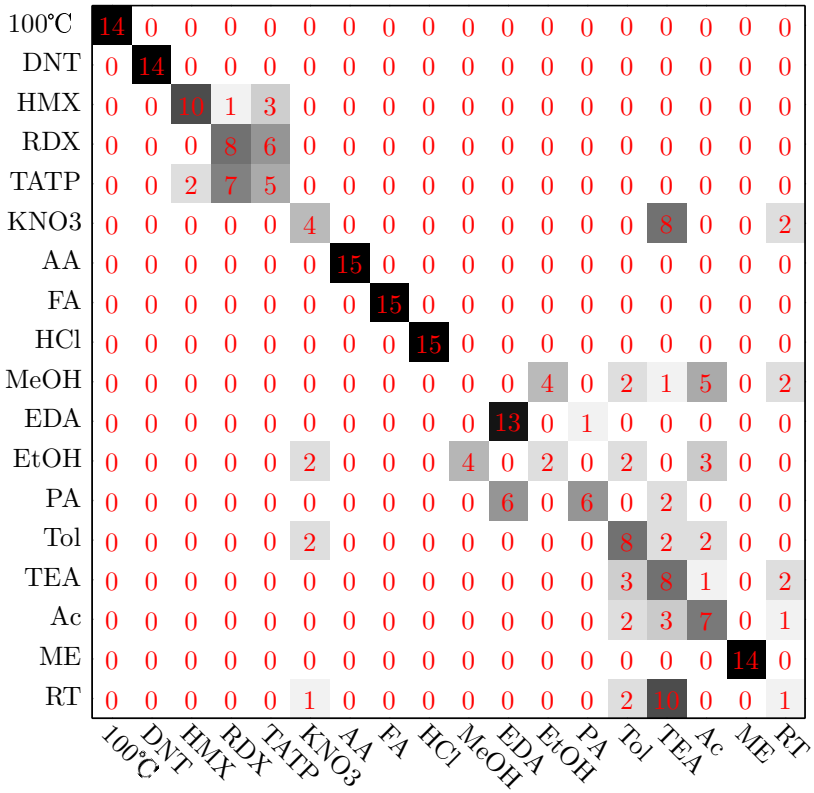

Figure 4.16: Confusion matrix calculated using k-nearest-neighbor on adjusted values according to model (4.15). The overall accuracy is 62.8%.

4.6 Using histogram and manifold methods

In the lack of conclusive results based on single feature methods, a natural step is to use other measures to represent the color from the sensor response. One idea is to make better use of the pixels that constitutes a measurement. One measurement can consist of up to 1000 pixels so reducing a measurement to just one number is a drastic compression and it is likely that valuable information is lost due to this compression. Two family of methods as applied; distance measures based on the Hellinger distance and distance measures based on the Hausdorff distance. Each of these distance measures come in different flavors, which will be explained in depth in this section.

The i'th example (dye) is represented by $X_i = \{x_{i1}, \ldots, x_{in_i}\}$, where x_{ij} is the j'th three–dimensional difference RGB pixel value between control and exposed, and n_i is the number of pixels considered for the representation of the i'th example. For several classifiers a notion of distance between examples is a key component. To construct a distance between two examples in the bag-of-words representation, we propose to represent each multi-instance example with a distribution and use the Hellinger distance as a metric between two examples. The motivation behind this approach is that differences between distributions, which are not directly measurable through the mean (or other moments), can still be detected. This approach was demonstrated to be effective in several application areas, e.g., disease classification using flow cytometry [Carter et al., 2009a] and document classification [Carter et al., 2009b].

4.6.1 Hellinger Distance

The Hellinger distance measures similarity between two probability measures $f_i(\mathbf{x})$ and $f_k(\mathbf{x})$ and is given by

$$d_{\mathrm{He}}(f_i, f_k)^2 = \int \left(\sqrt{f_i(\mathbf{x})} - \sqrt{f_k(\mathbf{x})}\right)^2 d\mathbf{x} \tag{4.17}$$

i.e., the Euclidean distance between the square-root of the PDFs.By completing the square of the integrand, the Hellinger distance can be rewritten to the following equivalent alternative:

$$d_{\mathrm{He}}(f_i, f_k)^2 = 2 - 2\int \sqrt{f_i(\mathbf{x}) f_k(\mathbf{x})} d\mathbf{x} \tag{4.18}$$

If the probability measures are equal the Hellinger distance is $d_{\mathrm{He}}(f_i, f_j)^2 = 0$. On the contrary, if the probability measures $f_i(\mathbf{x})$ and $f_k(\mathbf{x})$ are completely non-overlapping, then $d_{\mathrm{He}}(f_i, f_j)^2 = 2$.

Parzen window Kernel density estimator

The Hellinger distance requires a choice of model to construct the probability measure. The first one to consider is the Parzen window Kernel density estimator. Assuming an underlying probability density function f_i such that $x_{ij} \sim f_i$ for $j = 1, 2, \ldots, n_i$, one can associate X_i with the following kernel density estimate

$$f_i(\mathbf{x}) = \frac{1}{n_i} \sum_{k=1}^{n_i} K(\mathbf{x} - \mathbf{x}_{ik}) \tag{4.19}$$

where the kernel used is the isotropic squared exponential kernel

$$K(\mathbf{x}) = 1/(2\pi\sigma^2)^{D/2} \exp(-\|\mathbf{x}\|_2^2/2\sigma^2) \tag{4.20}$$

As the sensor responses are RGB values the dimensionality is $D = 3$. The kernel parameter is chosen to be $\sigma^2 = 1$ which seems like a reasonable smoothing.

To utilize the KDE a revision of the Hellinger distance expression is required. Looking at the integral term in (4.18), we inject a new term

$$\int \sqrt{f_i(\mathbf{x}) f_k(\mathbf{x})} d\mathbf{x} = \int \frac{f_i(\mathbf{x}) + f_k(\mathbf{x})}{f_i(\mathbf{x}) + f_k(\mathbf{x})} \sqrt{f_i(\mathbf{x}) f_k(\mathbf{x})} d\mathbf{x} \tag{4.21}$$

which enables us to split the integral in two:

$$\begin{aligned} &\int \sqrt{f_i(\mathbf{x}) f_k(\mathbf{x})} d\mathbf{x} = \\ &\int \frac{f_i(\mathbf{x})}{f_i(\mathbf{x}) + f_k(\mathbf{x})} \sqrt{f_i(\mathbf{x}) f_k(\mathbf{x})} d\mathbf{x} + \int \frac{f_k(\mathbf{x})}{f_i(\mathbf{x}) + f_k(\mathbf{x})} \sqrt{f_i(\mathbf{x}) f_k(\mathbf{x})} d\mathbf{x} \end{aligned} \tag{4.22}$$

Rearranging by moving the denominator into the square root yields

$$\begin{aligned} &\int \sqrt{f_i(\mathbf{x}) f_k(\mathbf{x})} d\mathbf{x} = \\ &\int f_i(\mathbf{x}) \sqrt{\frac{f_i(\mathbf{x}) f_k(\mathbf{x})}{(f_i(\mathbf{x}) + f_k(\mathbf{x}))^2}} d\mathbf{x} + \int f_k(\mathbf{x}) \sqrt{\frac{f_i(\mathbf{x}) f_k(\mathbf{x})}{(f_i(\mathbf{x}) + f_k(\mathbf{x}))^2}} d\mathbf{x} \end{aligned} \tag{4.23}$$

Defining a new function $T(\mathbf{x})$ enables further simplification

$$T(\mathbf{x}) = \frac{f_i(\mathbf{x})}{f_i(\mathbf{x}) + f_k(\mathbf{x})} \tag{4.24}$$

Also notice that the two terms on the RHS in equation (4.23) are on the form of expectation. Combining $T(\mathbf{x})$ and expectation yields

$$\int \sqrt{f_i(\mathbf{x}) f_k(\mathbf{x})} d\mathbf{x} \;=\; \mathbb{E}_{f_i}\left[\sqrt{T(\mathbf{x})(1 - T(\mathbf{x}))}\right] \;+\; \mathbb{E}_{f_k}\left[\sqrt{T(\mathbf{x})(1 - T(\mathbf{x}))}\right] \tag{4.25}$$

Substituting the result from (4.25) into (4.18) finally yields the Hellinger distance on the alternative form

$$d_{\mathrm{He}}(f_i, f_k)^2 = 2 - 2\left(\mathbb{E}_{f_i}\left[\sqrt{T(\mathbf{x})(1 - T(\mathbf{x}))}\right] + \mathbb{E}_{f_k}\left[\sqrt{T(\mathbf{x})(1 - T(\mathbf{x}))}\right]\right) \tag{4.26}$$

where $\mathbb{E}_h[f] = \int f(\mathbf{x})h(\mathbf{x})d\mathbf{x}$. A sample-based version of this expression is computed by replacing the expectations with their sample averages and the distributions with their kernel estimates,

$$E_{f_i}[\sqrt{T(x)(1-T(x))}] \approx \frac{1}{n_i}\sum_{j=1}^{n_i}\sqrt{T(x_{ij})(1-T(x_{ij}))}$$

Naturally, the distance calculation can be directly applied to a K-NN classifier. This approach can be considered an alternative to a set distance between two collections instances.

Gaussian distribution

The second approach applied to the Hellinger distance is the multivariate normal distribution using a full covariance matrix

$$f_i(\mathbf{x}) = \frac{1}{(2\pi)^{d/2}|\mathbf{\Sigma}_i|^{d/2}}\exp\left(-\frac{1}{2}(\boldsymbol{\mu}_i-\mathbf{x})^\top {\mathbf{\Sigma}_i}^{-1}(\boldsymbol{\mu}_i-\mathbf{x})\right) \tag{4.27}$$

where $\boldsymbol{\mu}_i$ is the mean and $\mathbf{\Sigma}_i$ the covariance matrix. Both parameters are estimated by maximum likelihood. Once the parameters are estimated the Hellinger distance can be calculated in closed form. The result is derived by [Jebara et al., 2004] for the general case of a product probability kernel. Such a kernel is on the form

$$K_p(f_i,f_j) = \int_{\mathbb{R}^D} f_i(\mathbf{x})^p f_k(\mathbf{x})^p d\mathbf{x} \tag{4.28}$$

Setting $p = 1/2$, we get the integral on the RHS of equation (4.18). Using the result derived by [Jebara et al., 2004] when f_i and f_j are Gaussian distributions with $D = 3$ yields

$$d_{\mathrm{He}}(f_i,f_k)^2 = 2 - 4\sqrt{2}\frac{|\mathbf{\Sigma}^\dagger|^{1/2}}{|\mathbf{\Sigma}_i||\mathbf{\Sigma}_k|}\exp\left(-\frac{1}{4}\left(\boldsymbol{\mu}_i^\top\mathbf{\Sigma}_i^{-1}\boldsymbol{\mu}_i + \boldsymbol{\mu}_k^\top\mathbf{\Sigma}_k^{-1}\boldsymbol{\mu}_k + {\boldsymbol{\mu}^\dagger}^\top\mathbf{\Sigma}^\dagger\boldsymbol{\mu}^\dagger\right)\right) \tag{4.29}$$

where $\mathbf{\Sigma}^\dagger = (\mathbf{\Sigma}_i^{-1} + \mathbf{\Sigma}_k^{-1})^{-1}$ and $\boldsymbol{\mu}^\dagger = \mathbf{\Sigma}_i^{-1}\boldsymbol{\mu}_i + \mathbf{\Sigma}_k^{-1}\boldsymbol{\mu}_k$.

4.6.2 The Hausdorff Distance

The Hausdorff distance measures distance between two point sets, and it is small if all points in each set are close to some point in the other set. It is a

Chemical	M	P	IM	MH	G	E[pFD]	#Significant
Acids	1	2	2	6	0	0.89	11
Alcohols	0	0	0	0	3	0.15	3
Amines	1	0	1	0	0	1.02	2
Explosives	0	3	0	7	1	0.98	11

Table 4.5: Number of instances the best performing method is significantly better than another method. The methods are Mean, Parzen, Inner Mean, Mod. Hausdorff and Gaussian. E[pFD] is the expected positive false discoveries and n is the number of significant results. The inner mean is explained in appendix E.

fundamentally different measure than the Hellinger distance, e.i. the Hausdorff distance becomes larger as the two point sets becomes further apart. On the contrary, having to completely separating point sets the Hellinger distance will at most be two, no matter how far apart the point sets are. This property could be useful for comparing sensor color, as the amount of color change could be important.

First define the distance between two points $\mathbf{x}_i$ and $\mathbf{x}_k$ as the Euclidean distance $d(\mathbf{x}_i, \mathbf{x}_k) = \|\mathbf{x}_i - \mathbf{x}_k\|_2$. The distance between a point $\mathbf{x}_i$ and a set $\mathbf{X}_k$ is then $d(\mathbf{x}_i, \mathbf{X}_k) = \min_{\mathbf{x}_k \in \mathbf{X}_k} d(\mathbf{x}_i, \mathbf{x}_k)$. The Hausdorff distance is defined as

$$d_{\text{Ha}}(\mathbf{X}_i, \mathbf{X}_k) = \max \left\{ \max_{\mathbf{x}_i \in \mathbf{X}_i} d(\mathbf{x}_i, \mathbf{X}_k), \max_{\mathbf{x}_k \in \mathbf{X}_k} d(\mathbf{x}_k, \mathbf{X}_i) \right\} \tag{4.30}$$

As an alternative approach one can use the modified Hausdorff distance which is more robust in the presence of noise and outliers

$$d_{\text{MH}}(\mathbf{X}_i, \mathbf{X}_k) = \max \left\{ \frac{1}{N_{\mathbf{X}_i}} \sum_{\mathbf{x}_i \in \mathbf{X}_i} d(\mathbf{x}_i, \mathbf{X}_k), \frac{1}{N_{\mathbf{X}_k}} \sum_{\mathbf{x}_k \in \mathbf{X}_k} d(\mathbf{x}_k, \mathbf{X}_i) \right\} \tag{4.31}$$

It should be noted that this distance is not a metric as the triangle inequality is not fulfilled [Dubuisson and Jain, 1994].

4.6.3 Evaluation using k-nearest-neighbor

The k-nearest-neighbor classifier is applied to each sensor for each representation technique. The dataset presented in table 4.3 is used to investigate the proposed methods. The dataset is reduced to a five-class dataset as we only want to investigate the performance on the chemical families that the sensor has proven

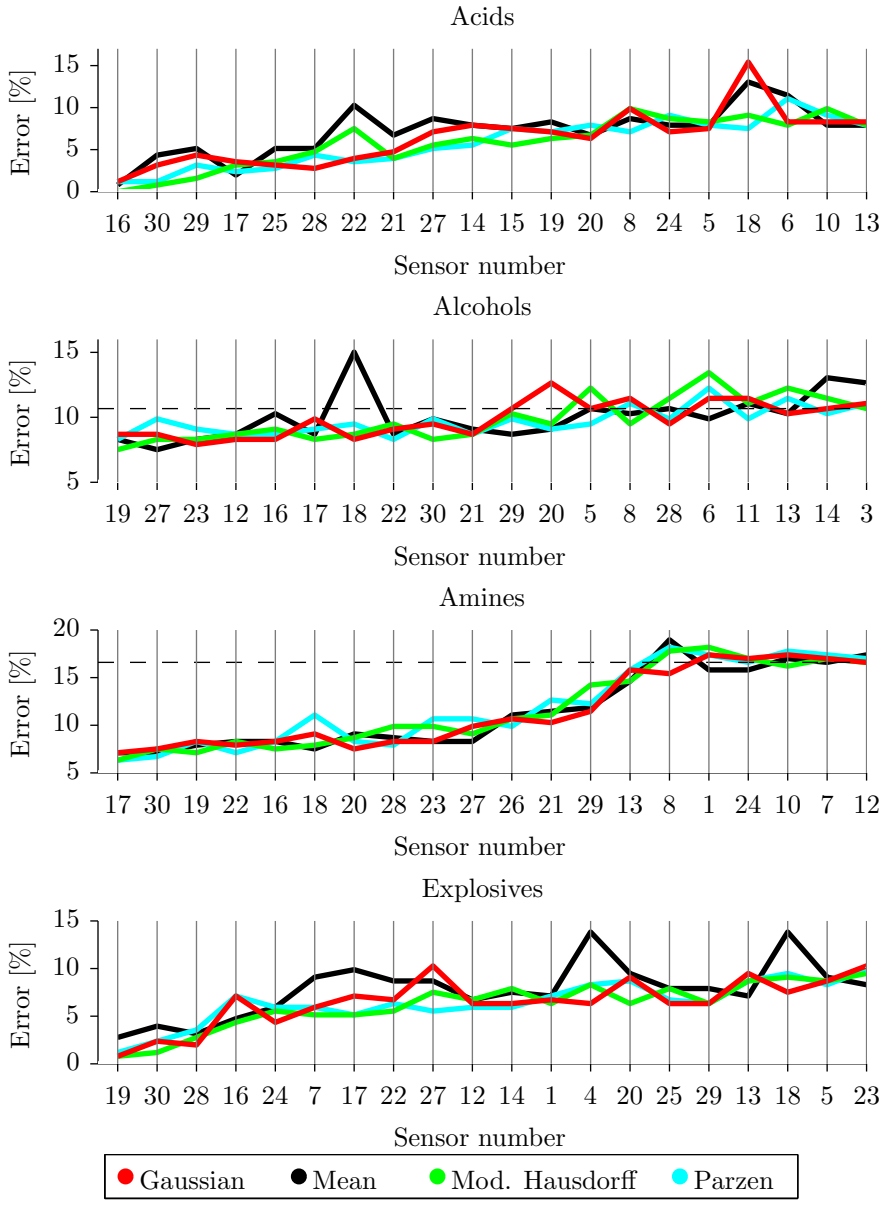

Figure 4.17: Individual error for the sensors. The dotted line corresponds to random guessing. For acids and explosives it is 17.8% and 22.1% respectively.

able to detect. Based on the results shown in figure 4.13 the chemical families are: acids, alcohols, amines and explosives. For each of the labels, the accuracy for each sensor is calculated using 1-vs-all. In this setting, the chosen chemical family that is to be detected is kept as the class label and all other measurements are labeled as 'other'.

To judge the differences in classification performance the McNemar significance test [McNemar, 1947] is employed. The McNemar significance is a paired test which uses the the number of instances where two classifiers disagree about a decision. From this test p–values for each comparison is calculated[21] and use the multiple hypothesis framework proposed by Storey [Storey, 2002]. Based on the p–values the expected positive false discoveries (E[pFD]) for our significant differences is calculated, that is, the expected quantity of wrongly significant results among all identified significant results. These finding are summarized in table 4.5 and the performance of the individual sensors are displayed in figure 4.17.

The overall best performing distance measure is the modified Hausdorff method although it is notable that this method is not best even once for alcohols whereas it is best on numerous occasions for acids and explosives. Looking into the individual sensors reveal that the top sensor for acids largely overlap with the top sensors for explosives (also see appendix F).

4.6.4 Evaluation using Gaussian process classification

It is clear that the distance measures are capturing "something" that the mean cannot and that the distance measures generally performs on par or better than the mean. However, using distance measures it is no longer applicable to fuse the sensors simply by stacking the responses in a vector-space model. One solution is to use a classifier that is designed to work on distances, i.e. a kernel classifier. Having distance measure $d(\boldsymbol{X}_i, \boldsymbol{X}_j)$ we can apply a distance substitution approach [Haasdonk and Bahlmann, 2004] using the squared exponential kernel

$$k\left(\boldsymbol{X}_i, \boldsymbol{X}_j\right) = \exp\left(-\frac{1}{\ell} d(\boldsymbol{X}_i, \boldsymbol{X}_j)\right) \tag{4.32}$$

where ℓ is the length scale. If the distance measure is a metric the corresponding Gram matrix produced using the above expression is guaranteed to be a positive semi-definite matrix [Haasdonk and Bahlmann, 2004].

[21] The null hypothesis is that the two classifiers have equal classification accuracy against the alternative that one classifier is better than the other.

We note that a valid covariance function may be constructed directly for the Hellinger distance by considering the inner product given by the integral which is known as the Probability Product Kernel [Jebara et al., 2004]; however, to make a fair comparisons we treat the Hellinger distance like the other distance measure and employ (4.32) when converting any distance measure to a Gram matrix Also note that since the modified Hellinger distance is not a metric, the distance substitution kernel may not be positive definite [Haasdonk and Bahlmann, 2004]. The same may apply to the Hellinger distances based on Parzen windows as these distances are calculated using approximations.

The use of kernels provides a convenient way of integrating information from different sensors by combining different kernels as a weighted sum. Thus, different sensors can be combined by constructing the following kernel

$$k\left(\boldsymbol{X}_i, \boldsymbol{X}_j\right) = \sigma^2 \mathbf{I} + \sum_{m=1}^{M} \alpha_m k\left(\boldsymbol{X}_i^m, \boldsymbol{X}_j^m\right) \tag{4.33}$$

where each kernel function is the distance substitution kernel with one of the respective metrics.

Initially we want to establish the performance of GP in the same setting as k-NN. The results from this approach are shown in figure 4.18. In the case of explosives, the modified Hausdorff is again the top performer for the first two dyes, which is again dye 19 and 30. However for dye 28 and 24 the modified Hausdorff coupled with GP yields an error of 21% and 30% respectively. This might very well be an effect of the modified Hausdorff not being a valid metric and as such the corresponding kernel might not be psd [Dubuisson and Jain, 1994]. But as the case of k-NN, the figure does not show a clear indication of which method is superior although it seems that modified Hausdorff is able to capture more information about dye 19 and 30 than the the methods.

To fuse the different sensors a forward selection method using the following steps is applied. 1) For a given sensor, perform a grid search of hyperparameters σ^2, α_m and ℓ. 2) Find the hyper parameters by optimizing the evidence in GP using the optimal point found in the grid as initial guess. 3) Perform *leave-one-out* cross validation to get classification error. 4) Choose the sensor that yields the lowest classification error.

When fusing the dyes one by one using forward selection we find no significant results between the methods (figure 4.19). To get a significant result (according to McNemar testing) the performance must at least differ 2.4 percent points but already with one dye we are below that margin.

The modified Hausdorff method is however the overall best performing method.

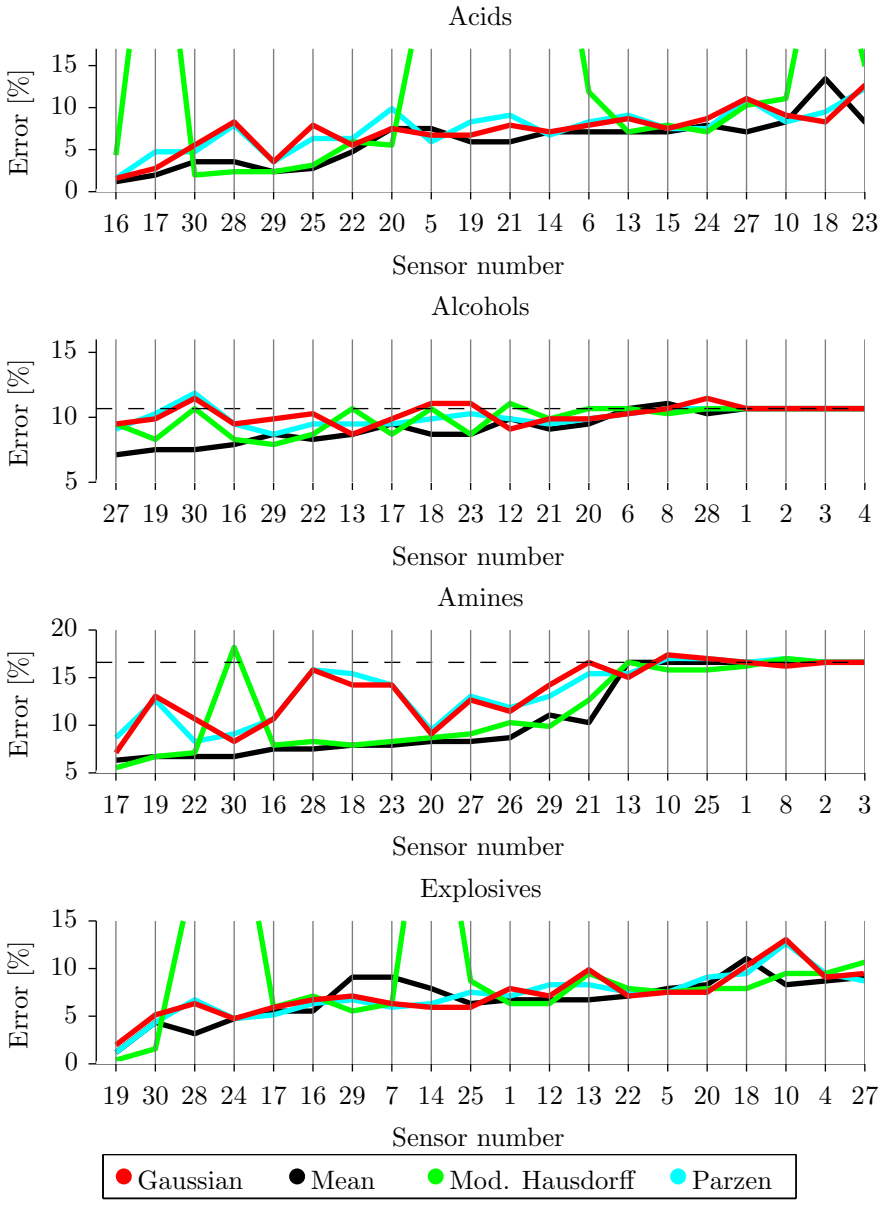

Figure 4.18: Confusion matrix calculated using k-nearest-neighbor on unadjusted values according to model (4.12). The overall accuracy is 45.1%.

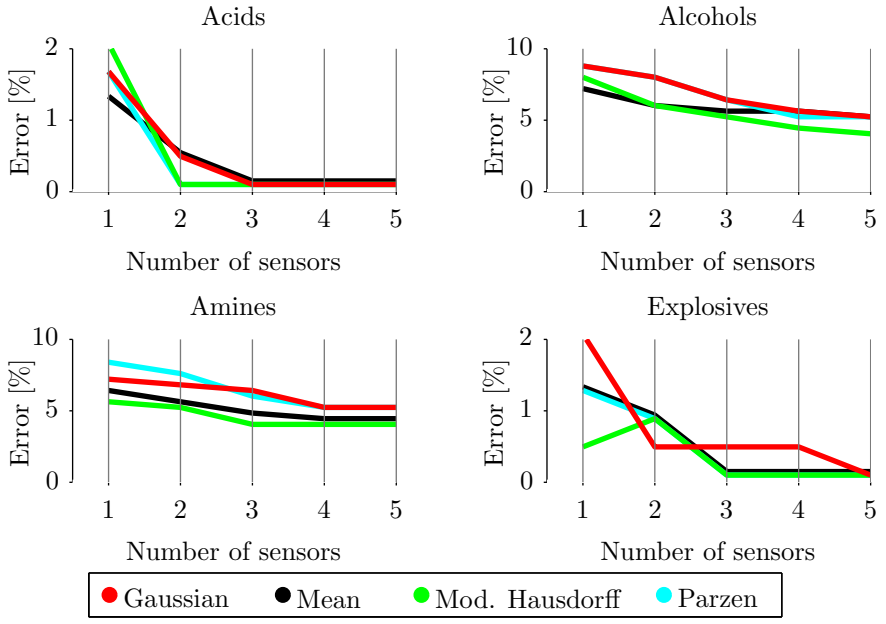

Figure 4.19: Confusion matrix calculated using k-nearest-neighbor on unadjusted values according to model (4.12). The overall accuracy is 45.1%.

It is particularly strong for classifying explosives. In the fusing scheme the modified Hausdorff method also works well and is the overall best performer.

4.7 Related work

Over the past years colorimetric sensor arrays has been developed and successfully applied in various areas. In 2000 a paper co-authored by Kenneth S. Suslick was published in Nature [Rakow and Suslick, 2000]. Since then, Suslick has pioneered work in applying the colorimetric sensor arrays in various areas, such as the application of the colorimetric sensor array for detecting volatile organic compounds in the gas phase [Suslick et al., 2004b, Rakow et al., 2005] as well as for identifying different organic compounds in the liquid phase [Zhang and Suslick, 2005, Zhang et al., 2006].

The colorimetric sensor is a fascinating technique for detecting different chemical compounds belonging to various classes, like amines, cyanides, alcohols, arenes,

ketones, aldehydes and acids in the parts-per-million (ppm) and parts-per-billion (ppb) ranges [Rakow et al., 2005, Lim et al., 2009, Zhang and Suslick, 2007]. A more elaborate description on the state-of-the-art for chemical sensing is given in paper found in appendix F.

The feature extraction and sensor evaluation has not been improved since the paper published by Suslick in 2004 [Suslick et al., 2004b]. All papers subsequent to this paper follows the same line of data processing. First, the data is extracted using dye localization, the dot size is reduced to accommodate for the coffee stain effect and the mean difference color response is extracted and represented in a vector-space model. The data is then visualized suing principal component analysis and hierarchical cluster analysis [Janzen et al., 2006, Suslick et al., 2010, Luo et al., 2010]. The hierarchical cluster analysis is carried out using the Euclidean distance between measurements so in essence this corresponds to performing 1-nearest-neighbor.

4.8 Summary

This chapter highlighted the major developments made for colorimetric sensor arrays. The entire processing pipeline was described, from the preprocessing of images to the classification of analytes and identification of important chemoselective compounds.

There are numerous ideas on how to further explore the results put forward in this chapter, especially the results presented in section 4.6. Obviously the issues for dye number 14, 24 and 28 (figure 4.18) when combining the modified Hausdorff with Gaussian process classification is an issue that must be put under scrutiny. The issue could be that the Modified Hausdorff distance is not a real metric which is required in order to guarantee that the resulting kernel is positive semi-definite. Another issue is that the Modified Hausdorff is quite prone to outliers. This is an issue only a few bad pixels are required to ruin a measurements. An easy way to solve this could be to remove the outliers by doing image smoothing as specified in section 4.1. Expanding the Hellinger distance measure by using Gaussian mixture models is also worthwhile to consider. Finally, in the lack of one distance measure clearly outperforming the others, it could be of interest to combine all the features extracting methods by either using multiple kernel learning or further developing the MKL-equivalent covariance function presented in equation (4.33)

Other ideas are to explore is based on the results in section 4.5. Measuring the dye color before exposing the sensor to analyte enhances the signal substan-

tially. These finding could possibly be build into the framework of Manifold and Histogram methods. The ideas presented here are currently being investigated in collaboration with Ryota Tomioka[22] and a paper is currently under development. This paper compiles the major research findings presented in this chapter as well as the possible enhancements listed.

[22] Assistant Professor at Department of Mathematical Informatics, The University of Tokyo

Chapter 5

Multisensor approach for dection of explosives

The other three sensors within the Xsense project were only briefly described. This is because all the work that has been carried on these sensors is contained within a recently submitted paper (appendix A), and it would make little sense to spend too much time on writing a chapter repeating everything in the same format. The main innovation of the paper is the multisensor approach, where measurements were collected under identical conditions utilizing all the sensors in the Xsense project. The highlights of the paper found in appendix A is briefly presented here.

By using the technologies shown in figure 5.1 it is possible to simultaneously detect explosives in trace concentrations. These are the sensors that were described in the introduction (section 1.4) and the working principles will not be repeated here. Instead readers are refered to appendix A.

A dataset consisting of the four analytes were collected; ammonium nitrate (AN), 2,4-diaminotoluene (DAT), 2,4-dinitrotoluene (DNT), and diesel. The dataset is inspired by a post-blast scenario of e.g. a car bomb. The number of measurements as well as the classification results (obtained using 1-nearest-neighbor) is shown in table 5.1.

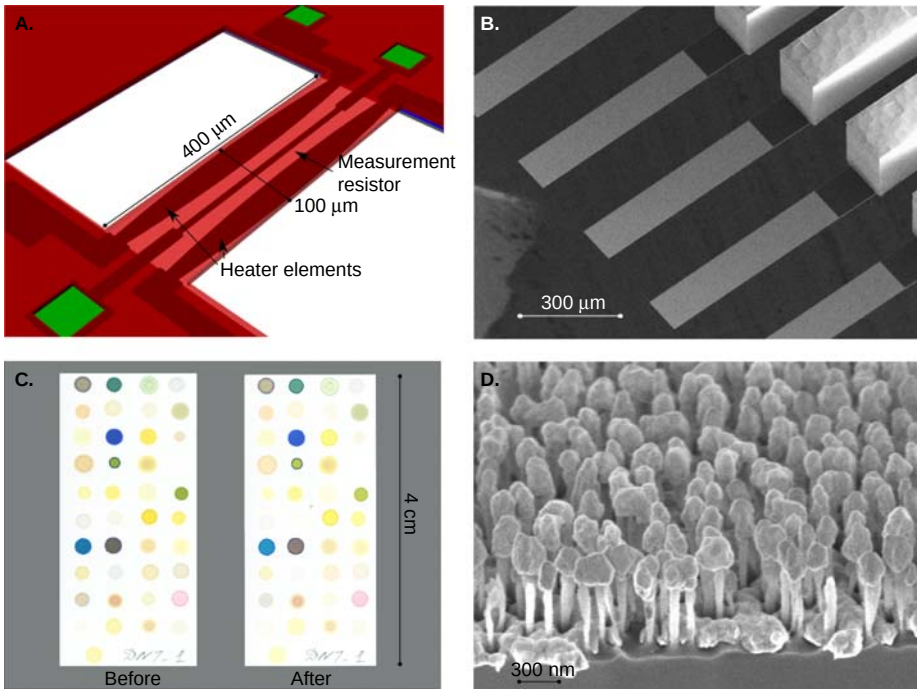

Figure 5.1: Illustration of the four sensing techniques: (A). Calorimetric sensor; (B). Cantilever sensor; (C). Colorimetric sensor; (D). SERS sensor.

Analyte	Calorimetric	Cantilever	Colorimetric	SERS
AN	2/3	N.D	2/2	8/8
DAT	3/3	N.D	6/7	5/5
DNT	3/3	3/3	5/5	6/6
Diesel	N.D	N.D	4/4	N.D

Table 5.1: Detection rates of the four sensors. False positives are not included in the table although it should be emphasized that there are neither false positives nor false negatives for DNT. Some scenarios are marked as no detection (N.D.) as by inspecting the sensor response it was deemed that the sensor was not able to detect the analyte in question, but only show that the analyte was not causing false alarms for DNT.

As described in the introduction, all of the Xsense sensors were designed to detect TNT so it is no surprise that all the DNT measurements were identified correctly for all the sensors. More interestingly it seems that the colorimetric sensor is the most versatile in the current setup. However, comparing e.g. the

cantilever and the colorimetric sensors on the grounds on these results is unfair. The cantilever is functionlized using just one chemoselective compound whereas the colorimetric sensor utilized 41 compounds. The situation more confirms two ideas: one) sensor fusion improves detection (as has been described in chapter 4, a colorimetric sensor array is sensor fusion, it is just that they are build on the same technology), and two) The sensors seems to compliment each other well, although it is questionable whether their detection patterns are independent.

Chapter 6

Conclusion and future work

This thesis has shown advanced on the data analysis of data collected using five different sensors. The first one was based on quartz crystal microbalance crystals (QCM). The inclusion of the QCM sensor was mostly an opportunity that presented itself back when the sensors within the Xsense project was still being developed. Handling the QCM data was a very good experience and given that QCM resembles cantilever sensing closely it also allowed me to be setup nicely for future data. The cantilever sensor is a sensor that is chemically coated just like QCM, so QCM and cantilevers can be considered very much alike, only the medium is different.

The task for the QCM sensor was the detection of benzodioxol, an important precursor for ecstasy. Despite the fact that QCM produces close to linear responses it has been a growing trend to apply artificial neural networks to both classify analytes and to perform density estimation. One of the hypothesis when the QCM data was analyzed (from a signal processing point of view), was that adequate performance would be obtained using linear methods to both classify and estimate concentration levels.

In chapter 3 [paper B] we showed that the linear method SVD greatly outperforms ANN in classification and given that SVD is much faster than ANN, based on the dataset, it makes little sense to apply ANN. In regression a similar picture showed. ANN was again outperformed by the linear PCR method but

also the GPR, and it actually turned out that GPR was overall the best method. Likely because GPR can adapt to the minor non-linearities that sneak into any dataset that is measured from real-world. To summarize, linear methods such as SVD and PCR are preferable over ANN. GPR might provide an extra edge when estimated concentrations but with the application of GPR some model complexity follows.

The majority of the work presented has mostly concerned colorimetric data handling and here a number innovations was proposed. The main hypothesis that we wanted to investigate was the possibility to improve the feature extraction for colorimetric sensors. In chapter 4 we showed that the traditional approach can be improved in two ways. First, ff the colors are calibrated, or the colors before exposure is included in the analysis the classification accuracy is improved. Secondly, by using more advanced methods to represent the sensor response, such as the modified Hausdorff, the overall system accuracy is improved.

In the same chapter, we also proposed satisfactory solutions to the important problem of sensor fusion for colorimetric sensor arrays. This was solved by a Gaussian Process approach, where the algorithm successfully identified sensors that improved the accuracy.

With the combination of Gaussian Process classification and the modified Hausdorff some issues arose. The modified Hausdorff is not a real metric and as such the Gram matrix that is calculated based on the modified Hausdorff might violate the requirements of positive semidefinite matrices. These issues will be looked upon in the near future and if we can solve them the results will be included in the upcoming paper. With this paper, a toolbox that contains all the code that I have written during the project will also be released. When we begun to use colorimetric sensors, we found that there was quite a lot of work required to even begin to handle the data. This toolbox should help making colorimetric sensor arrays more accessible to other research groups. Also, the results (and the accompanying software) on feature selection presented should enable researchers to analyze their sensors better and enable them to iteratively design better colorimetric sensor arrays.

The remaining three sensors within the Xsense project where briefly described in chapter 5. The main innovation of the work was the multisensor approach, where measurements were collected under identical conditions utilizing all the sensors in the Xsense project. The results should be considered as a proof of concept and they imply that the sensors within the Xsense project are suitable to be combined and that the overall accuracy would be improved in all four sensors were integrated.

The work within the Xsense group has spurred the project, “Multisensor DVD-

platform - MUSE", Danish Council for Strategic Research grant 11-115314 and led by Anja Boisen, DTU Nanotech. Within this project, future work will include system integration of sensors which will enable the possibility for collecting simultaneous measurements from all sensors. The system integration will facilitate automatic data collection that will provide sufficient data to enable the possibility of using data fusing. Only then can a full multisensor system utilizing sensors based on different physical properties be proclaimed.

The sensors included initially are SERS and cantilevers, as these are the technologies that fits into the designed integrated system. The application is different too, here the goal is to measure sepsis in blood and hormones in waste water. However, a lot of the work that was presented in thesis, and especially the work with sensor fusion developed for the colorimetric sensor array serve as a platform. Kernel methods are very suitable for data fusion as kernels naturally allow sensors with widely different signals to be merged. In this framework, one has to design kernels that fit the data well and then they can be merged. I am personally very excited and grateful that I can be apart of this new research project.

Appendix A

Miniaturized multisensory approach for the highly sensitive and selective detection of explosives

---

Tommy S. Alstrøm, Natalie V. Kostesha, Filippo G. Bosco, Michael S. Schmidt, Jesper K. Olsen, Michael Bache, Jan Larsen, Mogens H. Jakobsen, and Anja Boisen. Miniaturized multisensory approach for the highly sensitive and selective detection of explosives. *Submitted to Journal of Materials Chemistry*, 2013.

The paper was submitted to the Journal of American Chemical Society (JACS) and was rejected with the editor suggesting that we submit the paper to a more specialized journal. JACS being one of the most important journals in the field of chemisty with an impact factor of 9.91 (2011), we were happy they took the paper under consideration and gave reviews that have improved this work. The paper is now submitted to Journal of Materials Chemistry.

The layout of the paper has been revised.

Miniaturized multisensory approach for the highly sensitive and selective detection of explosives

Tommy S. Alstrøm,[†] Natalie V. Kostesha,[‡] Filippo G. Bosco,[‡] Michael S. Schmidt,[‡] Jesper K. Olsen,[‡] Michael Bache,[‡] Jan Larsen,[†] Mogens H. Jakobsen,[‡] and Anja Boisen[*,‡]

[†]*Department of Applied Mathematics and Computer Science, Building 305, DK-2800 Kgs. Lyngby, Denmark, and* [‡]*Department of Micro- and Nanotechnology, Ørsteds Plads, Building 345east, DK-2800 Kgs. Lyngby, Technical University of Denmark*

E-mail: Anja.Boisen@nanotech.dtu.dk

ABSTRACT

Substances like explosives, explosives derivatives, and energetic materials are extremely dangerous, even in small quantities. To this date no single measurement technology has demonstrated the desired detection performance. In the attempt to improve the overall detection accuracy, we propose a miniaturized multisensory approach for sensing explosives, in real-time with the perspective of integrating them into a handheld device. This makes our approach relevant for defense, clearance, and security applications. The sensing system, which is similar to an electronic nose, is based on the application of a unique setup of four sensors based on calorimetric, cantilever, colorimetric, and surface enhanced Raman spectroscopy. Although the sensors are yet to be integrated, we have conducted an experiment where the measurements are collected simultaneously utilizing all sensors. Hence, it is garanteed that the sensors worked under identical conditions. The identification of 2,4–dinitrotoluene as well as background molecules such as ammonium nitrate, 2,4–diaminotoluene, and diesel is demonstrated. To improve the responses from the sensors, the data is preprocessed and enhanced using methods such as least squares regression and Gaussian process regression. The preprocessed sensor responses are then identified as one

[*]To whom correspondence should be adressed

of the target analytes using a 1–nearest neighbor approach. Finally the performance of each the sensors are compared. All of the sensors were able to detect 2,4–dinitrotoluene without error, even though the chemically closely related 2,4–diaminotoluene was in the dataset. Further, it turned out at the sensors were no able to detect the other analytes without error. The individual error patterns for the sensors are not identical either, which indicates that a single integrated device containing all sensors would enhance detection performance.

A.1 Introduction

Preventing the development, production, stockpiling, transport and use of illegal explosives, is one of the most significant challenges for law enforcement agencies. The detection techniques and equipment (sensors) must not only detect a variety of hidden explosives, but must also be able to detect components that can be used for fabrication of such explosives.

For most explosives the equilibrium vapor concentration is in the range from parts-per-million (ppm) to parts-per-billion (ppb) range, making detection a challenging task. Ideally, explosive identification systems have to be quick, precise and deliver a high level of confidence. This requires reliable, selective and sensitive detection techniques that provide identification of trace amounts of explosives within a few minutes.

The minimization of false alarms[1,2] is identified as a priority in chemical sensing devices. Currently, the screening and identification of suspicious substances is often done by canine units or specialized teams which employ sophisticated methods e.g. terahertz pulsed spectroscopic imaging[3,4], gas chromatography, mass spectroscopy[5] or long-range Raman spectrometry[6]. The screening is characterized by a high assignment of personnel and high costs[7]. Furthermore, in relation to the requested volume the methods are often slow. Airport screening requires systems to handle up to 10 passengers per minute[7]. Canine units work swiftly but require breaks, have significant upkeep cost and can only be applied by expert handlers[7]

The use of detection systems based on multisensory approaches could tremendously help in the fast identification of explosives, reduce false alarms and provide new opportunities for the real-time analysis of explosives[8]. A simultaneous application of a variety of sensor techniques, which are based on different measurement principles, will enhance the collection of data where erroneous detections are statistically independent. This improves the possibility to reliably detect presence of explosives molecules with a high confidence[9,10].

The application of multisensory detection technologies has a great perspective in the identification of different analytes and today's market also show a demand for portable multisensory instruments[11–13]. These instruments are sensitive enough to detect low concentrations of analytes and can within few seconds identify common volatile compounds, such as ammonia, methane, phosphine, chlorine, carbon monoxide, hydrogen sulfide and other dangerous gases in air. For example, in the product "GDA 2" by AirSense Analytics, a combination of different sensors is applied. The product comprises an ion mobility spectrometer, a photo ionization detector, two semiconductor gas sensors and an electrochemical cell. Other detecting combinations like an array of chemical sensors[9,14,15] or a surface modified with different sensing layers can also be called a multisensory approach. While the "GDA 2" is a handheld device with a weight of 4.2 kg, we propose the use of micro- and nano sized sensors which can facilitate a handheld device that is even lighter and which can contain a multitude of sensors. These sensors also facilitate the realization of miniaturized sensor systems to be used in for example security and surveillance, potentially allowing the sensor unit to have a footprint of only a few mm^2.

The four measurement techniques that are being investigated are : calorimeter, cantilever, colorimetric array, and surface enhanced Raman spectroscopy (SERS). The utilized sensors are shown on Figure A.1.

Calorimetry is widely applied to investigate thermal properties of various samples analytes. In this work we present a micro-calorimetric sensing device (Figure A.1A) that is based on differential thermal analysis (DTA) where the temperature difference between two highly sensitive temperature sensors is measured[16–19]. One sensor is loaded with a sample analyte and the other is left blank. Using integrated heating elements both sensors are heated at a constant rate while the differential temperature is continuously measured. At certain temperatures the sample will sublimate, melt, evaporate or deflagrate which results in a change in differential temperature. Using the calorimetric sensor, we have previously demonstrated successful detection of TNT, PETN and RDX molecules[20,21].

The cantilever based sensor is an established micro- and nano-mechanical sensing tool for trace detection of bio-chemical compounds[22–24]. The response of cantilever-based sensors can be measured by monitoring change in resonance frequency of the cantilevers. A negative frequency shift is generated through mass added to the surface of the cantilevers[25,26]. Generally, the larger the resonance frequency change, the higher the amount of a given analyte is present in the sample. We measure the change in resonance frequency on chips each containing eight cantilevers (Figure A.1B)[27]. The cantilever's surface is functionalized with receptor molecules designed to specifically bind target analytes[28]. In this work cantilevers are employed in the detection of DNT molecules. For this

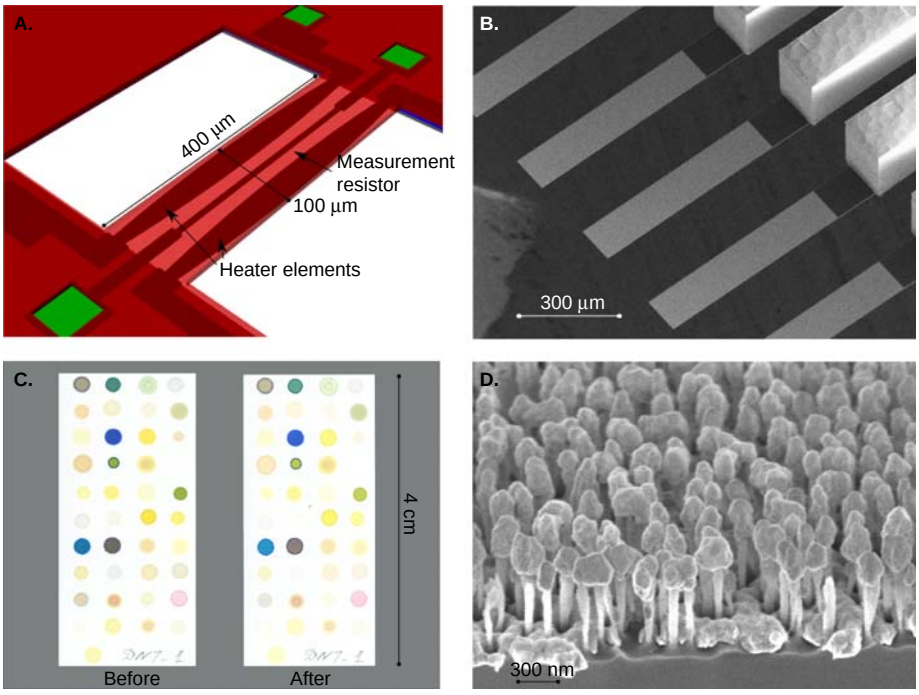

Figure A.1: Illustration of the four sensing techniques: (A). Calorimetric sensor; (B). Cantilever sensor; (C). Colorimetric sensor; (D). SERS sensor.

purpose the gold coated surface of the cantilever beams is functionalized with a tetraTTF-calix[4]pyrrole (TTF) molecule, specifically synthesized to bind nitroaromatic compounds, such as 1,3,5-trinitrobenzene (TNB), DNT and TNT[29,30]. We deploy TTF coated cantilever chips as well as untreated reference chips

Colorimetric sensing is a chemo-sensing technique which can be useful in both detection and identification of volatile organic compounds in air and liquids[31–33]. Chemo-selective compounds are capable of changing colors when exposed to analytes or analyte mixtures. The colorimetric sensor array technique (Figure A.1C) presented by Kostesha et al. showed great potential for real-time (2 minutes of analyte exposure is needed for the current sensor) monitoring of analytes such as DNT, acids, alcohols and arenes with sensitivity below ppm[15,34]. Chemo-selective compounds are capable of recognizing specific analytes; this recognition is a function of intermolecular interactions, basically weak, non-covalent interactions or donor-acceptor interactions.

SERS is increasingly used as a versatile analytical tool for both chemical and

biochemical sensors in liquid and gas phase. In fact, single molecule detection with SERS has been demonstrated[35]. SERS-based sensors rely on increasing the number of inelastically scattered photons from an analyte adsorbed on a so-called SERS substrate. A new class of SERS substrates have been developed at DTU Nanotech using standard cleanroom silicon processing techniques (Figure A.1D)[36]. This class of substrates demonstrates a signal enhancement factor of up to $7.8 \cdot 10^6$ due to plasmonic effects from a nanostructured and silver coated surface. In this paper we demonstrate how this new class of substrates can be used to greatly improve the Raman enhancement thus enabling explosives detection which is approximately a factor of 100 more sensitive than commercially available SERS substrates[36,37].

In the strategic research project Xsense funded by the Danish Agency for Science and Technology we work towards the development and implementation of four individual miniaturized sensor technologies for detection of military and improvised explosives [8,38]. By using the technologies described above (Figure A.1) it is possible to simultaneously detect explosives in trace concentrations. Our hypothesis is that sufficient reliability can be ensured by merging several independent and sensitive measuring principles. The basic scientific goal of the Xsense project is to focus on the development and refinement of the miniaturized sensors in order to achieve a detection limit towards explosives of 1 ppb (DNT and TNT being the major test molecules). A summary of the sensors characteristics and sensing principles are given in Table A.1.

A.2 Results and discussion

To confirm that our sensors work independently we conducted experiments where the sensors were sequentially exposed to the analytes: ammonium nitrate (AN), 2,4-diaminotoluene (DAT), 2,4-dinitrotoluene (DNT), and diesel. All sensors have previously been individually used for DNT detection – here we for the first time present combined measurements and data analysis on four common analytes, including potentially highly disturbing background molecules. We chose DNT as the explosive molecule as DNT is a decomposition product of TNT, the explosive most commonly deployed in landmines in the ground today. Ammonium nitrate is widely used as a fertilizer and is thus a common background molecule. Also, ammonium nitrate is a main compound in production of improvised homemade-fertilizer based bombs. DAT has been chosen since this molecule is chemically closely related to DNT; DNT carries two nitro-groups in the structure, DAT carries two amino-groups in the same positions.. Thus, DAT could cause concern about sensor selectivity and heighten false alarm rate. Diesel is chosen as an environmental disturbance that would often be present in a mine field and in post-blast scenarios, e.g. a detonated car bomb. Diesel is

Table A.1: Comparison of sensor characteristics.

Sensor characteristics	Calorimetric	Cantilever	Colorimetric	SERS
Sensing principle:	Thermal analysis of sample molecules.	Determination of mass and surface stress change	Chemical interactions: donor-acceptor, non-covalent, covalent, van der Waals, host-guest	Identification of vibrational scattering profile through Raman-based spectroscopy
Lower detection limit:	ppt [18]	ppb [39]	ppm [40]	ppm [41]
Measurement time:	1 minute	2 min for indication, 10 min for equilibrium response	2 min	5-10 min
Robustness:	Very robust	Sensitive to abrupt changes in humidity and temperature	Sensitive to light and oxygen. Robust to mechanical stress	Mechanically fragile
Working Conditions:	Gas phase	Gas and liquid phase	Gas and liquid phase	Gas and liquid phase
Sensor shelf-life [42]:	Years	Several months	Several months	Several months
Recycling time:	Chip cleaning after ∼1000 measurements	Sensor regeneration after positive detection	Single time use	Single time use
Feasibility:	Compatible with silicon-based mass production	Compatible with silicon-based mass production	Compatible with chemical micro-array mass production	Compatible with silicon-based mass production
Scalability:	Extendable to some other target analytes	Applicable to virtually any receptor-analyte assay	Applicable to almost all classes of chemical compounds	Applicable to detection of virtually any Raman-active compound

also the most widely employed fuel in heavy truck and automotive engines used by military forces and mine clearance agencies. The signal processing of the sensors responses was tailored to each sensor as the responses are very different in nature. Elaborate details on the signal processing can be found in the Supporting Information. In this section we discuss the individual response of each sensor to the four chemical compounds and show examples of sensor responses.

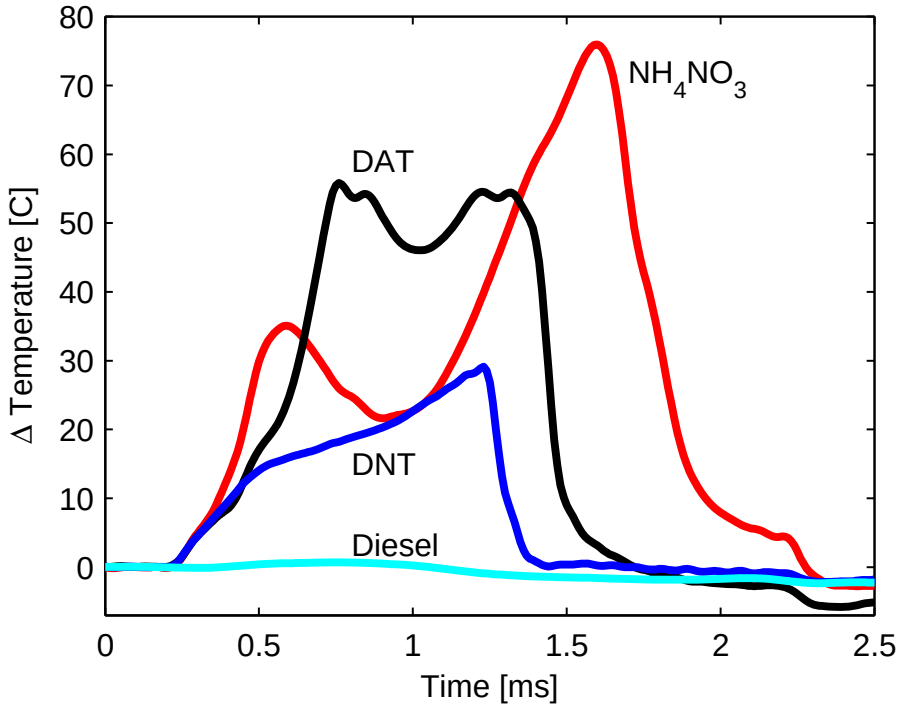

Figure A.2: Example calorimetric responses of the four target analytes after trimming and smoothing. A distinct response is obtained for each analyte due to the different thermal properties. Additional responses are found in the Supporting Information.

A.2.1 Calorimetric responses

A sample will at certain temperatures change phases and either sublimate, melt, evaporate or deflagrate which results in a change in the differential temperature in a differential thermal analysis. Figure A.2 shows the calorimetric response from the calorimetric sensor, of ammonium nitrate, DAT, DNT and diesel.

Significant and distinct responses are obtained for ammonium nitrate, DAT and DNT. A very limited response is observed for diesel. A positive ΔT means that the sample sensor is cooler than the reference sensor. The initial increase in ΔT is due to a higher thermal mass of the sensor containing the sample. Sublimation will start cooling the sample sensor further. The first peak observed for DAT and ammonium nitrate and the change in slope observed for DNT (at $\sim$0.5 ms) is due to melting of the sample. The last peak is due to sample depletion. From

an analysis of the responses after the last peaks the signal decay is observed to be fastest for DNT[21]. This is interpreted as due to deflagration whereas DAT and ammonium nitrate decay at a rate determined by the characteristic time constant of the integrated temperature sensor. The different calorimetric signatures are a result of different analytes having different vapor pressures, phase change temperatures, phase change enthalpies and thermal mass for the different phases.

The responses of the calorimetric sensor can be handled using various approaches, e.g., as described by Olsen[43]. The peak value of the sensor response gives an indication of the amount of analyte on the sensor as well as the type. Studies have shown that for explosives the shape of the sensor response is highly discriminative[43].

A.2.2 Cantilever responses

For analyte detection eight silicon-gold-coated cantilevers were functionalized using TTF molecules. As a control we used eight blank silicon-gold-coated cantilevers without immobilized TTF on the surface. The measuring principle has been described elsewhere[44].

The results show how TTF-coated cantilevers shift their resonance frequencies up to one order of magnitude more when exposed to DNT than when exposed to the other vapor samples. This behavior indicates a higher selectivity for DNT with respect to a control. As has been shown before, TTF molecules can interact with electron-deficient molecules[30], and have demonstrated high specificity to nitro-aromatic explosives such as 2,4,6-trinitrotoluene, trinitrobenzene and picric acid, respectively[45]

To evaluate signals obtained from the cantilever-based sensor a statistical analysis was performed. Figure A.3 presents the response of 64 independent cantilevers with and without TTF as a cumulative distribution function (CDF). For small sample sizes (in our case each chip provide up to N=8 measurements), the CDF will more accurately display the nature of the data compared to a plot with mean and variance. Using the CDF we can graphically display whether we expect the detection to fail or succeed.

From Figure A.3 we can see that TTF–coated cantilevers also react to DAT where a slight positive frequency shift is observed. This positive change is likely caused by both mass addition and surface properties modifications, generated from unspecific binding of molecules on both cantilever surfaces[46]. The blank cantilevers partially respond when exposed to ammonium nitrate (negative shift)

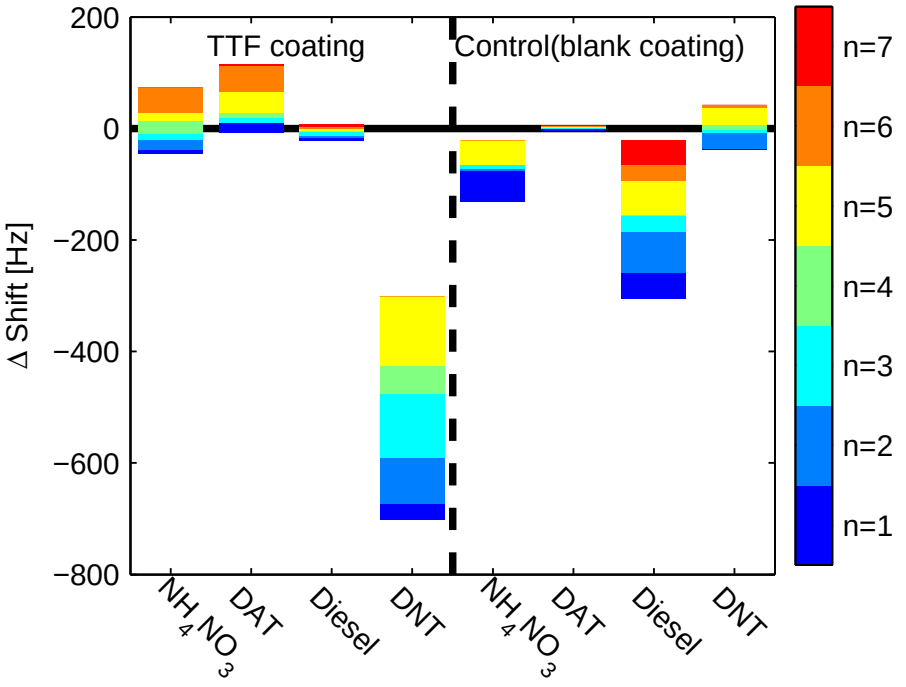

Figure A.3: Data analysis obtained from the cantiliver-based sensor on the presence of the target analytes. Data was collected from 64 independent cantilevers (eight chips), exposed to the four selected analytes. The destribution of responses are presented as a cumulative distribution function (CDF). The value of CDF is initially 0 (below the bars) and once n cantilevers have been measured, the CDF function will be n/N, where N is to total amount of measured cantilevers. Above the bars the CDF has the value 1. Due to sporadic malfunction of cantilevers, N=6 for DNT-TTF and AN-Control, N=7 for AN-TTF and DNT-Control, N=8 for remaining bars. The number of event is marked by color. Additional cantilever responses are found in the Supporting Information.

and diesel (positive shift), while they don't present significant frequency change for DAT and DNT. The blank cantilevers' response is used as reference for eliminating measurement artifacts on the TTF functionalized sensors.

The negative frequency shift generated by diesel is attributed to sticking of hydrocarbons on the cantilever surfaces. The TTF layer which covers the specific cantilevers probably acts as an oleophobic protective coating that prevents unspecific sticking of diesel on the treated surface.

A.2.3 Colorimetric responses

In the colorimetric sensor 41 chemo-selected compounds (dyes) which are able to change color in the presence of different molecules were chosen. The detecting principle of the colorimetric sensor array and the data analysis using a difference map (DM) have been described previously [15,40].

Results demonstrate that the colorimetric sensor is able to detect vapor emanating by DAT, DNT, ammonium nitrate and diesel. From the data analysis it seems that almost each chosen dye in the array reacts with the analytes of interest. Ammonium nitrate was detected by 8 dyes out of 41; where only 3 dyes in the array were particularly specific to ammonium nitrate. Diesel was detected by 5 dyes; where only 1 dye was particularly specific to diesel. DAT was detected by 6 dyes where 1 dye was specific to DAT. Finally, DNT was detected by 9 dyes where 4 of the dyes were particularly specific to DNT.

Using DM analysis it is observe that a combination of chemo-selective dyes compose a unique fingerprint for each analyte. Also, with DM analysis it is possible to study the unspecific cross-reactivity for our applied dyes. In total 10 of the dyes show similar color-change response to the analytes. Specific cross-reactivity is observed during detection of DAT and DNT, where 2 dyes demonstrated similar color change. For ammonium nitrate and DAT 3 dyes show cross-reactivity. Cross-reactivity is also observed between ammonium nitrate, DAT and diesel, as well as between DNT and diesel. However, there is no cross-reactivity observed between ammonium nitrate and DNT. DM is widely used in colorimetry. However, the color representations in DM is weak and furthermore negative color change values are eliminated (a color difference is basically calculated by taking the absolute value of a pixel value before and after exposure to an analyte). Also, for most dyes scaling is needed in order to make color differences visible. As an alternative to DM we suggest to use bar plots where each bar represents the CDF of the color change for a given dye color (RGB) when exposed to a given analyte.

Data analysis is here generated after the mathematical analysis of color changes. Mathematical algorithms were applied in order to analyze positive and negative values during color changes with statistical methods; the sensory output was put into a numerical form. As an example, Figure A.4 shows exposure responses from dye 4, dye 22 and dye 28., Those dyes were identified as significant in the array. The CDF plotting offers some advantages over the traditional DM analysis as no scaling is needed and negative values can be plotted directly on the graph.

From Figure A.4 dye number 4 shows a cross-reactive signal to ammonium

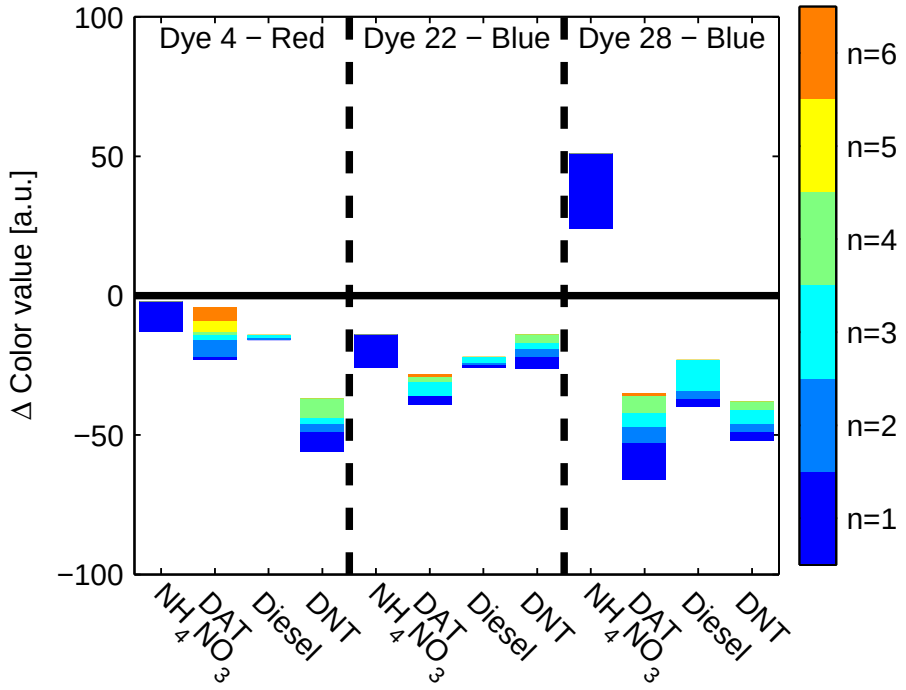

Figure A.4: Representation of response as cumulative densities function analysis for chemo-selective compounds of 4, 22 and 28 in the colorimetric sensor array when target analytes were present. Up to seven repetitions (color bar) were performed to evaluate color changes of the dyes (left axis). Bars on the scheme represent color changes after calculation of the median and probability values of the signal. N=2 for AN, N=7 for DNT, N=4 for Diesel and N=5 for DNT. Additional responses are found in the Supporting Information.

nitrate, DAT and diesel; however the specific signal is demonstrated for DNT only. Dyes number 22 and 28 show unique responses to all analytes. In the presence of DAT the dye number 22 turned from green to pink. However, in the presence of other analytes the same dye exhibited color change from green to transparent or light green in different intensity. For dye number 28 a positive value for color changes was observed for ammonium nitrate. In the presence of ammonium nitrate the light green color of the dye turned to dark green, while in the presence of other analytes the dye changed color from light green to yellow.

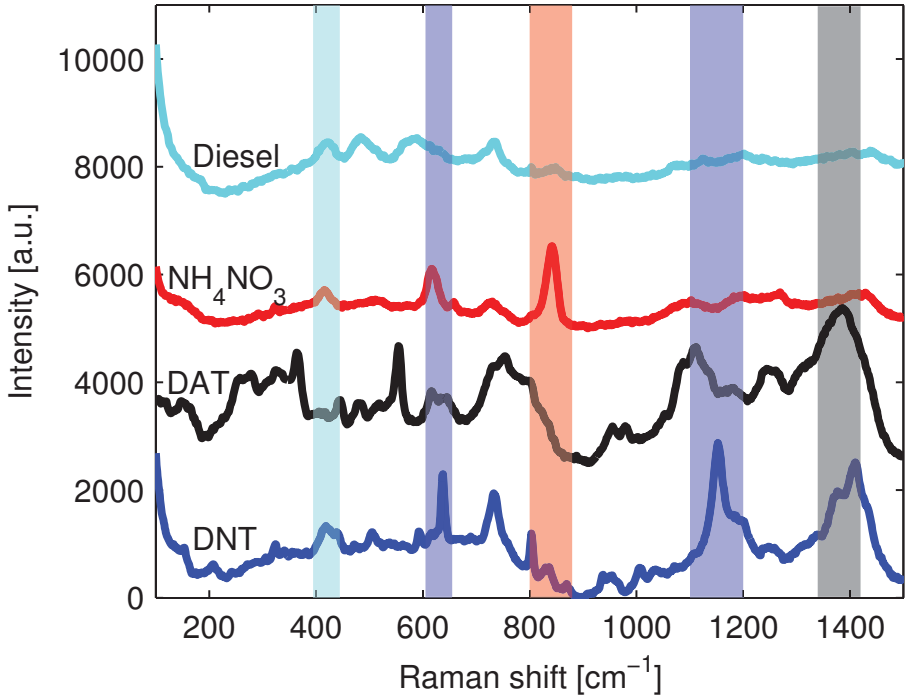

Figure A.5: Example responses of Raman signals from SERS substrates when exposed to target. It is seen that the peaks defining DNT are not found in the spectra from the other substances thus enabling DNT to be distinguished from the potential background substances. The horizontal bars mark the frequency intervals where notable peaks should occur for the given analyte. Additional details on responses are found in the Supporting Information.

A.2.4 SERS responses

The exposure results of the SERS surface to DAT, DNT, ammonium nitrate and diesel show a specific spectrum for each compound. Figure A.5 shows the various spectra with the peak areas of interest highlighted.

For the recorded DNT spectrum the areas of interest are around 650 cm^{-1} and 1150 cm^{-1}. These peaks are shifted compared to the bulk Raman values of pure DNT crystals found in literature where the nitro groups give origin to a distinct peak at around 1350 cm^{-1} and 1530 cm^{-1}. The origin of the measured peaks is thus difficult to identify[47]. Ammonium nitrate has a single distinct peak at 850 cm^{-1} and 650 cm^{-1}, again this is $\sim$200 cm^{-1} lower when comparing with

bulk measurements in literature, where the nitrate symmetric stretch at 1040 cm^{-1} and the nitrate in-plane bending mode at 712 cm^{-1} are the recognizable peaks[48].

When comparing the DNT spectrum with the DAT spectrum a clear distinction to DNT can be seen as DAT has a large peak at 1300-1400 cm^{-1} and an additional peak at 500 cm^{-1}.

The spectrum of diesel shows a comparable flat profile. This is expected as diesel is usually composed by a complex mixture of saturated and aromatic carbon compounds of a 8-22 chain length and often diesel includes other additives to improve the engines combustion performance. The fouling properties of diesel and large variety of composition can thus coat a sensor surface and potentially overshadow a signal from DNT[49,50].

A.2.5 Classification and combined responses

A careful mathematical analysis was performed to statistically analyze responses obtained from calorimetric, cantilever, colorimetric and SERS-based sensors. In this paper we used new methods for extracting features from all sensors and to categorize and evaluate signals in order to understand the efficiency of sensing technologies for detecting military and improvised explosives. By using machine learning classifiers the quality and robustness of these features were determined.

Applied sensors must not only be able to classify explosives, explosive derivatives and volatile organic compounds. They must also be able to measure the certainty of the classifier. This means there is a need for classifiers that not only give a decision, but also give a posterior probability about the decision. The pre-calibration of the system or the application of libraries (classifiers) allows with high precision to identify a broad range of target compounds.

All the sensors were able to give positive responses to DNT, but in order to assess the recognition performance of each sensor we have created an artificial classification system. Prior to the classification system each sensor output is processed using a custom made signal processing system. As the sensor responses are of very different nature each sensor has a unique signal processing system which is described in the supporting information. The classification system consists of the 1-Nearest Neighbor classification method[51] as this method is easy to apply when few examples of measurements exist. The method classifies each measurement in turn and treats this measurement as unknown. The measurement is compared to all the other measurements which are treated as known and then selecting the measurement that most resembles the unknown

measurement. The unknown measurement is classified as the same analyte as the known measurement. The classification results are illustrated as confusion matrices shown in Figure A.6.

The array of sensors demonstrated a high classification rate for explosives, like DNT with zero false negatives. The calorimetric sensor (Figure A.6A) made one misclassification which is an ammonium nitrate sample which was detected as DAT. The cantilever sensor (Figure A.6B) was very unreliable for ammonium nitrate, DAT and diesel; DNT was detected with high precision. This was expected as the cantilever-based sensor only operated with a TTF-coating that is specifically designed to detect DNT and similar analytes. The colorimetric sensor is a more specific sensor compared to calorimetric and cantilever sensors. The colorimetric sensor comprises 41 unique chemo-selective compounds, including 25 TTFs (Figure A.1C). The results (Figure A.6C) show that this sensor is able to detect all analytes; the sensor was able to detect DNT with both zero false negatives and zero false positives (all 5 measurements were classified correctly), also ammonium nitrate and diesel gave zero false negatives. DAT showed one false positive and control measurements (environment) gave two false positives responses (one for DAT and one for diesel).

The SERS sensor is a more specific sensor compared to the colorimetric sensor as our SERS sensor scans 2000 frequencies. SERS makes a perfect classification (Figure A.6D) although it should be remarked (as described in section 2.4) that diesel is not actually detected as it consists of a mixture of different length carbon chains that read out as a broad Raman signature overlapping with that of many carbon based analytes. The confusion matrix shows that diesel does not give rise to false alarms. In general, the sensors have a high detection rate and it is quite possible that the false alarms could be lowered significantly or even extinguished entirely if more measurements are made as this would not only give more knowledge of the sensor but also make more sophisticated classification systems applicable.

To summarize how the sensors complement each other we draft up all detection rates in Table A.2. The table shows that DNT is detected in all cases for all four sensors. The higher dimensional sensors (colorimetric and SERS) are the most specific making very few detection mistakes.

A.3 Conclusions

From our experiments we can conclude that the most versatile sensor seems to be the colorimetric sensor as this sensor was able to positively detect all the tested analytes only making one misclassification to DAT. However, the sensor also had

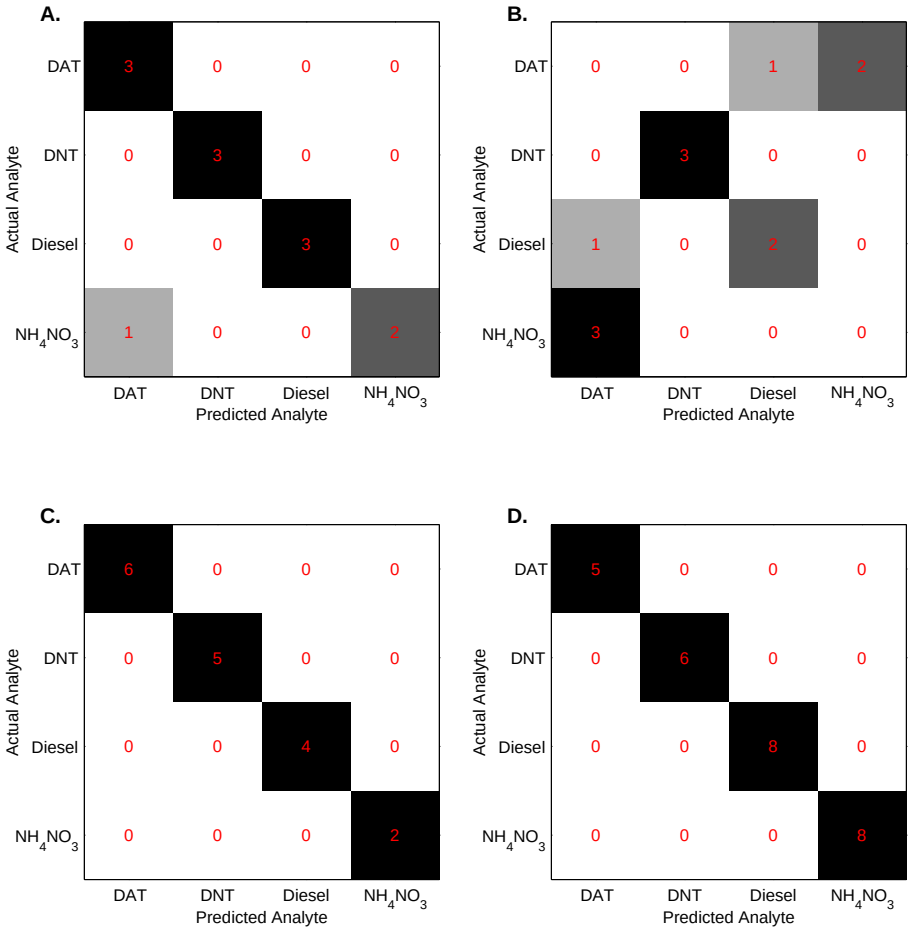

Figure A.6: Confusion matrix presenting the responses of the sensors on the presence of ammonium nitrate, DAT, DNT and diesel calculated using 1-NN. A. Calorimetry – classification rate of 11/12; B. Cantilever – classification rate of 5/12; C. Colorimetric – classification rate of 17/17[52]; D. SERS – classification rate of 27/27. Herein, rows indicate the true class; columns indicate the predicted class and the number indicate the counts; e.g. for A. two of the ammonium nitrate measurements was correctly identified as ammonium nitrate while one measurement was incorrectly identified as DAT. Each element in the matrix is colored based on the number of measurements classified according to the given matrix element relative to the total number of measurements. The more measurements in the element the darker the element is.

Table A.2: Detection rates of the four sensors. False positives are not included in the table although it should be emphasized that there are neither false positives nor false negatives for DNT. Some scenarios are marked as no detection (N.D.) as by inspecting the sensor response it was deemed that the sensor was not able to detect the analyte in question, but only show that the analyte was not causing false alarms for DNT.

Analyte	Calorimetric	Cantilever	Colorimetric	SERS
DAT	3/3	N.D	6/7	5/5
DNT	3/3	3/3	5/5	6/6
Diesel	N.D	N.D	4/4	N.D
NH_4NO_3	2/3	N.D	2/2	8/8

two false alarms, one for DAT and one for diesel which indicates that the sensor at times may be too sensitive. Based on Table A.2 the calorimetric and SERS sensors have in this experimental setup very similar properties. The advantage of the calorimetric sensor (Table A.1) is that the sensor can conduct hundreds of repeated measurements without requiring cleaning or manual operation, and therefore this sensor is ideal to use as a screener before applying samples to the other sensors. The cantilever requires cleaning between each measurement while colorimetric and SERS are single disposable sensors, thus it is desirable to apply these sensors only if a sample has a suspicious content. These results encourage the fabrication of a sensor network of the sensors and conduct a larger scale experiment where sensor fusion is applied.

In this paper we have shown that by establishing a network of four miniaturized independent sensors the reliability in explosives detection can potentially be improved significantly. Proof of the concept has been confirmed for all four sensor technologies hence the ongoing effort is thus in optimizing sensitivity and integrating all the sensors into one device. The inherent design qualities of the completed device should enable its use by personnel with minimal training thus making explosives detection capabilities accessible beyond trained dog teams. The proposed system has potential to be highly suitable for the use in anti-terror efforts, border control, monitoring of environment and mine clearance. Future work will include system integration of sensors which would enable the possibility for collecting simultaneous measurements from all sensors. The system integration would facilitate automatic data collection that will provide sufficient data to enable the possibility of using a data fusing classification algorithm.

A.4 Experimental

Analytes that has been exposed to sensors: 2,4-diaminotoluene (DAT), 2,4-dinitrotoluene (DNT), ammonium nitrate were all from Sigma (St. Louise, MO, USA). Diesel was used as received from a Shell petrol station.

A.4.1 Sensor preparations

The colorimetric sensor array consists of 41 different chemo-selective compounds selected from a set of compounds described by Kostesha et al[53]. SERS substrates were developed as described by Schmidt et al[54]. The cantilevers fabrication and modification was reported by Bosco et al[44]. Calorimetric chips were fabricated following the protocol developed by Olsen et al[16–19]. Tetrathiafulvalene–Calix[4]pyrroles are used in the fabrication of the colorimetric sensor array as well as coating for the cantilevers[30].

A.4.2 Experimental setup

All the measurements were conducted using a vapor generator which was built and tested at Technical University of Denmark, Department of Micro- and Nanotechnology. The generator used the principle where a nitrogen gas is passed through a heated reservoir containing the analyte of interest. An illustration of the vapor generator system can be seen in Figure A.7. Deposition is done by placing a sensor close to the exhaust of the system making the analyte condense on the sensor surface.

It consists of an explosive reservoir, an oven, a mass flow controller and various fittings. The explosive reservoir is a copper tube containing glass wool. The analytes DAT, DNT and ammonium nitrate was first dissolved and then injected in the glass wool using a syringe whereas diesel was injected without treatment. Ethanol was used for DAT and DNT and water for ammonium nitrate. Before the reservoir was ready for use solvent was first evaporated at low temperature. The copper tube was inserted into the heating oven and connected to a nitrogen flow connector, controlled by a mass flow controller. When the nitrogen flowed through the heated reservoir it became saturated with the analyte. By reducing the nozzle diameter to 2 mm the velocity of the hot saturated vapor was increased. The cantilever, calorimetry and SERS surface sensors were kept at approximately 1 mm distance from the nozzle opening for 2 minutes, thus a part of the analyte condensated on the sensor surface. The colorimetric sensor

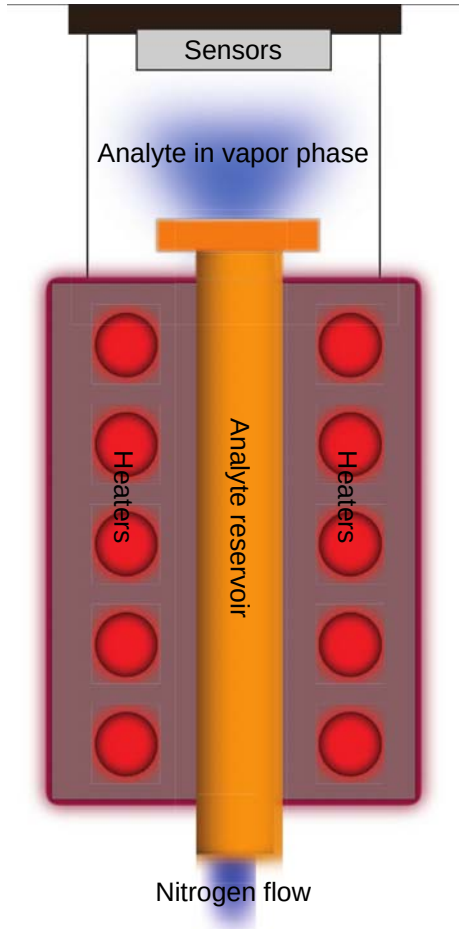

Figure A.7: Illustration of the vapor generator used for deposition of analytes onto the sensors.

was only exposed to the analyte vapors at a greater distance from the nozzle opening.

Pictures from the colorimetric sensor were scanned through an ordinary flatbed scanner (Epson V750-M Pro Perfection scanner) immediately after immobilization of dyes and after exposure of analytes. Pictures were obtained at 600 dots per inch in RGB color format. Data analysis obtained from the colorimetric sensor was analyzed as described in earlier work[31,34]. Raman measurements were performed using 780 nm wavelength excitation at a power of 0.5 mW for 2 seconds. The laser spot diameter was 3.1 μm. Raman measurements were made

on SERS substrates where silver coated nanopillars were in the pre-leaned, post-leaned and non-leaning configurations[54]. The nanopillars were brought to lean by 1 μL water.

A.4.3 Signal Processsing

The calorimetry sensor response is contaminated by white measurement noise. We smooth the response by using Gaussian Process regression[55] as this method effectively removes the noise and at the same time we do not need to concern about choosing model parameters. The smoothed responses are directly applied to the 1-NN classifier.

Our cantilever measurement system collects readout of the entire cantilever surface for each cantilever on the chip, thus one measurement consist of 8 cantilever surface readouts, where one surface contains multiple readouts. These readouts are reduced to a single value by taking the mean bending of the entire surface[44]. All measurements are manually inspected as cantilevers on occasion malfunctions. In these cases the measurement is regarded as not available. The final measurement that is applied to the 1-NN classifier is the mean value of the TTF coated cantilevers subtracted with the mean value of the blank cantilevers.

The colorimetric sensor response is a pair of images; an image of the clean sensor and an image of the exposed sensor. The colorimetric sensor response undergoes several steps before the response is applied to the 1-NN classifier[56]. The final result is one RGB value from each dye is selected and concatenated into one vector for each measurement. These vectors are applied to the classifier.

The SERS responses are baseline corrected using a 5th order polynomial calculated using least squares regression. The functional values of the polynomial is then subtracted from the original response and then normalized. The spectrum in the interval [100,1000] is then applied to the 1-NN classifier. To make the classification we train one 1-NN classifier per reading mode (pre-bending, post-bending, no bending) and then make the final prediction using majority voting.

Acknowledgement

We acknowledge the financial support from the Danish Agency for Science and Technology's, Program Commission on Nanoscience Biotechnology and IT (NABIIT). Case number: 2106-07-0031 – Xsense - Miniaturized sensors for ex-

plosives detection in air. We acknowledge Kent A. Nielsen, Carsten Johnsen and Jan O. Jeppesen, Department of Physics and Chemistry, University of Southern Denmark for providing TTF molecules for the cantilever and colorimetric sensors. Finally we thank Mads S. Jensen from Danish Emergency Management Agency for providing insight regarding current challenges on explosives detection for intelligence agencies.

Supporting Information Available

The full data set will be described in the Supporting Information document. The data set is not showed in this text in completeness; however the full collection of data accompanied with supporting MATLAB^{TM} scripts that was used to produce all figures in this paper as well as the signal processing modules can be downloaded at http://www.imm.dtu.dk/pubdb/p.php?6401

A.5 REFERENCES

[1] Yanghai Gui, Changsheng Xie, Jiaqiang Xu, and Guoqing Wang. Detection and discrimination of low concentration explosives using MOS nanoparticle sensors. *Journal of hazardous materials*, 164(2-3):1030–5, May 2009. ISSN 1873-3336. doi: 10.1016/j.jhazmat.2008.09.011.

[2] Jehuda Yinon. Detection of Explosives by Electronic Noses. *Analytical Chemistry*, 75(5):98 A–105 A, March 2003. ISSN 0003-2700. doi: 10.1021/ac0312460.

[3] Michael J. Fitch, Megan R. Leahy-Hoppa, Edward W. Ott, and Robert Osiander. Molecular absorption cross-section and absolute absorptivity in the THz frequency range for the explosives TNT, RDX, HMX, and PETN. *Chemical Physics Letters*, 443(4–6):284–288, August 2007. ISSN 0009-2614. URL http://www.sciencedirect.com/science/article/pii/S0009261407008676.

[4] Jeffrey Barber, Daniel E. Hooks, David J. Funk, Richard D. Averitt, Antoinette J. Taylor, and Dmitri Babikov. Temperature-Dependent Far-Infrared Spectra of Single Crystals of High Explosives Using Terahertz Time-Domain Spectroscopy. *The Journal of Physical Chemistry A*, 109 (15):3501–3505, March 2005. ISSN 1089-5639. doi: 10.1021/jp044384h. URL http://dx.doi.org/10.1021/jp044384h.

[5] Stacy-Ann Barshick and Wayne H. Griest. Trace Analysis of Explosives in Seawater Using Solid-Phase Microextraction and Gas Chromatography/Ion

Trap Mass Spectrometry. *Analytical Chemistry*, 70(14):3015–3020, May 1998. ISSN 0003-2700. doi: 10.1021/ac980060b. URL http://dx.doi.org/10.1021/ac980060b.

[6] J. Chance Carter, S. Michael Angel, Marion Lawrence-Snyder, Jon Scaffidi, Richard E. Whipple, and John G. Reynolds. Standoff Detection of High Explosive Materials at 50 Meters in Ambient Light Conditions Using a Small Raman Instrument. *Applied spectroscopy*, 59(6):769–775, June 2005. URL http://as.osa.org/abstract.cfm?URI=as-59-6-769.

[7] Dana A. Shea and Daniel Morgan. Detection of explosives on airline passengers: Recommendation of the 9/11 Commission and related issues. *CRS Report for Congress*, April(RS21920):1–6, 2007. URL http://oai.dtic.mil/oai/oai?verb=getRecord&metadataPrefix=html&identifier=ADA453711.

[8] Xsense. Xsense - Miniaturized Sensors for Explosives Detection in Air, 2012. URL http://www.xsense.dk.

[9] Joseph R. Stetter, S. Strathmann, Carol McEntegart, Maylin Decastro, and William R. Penrose. New sensor arrays and sampling systems for a modular electronic nose. *Sensors and Actuators B: Chemical*, 69(3):410–419, October 2000. ISSN 0925-4005. URL http://www.sciencedirect.com/science/article/pii/S0925400500005037.

[10] Baranidharan Raman, Douglas C. Meier, Jon K. Evju, and Steve Semancik. Designing and optimizing microsensor arrays for recognizing chemical hazards in complex environments. *Sensors and Actuators B: Chemical*, 137(2):617–629, April 2009. ISSN 0925-4005. URL http://www.sciencedirect.com/science/article/pii/S0925400508008125.

[11] AIRSENSE Analytics, 2012. URL http://www.airsense.com/en.

[12] RKI Instruments, Inc., 2012. URL http://www.rkiinstruments.com.

[13] Industrial Scientific, 2012. URL http://www.indsci.com.

[14] Kenneth S. Suslick, Keren I. Hulkower, Avijit Sen, Mitchell A. Sroka, and William B. McNamara III. Method and apparatus for detecting ammonia from exhaled breath, August 2004.

[15] Natalie V. Kostesha, Tommy S. Alstrøm, Carsten Johnsen, Kent A. Nielsen, Jan O. Jeppesen, Jan Larsen, Mogens H. Jakobsen, and Anja Boisen. Development of the colorimetric sensor array for detection of explosives and volatile organic compounds in air. In *Proceedings of SPIE*, volume 7673, pages 76730I–76730I–9, 2010. doi: 10.1117/12.850310.

[16] Dechang Yi, Anders Greve, Jan H. Hales, Larry R. Senesac, Zachary J. Davis, Don M. Nicholson, Anja Boisen, and Thomas Thundat. Detection of adsorbed explosive molecules using thermal response of suspended microfabricated bridges. *Applied Physics Letters*, 93(15): 154102, October 2008. ISSN 00036951. doi: DOI:10.1063/1.3002285. URL http://dx.doi.org/doi/10.1063/1.3002285http://link.aip.org/link/?APPLAB/93/154102/1.

[17] Dechang Yi, Larry Senesac, and Thomas Thundat. Speciation of Energetic Materials on a Microcantilever Using Surface Reduction. *Scanning*, 30(2):208–212, 2008. ISSN 1932-8745. doi: 10.1002/sca.20096. URL http://dx.doi.org/10.1002/sca.20096http://www.ncbi.nlm.nih.gov/pubmed/18288710.

[18] Larry R. Senesac, Dechang Yi, Anders Greve, Jan H. Hales, Zachary J. Davis, Don M. Nicholson, Anja Boisen, and Thomas Thundat. Micro-differential thermal analysis detection of adsorbed explosive molecules using microfabricated bridges. *Review of Scientific Instruments*, 80 (3):35102, March 2009. ISSN 1089-7623. doi: 10.1063/1.3090881. URL http://link.aip.org/link/?RSI/80/035102/1http://link.aip.org/link/?RSINAK/80/035102/1.

[19] Anders Greve, Jesper K. Olsen, Natalya L. Privorotskaya, Larry R. Senesac, Thomas Thundat, William P. King, and Anja Boisen. Micro-calorimetric sensor for vapor phase explosive detection with optimized heat profile. *Microelectronic Engineering*, 87(5-8):696–698, May 2010. ISSN 0167-9317. doi: 10.1016/j.mee.2009.12.069. URL http://www.sciencedirect.com/science/article/pii/S0167931709009125http://dx.doi.org/10.1016/j.mee.2009.12.069.

[20] Jesper K. Olsen, Anders Greve, Larry R. Senesac, Thomas Thundat, and Anja Boisen. Differential thermal analysis microsystem for explosive detection. In Thomas George, M Saif Islam, and Achyut K Dutta, editors, *Micro- and Nanotechnology Sensors, Systems, and Applications III*, volume 8031, page 80312P. SPIE, 2011. doi: 10.1117/12.883960. URL http://link.aip.org/link/?PSI/8031/80312P/1.

[21] Jesper K. Olsen, Larry R. Senesac, Thomas Thundat, and Anja Boisen. Trace explosives detection by micro differential thermal analysis. In *Micro Electro Mechanical Systems (MEMS), 2011 IEEE 24th International Conference on*, pages 984–987, 2011. ISBN 1084-6999 VO -.

[22] Roberto Raiteri, Massimo Grattarola, Hans-Jürgen Butt, and Petr Skládal. Micromechanical cantilever-based biosensors. *Sensors and Actuators B: Chemical*, 79(2–3):115–126, October 2001. ISSN 0925-4005. URL http://www.sciencedirect.com/science/article/pii/S0925400501008565.

[23] Jurgen Fritz. Cantilever biosensors. *Analyst*, 133(7):855–863, 2008. ISSN 0003-2654. URL http://dx.doi.org/10.1039/B718174D.

[24] Anja Boisen, Søren Dohn, Stephan S. Keller, Silvan Schmid, and Maria Tenje. Cantilever-like micromechanical sensors. *Reports on Progress in Physics*, 74(3):36101, 2011. ISSN 0034-4885. URL http://stacks.iop.org/0034-4885/74/i=3/a=036101.

[25] Jurgen Fritz, Marko K. Baller, Hans P. Lang, Hugo E. Rothuizen, Peter Vettiger, Ernst Meyer, Hans-Joachim Güntherodt, Christoph Gerber, and James K. Gimzewski. Translating Biomolecular Recognition into Nanomechanics. *Science*, 288(5464):316–318, 2000. doi: 10.1126/science.288.5464.316. URL http://www.sciencemag.org/content/288/5464/316.abstract.

[26] Maria L. Sushko, John H. Harding, Alexander L. Shluger, Rachel A. McKendry, and Moyu Watari. Physics of Nanomechanical Biosensing on Cantilever Arrays. *Advanced Materials*, 20(20):3848–3853, 2008. ISSN 1521-4095. doi: 10.1002/adma.200801344. URL http://dx.doi.org/10.1002/adma.200801344.

[27] Filippo G. Bosco, En-Te Hwu, and Anja Boisen. High-throughput readout system for cantilever-based sensing of explosive compounds. In Thomas George, M Saif Islam, and Achyut K Dutta, editors, *Micro- and Nanotechnology Sensors, Systems, and Applications II*, volume 7679, page 767925. SPIE, 2010. doi: 10.1117/12.850008. URL http://link.aip.org/link/?PSI/7679/767925/1.

[28] James K. Gimzewski, Christoph Gerber, Ernst Meyer, and Reto R. Schlittler. Observation of a chemical reaction using a micromechanical sensor. *Chemical Physics Letters*, 217(5–6):589–594, 1994. ISSN 0009-2614. doi: 10.1016/0009-2614(93)E1419-H. URL http://www.sciencedirect.com/science/article/pii/0009261493E1419H.

[29] Kent A. Nielsen, Won-Seob Cho, Jan O. Jeppesen, Vincent M. Lynch, Jan Becher, and Jonathan L. Sessler. Tetra-TTF Calix[4]pyrrole: A Rationally Designed Receptor for Electron-Deficient Neutral Guests. *Journal of the American Chemical Society*, 126(50):16296–16297, November 2004. ISSN 0002-7863. doi: 10.1021/ja044664a.

[30] Jung S. Park, Franck Le Derf, Christopher M. Bejger, Vincent M. Lynch, Jonathan L. Sessler, Kent A. Nielsen, Carsten Johnsen, and Jan O. Jeppesen. Positive Homotropic Allosteric Receptors for Neutral Guests: Annulated Tetrathiafulvalene–Calix[4]pyrroles as Colorimetric Chemosensors for Nitroaromatic Explosives. *Chemistry - A European Journal*, 16(3):848–54, January 2010. ISSN 1521-3765. doi: 10.1002/chem.200902924.

[31] Natalie V. Kostesha, Tommy S. Alstrøm, Carsten Johnsen, Kent A. Nielsen, Jan O. Jeppesen, Jan Larsen, Anja Boisen, and Mogens H. Jakobsen. Multi-colorimetric sensor array for detection of explosives in gas and liquid phase. In *Proceedings of SPIE*, volume 8018, pages 80181H–80181H–12, 2011. doi: 10.1117/12.883895.

[32] Chen Zhang and Kenneth S. Suslick. A colorimetric sensor array for organics in water. *Journal of the American Chemical Society*, 127(33):11548–9, August 2005. ISSN 0002-7863. doi: 10.1021/ja052606z.

[33] Kent A. Nielsen, Luis Martín-Gomis, Ginka H. Sarova, Lionel Sanguinet, Dustin E. Gross, Fernando Fernández-Lázaro, Paul C. Stein, Eric Levillain, Jonathan L. Sessler, Dirk M. Guldi, Ángela Sastre-Santos, and Jan O. Jeppesen. Binding studies of tetrathiafulvalene-calix[4]pyrroles with electron-deficient guests. *Tetrahedron*, 64(36):8449–8463, September 2008. ISSN 0040-4020. URL http://www.sciencedirect.com/science/article/pii/S0040402008010740.

[34] Tommy S. Alstrøm, Jan Larsen, Natalie V. Kostesha, Mogens H. Jakobsen, and Anja Boisen. Data representation and feature selection for colorimetric sensor arrays used as explosives detectors. In *IEEE International Workshop on Machine Learning for Signal Processing (MLSP)*, pages 1–6, 2011. doi: 10.1109/MLSP.2011.6064615.

[35] Kneipp Kneipp, Yang Wang, Harald Kneipp, Lev T. Perelman, Irving Itzkan, Ramachandra R. Dasari, and Michael S. Feld. Single molecule detection using surface-enhanced Raman scattering (SERS). *Physical Review Letters*, pages 1667–1670, 1997. URL http://link.aps.org/doi/10.1103/PhysRevLett.78.1667.

[36] Ivan Talian, Klaus B. Mogensen, Andrej Oriňák, Dušan Kaniansky, and Jörg Hübner. Surface-enhanced Raman spectroscopy on novel black silicon-based nanostructured surfaces. *Journal of Raman Spectroscopy*, 40(8):982–986, 2009. ISSN 1097-4555. URL http://dx.doi.org/10.1002/jrs.2213.

[37] Klarite. Klarite, 2012. URL http://www.d3technologies.co.uk.

[38] Michael S. Schmidt, Natalie V. Kostesha, Filippo G. Bosco, Jesper K. Olsen, Carsten Johnsen, Kent A. Nielsen, Jan O. Jeppesen, Tommy S. Alstrøm, Jan Larsen, Thomas Thundat, Mogens H. Jacobsen, and Anja Boisen. Xsense - a miniaturised multi-sensor platform for explosives detection. In *Proceedings of SPIE*, volume 8031, pages 803123–803123–7, 2011. doi: 10.1117/12.884050.

[39] Jessica L. Arlett, Edward B. Myers, and Michael L. Roukes. Comparative advantages of mechanical biosensors. *Nature Nanotechnology*, 6(4):203–215,

April 2011. ISSN 1748-3387. URL http://dx.doi.org/10.1038/nnano.2011.44.

[40] Kenneth S. Suslick, Neal A. Rakow, and Avijit Sen. Colorimetric sensor arrays for molecular recognition. *Tetrahedron*, 60(49):11133–11138, November 2004. ISSN 00404020. doi: 10.1016/j.tet.2004.09.007.

[41] Desiree S. Grubisha, Robert J. Lipert, Hye-Young Park, Jeremy Driskell, and Marc D. Porter. Femtomolar Detection of Prostate-Specific Antigen: An Immunoassay Based on Surface-Enhanced Raman Scattering and Immunogold Labels. *Analytical Chemistry*, 75(21):5936–5943, September 2003. ISSN 0003-2700. doi: 10.1021/ac034356f. URL http://dx.doi.org/10.1021/ac034356f.

[42] The sensors should be carefully sealed as they will react with the environment swiftly

[43] Jesper Kenneth Olsen. *Micro Calorimetric Sensors for Explosives Detection*. PhD thesis, Technical University of Denmark (DTU), 2011.

[44] Filippo G. Bosco, En-Te Hwu, Ching-Hsiu Chen, Stephan Keller, Michael Bache, Mogens H. Jakobsen, Ing-Shouh Hwang, and Anja Boisen. High throughput label-free platform for statistical bio-molecular sensing. *Lab Chip*, 11(14):2411–2416, 2011. doi: 10.1039/C1LC20116F. URL http://dx.doi.org/10.1039/C1LC20116F.

[45] Dae-Sik Kim, Vincent M. Lynch, Kent A. Nielsen, Carsten Johnsen, Jan O. Jeppesen, and Jonathan L. Sessler. A chloride-anion insensitive colorimetric chemosensor for trinitrobenzene and picric acid. *Analytical and bioanalytical chemistry*, 395(2):393–400, 2009. doi: 10.1007/s00216-009-2819-4.

[46] Javier Tamayo, Daniel Ramos, Johan Mertens, and Montserrat Calleja. Effect of the adsorbate stiffness on the resonance response of microcantilever sensors. *Applied Physics Letters*, 89(22):224104, 2006. doi: 10.1063/1.2388925. URL http://link.aip.org/link/?APL/89/224104/1.

[47] Alejandro Blanco, Nairmen Mina, Miguel E. Castro, Jairo Castillo-Chara, and Samuel P. Hernandez-Rivera. Spectroscopic investigation of the spectroscopic signatures of 2,4-DNT and 2,6-DNT: their interactions with sand particles. In Russell S Harmon, J Thomas Broach, John H Holloway, and Jr., editors, *Detection and Remediation Technologies for Mines and Minelike Targets IX*, volume 5415, pages 1357–1366. SPIE, 2004. doi: 10.1117/12.542870. URL http://link.aip.org/link/?PSI/5415/1357/1.

[48] Esam M. A. Ali, Howell G. M. Edwards, and Ian J. Scowen. In-situ detection of single particles of explosive on clothing with confocal Raman microscopy. *Talanta*, 78(3):1201–1203, May 2009. ISSN

0039-9140. URL http://www.sciencedirect.com/science/article/pii/S0039914008009211.

[49] Michael J. Kleeman, James J. Schauer, and Glen R. Cass. Size and Composition Distribution of Fine Particulate Matter Emitted from Motor Vehicles. *Environmental Science & Technology*, 34(7):1132–1142, February 2000. ISSN 0013-936X. doi: 10.1021/es981276y. URL http://dx.doi.org/10.1021/es981276y.

[50] John W. Haas III, James M. Sylvia, Kevin M. Spencer, Thomas M. Johnston, and Susan L. Clauson. Surface-enhanced Raman sensor for nitroexplosive vapors. In Abinash C Dubey, James F Harvey, and J Thomas Broach, editors, *Detection and Remediation Technologies for Mines and Minelike Targets III*, volume 3392, pages 469–476. SPIE, 1998. doi: 10.1117/12.324179. URL http://link.aip.org/link/?PSI/3392/469/1.

[51] Christopher M. Bishop. *Pattern Recognition and Machine Learning*. Springer, Secaucus, NJ, USA, 2006. ISBN 0387310738.

[52] The colorimetric sensor contained 5 additional control measurements where three of them resulted in false alarms; hence the classification rate is 19/22. See Supporting Information for details.

[53] Jan O. Jeppesen, Natalie V. Kostesha, Carsten Johnsen, Kent A. Nielsen, Anja Boisen, and Mogens H. Jakobsen. Multisensor array useful for detection and/or identification of an analyte (e.g. amines, alcohols, ketones and thiols) in the gas phase or in the liquid phase, comprises at least two different chemo-selective heteroaryl compounds, 2011.

[54] Michael S. Schmidt, Jörg Hübner, and Anja Boisen. Large Area Fabrication of Leaning Silicon Nanopillars for Surface Enhanced Raman Spectroscopy. *Advanced Materials*, pages OP11–OP18, November 2011. ISSN 09359648. doi: 10.1002/adma.201103496. URL http://www.ncbi.nlm.nih.gov/pubmed/22105972.

[55] Carl E. Rasmussen and Christopher K. I. Williams. *Gaussian Processes for Machine Learning*. MIT Press, April 2006. URL http://www.gaussianprocess.org/gpmlhttp://www.ncbi.nlm.nih.gov/pubmed/15112367.

[56] Tommy S. Alstrøm and Jan Larsen. Feature Extraction and Signal Representation for Colorimetric Sensor Arrays. Technical report, DTU Informatics, 2011. URL http://www.imm.dtu.dk/pubdb/p.php?5845.

A.6 Supporting Information for "Miniaturized multisensory approach for the highly sensitive and selective detection of explosives"

A.6.1 Sensor responses and signal processing

Herein the full data set will be described. The data set is not showed in this text in completeness; however the full collection of data accompanied with supporting MATLAB^{TM} scripts that was used to produce all figures in this paper as well as the signal processing modules can be downloaded at http://www.imm.dtu.dk/pubdb/p.php?6401.

The measurements are done in four consecutive days where each analyte is tested in one day. The reason for doing it on different days is that the vapor generator needs thorough cleaning when changing the analyte to avoid possible cross contaminations. The change takes some time and makes it impossible with our current experimental setup to measure on different analytes in the same day.

For all the sensors except SERS, DNT, DAT and diesel are all evaporated at 70°C with a 2 mm distance to a to a 2 mm nozzle opening for 2 minutes (DAT was handled differently for the calorimetric sensor, see 1.1 in this supporting information). Due to the much lower vapor pressure of ammonium nitrate the temperature was increased to 250°C to get comparable amounts of added mass for a 2 minute evaporation time. SERS chips are evaporated using the same settings except for evaporation time. Only a 1 minute evaporation time is used as 2 minute evaporation time causes crystallizations of analyte on the surface.

A.6.1.1. The calorimetric sensor

Figure A.8 shows a clean bridge of the calorimetric sensor. Figure A.9-A.12

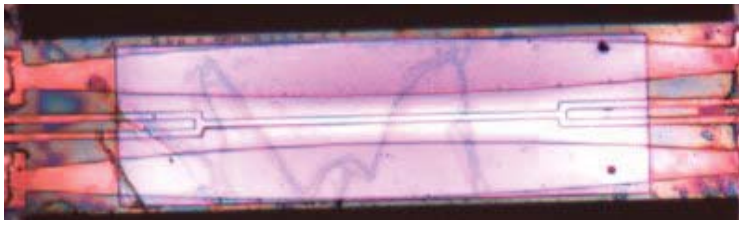

Figure A.8: An image of the bridge that is located on the calorimetric sensor in clean state.

shows the responses (after smoothing) for the calorimetric sensor when exposed

to the analytes. The condensation of DAT turned to be troublesome (Figure A.10). To force the DAT to condensate a droplet of nitrogen was put on the opposite side of the sensor thus cooling the sensor while depositing DAT. First the sensor was evaporated for 2 minutes, but this turned out to saturate the sensor (Figure A.10, top panel), so the evaporation time was reduced to one minute (middle and bottom panel).

When measuring, both reference and measurement sensor is calibrated in order to be heated with the same linear heating rate by applying a calibrated voltage waveform. Calibration ensures constant heating rate, and that reference and measurement chip signal is kept close together when no sample is present. As baseline correction, each time a sensor reading is performed, we also measure 10 times with no sample present. The median of these 10 samples is used to baseline correct the signal.

The baseline corrected signal is contaminated with noise. This noise is removed using Gaussian Process Regression (GPR). As fitting the hyper parameters when using GPR is not a convex optimization problem, we use 10 restarts and then select the model that has the maximum evidence. Readers interested in further details are referred to the downloadable package.

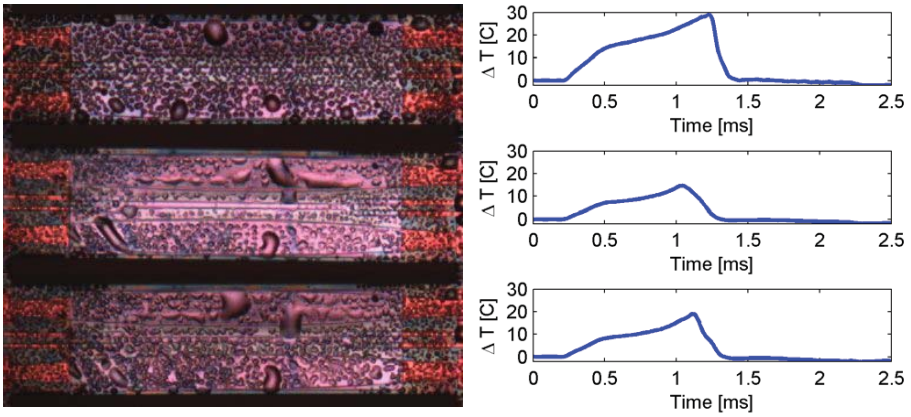

Figure A.9: The three runs for the calorimetric sensor when exposed to DNT. The shape is reproducible and distinct from the other responses. The left images are images of the bridge just before the heating pulse is applied to the sensor. Clearly the bridge is loaded with DNT molecules. The right hand images are the corresponding profiles obtained when the heating pulse is applied.

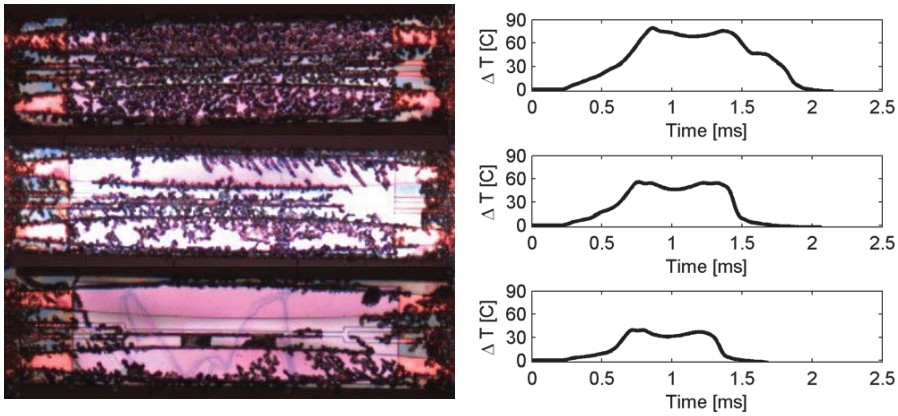

Figure A.10: The three runs for the calorimetric sensor when exposed to DAT.

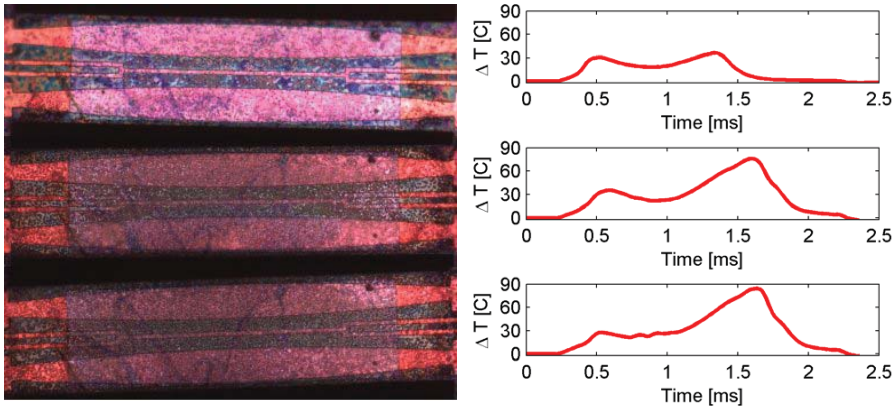

Figure A.11: The three runs for the calorimetric sensor when exposed to ammonium nitrate.

A.6.1.2. The cantilever sensor

A priori we know that cantilever measurements are prone to high variability so in order to improve robustness 16 cantilevers are used per measurement, 8 cantilevers with TTF coating and 8 cantilevers with no coating. If the sensor is able to make a detection there should be a significant difference between the changes of resonance frequency for TTF coating cantilevers vs. non-coated cantilevers.

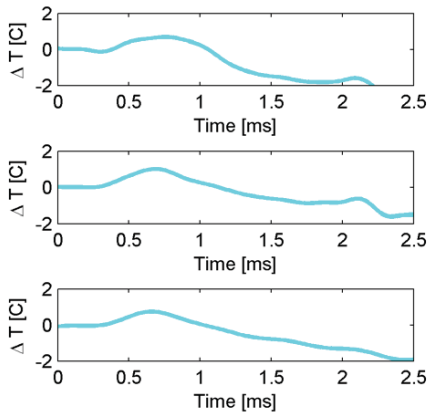

Figure A.12: The three runs for the calorimetric sensor when exposed to Diesel. No surface images of the calorimetric sensor are shown as it turned out that we were not able to condensate Diesel on the sensor.

Analysis of the data shows that the data is in general normally distributed but there are expectations. For this reason we employ the nonparametric method Kruskal-Wallis for significance test. Kruskal-Wallis assumes that the distributions to be tested are identically shaped. Since our data have few samples with high variance we don't have enough data to verify this claim hence we should use the conclusions with caution for p-values close to the significance level which we choose to 0.05. For all three cases the test show that there are significant differences when the target analyte is Diesel and DNT with p¡0.01. For DAT and ammonium nitrate the results are more ambiguous. For experiment 1 there was found a significant difference for DAT and ammonium nitrate however, for experiment 2 and 3 no significant differences was found.

In order to apply 1-NN the measurements for each experiment are reduced to a single number by using the median response of an experience subtracting the median response for the blank cantilever.

Figure A.13-A.16 contains the complete data gathered from the cantilever sensor. The entries with "n.a." represent a cantilever that could not be read with the optical system, i.e., some kind of malfunction with the cantilever in question.

A.6.1.3. The colorimetric sensor

The colorimetric sensor responses is a series of images pairs (before exposure to

		DAY 1		DAT			
		TTF			Blank		
EXP	Cantilever #	Before exposure (Hz)	After exposure (Hz)	Shift (Hz)	Before exposure (Hz)	After exposure (Hz)	Shift (Hz)
1	1	4964.6	4957.6	-7	4929.7	4935.8	6.1
	2	4991.1	5001.3	10.2	4942.3	4943.4	1.1
	3	5032.6	5042.2	9.6	4944.5	4947.8	3.3
	4	5133.4	5153.3	19.9	4947	4943.7	-3.3
	5	5258.7	5285.9	27.2	4949.1	4951.1	2
	6	5454.6	5520.8	66.2	4952.7	4951.3	-1.4
	7	5731	5846.1	115.1	4968	4973.3	5.3
	8	5543.2	5655.2	112	4976.1	4976	-0.1
2	1	n.a.	n.a.	n.a.	4988.7	4917.7	-71
	2	5165.5	4999.1	-166.4	4934.3	4914.4	-19.9
	3	4886.1	4979.4	93.3	4985.5	4939.2	-46.3
	4	4955.6	5023	67.4	4754.4	4922.9	168.5
	5	5214.4	5139.1	-75.3	4877.58	4936.8	59.22
	6	5011.7	5280.7	269	4972.8	4957.8	-15
	7	5234.6	5321.8	87.2	5011	4962.5	-48.5
	8	5144.56	5182.9	38.34	4971.5	4972.25	0.75
3	1	4934.5	4946	11.5	4829.7	4917.1	87.4
	2	4897.9	4981.3	83.4	4778.2	4870.3	92.1
	3	5033.9	5021.9	-12	4922.9	4928.9	6
	4	5229.2	5137.2	-92	4717.3	4923	205.7
	5	5198.2	5283.1	84.9	4881.2	4930.9	49.7
	6	5298.4	5529.5	231.1	4959.1	4956	-3.1
	7	5633.1	5728.7	95.6	4958.2	4958.9	0.7
	8	n.a.	n.a.	n.a.	5001.1	4877.5	-123.6
	AVERAGES	5179.403	5228.005	**48.60182**	4923.037	4937.856	**14.81958**
		Differential averaged shift			**33.7822**	Hz	

Figure A.13: Cantilever measurements for DAT.

analyte, after exposure to analyte and difference maps). Examples are shown figure s10 but otherwise the raw images can be found in the data set download.

		DAY 2			DNT		
		TTF			Blank		
EXP	*Cantilever #*	*Before exposure (Hz)*	*After exposure (Hz)*	***Shift*** *(Hz)*	*Before exposure (Hz)*	*After exposure (Hz)*	***Shift*** *(Hz)*
1	1	4573.7	4098	-475.7	4697.2	4702.9	5.7
	2	4581.6	4280.7	-300.9	4711.5	4673.8	-37.7
	3	n.a.	n.a.	n.a.	4692.7	4656.8	-35.9
	4	n.a.	n.a.	n.a.	4721.6	4713.9	-7.7
	5	4552	3850	-702	4716.2	4714.8	-1.4
	6	4564.9	3891.4	-673.5	4651.6	4689.3	37.7
	7	4582.1	3991.4	-590.7	4674.7	4717.3	42.6
	8	4350.1	3923.8	-426.3	n.a	n.a.	n.a.
2	1	n.a.	n.a.	n.a.	4903.4	4896.9	-6.5
	2	3714	3611.7	-102.3	4899.1	4907.9	8.8
	3	4293.6	4007.8	-285.8	4912.5	4803.8	-108.7
	4	4621.1	4226.3	-394.8	4907.3	4903	-4.3
	5	4763.6	4542.4	-221.2	4915.5	4912.3	-3.2
	6	4921.2	4799.3	-121.9	4932.8	4901.7	-31.1
	7	5091	4852.3	-238.7	4947.6	4939.7	-7.9
	8	4572.7	4269.5	-303.2	n.a.	n.a.	n.a.
3	1	3733	3597.5	-135.5	4899.1	4835.2	-63.9
	2	4288.7	4156.3	-132.4	4704.2	4762.4	58.2
	3	4711.1	4482.4	-228.7	4918.2	4872.5	-45.7
	4	4788.6	4619.7	-168.9	4972.3	4977.8	5.5
	5	4986.1	4792	-194.1	4921.4	4899.8	-21.6
	6	5109.4	4985	-124.4	4908.9	4915	6.1
	7	4674.1	4511.2	-162.9	4829.1	4930.4	101.3
	8	n.a.	n.a.	n.a.	4912.6	4909.4	-3.2
	AVERAGES	4573.63	4274.435	**-299.195**	4834.068	4828.936	**-5.13182**
		Differential averaged shift			**-294.06**	Hz	

Figure A.14: Cantilever measurements for DNT.

Images of the sensor were scanned using an ordinary flatbed scanner immediately

		DAY 3			Ammonium Nitrate		
		TTF			Blank		
EXP	*Cantilever #*	*Before exposure (Hz)*	*After exposure (Hz)*	***Shift*** *(Hz)*	*Before exposure (Hz)*	*After exposure (Hz)*	***Shift*** *(Hz)*
1	1	5684.5	5646.6	-37.9	n.a	n.a.	n.a.
	2	5547.1	5574.8	27.7	4802.6	4730.6	-72
	3	5688.4	5643.5	-44.9	4779.3	4714.2	-65.1
	4	5584.3	5599.3	15	4834	4702.7	-131.3
	5	5702.9	5693.8	-9.1	4785.5	4720.2	-65.3
	6	5701.8	5680.9	-20.9	4767.6	4746.2	-21.4
	7	5599.7	5673.1	73.4	4792.1	4715.1	-77
	8	n.a	n.a.	n.a.	n.a	n.a.	n.a.
2	1	5994	6017.9	23.9	4986.9	4969.6	-17.3
	2	6109.4	6104.5	-4.9	4955	4940.4	-14.6
	3	6144.5	6112	-32.5	4945.7	4923.9	-21.8
	4	6168.8	6164.4	-4.4	4936	4902.5	-33.5
	5	6202.2	6203.2	1	4914.2	4891.5	-22.7
	6	6201.5	5881.9	-319.6	4912.7	4877.4	-35.3
	7	6260.4	6139.1	-121.3	4897.1	4846.5	-50.6
	8	6293.9	6327.2	33.3	4849.1	4335	-514.1
3	1	6105.4	6035.8	-69.6	n.a	n.a.	n.a.
	2	6122.3	6099	-23.3	5002.1	4952.5	-49.6
	3	6198.5	6109.5	-89	5025.6	4994.4	-31.2
	4	6215	6101.4	-113.6	5147.8	5092.3	-55.5
	5	6203.1	6214.5	11.4	5244.9	5232.7	-12.2
	6	6274.9	6210.8	-64.1	5598.7	5452.3	-146.4
	7	n.a	n.a.	n.a.	5841.6	5767.4	-74.2
	8	n.a	n.a.	n.a.	n.a	n.a.	n.a.
	AVERAGES	6000.124	5963.486	**-36.6381**	5000.925	4925.37	**-75.555**
		Differential averaged shift				**38.9169**	Hz

Figure A.15: Cantilever measurements for ammonium nitrate.

after immobilization of dyes and then again after exposure of target analytes. The images were encoded in a lossless format using the red-green-blue (RGB) color scheme with 8 bits per color. The images were used to generate color

		DAY 4		DIESEL			
		TTF			Blank		
EXP	*Cantilever #*	*Before exposure (Hz)*	*After exposure (Hz)*	***Shift*** *(Hz)*	*Before exposure (Hz)*	*After exposure (Hz)*	***Shift*** *(Hz)*
1	1	5867.6	5864	-3.6	4863.6	4769.9	-93.7
	2	5947.7	5956	8.3	4868	4847.5	-20.5
	3	6071	6074.8	3.8	4805.9	4501.2	-304.7
	4	6079.4	6062.3	-17.1	4583	4325.1	-257.9
	5	6156.8	6150.9	-5.9	4808	4652.7	-155.3
	6	6154.5	6153	-1.5	4868.1	4682.4	-185.7
	7	6225.5	6213.2	-12.3	4923.9	4768.5	-155.4
	8	6288.4	6265.8	-22.6	4933.3	4868.9	-64.4
2	1	n.a	n.a.	n.a.	n.a	n.a.	n.a.
	2	6118	6115.8	-2.2	4719.1	4408.1	-311
	3	6149.4	6123.1	-26.3	4706.3	4524	-182.3
	4	6239	6221.5	-17.5	4712.5	4544.2	-168.3
	5	6281.7	6205.9	-75.8	4672.8	4588.8	-84
	6	6144.9	6138.7	-6.2	4877.6	4689.5	-188.1
	7	6197.3	6157.8	-39.5	4709.6	4597.2	-112.4
	8	6087.1	6077.5	-9.6	4801.2	4621.7	-179.5
3	1	n.a	n.a.	n.a.	4788.6	4598.5	-190.1
	2	6219.1	6182.5	-36.6	4871.6	4602.7	-268.9
	3	6084.5	6022.8	-61.7	4821.1	4716.9	-104.2
	4	6138.8	6122.9	-15.9	4863.6	4703.2	-160.4
	5	n.a	n.a.	n.a.	4796.5	4688.4	-108.1
	6	6212.3	6189.7	-22.6	4768.1	4695.2	-72.9
	7	6109.6	6087.4	-22.2	4824.2	4711.6	-112.6
	8	n.a	n.a.	n.a.	4799.3	4710.2	-89.1
	AVERAGES	6138.63	6119.28	**-19.35**	4799.387	4644.191	**-155.196**
		Differential averaged shift			**135.846**	Hz	

Figure A.16: Cantilever measurements for diesel.

difference images by pixel subtraction (Figure A.17).

To align the two images a cost function that measures the L1 norm error per pixel is minimized The L1 norm error can be interpreted as the amount of color per pixel where a fully black pixel is fixed at a value of zero. At perfect image alignment, all the background pixels will be black and all dye pixels will have the weakest possible color, hence, blackness per pixel should be maximized.

Once the images are digitalized feature extraction is employed using the mean pixel value. Chemically we know that a dye should only have one color, as the dye is homogeneous and exposed to a homogeneous vapor. However, noise is induced from: the scanner, the drying process of the dye, external light, and roughness of surface. Some of these effects can be handled easily. The drying of the dyes often results in a ring near the perimeter (the coffee stain effect) and this area of the dye is unreliable. To accommodate for this effect, a smaller area of a dye is used for feature extraction, corresponding to 2/3 of the dye radius.

The full list of chemoselective compounds used to manufacture the colorimetric sensor arrays are also included, see Table A.3.

A.6.1.4. SERS Sensor Responses

Examples of the SERS signals have been shown in the main paper, and the data is too large to print in this document. Interested readers are referred to the downloadable package.

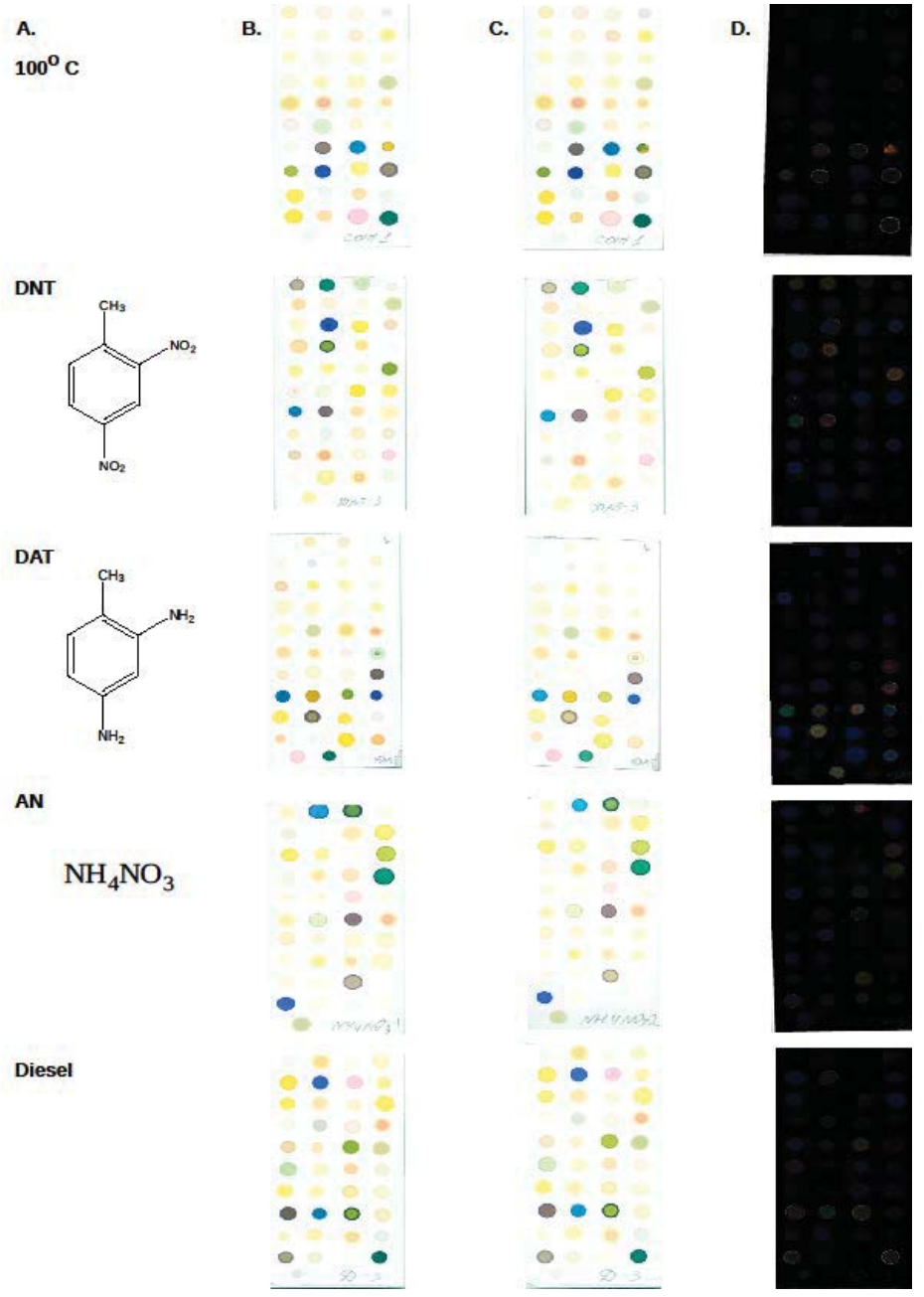

Figure A.17: Examples of the colorimetric sensor. B is the sensor before exposure; C is the sensor after exposure; and D is the difference map.

A.6.2 Confusion matrices and 1-Nearest Neighbor

The confusion matrices on Figure 6 are calculated using 1-Nearest Neighbor (1-NN). The 1-NN technique which works as follows: a given sensor response is considered to be a single point in a high dimensional vector space. E.g. for the colorimetric sensor, the dimensionality of the space becomes the number of dyes multiplied by three, as each dye is represented using one RGB color, which again is a three dimensional number. When testing an unknown data point, the Euclidean distances for all known points are calculated. The analyte of the closest point is then identified and the unknown point is classified as the identified analyte.

A.6.2.1. Colorimetric confusion matrix

Since the colorimetric sensor is a chemical sensor that immediately reacts with the environment, control measurements for the surrounding environment were included. The control measurements resulted in misclassification on three occasions as can be seen shown on Figure A.18.

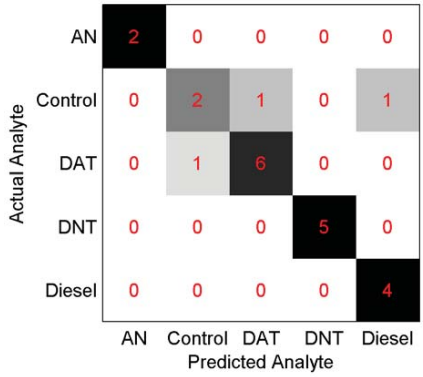

Figure A.18: The three runs for the calorimetric sensor when exposed to Diesel. No surface images of the calorimetric sensor are shown as it turned out that we were not able to condensate Diesel on the sensor.

Table A.3: List of the 41 chemoselective compounds tested and applied further in the colorimetric sensor array for detection of ammonium nitrate, DAT, DNT, and diesel.

№	CAS-№.:	Formula	M_w	Structure and Name	Availability
1	NA	$C_{13}H_{25}N_3O_6S_7$	760.00	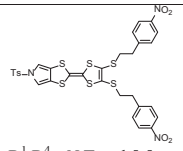 R^1,R^4 : *N*-Tosyl-[*c*]pyrrolo R^2,R^3 : 2-(4-Nitrophenyl)ethylthio	Synthetic procedure described in [1]
2	NA	$C_{38}H_{30}N_4O_8S_{12}$	1055.45	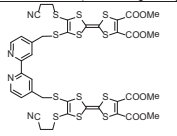 R^1 : (4'-{[7-(2-Cyanoethylthio)-2,3-Dimethoxy-carbonyl-6-thiomethylene]tetrathiafulvalene}-4-bipyridine)methylethio R^2,R^3 : Methoxycarbonyl R^4 : 2-Cyanoethylthio	Synthetic procedure described in [1]
3	NA	$C_{28}H_{28}N_4O_6S_8$	773.07	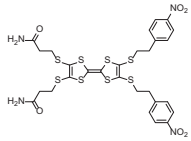 R^1,R^4 : 2-(Carboxamide)ethylthio R^2,R^3 : 2-(4-Nitrophenyl)ethylthio	Synthetic procedure described in [1]
4	26314-39-6	$C_{14}H_{12}O_8S_8$	436.50	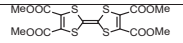 R^1,R^2,R^3,R^4 : Methoxycarbonyl	[2]
5	300766-19-2	$C_{25}H_{31}NO_2S_7$	601.97	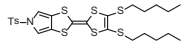 R^1,R^4 : *N*-Tos yl-[*c*]pyrrolo R^2,R^3 : Pentylthio	[3]
6	NA	$C_{25}H_{35}NO_2S_7$	606.01	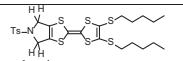 R^1,R^4 : *N*-Tosyl-2,5-Dihydro-[*c*]pyrrolo	Synthetic procedure described in [1]

				R^2,R^3 : Pentylthio	
7	NA	$C_{19}H_{15}NO_6S_5$	516.65	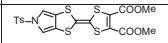 R^1,R^4 : *N*-Tosyl-[*c*]pyrrolo R^2,R^3: Methoxycarbonyl	Synthetic procedure described in [1]
8	NA	$C_{25}H_{31}N_3S_6$	565.92	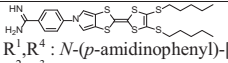 R^1,R^4 : *N*-(*p*-amidinophenyl)-[*c*]pyrrolo R^2,R^3 : Pentylthio	Synthetic procedure described in [1]
9	NA	$C_{23}H_{35}NO_6S_6$	613.92	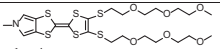 R^1,R^4 : *N*-Methyl-[*c*]pyrrolo R^2,R^3 : 2-(2-(2-Methoxyethoxy)ethoxy)ethylthio	Synthetic procedure described in [1]
10	132765-36-7	$C_{18}H_{16}N_4S_8$	544.87	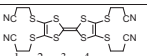 R^1,R^2,R^3,R^4 : 2-Cyanoethylthio	Synthetic procedure described in [4]
11	NA	$C_{14}H_{14}Br_2S_{12}$	566.52	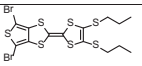 R^1,R^4 : 2,5-Dibromo-[*c*]thieno R^2,R^3 : Propylthio	Synthetic procedure described in [5]
12	31366-25-3	$C_6H_4S_4$	204.36		Sigma-Aldrich.Co.LLC.
13	55259-49-9	$C_{10}H_{12}Se_4$	448.04	 R^1,R^2,R^3,R^4 : Methyl	Sigma-Aldrich.Co.LLC.
14	NA	$C_{100}H_{148}N_4O_{24}S_{24}$	2559.82	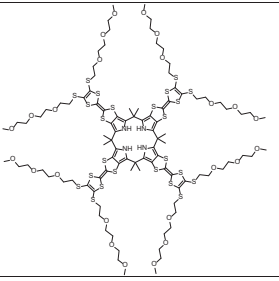	[6]

15	NA	$C_{68}H_{84}N_4S_{24}$	1727,01	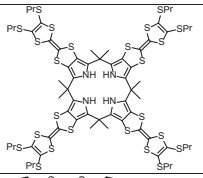	7
16	61940-34-9	$C_{16}H_{20}S_4$	340.59	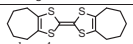 R^1, R^4: Tetramethylelethio R^2, R^3: Tetramethylelethio	Sigma-Aldrich.Co.LLC.
17	S926035	$C_{38}H_{52}O_4S_4$	701.09		Sigma-Aldrich.Co.LLC.
18	75258-46-7	$C_{22}H_{20}O_2S_4$	444.56		Sigma-Aldrich.Co.LLC.
19	83362-96-3	$C_{20}H_{14}Cl_2S_4$	453.49	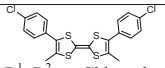 R^1, R^2 : p-Chlorophenyl R^3, R^4 : Methyl	Sigma-Aldrich.Co.LLC.
20	56851-13-9	$C_{20}H_{16}S_4$	384.60	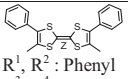 R^1, R^2 : Phenyl R^3, R^4 : Methyl	Sigma-Aldrich.Co.LLC.
21	61485-52-7	$C_{18}H_{10}Br_2S_4$	514.35		Sigma-Aldrich.Co.LLC.
22	40210-84-2	$C_6H_4S_4\times C_{12}H_4N_4$	408.54		Sigma-Aldrich.Co.LLC.
23	100760-57-4	$C_{20}H_{16}S_4$	384.60	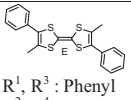 R^1, R^3 : Phenyl R^2, R^4 : Methyl	Sigma-Aldrich.Co.LLC.
24	71938-96-0	$C_{22}H_{16}S_4$	408.62	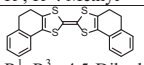 R^1, R^3 : 4,5-Dihydronaphto R^2, R^4 : 4,5-Dihydronaphto	Sigma-Aldrich.Co.LLC.
25	24648-13-3	$C_{14}H_8S_4$	304.47	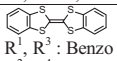 R^1, R^3 : Benzo R^2, R^4 : Benzo	Sigma-Aldrich.Co.LLC.
26	72-48-0	$C_{14}H_8O_4$	240.21	Alizarin	Sigma-Aldrich.Co.LLC.
27	76-60-8	$C_{21}H_{14}Br_4O_5S$	698.01	Bromocresol Green	Sigma-Aldrich.Co.LLC.
28	115-40-2	$C_{21}H_{16}Br_2O_5S$	540.22	Bromocresol Purple	Sigma-Aldrich.Co.LLC.
29	34722-90-2	$C_{27}H_{27}Br_2NaO_5S$	646.36	Bromothymol Blue sodium salt	Sigma-Aldrich.Co.LLC.

30	115-39-9	$C_{19}H_{10}Br_4O_5S$	669.96	Bromphenol Blue	Sigma-Aldrich.Co.LLC.
31	125-31-5	$C_{23}H_{22}O_5S$	410.48	Xylenol Blue	Sigma-Aldrich.Co.LLC.
32	4430-20-0	$C_{19}H_{12}Cl_2O_5S$	423.27	Chlorphenol Red	Sigma-Aldrich.Co.LLC.
33	1733-12-6	$C_{21}H_{18}O_5S$	382.43	Cresol Red	Sigma-Aldrich.Co.LLC.
34	1552-42-7	$C_{26}H_{29}N_3O_2$	415.53	Crystal Violet Lactone	Sigma-Aldrich.Co.LLC.
35	121792-58-3	$C_{29}H_{19}Cl_2NO$	468.37	2,6-Dichloro-4-(2,4,6-triphenyl-1-pyridinio)phenolate	Sigma-Aldrich.Co.LLC.
36	10081-39-7	$C_{41}H_{29}NO$	551.68	Reichardt's dye	Sigma-Aldrich.Co.LLC.
37	143-74-8	$C_{19}H_{14}O_5S$	354.38	Phenol Red	Sigma-Aldrich.Co.LLC.
38	603-45-2	$C_{19}H_{14}O_3$	290.31	Rosolic acid	Sigma-Aldrich.Co.LLC.
39	493-52-7	$(CH_3)_2NC_6H_4N=NC_6H_4CO_2H$	269.30	Methyl Red	Sigma-Aldrich.Co.LLC.
40	5423-07-4	$C_{16}H_8N_4Na_2O_{11}S_2$	542.36	Nitrazine yellow	Sigma-Aldrich.Co.LLC.
41	2374-05-2	$BrC_6H_2(CH_3)_2OH$	201.06	4-Bromo-2,6-Dimethylphenol	Sigma-Aldrich.Co.LLC.

(1) Jeppesen, J. O.; Kostesha, N. V.; Johnsen, C.; Nielsen, K. A.; Boisen, A.; Jakobsen, M. H. Multisensor array useful for detection and/or identification of an analyte (e.g. amines, alcohols, ketones and thiols) in the gas phase or in the liquid phase, comprises at least two different chemo-selective heteroaryl compounds **2011**, 73.

(2) Le Coustumer, G.; Mollier, Y. *J. Chem. Soc., Chem. Commun.* **1980**, 38–39.

(3) Rice, J. E.; Okamoto, Y. *J. Org. Chem.* **1981**, *42*, 446–447.

(4) Svenstrup, N.; Rasmussen, K. M.; Hansen, T. K.; Becher, J. *Synthesis* **1994**, 809–812.

(5) Kim, D.-S.; Lynch, V. M.; Nielsen, K. a; Johnsen, C.; Jeppesen, J. O.; Sessler, J. L. *Analytical and bioanalytical chemistry* **2009**, *395*, 393–400.

(6) Larsen, J.; Lenoir, C. *Synthesis* **1989**, 134.

(7) Nielsen, K. A.; Cho, W. S.; Lyskawa, J.; Levillain, E.; Lynch, V. M.; Sessler, J. L.; Jeppesen, J. O. *Journal of the American Chemical Society* **2006**, *128*, 2444–2451.

Appendix B

Data-driven modeling of nano-nose gas sensor arrays

Tommy S. Alstrøm, Jan Larsen, Claus H. Nielsen, and Niels B. Larsen. Data-driven modeling of nano-nose gas sensor arrays. In Ivan Kadar, editor, *Proceedings of SPIE*, volume 7697, pages 76970U–76970U–12. SPIE, 2010. doi: 10.1117/12.850314.

The layout of the paper has been revised.

Data–driven modeling of nano-nose gas sensor arrays

Tommy S. Alstrøm[a], Jan Larsen[a], Claus H. Nielsen[b,c] and Niels B. Larsen[b]

[a]DTU Informatics, Technical Univ. of Denmark, DK-2800 Kongens Lyngby, Denmark;
[b]DTU Nanotech, Technical Univ. of Denmark, DK-2800 Kongens Lyngby, Denmark;
[c]Dept. of Chemistry, Univ. of Copenhagen, DK-2100 Copenhagen Ø, Denmark.

ABSTRACT

We present a data-driven approach to classification of Quartz Crystal Microbalance (QCM) sensor data. The sensor is a nano-nose gas sensor that detects concentrations of analytes down to ppm levels using plasma polymorized coatings. Each sensor experiment takes approximately one hour hence the number of available training data is limited. We suggest a data-driven classification model which work from few examples. The paper compares a number of data-driven classification and quantification schemes able to detect the gas and the concentration level. The data-driven approaches are based on state-of-the-art machine learning methods and the Bayesian learning paradigm.

Keywords: Polymer Coated Quartz Crystal Microbalance Sensor (QCM), Gaussian Process Regression (GPR), Artificial Neural Network (ANN), Non–negative Matrix Factorization (NMF), Principal Component Analysis (PCA), Principal Component Regression (PCR), Classification, Concentration Level Estimation.

B.1. INTRODUCTION

The development of gas sensors is a field of great activity. Particularly the development of electronic noses for use in process control, quality control in the food and beverage industry, pollution monitoring and airport security[1,2].

Further author information: (Send correspondence to T.S.A.)
T.S.A.: E-mail: tsal@imm.dtu.dk, Telephone: (+45) 45 25 39 04
J.L.: E-mail: jl@imm.dtu.dk, Telephone: (+45) 45 25 39 23
C.H.N.: E-mail: chn@chn-analytical.dk
N.B.L: E-mail: niels.b.larsen@nanotech.dtu.dk

Ideally such an electronic nose should be portable, provide both a qualitative and quantitative determination of analytes as well as offer stable performance over extended periods of time. This means that the sensor element(s) must operate in a reversible manner and show an affinity towards target analytes.

Many different strategies have been pursued to develop selective gas sensors. One approach is to functionalize the physical sensor device with chemical coatings. Molecularly imprinted polymers (MIPs) seek to mimic biological antibodies. The selectivity of these "plastic antibodies" has been shown to be somewhat random and not easily controlled[3]. Several macromolecules have been evaluated as potential gas sensors. One of the more popular choices are cyclodextrins, which are cage-like molecules with hydrophobic cavities and hydrophilic edges[4]. These molecules offer both chemical and steric selectivity and serve as a platform for a vast group of derivatives that tune the specificity towards certain compounds or classes of compounds. However, the selective modification of cyclodextrins is not a simple process and requires elaborate synthesis and isolation steps[5]. Another drawback is the fact that these substances must be dissolved in a solvent from which a film can be cast by for example spin or spray coating in order to functionalize a sensor surface.

In this work an alternative methodology known as plasma polymerization is used for sensor functionalization. This method allows for solvent free deposition of a wide range of thin polymer films on the surface of most sensors including cantilever and quartz crystal microbalance (QCM) based sensors[6]. Plasma polymerization also offers excellent control over film thickness since it is directly proportional to polymerization time as confirmed by Kurosawa et al.[7]. A wide selection of monomers with many different functional groups can be used for plasma polymerization making it a very versatile technique. The choice of monomer naturally depends on the target analytes to be detected. As described by Grate and Abraham the choice of coatings can advantageously be based on the main interaction parameters that are responsible for the sorption of gases into solids[8]. According to the linear solvation energy relationship (LSER) model these parameters are: dispersion interactions, polarizability, dipolarity and hydrogen bonding. Ideally one would develop a selection of coatings where each coating is representing only one of the above interaction parameters. This is however not easily done in practice, but Grate and Abraham suggest several good candidates that can be assumed to primarily interact via one parameter only. The coatings are deposited on a QCM based sensor. The working principle of QCM sensors resemble tuning forks. The resonance frequency response of QCM sensors is close to linear with respect to mass change[6]. Coating the quartz crystals make them selective towards various analytes making them suitable as gas sensors. In order to verify the selectivity of the coatings the sensor is tested using six different analytes. The response data is subject to data analysis methods. A number of methods have been applied to polymer coated QCM sensors.

Often QCM sensors selectivity has been analyzed by using principal component analysis (PCA)[9–11] or hierarchical cluster analysis (HCA)[12,13]. Recently the application of artificial neural networks (ANN) evolved as the dominant method[14].

As described earlier the response of QCM sensors is sensitive to mass changes making them viable for detecting concentration levels of analytes. Various methods have been used to construct QCM based concentration level estimators such as partial least squares (PLS)[11] and multivariate linear regression[15]. Artificial neural networks have been applied as concentration level estimators in a broad range of applications[14,16–18].

In this paper we compare classification using ANN and PCA with a Non–negative Matrix Factorization (NMF) classification scheme. NMF was introduced by Lee and Seung[19] as an alternative to PCA for feature extraction applied to identifying facial features but have found use in a vast range of areas. Further we propose a QCM sensor consisting of 8 crystals with different coatings. The sensor is able to classify the test analytes with high accuracy even though the available training data is limited. In order to perform concentration level estimation the analytes are measured at various concentrations. Three different methods for concentration level estimation are evaluated; Principal component regression (PCR), ANN and Gaussian process regression (GPR). PCR is a linear method that performs well with a limited amount of training points although it handles non–linearity in data poorly. To overcome this problem neural networks has usually been applied as ANN can model non–linearities. GPR is so far an untried method for QCM data. GPR is a non–linear method as ANN but GPR should be able to perform well with a limited amount of data points.

B.2. SENSORS AND MEASUREMENT SYSTEM

A selection of eight monomers were chosen based on the single interaction parameter. All monomers used, dodecane (DOD), heptadecafluoro-1-decene (HDFD), maleic anhydride (MAH), methylene dioxobenzene (MDOB), methyl methacrylate (MMA), styrene (STY) and vinyl pyrrolidone (VP), were of at least $\geq 99\%$ purity except di(ethylene glycol) vinyl ether (DEGVE), which was of 98% purity, and all of them were used without further purification. The monomers were polymerized at a total pressure of 10-13 Pa and at a power of $0.5\frac{W}{l}$ in a 50 Hz (i.e. low frequency) plasma chamber[20]. Argon was used as a carrier gas. Surfaces were activated for 2 min in argon plasma followed by addition of monomer to initiate polymerization. After polymerization power was turned off, but the monomer was allowed to flow for another 2 min. This "afterglow polymerization" is believed to reduce the amount of free radicals on the

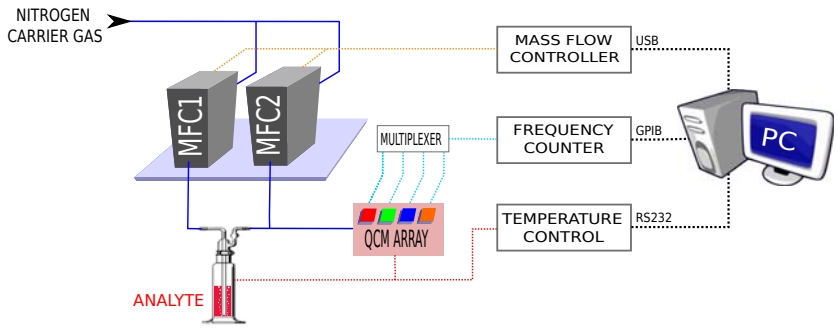

Figure B.1: Experimental setup used for gas sorption measurements of QCMs coated with thin polymer films.

polymer surface by reaction with monomer species. For gas sorption measurements 10 MHz, 0.538“ diameter AT-cut quartz crystals with 10Å Ti + 1000Å Au electrodes driven by 10 MHz QCM lever oscillators (all from International Crystal Manufacturing Co.) were used. Crystals were coated on one side only by masking one side with SWT 20+ semiconductor dicing tape (from Nitto Denko). Crystals were mounted in a home built flow system made from poly(methyl methacrylate) (PMMA) which was placed on top of an aluminum block held at a 33°C(±0.1°C) throughout the duration of the experiments. The entire flow system and all oscillators were placed inside a closed box to shield the QCMs from excessive temperature variations (the temperature in the laboratory varied up to 5°C between day and night time). Figure B.1 shows a schematic of the experimental setup. Analytes used were acetone ($\geq$ 99.8%), anhydrous ethanol ($\geq$ 99.9%), heptane ($\geq$ 99%), 1-pentanol ($\geq$ 99%), 1,3-Benzodioxole ($\geq$ 99%) and Milli-Q purified water (Millipore). The analyte vapors were produced by bubbling nitrogen through gas wash bottles containing analyte. Analyte concentrations were defined by adjusting the ratio of nitrogen flowing through and bypassing the wash bottle respectively. A constant flow rate of 100 sccm was maintained throughout the entire duration of the experiments using mass flow controllers (mks Instruments, type 1179A). With an internal volume of the flow system of about 2.5 cm^3 this corresponds to about 39 exchanges per minute. For this reason the concentration of analyte in the gas phase is assumed to be constant. The setup allows for sequential measurement of four crystals. Each crystal was measured every 4 seconds and each measurement was taken as the median of 10 measurements. Of the 4 crystals being measured one was always a blank (i.e. uncoated) crystal. The gold surface of the blank crystal provided information about unspecific adsorption and deviations due to temperature changes. Resonant frequencies were measured using a Fluke PM6681 high resolution frequency counter. The sorption measurements consisted of re-

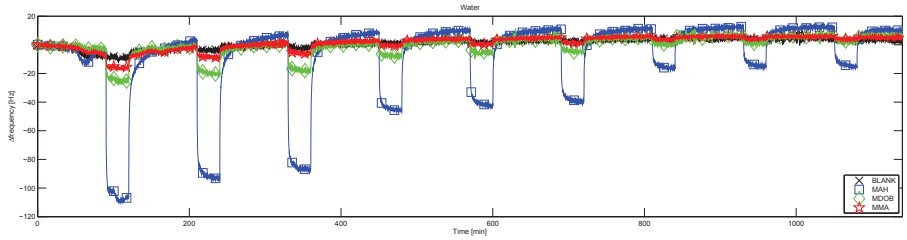

Figure B.2: Δfrequency responses for MAH, MDOB, MMA and a blank quartz crystal for nine measurement cycles. The first three measurement cycles is water at 9200 parts per million (ppm), the next three cycles the concentration is at 4600 ppm and the last three cycles has a concentration level at 2300 ppm. The sign reversed peak value during a measurement cycle is recorded as representative for the cycle.

peated cycles of 100 min pure nitrogen flow followed by 40 min of analyte-spiked flow. The response was measured at six different concentrations, three times at each concentration, for each analyte. Figure B.2 shows the response for MAH, MDOB and MMA using water as analyte. A measurement cycle consist of filling the chamber with pure nitrogen for 100 minutes allowing the coatings to get a known steady state response. After the 100 minutes have passed an analyte at a given concentration level is added to the flow maintained for 40 minutes. The peak response is recorded as representative for the measurement cycle. Figure B.3 shows the measured (peak sign reversed) frequency responses for all analytes. The frequency readings show a near linear response with respect to mass for most coatings. Other coatings such as STY for heptane show a non-linear response. All responses but one are of the same sign. HDFD shows a negative response towards pentanol. This is because HDFD is a teflon-like coating onto which condensation of pentanol is less likely to occur compared to the uncoated reference quartz crystal.

B.3. ALGORITHM TRAINING AND EVALUATION

B.3.1 Data partitioning

As described in section B.2 we have conducted experiments on six different analytes. Each analyte is measured at 6 different concentration levels and each experiment is repeated 3 times. Therefore the dataset has 108 data points in total, 18 data points per analyte. The data is partitioned into a training set

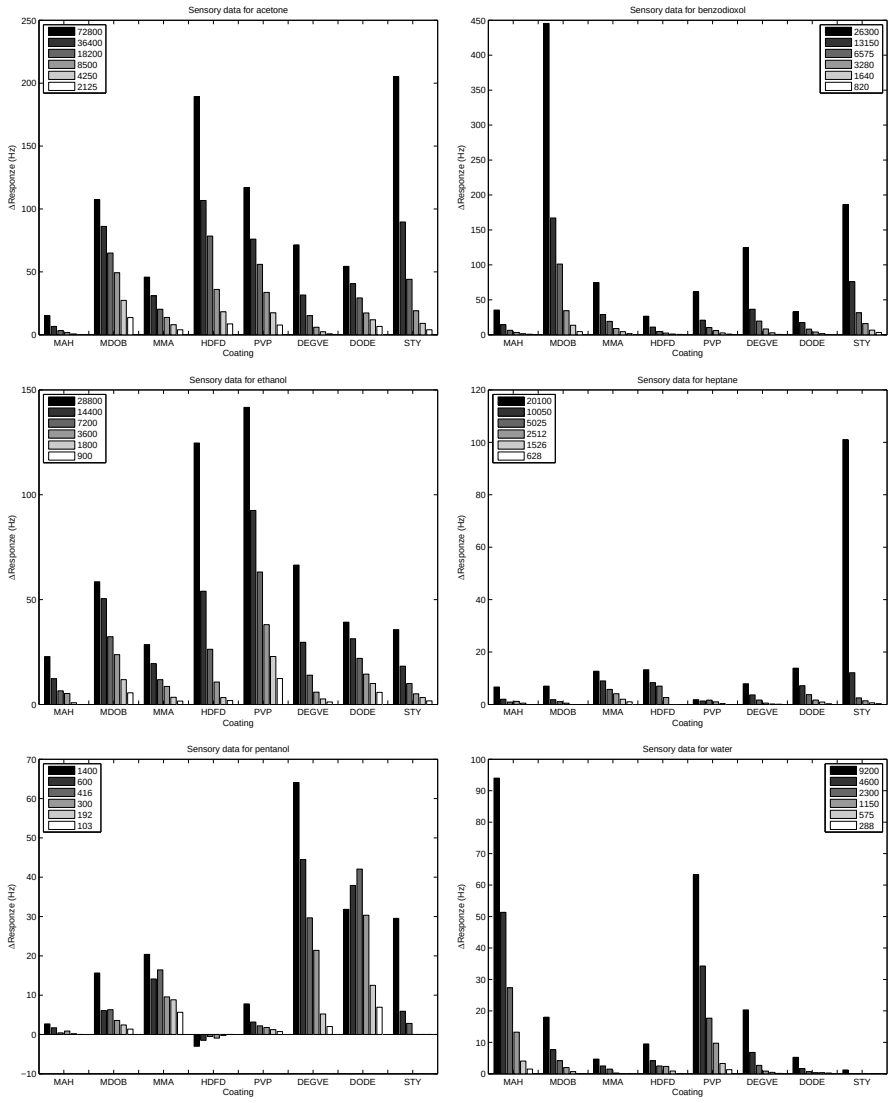

Figure B.3: The bars are averages of the measured responses. Inspection of the data shows that only on one occasion does a crystal give a negative Δfrequency response, namely HDFD for pentanol. Note both the concentration levels and the y–axis scaling varies between analytes. The concentration levels is in parts per million (ppm).

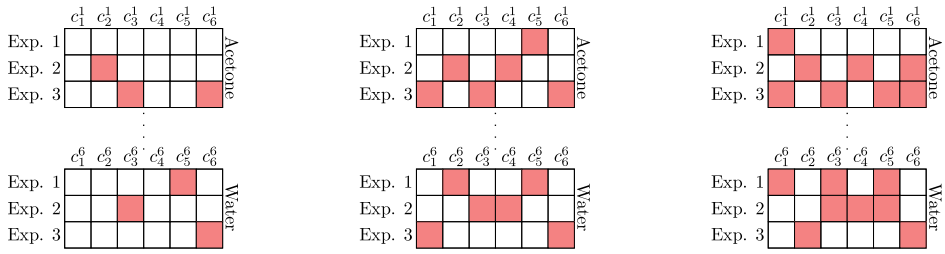

Figure B.4: The figure illustrate three different data partitioning scenarios. Left has $N_{train} = 3$, center has $N_{train} = 6$ and right has $N_{train} = 8$. Each square corresponds to one data point. The test set comprise the blank squares and the training set comprise the colored squares. c_i^a denoted that concentration level i for analyte a. Here acetone corresponds to $a = 1$ and water is $a = 6$.

and a test set. We want to produce learning curves for the different algorithms so the size of the training set will vary. Our minimum training set size will be three training points per analyte – the minimum number of points that can reveal non–linearities in the sensor response. The maximum trained set size is chosen to be twelve training points per analyte, denoted as $N_{train} = 12$. This corresponds to an experimental setup where all concentration levels per analyte is included twice. We want to increase the training set size in roughly the same manner as an experimenter would include more and more experiments. To achieve this we impose constraints on how the data is partitioned. Each analyte must be represented evenly in training set - thus the training set size must be a multiple of six. Further each concentration level within each analyte, should be represented as evenly as possible. Choosing $N_{train} = 6$ we have each concentration represented exactly once. Figure B.4 shows examples of data partitioning for $N_{train} = 3$, $N_{train} = 6$ and $N_{train} = 8$. Each data partitioning and subsequent model training and evaluation is performed 100 times. This is done to ensure that we are not comparing the algorithms on a training/test set that turned out to be an exception rather than the norm.

B.3.2 Model training and evaluation

The proposed methods have several parameters that can have a huge impact of performance. These parameters are often set using model selection. In order to select the model that has the lowest generalization error[21] model selection methodology must be applied. We will work with both cross validation[21] (CV) and marginal likelihood[22] (ML) depending on the method in question. Model selection for classification using SVD and NMF will use leave–one–out cross val-

idation (LOO-CV). Due to computational limitations model selection for ANN classification will use a 6–fold cross validation scheme (6F-CV) instead of LOO-CV . The 6F-CV set will contain one data point per analyte. Model selection for PCR and ANN regression will use LOO-CV. Model selection for GPR will use ML as described by Rasmussen and Williams[22]. The performance of the classifiers are evaluated based on the misclassification rate defined as

$$E_{mis} = \frac{N_{error}}{N} \tag{B.1}$$

where N_{error} is the amount of misclassified points and N is the total amount of points that was classified. Evaluating performance on quantifiers must be done differently than for the classifiers. The performance criterion used is the mean relative absolute error as has been used by others[14,17]. It is defined as

$$E(RAE) = \frac{1}{N}\sum_{n=1}^{N}\left|\frac{y_n - \hat{y}_n}{y_n}\right| \tag{B.2}$$

where y_n is the true concentration, $\hat{y}_n$ is the predicted concentration and N is the amount of data points estimated. The advantage of this performance criterion is that errors at both high and low concentrations are penalized equally.

B.3.3 Data analysis framework

We adopt a two–tiered model where classification and concentration level estimation (quantification) is handled separately[14]. Figure B.5 shows how data and decisions are made throughout the data processing pipeline. Output from the QCM sensor is applied to a classifier. Based on the decision made by the classifier a given quantifier is selected. There is one quantifier trained per analyte. The output from the model is a class given as an analyte name and a concentration level given in ppm.

We will use past implementations in MATLAB™ of most of the algorithms. The neural network algorithms has been developed during the past years at DTU Informatics and is freely available for download at DTU ISP toolbox[23]. The NMF algorithm is implemented by Lin[24] and is freely available from Lin's website but can be found in the DTU ISP Toolbox as well. The Gaussian process regression implementation used is published by Rasmussen and Williams[25]. The SVD and PCR algorithms are implemented by the authors.

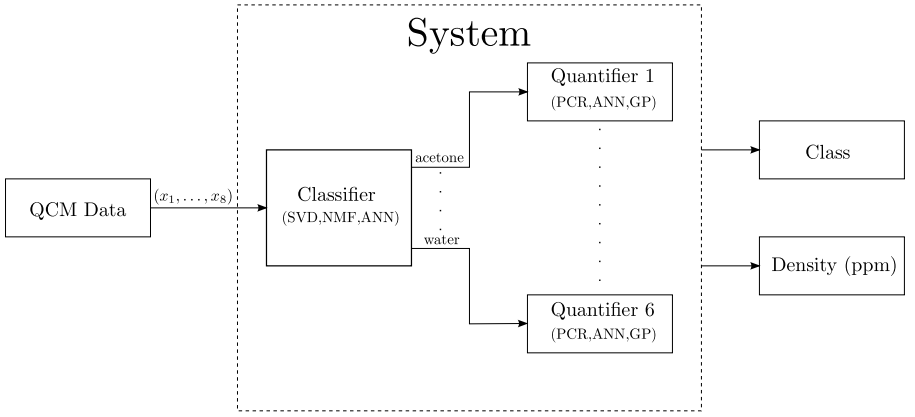

Figure B.5: The schematic setup of the classification/quantification framework.

B.3.4 Gaussian Process regression

Gaussian process regression is an extension of the linear Bayesian regression framework. A recent textbook on Gaussian processes in a machine learning context is written by Rasmussen and Williams[22]. A Gaussian process is completely specified by its mean function and covariance function. Using Gaussian processes for regression requires two choices: a prior and a covariance function. We choose a zero mean Gaussian prior with unit variance. To make this prior plausible we subtract the empirical mean from the data and scale the data to unit variance. The empirical mean and empirical variance is calculated using the training set alone and as such the test data is not guaranteed to neither zero mean nor unit variance. We try three different covariance functions all based on the squared exponential covariance function[22]

$$k(\boldsymbol{x}_p, \boldsymbol{x}_q) = \sigma_f^2 \exp\left(-\frac{1}{2}(\boldsymbol{x}_p - \boldsymbol{x}_q)^\top \boldsymbol{M}(\boldsymbol{x}_p - \boldsymbol{x}_q)\right) + \sigma_n^2 \delta_{pq} \qquad \text{(B.3)}$$

where σ_f^2, σ_n^2 and M are called the *hyper–parameters*. Typically σ_f^2 is called the signal variance and σ_n^2 the noise variance. Choosing $\boldsymbol{M}_{iso} = \ell^{-2}\boldsymbol{I}$ yields the isotropic squared exponential function where ℓ is called the length–scale. Choosing $\boldsymbol{M}_{ard} = \text{diag}(\boldsymbol{\ell})^{-2}\boldsymbol{I}$ yields a covariance function that implements automatic relevance determination[22,26]. The two approaches can be combined by adding the covariance functions together thus creating the third covariance function. Model selection consists of choosing suitable values for the hyper-parameters. This is done using the marginal likelihood approach as discussed

by Rasmussen and Williams[22] allowing 1000 function evaluations during the optimization. The initial values for hyper–parameters are drawn from a zero–mean Gaussian distribution with unit variance. In order to avoid bad local minima 10 restarts is tried picking the hyper–parameters that yields the best marginal likelihood.

B.3.5 Artificial Neural Networks

The neural network classifier is a two–layered feed forward network (one hidden layer). Neural networks with one hidden layer are general approximators[21] so it is sufficient to use just one hidden layer. The network has eight inputs – one per polymer, and six outputs – one per analyte. Prior to training the entire data set whitened (made zero mean and scaled to unit variance). The hidden units use tangent hyperbolic sigmoidal function as transfer function. The network is trained using the BFGS optimization algorithm as described by Nielsen[27]. The cost function (that is used by the optimizer) is a quadratic cost function augmented with outliers detection and weight decay. The cost function $S(\boldsymbol{w})$ has two hyper–parameters α and β.

$$S(\boldsymbol{w}) = E_D(\boldsymbol{w}, \beta) + \alpha E_W(\boldsymbol{w}) \tag{B.4}$$

where $E_D(\boldsymbol{w}, \beta)$ is the cross-entropy error function and $E_W(\boldsymbol{w})$ is a regularization term[28]. Both hyper–parameters are updated after each iteration using MacKays Bayesian maximum likelihood II (MLII) scheme[29,30]. The hyper-parameters are initialized to $\alpha = 8$ and $\beta = 1$ and the network weights are initialized using a zero mean Gaussian with variance equal to α. The stopping criterion for the network training is either 100 iterations or if the hyper-parameters are updated with a margin lower that 10^{-5}. Each network training cycle is repeated 10 times and the network with the lowest training error $E_D(\boldsymbol{w}, \beta)$ is selected for concentration level estimation. The network training and cost function is described in details by Sigurdsson et. al.[28]. The neural network regressor is almost identical to the neural network classifier. The cost function does not have outliers detection and the regressor uses just one output neuron which hold the estimated concentration level.

The tunable parameters subject to cross validation is the number of hidden units. For the model selection part two to six hidden units were tested. The most often number of hidden units chosen was three which was chosen in 52.3% of the runs. The number of hidden units chosen for the regressor turned out to depend heavily on the analyte and the amount of training points available. Making a histogram on all runs put together showed an almost uniform histogram. However if the histogram is calculated for each value of N_{train} the most common choice for hidden units was 2 (for N_{train} in range 6–9)

B.3.6 Non–negative Matrix Factorization

Classification using NMF is a linear vector–space method. The data is represented in a 8–dimensional vector space and training consist of finding a suitable subspace as representative for each analyte. When classifying an unknown data point, the date point is projected into each subspace. The subspace that represents the data point best (calculated as residuals) is chosen as the correct analyte. This is done as follows; the training points for each analyte is stored as columns in a data matrix $\boldsymbol{X}_{analyte} \in \mathbb{R}^{8\times N_{train}}$. NMF factorizes $\boldsymbol{X}$ into two new matrices

$$\boldsymbol{W}\boldsymbol{H} \approx \boldsymbol{X}, \qquad \boldsymbol{W} \in \mathbb{R}_{0+}^{8\times b}, \quad \boldsymbol{H} \in \mathbb{R}_{0+}^{b\times N_{train}}, \quad \boldsymbol{X} \in \mathbb{R}_{0+}^{8\times N_{train}} \tag{B.5}$$

NMF assumes that all values in $\boldsymbol{X}$ is non–negative so all negative values in the data set are set to zero. Effectively it means pentanol will be classified without using the contribution from HDFD, see figure B.3. The matrix $\boldsymbol{W}$ is the basis and the columns of matrix $\boldsymbol{H}$ is the data points represented in the basis $\boldsymbol{W}$. After training we have one $\boldsymbol{W}$ matrix per analyte (it is enforced that all subspaces are of the same size). When classifying data points the NMF factorization is run with $\boldsymbol{W}$ held fixed. This procedure is carried out for all six $\boldsymbol{W}$ matrices resulting in six different $\boldsymbol{H}$ matrices. The $\boldsymbol{H}$ matrix that represent the data point best is chosen as the correct analyte.

The factorization is calculated using the approach by Lin[24]. Each element of matrices $\boldsymbol{W}$ and $\boldsymbol{H}$ are initialized to a value drawn from a uniform distribution in the interval $]0;1[$. The stopping criterion for the algorithm is either 30 iterations or 10^{-4} as relative error. The amount of basis vectors to use per subspace b is a model parameter that is allocated by LOO-CV. Allowable subspace size is in the interval $b \in \{2,\ldots,\min(N_{train}-1,10)\}$. The most often value chosen was $b = 2$. Note that b must be less that the amount of training points – so if $N_{train} = 3$ the subspace size is automatically chosen to $b = 2$. If we look at the case where $N_{train} = 12$ the subspace size was mostly chosen to $b = 2$ but only for 20% of the runs.

B.3.7 Principal component regression

Principal component regression is a linear regression method that is related to regularized least squares regression and partial least squared regression (PLS)[21,31]. The parameters to be chosen when using principal component regression is which principal components to include in the regression. We include principal components in the model ordered by their variance choosing the highest variance component. To determine the amount of components k to include in the model we use LOO-CV. The number of allowable components is

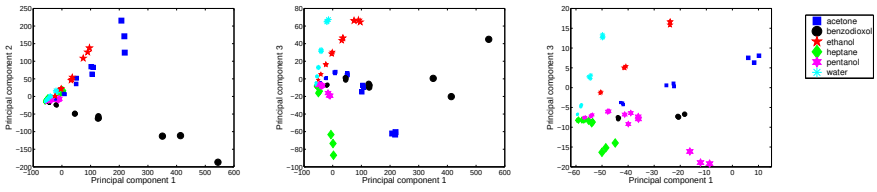

Figure B.6: QCM data visualized using PCA. The size of the squares represent the concentration. Panel 3 is a zoomed in version of panel 2.

$k \in \{1, \ldots, \min(N_{train}, 8)\}$. For $N_{train} = 12$ the most commonly chosen value was $k = 6$, but only in 22.3% of the runs.

B.3.8 Singular Value Decomposition

Classification using SVD is identical to the NMF classification method except for the matrix factorization. The matrix factorization is carried out using SVD instead and basis vectors are included based on their eigenvalues, always choosing the basis vector with the highest eigenvalue. The SVD classification method used is described in details by Eldén[31]. As with NMF the model selection parameter is the subspace size. For model selection the allowable subspace size of is $b \in \{1, \ldots, \min(N_{train} - 1, 7)\}$. For $N_{train} = 12$ the most commonly chosen subspace size was $b = 2$ which was chosen in 90% of the runs.

B.4. RESULTS

Principal component analysis is used to visualize the entire data set more effectively, see figure B.6. The plots illustrate that the analytes lying on their own almost linear manifold thus motivating the use of linear methods. The plots imply (but do not verify) that clustering methods such as K–nearest neighbor[21] would not perform well given a small amount of training points. If all concentrations are not represented by a cluster a substantial amount of data points would likely be misclassified. Table B.1 lists the classification accuracy for the tested classification algorithms. The performance of SVD classification is superior to both ANN and NMF. Using only 3 training points per analyte we gain remarkable accuracy – only misclassifying 3% of the test points. ANN is quite poor initially but as the amount of training point increases ANN classification catches up. NMF performance is similar to SVD although not quite

Algorithm	N_{train}				
	3	4	5	6	12
ANN	0.611 ± 0.027	0.200 ± 0.024	0.076 ± 0.003	0.023 ± 0.002	0.003 ± 0.001
NMF	0.039 ± 0.004	0.028 ± 0.004	0.025 ± 0.003	0.017 ± 0.003	0.009 ± 0.002
SVD	0.032 ± 0.004	0.012 ± 0.002	0.006 ± 0.001	0.002 ± 0.001	0.001 ± 0.000

Table B.1: Classification error on test sets calculated as the mean over a 100 runs $\pm$ the standard deviation of the mean. Note N_{train} is the amount of training points per analyte – the total amount of training points is N_{train} multiplied with six.

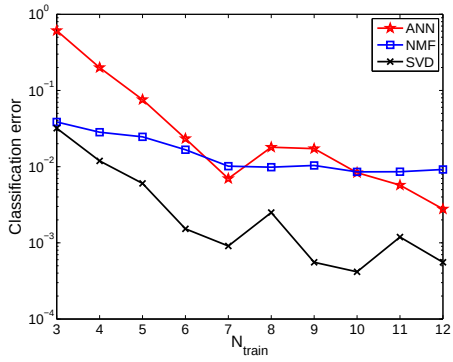

Figure B.7: Learning curves for the classification algorithms on a test set. Note N_{train} refers to the amount of training points per analyte. The total amount of training points is $6N_{train}$.

as good. Figure B.7 shows learning curves for the three algorithms. The SVD classifier is the preferred method regardless of the amount of training points. Concentration level estimation results are listed in table B.2. There is no clear indication of which algorithm should be the preferred choice although it shows that ANN is consistently the poorest performer. As with classification there are too few training points to train an adequate neural network solution. The best regressor for $N_{train} = 3$ is PCR regardless of analyte except for Benzodioxol where the GPAI approach is the best. At $N_{train} = 4$ the GPR method performs similar to PCR and for $N_{train} \geq 5$ GPR is either the superior method or on par for all choices of analyte. At $N_{train} = 12$ the GPR method offers superior accuracy. There is no significant indication of which of the three covariance functions is the best although the combined covariance function (GPAI) seems slightly better. Figure B.8 shows learning curves for the concentration level estimators. The learning curves clearly illustrates the troubles of ANN using a limited amount of training points. Another interesting observation is that PCR does not seem to improve significantly once N_{train} reaches 6.

Analyte	Algorithm	N_{train}				
		3	4	5	6	12
Acetone	PCR	0.14 ± 0.009	0.09 ± 0.004	0.07 ± 0.003	0.08 ± 0.003	0.07 ± 0.003
	GPI	0.56 ± 0.094	0.12 ± 0.010	0.06 ± 0.004	0.04 ± 0.001	0.04 ± 0.001
	GPA	0.52 ± 0.088	0.09 ± 0.020	0.06 ± 0.006	0.04 ± 0.001	0.03 ± 0.002
	GPAI	0.30 ± 0.047	0.09 ± 0.008	0.05 ± 0.003	0.04 ± 0.001	0.04 ± 0.002
	ANN	1.05 ± 0.060	0.58 ± 0.021	0.56 ± 0.026	0.48 ± 0.015	0.40 ± 0.024
Benzodioxol	PCR	0.22 ± 0.008	0.17 ± 0.008	0.13 ± 0.005	0.12 ± 0.003	0.14 ± 0.011
	GPI	0.24 ± 0.024	0.07 ± 0.004	0.05 ± 0.001	0.05 ± 0.001	0.04 ± 0.001
	GPA	0.22 ± 0.027	0.12 ± 0.005	0.08 ± 0.003	0.06 ± 0.002	0.04 ± 0.002
	GPAI	0.16 ± 0.011	0.12 ± 0.006	0.08 ± 0.004	0.06 ± 0.003	0.04 ± 0.001
	ANN	0.87 ± 0.057	0.68 ± 0.043	0.63 ± 0.036	0.46 ± 0.018	0.49 ± 0.034
Ethanol	PCR	0.10 ± 0.005	0.09 ± 0.003	0.07 ± 0.002	0.05 ± 0.002	0.04 ± 0.001
	GPI	0.36 ± 0.053	0.10 ± 0.006	0.05 ± 0.002	0.03 ± 0.000	0.03 ± 0.001
	GPA	0.61 ± 0.108	0.15 ± 0.021	0.07 ± 0.004	0.05 ± 0.001	0.04 ± 0.001
	GPAI	0.29 ± 0.049	0.14 ± 0.019	0.07 ± 0.003	0.05 ± 0.001	0.03 ± 0.001
	ANN	0.81 ± 0.047	0.55 ± 0.015	0.56 ± 0.041	0.47 ± 0.021	0.41 ± 0.023
Heptane	PCR	0.31 ± 0.014	0.26 ± 0.009	0.22 ± 0.007	0.17 ± 0.004	0.16 ± 0.008
	GPI	1.21 ± 0.161	0.41 ± 0.034	0.28 ± 0.015	0.17 ± 0.004	0.13 ± 0.002
	GPA	0.68 ± 0.098	0.23 ± 0.012	0.16 ± 0.006	0.12 ± 0.002	0.13 ± 0.003
	GPAI	0.44 ± 0.059	0.26 ± 0.019	0.17 ± 0.008	0.12 ± 0.003	0.12 ± 0.003
	ANN	$NaN \pm NaN$	0.83 ± 0.043	0.57 ± 0.016	0.56 ± 0.022	0.54 ± 0.032
Pentanol	PCR	0.35 ± 0.007	0.25 ± 0.010	0.13 ± 0.004	0.12 ± 0.002	0.12 ± 0.003
	GPI	0.60 ± 0.058	0.24 ± 0.019	0.12 ± 0.004	0.10 ± 0.002	0.06 ± 0.002
	GPA	0.38 ± 0.026	0.19 ± 0.008	0.14 ± 0.005	0.12 ± 0.003	0.04 ± 0.005
	GPAI	0.37 ± 0.024	0.19 ± 0.008	0.14 ± 0.004	0.12 ± 0.003	0.04 ± 0.004
	ANN	$NaN \pm NaN$	0.81 ± 0.024	0.73 ± 0.026	0.58 ± 0.002	0.37 ± 0.003
Water	PCR	0.18 ± 0.002	0.17 ± 0.002	0.17 ± 0.003	0.17 ± 0.003	0.17 ± 0.007
	GPI	0.44 ± 0.038	0.18 ± 0.012	0.13 ± 0.007	0.10 ± 0.003	0.07 ± 0.003
	GPA	0.30 ± 0.037	0.16 ± 0.013	0.12 ± 0.009	0.10 ± 0.005	0.07 ± 0.003
	GPAI	0.31 ± 0.037	0.19 ± 0.018	0.12 ± 0.011	0.11 ± 0.010	0.07 ± 0.003
	ANN	$NaN \pm NaN$	0.89 ± 0.032	0.70 ± 0.021	0.64 ± 0.012	0.50 ± 0.026

Table B.2: Estimation error on test sets calculated as the mean over a 100 runs $\pm$ the standard deviation of the mean. The three instances where ANN is listed as NaN means that there was occurrences where the network failed to train due to an unlucky choice of training set. GP* refers to Gaussian process regression using the different covariance functions. GPI is the isotropic covariance function, GPA is the ARD covariance function and GPAI is the combined covariance function.

B.5. CONCLUSSION

Eight different polymer coatings have been evaluated for their suitability as gas sensors by exposing polymer coated QCMs to volatile organic compounds. The high classification accuracy implies that the coatings do indeed represent the range of interactions described by the LSER model very well. Each polymer film seems to contribute with unique data. According to our analysis the coatings are useful as gas sensing elements and can thus advantageously be used to functionalize many other types of sensors. Deposition of multiple types of sensor coatings by plasma polymerization is compatible with practically any sensing device, and circumvents the use of solvents and subsequent drying processes during deposition which can often damage fragile device components.

We presented a two–tiered data analysis framework that successfully classified responses from an eight–dimensional polymer coated QCM sensor. By using linear methods such as SVD and NMF we get remarkable high accuracy ($> 96\%$)

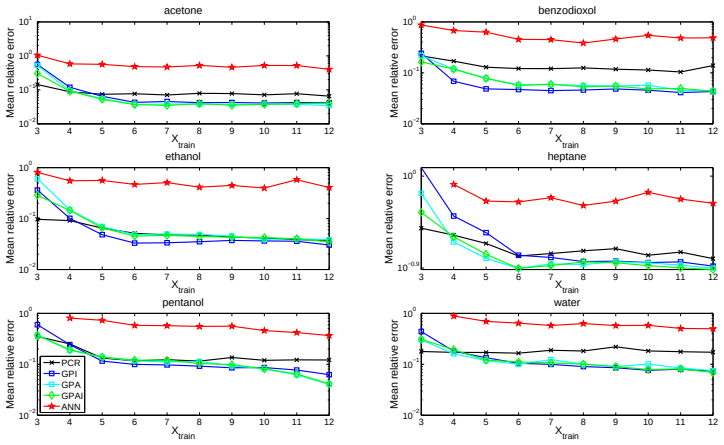

Figure B.8: Learning curves for the concentration level estimation.

with only 3 training points per analyte. Having one training point per analyte per concentration level SVD have an classification accuracy of 99.8%. NMF does not perform to the level of SVD, but is still better than ANN for a limited amount of training points. The NMF classification algorithm is fairly simple and more sophisticated approaches could be developed. One could perform NMF on the entire data set instead of per analyte and then map the basis vectors to classes using a probabilistic approach[32]. The model selection for NMF and SVD can be improved further as well. If there is more than one choice of b tied for the best model, b is assigned randomly to a value among the best choices. One could construct a cost function that takes the residual values into account and then select the value of b based on the cost function.

For concentration level estimation the Gaussian process regression is better than the linear method PCR (when $N_{train} \geq 5$). Both of these methods are markedly better than the ANN. The issue with ANN regression being that the system is underspecified. For the smallest possible neural network with two hidden units, the number of parameters in the model is 18 (16 weights in the first layer, 2 weights in the second layer), but the network only have up to 12 training points. One could possibly improve ANN performance by reducing the dimension of the data before applying the data to the neural network (for example using PCA) thus reducing the number of input neurons.

The best case scenario for GPR is a mean relative error of 3%. However the GPR method does have difficulties when having just three training points per

analyte. This can be explained by the zero mean Gaussian prior and the way data partitioning is performed. For training sets where the lowest and/or highest concentrations levels are omitted the GPR will perform poorly. In general the GPR will return to zero when estimating points outside the training interval. The performance outside the training interval could probably be improved by adding a growing term to the prior or using a thin–plate spline kernel as covariance function[33].

B.6. ACKNOWLEDGMENTS

We acknowledge the support from the Danish Agency for Science and Technology's, Program Commission on Nanoscience Biotechnology and IT (NABIIT), grant: 2106-07-0031 and 2106-05-0039.

REFERENCES

[1] Hamdi M. Saraoğlu and Burçak Edin. E-Nose System for Anesthetic Dose Level Detection using Artificial Neural Network. *Journal of Medical Systems*, 31(6):475–482, August 2007. ISSN 0148-5598. doi: 10.1007/s10916-007-9087-7.

[2] J. Yinon. Detection of Explosives by Electronic Noses. *Analytical Chemistry*, 75(5):98 A–105 A, March 2003. ISSN 0003-2700. doi: 10.1021/ac0312460.

[3] J.O. O. Mahony, K. Nolan, M.R. R. Smyth, and B. Mizaikoff. Molecularly imprinted polymers—potential and challenges in analytical chemistry. *Analytica Chimica Acta*, 534(1):31–39, April 2005. ISSN 00032670. doi: 10.1016/j.aca.2004.07.043.

[4] József Szejtli. Introduction and General Overview of Cyclodextrin Chemistry. *Chemical Reviews*, 98(5):1743–1754, July 1998. ISSN 0009-2665. doi: 10.1021/cr970022c.

[5] Abdul R. Khan, Peter Forgo, Keith J. Stine, and Valerian T. D'Souza. Methods for Selective Modifications of Cyclodextrins. *Chemical Reviews*, 98(5):1977–1996, July 1998. ISSN 0009-2665. doi: 10.1021/cr970012b.

[6] Günter Sauerbrey. Verwendung von Schwingquarzen zur Wägung dünner Schichten und zur Mikrowägung. *Zeitschrift für Physik*, 155(2):206–222, April 1959. ISSN 1434-6001. doi: 10.1007/BF01337937.

[7] Shigeru Kurosawa, Tomoya Hirokawa, Kazuya Kashima, Hidenobu Aizawa, Dae-Sang Han, Yasuo Yoshimi, Yuji Okada, Kiyoshi Yase, Jun Miyake, Minoru Yoshimoto, and Jöns Hilborn. Detection of deposition rate of plasma-polymerized films by quartz crystal microbalance. *Thin Solid Films*, 374(2):262–267, October 2000. ISSN 00406090. doi: 10.1016/S0040-6090(00)01161-5.

[8] Jay W. Grate and Michael H. Abraham. Solubility interactions and the design of chemically selective sorbent coatings for chemical sensors and arrays. *Sensors and Actuators B: Chemical*, 3(2):85–111, February 1991. ISSN 09254005. doi: 10.1016/0925-4005(91)80202-U.

[9] Hsin-Hsien Lu, Yerra Koteswara Rao, Tzong-Zeng Wu, and Yew-Min Tzeng. Direct characterization and quantification of volatile organic compounds by piezoelectric module chips sensor. *Sensors and Actuators B: Chemical*, 137(2):741–746, April 2009. ISSN 09254005. doi: 10.1016/j.snb.2009.01.060.

[10] Annika M. Rosengren, Kerstin Golker, Jesper G. Karlsson, and Ian A. Nicholls. Dielectric constants are not enough: principal component analysis of the influence of solvent properties on molecularly imprinted polymer-ligand rebinding. *Biosensors & bioelectronics*, 25(3):553–7, November 2009. ISSN 1873-4235. doi: 10.1016/j.bios.2009.06.042.

[11] Pengchao Si, John Mortensen, Alexei Komolov, Jens Denborg, and Preben J. Mø ller. Polymer coated quartz crystal microbalance sensors for detection of volatile organic compounds in gas mixtures. *Analytica chimica acta*, 597(2):223–30, August 2007. ISSN 1873-4324. doi: 10.1016/j.aca.2007.06.050. URL http://www.ncbi.nlm.nih.gov/pubmed/17683733.

[12] Kelly Sepcic, Mira Josowicz, Jiri Janata, and Ted Selby. Diagnosis of used engine oil based on gas phase analysis. *The Analyst*, 129(11):1070, 2004. ISSN 0003-2654. doi: 10.1039/b406619g.

[13] Zhihua Ying, Yadong Jiang, Xiaosong Du, Guangzhong Xie, Junsheng Yu, and Huiling Tai. Polymer coated sensor array based on quartz crystal microbalance for chemical agent analysis. *European Polymer Journal*, 44 (4):1157–1164, April 2008. ISSN 00143057. doi: 10.1016/j.eurpolymj.2008.01.015.

[14] Ali Gulbag, Feyzullah Temurtas, and Ismihan Yusubov. Quantitative discrimination of the binary gas mixtures using a combinational structure of the probabilistic and multilayer neural networks. *Sensors and Actuators B: Chemical*, 131(1):196–204, April 2008. doi: 10.1016/j.snb.2007.11.008.

[15] Ya-Ling Wang and Jeng-Shong Shih. Multi-channel piezoelectric crystal gas sensor with principal component analysis for organic solvent pollutants

from polymer plants. *Journal of the Chinese Chemical Society*, 53(6):1427–1437, December 2006. ISSN 0009-4536.

[16] Hamdi M. Saraoglu and Mehmet Kocan. Determination of Blood Glucose Level-Based Breath Analysis by a Quartz Crystal Microbalance Sensor Array. *IEEE Sensors Journal*, 10(1):104–109, January 2010. ISSN 1530-437X. doi: 10.1109/JSEN.2009.2035769. URL http://ieeexplore.ieee.org/lpdocs/epic03/wrapper.htm?arnumber=5352205.

[17] Bekir Mumyakmaz, Ahmet Özmen, Mehmet A. Ebeoğlu, and Cihat Taşaltın. Predicting gas concentrations of ternary gas mixtures for a predefined 3D sample space. *Sensors and Actuators B: Chemical*, 128(2):594–602, January 2008. ISSN 09254005. doi: 10.1016/j.snb.2007.07.062.

[18] Ahmet Özmen, F. Tekce, Mehmet A. Ebeoğlu, Cihat Taşaltın, and Zafer Z. Öztürk. Finding the composition of gas mixtures by a phthalocyanine-coated QCM sensor array and an artificial neural network. *Sensors and Actuators B: Chemical*, 115(1):450–454, May 2006. ISSN 09254005. doi: 10.1016/j.snb.2005.10.007.

[19] Daniel D. Lee and H. Sebastian Seung. Learning the parts of objects by non-negative matrix factorization. *Nature*, 401(6755):788–791, October 1999. doi: 10.1038/44565.

[20] Bjø rn Winther-Jensen and Kristian Glejbø l. Method and apparatus for the excitation of a plasma, 2003.

[21] Christopher M. Bishop. *Pattern Recognition and Machine Learning*. Springer, Secaucus, NJ, USA, 2006. ISBN 0387310738.

[22] Carl E. Rasmussen and Christopher K. I. Williams. *Gaussian Processes for Machine Learning*. MIT Press, April 2006. URL http://www.gaussianprocess.org/gpmlhttp://www.ncbi.nlm.nih.gov/pubmed/15112367.

[23] DTUInformatics. DTU:Toolbox. URL http://cogsys.imm.dtu.dk/toolbox/.

[24] Chih-Jen Lin. Projected gradient methods for nonnegative matrix factorization. *Neural computation*, 19(10):2756–79, October 2007. ISSN 0899-7667. doi: 10.1162/neco.2007.19.10.2756.

[25] Carl E. Rasmussen and Christopher K. I. Williams. GPML code, 2006. URL http://www.gaussianprocess.org/gpml.

[26] Radford M. Neal. *Bayesian Learning for Neural Networks*. Springer-Verlag New York, lecture no edition, 1996. ISBN 0-387-94724-8.

[27] Hans B. Nielsen. UCMINF - an Algorithm for Unconstrained, Nonlinear Optimization. Technical Report IMM-TEC-0019, IMM, Technical University of Denmark, 2001.

[28] Sigurdur Sigurdsson, Jan Larsen, Lars K. Hansen, Peter A. Philipsen, and Hans C. Wulf. Outlier estimation and detection application to skin lesion classification. In *IEEE International Conference on Acoustics Speech and Signal Processing*, volume 1, pages I–1049–I–1052. IEEE, May 2002. ISBN 0-7803-7402-9. doi: 10.1109/ICASSP.2002.5743975.

[29] David J. C. MacKay. A Practical Bayesian Framework for Backpropagation Networks. *Neural Computation*, 4(3):448–472, May 1992. ISSN 0899-7667. doi: 10.1162/neco.1992.4.3.448.

[30] David J. C. MacKay. The Evidence Framework Applied to Classification Networks. *Neural Computation*, 4(5):720–736, September 1992. ISSN 0899-7667. doi: 10.1162/neco.1992.4.5.720.

[31] Lars Eldén. *Matrix Methods in Data Mining and Pattern Recognition*. Society for Industrial and Applied Mathematics, Philadelphia, PA, USA, 2007. ISBN 9780898716269.

[32] Thomas Kolenda, Lars K. Hansen, Jan Larsen, and Ole Winther. Independent component analysis for understanding multimedia content. In H Bourlard, T Adali, S Bengio, J Larsen, and S Douglas, editors, *Proceedings of the 12th IEEE Workshop on Neural Networks for Signal Processing*, pages 757–766, Piscataway, New Jersey, 2002. IEEE. ISBN 0-7803-7616-1. doi: 10.1109/NNSP.2002.1030096.

[33] Grace Wahba. *Spline Models for Observational Data*. Society for Industrial and Applied Mathematics, January 1990. ISBN 978-0-89871-244-5. doi: 10.1137/1.9781611970128.

Appendix C

Data representation and feature selection for colorimetric sensor arrays used as explosives detectors

Tommy S. Alstrøm, Jan Larsen, Natalie V. Kostesha, Mogens H. Jakobsen, and Anja Boisen. Data representation and feature selection for colorimetric sensor arrays used as explosives detectors. In *IEEE International Workshop on Machine Learning for Signal Processing (MLSP)*, pages 1–6, 2011. URL http://dx.doi.org/10.1109/MLSP.2011.6064615.

The layout of the paper has been revised.

DATA REPRESENTATION AND FEATURE SELECTION FOR COLORIMETRIC SENSOR ARRAYS USED AS EXPLOSIVES DETECTORS

Tommy S. Alstrøm[a], *Jan Larsen*[a], *Natalie V. Kostesha*[b], *Mogens H. Jakobsen*[b] *and Anja Boisen*[b]

[a]Dept. of Informatics and Mathematical Modeling,
Technical University of Denmark
Richard Petersens Plads 321, 2800 Kgs. Lyngby, Denmark
{tsal,jl}@imm.dtu.dk

[b]Dept. of Micro- and Nanotechnology,
Technical University of Denmark
Ørsteds Plads 345 East, DK-2800, Kgs. Lyngby, Denmark
{natalie.kostesha,mogens.jakobsen,anja.boisen}@nanotech.dtu.dk

ABSTRACT

Within the framework of the strategic research project *Xsense* at the Technical University of Denmark, we are developing a colorimetric sensor array which can be useful for detection of explosives like DNT, TNT, HMX, RDX and TATP and identification of volatile organic compounds in the presence of water vapor in air. In order to analyze colorimetric sensors with statistical methods, the sensory output must be put into numerical form suitable for analysis. We present new ways of extracting features from a colorimetric sensor and determine the quality and robustness of these features using machine learning classifiers. Sensors, and in particular explosive sensors, must not only be able to classify explosives, they must also be able to measure the certainty of the classifier regarding the decision it has made. This means there is a need for classifiers that not only give a decision, but also give a posterior probability about the decision. We will compare K–nearest neighbor, artificial neural networks and sparse logistic

We acknowledge the support from the Danish Agency for Science and Technology's, Program Commission on Nanoscience Biotechnology and IT (NABIIT). Case number: 2106-07-0031 - Miniaturized sensors for explosives detection in air.

regression for colorimetric sensor data analysis. Using the sparse solutions we perform feature selection and feature ranking and compare to Gram–Schmidt orthogonalization.

Index Terms— artificial neural networks (ANN), chemo–selective compounds, classification, colorimetric sensor array, DNT, explosives detection, feature ranking, Gram–Schmidt orthogonalization, K–nearest neighbor (KNN), sparse logistic regression (SLR), TNT

C.1 Introduction

Over the past decade, explosives have been a preferred tool for terrorists, yet there is no satisfactory mobile and portable solution to detect explosives. To detect a variety of military and industrial explosives easily, new technologies must be developed. There are several application areas for explosives sensors, such as anti-terrorism (screening luggage and mail packages, checking suspects and mass transit systems), demining and environmental monitoring of hazardous compounds.

Sensors must not only easily detect a variety of hidden explosives but they must also be able to detect illegal chemicals and products of the explosives industry. A further requirement is that the sensing device should be portable, rapid, highly sensitive, specific (minimize false alarms), and inexpensive [1].

Over the past years a number of detecting methods have been developed and successfully applied in explosives detectors. These include, but are not limited to, gas chromatography, Raman spectrometry, mass spectrometry, ion mobility spectrometry and colorimetric sensors. Suslick *et al.* described the application of the colorimetric sensor array for detecting volatile organic compounds in the gas phase [2, 3] as well as for identifying different organic compounds in the liquid phase [4, 5]. In our project we develop a colorimetric sensor array that can be useful in detecting and identifying explosives like TNT, DNT, HMX, RDX and TATP [6, 7]. The colorimetric sensor is a fascinating technique for detecting different chemical compounds belonging to various classes, like amines, cyanides, alcohols, arenes, ketones, aldehydes and acids in the parts-per-million (ppm) and parts-per-billion (ppb) ranges [3, 8, 9]. In our research we use a completely different class of chemo–selective compound which has already shown excellent results for detecting TNT. This type of colorimetric sensor could be successfully applied in homeland security and defense [10, 11].

A colorimetric sensor array consists of a number of chemo–selective compounds of various colors that will undergo a color change when subjected to an environ-

ment or a target substance, hereafter denoted an *analyte*. These chemo–selective compounds, which are typically called *dyes* are digitalized using a flatbed scanner. One dye consists of several hundred pixels, but a dye is considered to have only one color which is typically found by calculating the mean pixel value. We investigate how feature extraction using the mean pixel value compares to alternatives.

Having acquired the sensor response digitally enables the application of signal processing and statistic methods such as principal component analysis (PCA) and hierarchical cluster analysis (HCA) [12–14]. In the domains where colorimetric sensors have been investigated, HCA shows high accuracy and low false alarm rate. The closely related K-Nearest Neighbor (KNN) classifier [15] with $K = 1$ set to one has evolved as the de–facto method.

Our requirements for a classifier go beyond what KNN offers. As we are detecting hazardous compounds, we require the classifier to offer posterior probabilities and not only decisions. Further we seek to qualify which compounds in the colorimetric sensor are important, and which are less important. This knowledge enables the ability to either reduce the size of the sensor or replace less sensitive and unimportant compounds with more selective and responsive compounds. Various feature selection strategies can be employed to select the dyes but so far none have been applied to colorimetric sensor arrays. Our preference would be to use a sparse classifier thus making the feature selection an inherent part of the classification. Our main goal is not to find the classifier that has the best classification rate but to identify a classifier with these attributes and at the same time delivers comparable or better performance compared to KNN. We will consider two classifiers: sparse logistic regression (SLR) [16] which is a linear classifier that is extended to model posterior probabilities and implement sparsity, and artificial neural networks (ANN) [17] which is a proven non–linear classifier. Our primary motivation to include a non–linear classifier is to investigate if non–linear models are better suited for colorimetric sensor arrays.

C.2 Colorimetric sensors

We have operated with three different sensors: sensor A comprised 15 dyes [6]; sensor B equal to sensor A with one added dye [7]; sensor C which is a further extension adding 15 dyes to sensor B (unpublished results). Fig. C.1A shows sensor B when exposed to the explosive analyte RDX. The sensors have been exposed to analytes belonging to the various chemical families (Table C.1). For a more elaborate description of sensor fabrication, dyes and target analytes we refer to our earlier published work [6, 7].

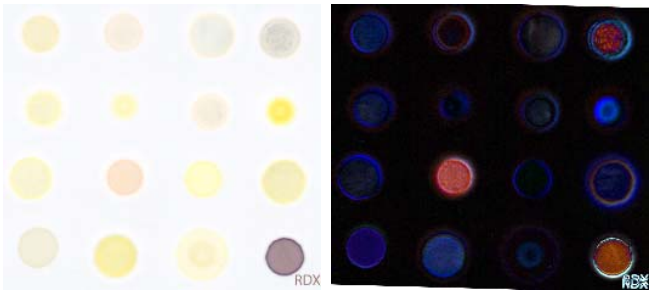

Figure C.1: An example of a colorimetric sensor exposed to the explosive analyte RDX. A: sensor before exposure. B: enhanced difference image.

Chemical family	A	B	C
Acids	32		45
Alcohols	26		27
Aldehydes	6		
Amines			42
Arenes	10		13
Drugs		6	
Environment	12	8	28
Explosives	20	8	56
Inorganic Explosives			14
Ketones	7		13
Thiols			14
Total measurements:	129	22	253

Table C.1: The different chemical families and how many measurements were applied to the sensors, i.e. sensor B has been measured 22 times in total, where 6 of the measurements were drugs. Each family comprises several compounds.

C.2.1 Data acquisition

Images of the sensor were scanned using an ordinary flatbed scanner immediately after immobilization of dyes and then again after exposure of target analytes. The images were encoded in a lossless format using the red-green-blue (RGB) color scheme with 8 bits per color. The images were used to generate color difference images by pixel subtraction (Fig. C.1). To align the two images a cost function that measures the L1 norm error per pixel is minimized:

$$\min_{\boldsymbol{t},\theta} \|\mathbf{I}_{\text{before}} - g(\mathbf{I}_{\text{after}}, \boldsymbol{t}, \theta)\|_1 / N_{pixels} \tag{C.1}$$

where I is an image matrix, $\mathbf{t}$ is an (x, y) translation, θ is a rotation and $g(\cdot)$ is the function that implements the transformation: first rotating the images using nearest neighbor interpolation, then translating (x, y)–pixels according to $\boldsymbol{t}$. The parameters $(\boldsymbol{t}, \theta)$ are initialized to zero.

The L1 norm error can be interpreted as the amount of *color* per pixel where a fully black pixel is fixed at a value of zero. At perfect image alignment, all the background pixels will be black and all dye pixels will have the weakest possible color, hence, blackness per pixel should be maximized. Dye localization and generation of colorimetric difference maps are described in detail in [18].

C.2.2 Data extraction

Once the images are digitalized feature extraction is employed typically using the mean pixel value. In order for the mean to be a robust measure of color change, the pixels of a dye have to be normally distributed (or at least have a symmetric distribution with one mode) and relatively free from outliers. As can be seen in Fig. C.2 this is may not always be the case. Chemically we know that a dye should only have one color, as the dye is homogeneous and exposed to a homogeneous vapor. However, noise is induced from: the scanner, the drying process of the dye, external light, and roughness of surface. Some of these effects can be handled easily. The drying of the dyes often results in a ring near the perimeter (the coffee stain effect) and this area of the dye is unreliable. To accommodate for this effect, a smaller area of a dye is used for feature extraction, corresponding to 2/3 of the dye radius. To handle the other noise effects that cause pixel outliers, the median or mode can be used as both statistics are more robust to outliers. Just as the case with the mean, the median requires a symmetric distribution with one mode. On the other hand the mode does not require the distribution to be symmetric and could potentially be more robust. However, these three statistics have the weakness that they consider the RGB colors as independent since an RGB color value is a 3 dimension vector. The multinomial mode does not have this weakness and will find the most occurring color in the dye hence we expect the multinomial mode to be the best representation. The entire data acquisition and extraction pipeline is described in detail in [18].

C.2.3 Data visualization

Data from colorimetric sensors can be visualized using principal component analysis (PCA) with a certain degree of success. However, once the sensor has

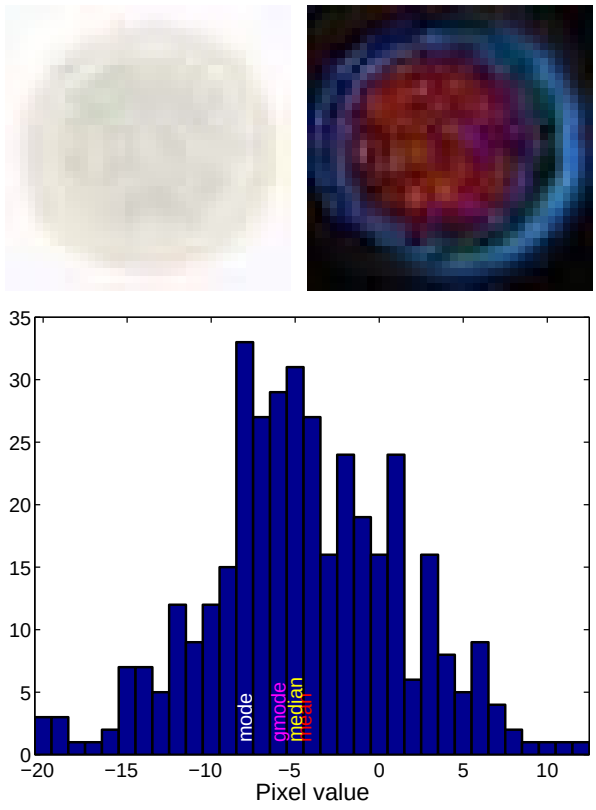

Figure C.2: An example of colorimetric sensor B exposed to the explosive analyte RDX. A: the sensor before exposure. B: the enhanced difference image. C: histogram of the green value and the value of the statistics.

been applied to many different classes, this kind of data visualization is of limited value. Fig. C.3 shows how PCA can be used to plot data for the sensor B case. However for sensors A and C the data collected is too high dimensional for a PCA plot to show the entire structure of the data [6]. Fig. C.4 shows how the variance in the data is distributed among the different dimensions. While the figure implies that sensor C is a higher dimensional sensor, the plot does not merit conclusions about the true dimensionality of the sensor. The dyes are highly correlated, especially the red-green-blue dimensions within each dye, but even more so there may be a lot of uncorrelated noise. PCA requires one dimension per uncorrelated signal channel and if the noise channels are sufficiently strong more dimensions will be needed to represent the data accurately. Observe that for three dimensions the sensors are almost equal, even though sensor C has

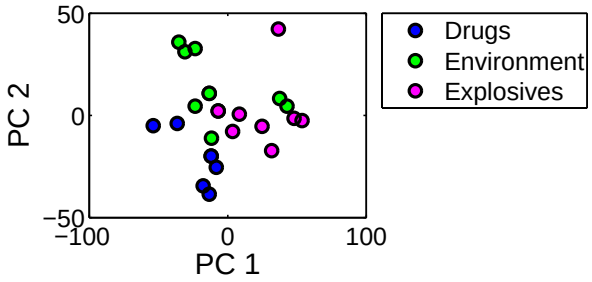

Figure C.3: PCA plot from sensor B. The PCA plot implies that the sensor should be able to separate well although there is an explosive outlier.

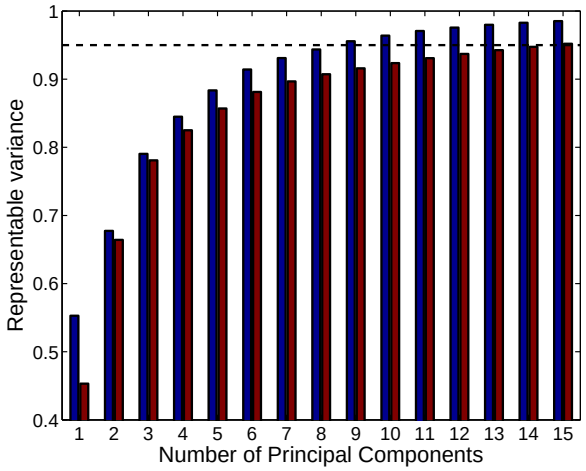

Figure C.4: The colorimetric sensor is a high dimensional sensor. For sensor A (blue) it requires 9 dimensions to represent 95% of the variance, whereas for sensor C (red) it requires 15 dimensions.

twice as many dyes as sensor A.

C.3 Methods

Each classification method is evaluated using 10–fold double cross validation (CV) partitioning used is a stratified approach. The partitioning of the outer fold that is used to estimate the test error remains fixed, while the partitions

that are used for model selection are regenerated in each run.

C.3.1 K–nearest neighbor

Despite its simplicity the K–nearest neighbor is an effective classification technique [15] which works as follows: when testing an unknown data point, the Euclidean distances for all known points are calculated. The classes of the closest K points are then identified and the unknown point is classified using majority voting of these known points. In the event of a tie, the algorithm uses the nearest neighbor among the tied classes to break the tie selecting the closest point as the class. All possible values of K are probed during model selection.

C.3.2 Sparse multinomial logistic regression

The multinomial logistic regression model offers a posterior probability of a class given a measurement. The model is written as

$$p(\mathcal{C}_k|\mathbf{x}) = \frac{\exp(\mathbf{w}_k^{\mathrm{T}}\mathbf{x})}{\sum_j \exp(\mathbf{w}_j^{\mathrm{T}}\ \mathbf{x})} \tag{C.2}$$

where $p(\mathcal{C}_k|\mathbf{x})$ is the probability of class $\mathcal{C}_k$ given a data point $\mathbf{x}$. To promote a sparse solution and to handle over-fit, we use L1 regularization. This is achieved by adding the term $\lambda\|\mathbf{w}\|_1$ to the cost function where λ is the model selection parameter. The cost function is minimized using the *Projection L1* method described by Schmidt *et al.* [16]. To further promote sparse solutions, the weights are initialized to zero. The optimal λ is searched for in the interval $[0; 10]$.

C.3.3 Artificial neural networks

The artificial neural network classifier used is a two–layered feed-forward with the hidden units using tangent hyperbolic sigmoidal function as the transfer function. A quadratic cost function augmented with outlier detection and weight decay is used. $S(\mathbf{w})$ has two hyper–parameters; the regularization parameter α and outlier probability β:

$$S(\mathbf{w}) = E_D(\mathbf{w}, \beta) + \alpha E_W(\mathbf{w}) \tag{C.3}$$

where $E_D(\mathbf{w}, \beta)$ is the cross-entropy error function and $E_W(\mathbf{w})$ is a regularization term. The hyper-parameter α is initialized to the number of inputs, i.e.,

Method	Median	Mode	MMode	Mean	Comb.
A-1NN	5.40	**5.83**	5.27	5.33	5.40
A-KNN	5.77	**6.20**	5.40	5.15	5.52
A-SLR	5.71	5.52	**6.08**	5.71	5.71
A-ANN	5.52	5.40	5.52	**5.71**	5.64
B-1NN	1.77	1.77	**2.18**	1.91	1.77
B-KNN	1.64	1.50	**1.91**	1.64	1.64
B-SLR	1.36	1.36	**1.91**	1.36	1.36
B-ANN	1.36	1.09	**1.50**	1.36	1.36
C-1NN	6.05	6.12	**6.15**	6.05	6.05
C-KNN	5.91	6.05	5.94	**6.12**	6.05
C-SLR	**6.79**	6.69	6.65	6.72	**6.79**
C-ANN	6.40	6.37	6.19	**6.47**	NaN
Total	1	2	**6**	3	1

Table C.2: Summary of how well the features and classifiers perform compared to random guessing, with the best performers highlighted.

the more inputs, the stronger regularization needed. The hyper-parameter β is initialized to zero as a priori there are no known outliers. The network weights are initialized using a zero mean Gaussian with variance equal to $1/\alpha$. Each network training cycle is repeated ten times and the network with the lowest training error $E_D(\mathbf{w}, \beta)$ is selected for classification. The outputs are converted to probabilities using the soft–max function. The network training and cost function are described in detail by Sigurdsson *et al.* [17].

C.4 Results and discussion

Since the sensors have a different amount of classes, we find it better to assess the quality of the classifiers by using the classification rate relative to random guessing as the classification rate alone can be misleading. For example a classification rate of 0.33% for sensor B would only be as good as random guessing while for sensor A and C it would be better than random guessing. The ratio is calculated as $(N_{correct} \cdot N_C)/N$, where N_C is the number of points correctly classified, N is the total number of points and N_C is the number of classes.

Table C.2 shows the best statistic is the multivariate mode which is the best performer in six out of twelve cases. However, all the other features are also represented at least once as the top performer, so the results indicate that in order to build the most accurate classifier one must extract all of the proposed

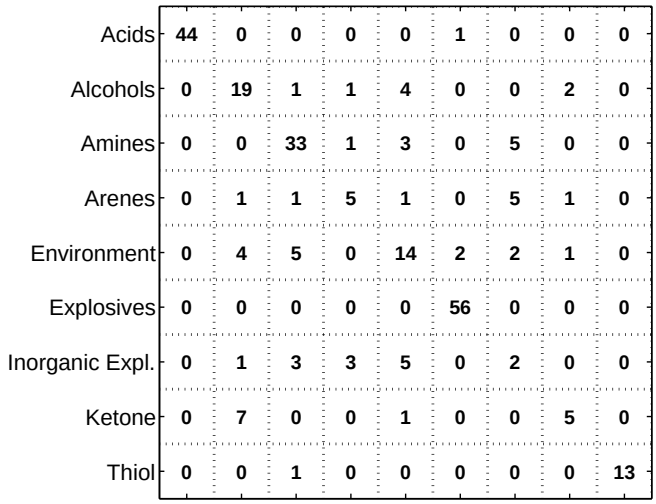

Figure C.5: Confusion matrix for C-SLR-Median where rows indicate the true class, columns indicate the predicted class and the number indicate the counts [19]. The sensor has a high classification rate for explosives with zero false negatives (all 56 measurements are classified correctly) but three false positives.

features from the colorimetric sensor and then let the feature selection be part of the model selection process.

The considered classification methods all perform similarly. As expected the simplest method, 1NN, is the best performer on the smallest dataset B. For sensor A, the KNN method is the best performer and on C the SLR is the best performer.

Sensor C is the richest sensor, with respect to data points, dyes and classes, and we will now discuss the results from this sensor in more detail. The best performing classifier for sensor C is SLR using median as feature extraction statistic. Fig. C.5 shows the confusion matrix for this situation and clearly shows that the sensor is very good for detecting especially acids and explosives, although some chemicals, such as arenes, pose a greater challenge. Having established that SLR is the classifier with the highest accuracy, we will now investigate how well SLR detects informative dyes by scrutinizing the sparse solutions.

A colorimetric sensor array is likely to have redundant features, as some dyes will

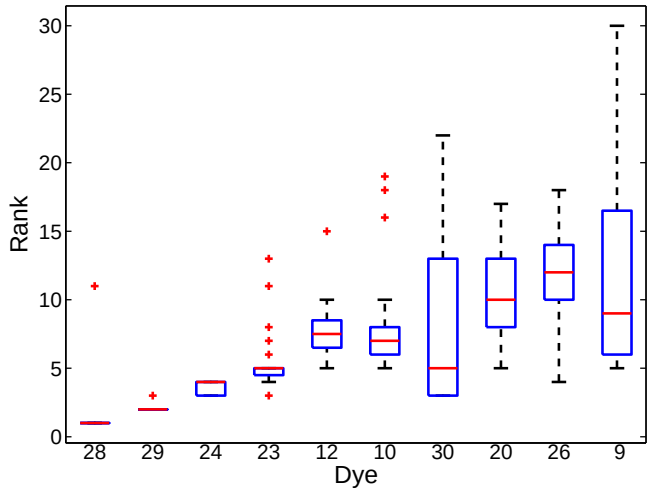

Figure C.6: Dyes ranked according to their mean rank for sensor C. The dye significance is listed from left to right where the more significant dye is the left.

react similarly, and it is not clear for the experimenter which dyes should be used in the next iteration of the sensor. We want to explore how well SLR identifies important dyes compared to the simple forward selection method based on the Gram–Schmidt orthogonalization [20].

For the feature selection process we convert the classification problem into a binary problem; explosives versus non-explosives (inorganic explosives will be part of the non-explosives group, as these explosives are not part of our detection focus). For each of the four feature extraction statistics, we will train ten models using the same data partitioning that was used in the multinomial classification case, hence forty models are trained in total. The sparsity parameter λ will start from zero and be incremented slowly, removing one feature at a time from the model. Each dye consist of three values (the RGB values) so in order to remove a dye all three features belonging to a dye have to be eliminated from the model. A dye is considered as completely removed once the weights for all the values are below a threshold which we set to 10^{-3}. Fig. C.6 shows how the dyes for sensor C rank according to their mean ranking. The top ten ranked dyes using the median as the feature extraction statistic are used to detect explosives. Fig. C.7 shows how well suited the dyes are for classification. Using three dyes the classification error is below 0.01% and after this adding more dyes only decreases the error marginally. Comparing the dyes identified by SLR to GS, the SLR dyes are clearly more suited, however if whitening is used GS show similar performance as SLR.

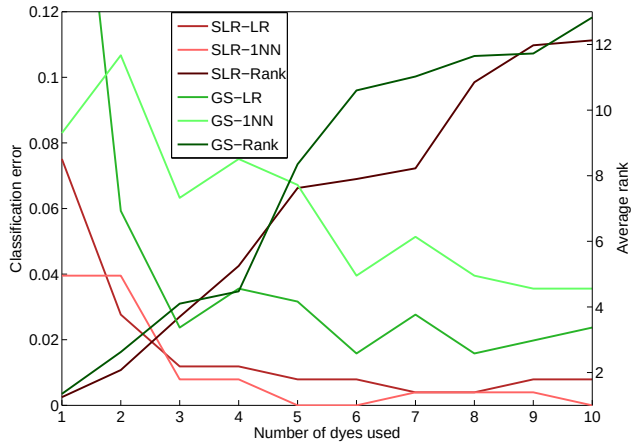

Figure C.7: Classification error with respect to number of dyes used, based on sensor C–Median. The classification error decreases to a certain point as dyes are added. SLR-LR is logistic regression classifier applied on the dyes identified by SLR. SLR-1NN used 1NN as classifier instead. SLR-Rank indicates the mean feature rank of dye i as shown on Fig. C.6. Similarly GS-X uses the features found by the GS based feature selection method.

C.5 Conclusion

We have tried five different feature sets of four different classifiers on three different colorimetric sensor arrays. The logistic regression method demonstrated equal classification ability compared to KNN and due to the added perks in terms of sparsity and probabilistic decisions, SLR is preferable to KNN. The results do not merit the use of a non–linear method such ANN. This is likely because there is not enough training data and since the experimental process of colorimetric sensors is time consuming, methods that work with fewer points are more appealing.

The classification results allow us to make a recommendation about which statistic to use for feature extraction. The de–facto approach is to use the mean but as the results show, this statistic only gives the best results on three instances, and never when combined with SLR. When using SLR the multivariate mode proved to be the best statistic. For sensor A and B the multivariate mode scores highest although for sensor C the median scored 2% higher than the multivariate mode.

SLR showed remarkable ability to identify a subset of dyes that could accurately

identify explosives from non–explosives. SLR did not reliably estimate the same features as important, but using the average rankings proved to be an adequate solution. Using the top 5 identified compounds we were are able to train a classifier that identified explosives without any false negatives (Fig. C.7).

Other popular classification methods such as linear discriminant analysis (LDA) and support vector machines (SVM) was not considered since they do not *both* model posterior probabilities and implement sparsity although one could consider using sparse relevance vector machines. Further, the dyes contribute with three features each (the RGB values) so one could also consider using group lasso instead of traditional regularization. This will be subject for future study.

References

[1] Michael S. Schmidt, Natalie V. Kostesha, Filippo G. Bosco, Jesper K. Olsen, Carsten Johnsen, Kent A. Nielsen, Jan O. Jeppesen, Tommy S. Alstrøm, Jan Larsen, Thomas Thundat, Mogens H. Jacobsen, and Anja Boisen. Xsense - a miniaturised multi-sensor platform for explosives detection. In *Proceedings of SPIE*, volume 8031, pages 803123–803123–7, 2011. doi: 10.1117/12.884050.

[2] Kenneth S. Suslick, Neal A. Rakow, and Avijit Sen. Colorimetric sensor arrays for molecular recognition. *Tetrahedron*, 60(49):11133–11138, November 2004. ISSN 00404020. doi: 10.1016/j.tet.2004.09.007.

[3] Neal A. Rakow, Avijit Sen, Michael C. Janzen, Jennifer B. Ponder, and Kenneth S. Suslick. Molecular recognition and discrimination of amines with a colorimetric array. *Angewandte Chemie (International ed. in English)*, 44(29):4528–32, July 2005. ISSN 1433-7851. doi: 10.1002/anie.200500939.

[4] Chen Zhang and Kenneth S. Suslick. A colorimetric sensor array for organics in water. *Journal of the American Chemical Society*, 127(33):11548–9, August 2005. ISSN 0002-7863. doi: 10.1021/ja052606z.

[5] Chen Zhang, Daniel P. Bailey, and Kenneth S. Suslick. Colorimetric sensor arrays for the analysis of beers: a feasibility study. *Journal of agricultural and food chemistry*, 54(14):4925–31, July 2006. ISSN 0021-8561. doi: 10.1021/jf060110a.

[6] Natalie V. Kostesha, Tommy S. Alstrøm, Carsten Johnsen, Kent A. Nielsen, Jan O. Jeppesen, Jan Larsen, Mogens H. Jakobsen, and Anja Boisen. Development of the colorimetric sensor array for detection of explosives and volatile organic compounds in air. In *Proceedings of SPIE*, volume 7673, pages 76730I–76730I–9, 2010. doi: 10.1117/12.850310.

[7] Natalie V. Kostesha, Tommy S. Alstrøm, Carsten Johnsen, Kent A. Nielsen, Jan O. Jeppesen, Jan Larsen, Anja Boisen, and Mogens H. Jakobsen. Multi-colorimetric sensor array for detection of explosives in gas and liquid phase. In *Proceedings of SPIE*, volume 8018, pages 80181H–80181H–12, 2011. doi: 10.1117/12.883895.

[8] Sung H. Lim, Liang Feng, Jonathan W. Kemling, Christopher J. Musto, and Kenneth S. Suslick. An Optoelectronic Nose for Detection of Toxic Gases. *Nature chemistry*, 1:562–567, September 2009. ISSN 1755-4349. doi: 10.1038/nchem.360.

[9] Chen Zhang and Kenneth S. Suslick. Colorimetric sensor array for soft drink analysis. *Journal of agricultural and food chemistry*, 55(2):237–42, January 2007. ISSN 0021-8561. doi: 10.1021/jf0624695.

[10] Dae-Sik Kim, Vincent M. Lynch, Kent A. Nielsen, Carsten Johnsen, Jan O. Jeppesen, and Jonathan L. Sessler. A chloride-anion insensitive colorimetric chemosensor for trinitrobenzene and picric acid. *Analytical and bioanalytical chemistry*, 395(2):393–400, 2009. doi: 10.1007/s00216-009-2819-4.

[11] Jung S. Park, Franck Le Derf, Christopher M. Bejger, Vincent M. Lynch, Jonathan L. Sessler, Kent A. Nielsen, Carsten Johnsen, and Jan O. Jeppesen. Positive Homotropic Allosteric Receptors for Neutral Guests: Annulated Tetrathiafulvalene–Calix[4]pyrroles as Colorimetric Chemosensors for Nitroaromatic Explosives. *Chemistry - A European Journal*, 16(3):848–54, January 2010. ISSN 1521-3765. doi: 10.1002/chem.200902924.

[12] Michael C. Janzen, Jennifer B. Ponder, Daniel P. Bailey, Crystal K. Ingison, and Kenneth S. Suslick. Colorimetric sensor arrays for volatile organic compounds. *Analytical chemistry*, 78(11):3591–600, June 2006. ISSN 0003-2700. doi: 10.1021/ac052111s.

[13] Benjamin A. Suslick, Liang Feng, and Kenneth S. Suslick. Discrimination of complex mixtures by a colorimetric sensor array: coffee aromas. *Analytical chemistry*, 82(5):2067–73, March 2010. ISSN 1520-6882. doi: 10.1021/ac902823w.

[14] Xiao-gang Luo, Ping Liu, Chang-jun Hou, Dan-qun Huo, Jia-le Dong, Huan-bao Fa, and Mei Yang. A novel chemical detector using colorimetric sensor array and pattern recognition methods for the concentration analysis of NH3. *The Review of scientific instruments*, 81(10):105113, October 2010. ISSN 1089-7623. doi: 10.1063/1.3501965.

[15] Christopher M. Bishop. *Pattern Recognition and Machine Learning*. Springer, Secaucus, NJ, USA, 2006. ISBN 0387310738.

[16] Mark Schmidt, Glenn Fung, and Rómer Rosales. Fast Optimization Methods for L1 Regularization: A Comparative Study and Two New Approaches. In Joost Kok, Jacek Koronacki, Raomon Mantaras, Stan Matwin, Dunja Mladenic, and Andrzej Skowron, editors, *Machine Learning: ECML 2007*, volume 4701 of *Lecture Notes in Computer Science*, pages 286–297. Springer Berlin / Heidelberg, 2007. doi: 10.1007/978-3-540-74958-5_28.

[17] Sigurdur Sigurdsson, Jan Larsen, Lars K. Hansen, Peter A. Philipsen, and Hans C. Wulf. Outlier estimation and detection application to skin lesion classification. In *IEEE International Conference on Acoustics Speech and Signal Processing*, volume 1, pages I–1049–I–1052. IEEE, May 2002. ISBN 0-7803-7402-9. doi: 10.1109/ICASSP.2002.5743975.

[18] Tommy S. Alstrøm and Jan Larsen. Feature Extraction and Signal Representation for Colorimetric Sensor Arrays. Technical report, DTU Informatics, 2011. URL http://www.imm.dtu.dk/pubdb/p.php?5845.

[19] Ian T. Nabney. Netlab 3.3: Algorithms for Pattern Recognition, 2004. URL http://www1.aston.ac.uk/eas/research/groups/ncrg/resources/netlab/.

[20] Isabelle Guyon and André Elisseeff. An introduction to variable and feature selection. *The Journal of Machine Learning Research*, 3:1157–1182, March 2003. ISSN 1532-4435. URL http://jmlr.csail.mit.edu/papers/v3/guyon03a.html.

Appendix D

Feature extraction using distribution representation for colorimetric sensor arrays used as explosives detectors

Tommy S. Alstrøm, Raviv Raich, Natalie V. Kostesha, and Jan Larsen. Feature extraction using distribution representation for colorimetric sensor arrays used as explosives detectors. In *IEEE International Conference on Acoustics, Speech, and Signal Processing (ICASSP)*, pages 2125–2128, 2012. doi: 10.1109/ICASSP.2012.6288331.

The layout of the paper has been revised.

FEATURE EXTRACTION USING DISTRIBUTION REPRESENTATION FOR COLORIMETRIC SENSOR ARRAYS USED AS EXPLOSIVES DETECTORS

Tommy S. Alstrøm[a], Raviv Raich[b], Natalie V. Kostesha[c], Jan Larsen[a]

[a]Dept. of Informatics and Mathematical Modeling, Technical University of Denmark
Richard Petersens Plads 321, 2800 Kgs. Lyngby, Denmark
{tsal,jl}@imm.dtu.dk

[b]School of Electrical Engineering and Computer Science
Oregon State University, Corvallis, OR 97331-5501
raich@eecs.oregonstate.edu

[c]Dept. of Micro- and Nanotechnology, Technical University of Denmark
ørsteds Plads 345 East, DK-2800, Kgs. Lyngby, Denmark
natalie.kostesha@nanotech.dtu.dk

ABSTRACT

We present a colorimetric sensor array which is able to detect explosives such as DNT, TNT, HMX, RDX and TATP and identifying volatile organic compounds in the presence of water vapor in air. To analyze colorimetric sensors with statistical methods, a suitable representation of sensory readings is required. We present a new approach of extracting features from a colorimetric sensor array based on a color distribution representation. For each sensor in the array, we construct a K–nearest neighbor classifier based on the Hellinger distances between color distribution of a test compound and the color distribution of all the training compounds. The performance of this set of classifiers are benchmarked against a set of K–nearest neighbor classifiers that is based on traditional feature representation (e.g., mean or global mode). The suggested approach of using the entire distribution outperforms the traditional approaches which use a single feature.

Index Terms— Hellinger distance, chemo–selective compounds, explosives detection, feature extraction, K–nearest neighbor classification

We acknowledge the support from the Danish Agency for Science and Technology's, Program Commission on Nanoscience Biotechnology and IT (NABIIT). Case number: 2106-07-0031 - Miniaturized sensors for explosives detection in air. Further we acknowledge Mikkel Schmidt, Dept. of Informatics and Mathematical Modeling, Technical University of Denmark and Ryota Tomioka, Dept. of Mathematical Informatics, University of Tokyo for invaluable and insightfull discussions.

1. INTRODUCTION

Over the past decade, explosives have been a preferred tool for terrorists, yet there is no satisfactory mobile and portable solution to detect explosives. To detect a variety of military and industrial explosives easily, new technologies must be developed. There are several application areas for explosives sensors, such as anti-terrorism (screening luggage and mail packages, checking suspects and mass transit systems), demining and environmental monitoring of hazardous compounds.

Sensors must not only easily detect a variety of hidden explosives, they must also be able to detect illegal chemicals and products of the explosives industry. Further requirements are that the sensing device should be portable, rapid, highly sensitive, specific (minimize false alarms), and inexpensive [1].

Over the past years a number of detection methods have been developed and successfully applied in explosives detectors. These include, but are not limited to, gas chromatography, Raman spectrometry, mass spectrometry, ion mobility spectrometry and colorimetric sensors. Suslick *et al.* described the application of the colorimetric sensor array for detecting volatile organic compounds in the gas phase [2, 3] as well as for identifying different organic compounds in the liquid phase [4, 5]. In our project we develop a colorimetric sensor array that can be useful in detecting and identifying explosives such as TNT, DNT, HMX, RDX and TATP [6, 7]. The colorimetric sensor is a fascinating technique for distinguishing different chemical compounds belonging to various classes, like amines, cyanides, alcohols, arenes, ketones, aldehydes and acids in the parts-per-million (ppm) and parts-per-billion (ppb) ranges [3, 8, 9]. In our research we use a com-

pletely different class of chemo–selective compound, which has already shown excellent results for detecting TNT. This type of colorimetric sensor could be successfully applied in national security and defense [10, 11].

A colorimetric sensor array consists of a number of chemo–selective compounds of various colors that will undergo a color change when subjected to an environment or a target substance, hereafter denoted an *analyte*. These chemo–selective compounds, which are typically called *dyes* are digitalized. Currently we use a flatbed scanner. One dye consists of several hundred pixels, but classically a dye is considered to have only one color, which is commonly found by calculating the mean or global mode pixel value [12]. We hypothesize that the complete distribution of color pixel value may contain additional information that can improve classification accuracy relative the information associated with a single pixel value such as the mean.

In this paper, we present a new method for representation and analyzing of the output of a colorimetric sensor array using the complete color distribution. To classify a given analyte, we propose a K-NN approach which uses the Hellinger distance between color distributions as a metric. By comparing this with a K-NN that use of a single feature such as the mean or global mode we are able to demonstrate significant improvement in accuracy.

2. COLORIMETRIC SENSORS

The colorimetric sensor array consists of a number of chemo–selective compounds immobilized onto silica gel resulting in circular spots (Fig. 1A). Each individual spot was approximately 3 mm in diameter with the total size of the sensor array of approximately 2.5 cm $\times$ 4.0 cm.

The dataset used in this paper has been discussed in detail in earlier work [12] but is summarized here for completeness. The sensor array has been exposed to analytes belonging to the various chemical families – 9 families in total, making it a multi-class dataset. The chemical families are: acids (45), alcohols (27), amines (42), arenes (14), environment (28), explosives (56), inorganic explosives (14), ketones (13) and thiols (14). The number in the parenthesis denotes the number of examples measured for the class in question, bringing to total number of examples to 253.

Data acquisition

Once the images of the sensor arrays have been digitalized, feature extraction is employed, typically using the mean pixel value. In order for the mean to be a robust measure of color change, the pixels of a dye have to be normally distributed (or at least have a symmetric distribution with one mode) and relatively free from outliers. As can be seen in Fig. 1 this may not always be the case. From a chemical point of view we know that a dye should only have one color, as the dye is homogeneous and exposed to a homogeneous vapor. However, noise is induced from: the scanner, the enhanced temperature for explosive detection, external light, and roughness of the surface. Some of these effects can be handled easily. The high temperature often results in a ring near the perimeter of the dyes (the coffee stain effect) and this area of the dyes is unreliable. In order to accommodate this effect, a smaller area of a dye is used for feature extraction, corresponding to 2/3 of the dye radius. To handle the other noise effects that cause pixel outliers, we have in earlier work suggested that the global mode is the most robust single value statistic compared to the mean, mode or median [12]. The global mode finds the most frequent pixel value occurring in a dye and as such is guaranteed to calculate a pixel value that exist in the given dye.

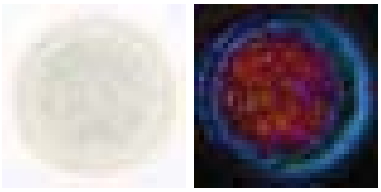

Fig. 1. An example of a specific dye of colorimetric sensor array exposed to the explosive analyte RDX. A: the sensor before exposure. B: the enhanced difference image.

Histogram features

In addition to the mean and global mode features used to characterize the color change response, we consider in this context the bag-of-words representation for multiple instance examples. The i'th example (dye) is represented by $X_i = \{x_{i1}, \ldots, x_{in_i}\}$, where x_{ij} is the j'th three–dimensional difference RGB pixel value between control and exposed, and n_i is the number of pixels considered for the representation of the i'th example. For several classifiers a notion of distance between examples is a key component. To construct a distance between two examples in the bag-of-words representation, we propose to represent each multi-instance example with a distribution and use the Hellinger distance as a metric between two examples. The motivation behind this approach is that differences between distributions, which are not directly measurable through the mean (or other moments), can still be detected. This approach was demonstrated to be effective in several application areas, e.g., disease classification using flow cytometry [13] and document classification [14].

Assuming an underlying probability density function f_i

such that $x_{ij} \sim f_i$ for $j = 1, 2, \ldots, n_i$, one can associate X_i with the following kernel density estimate

$$f_i(x) = \frac{1}{n_i} \sum_{j=1}^{n_i} K(x - x_{ij})$$

where $K(x) = 1/(2\pi\sigma^2)^{d/2} \exp(-||x||^2/2\sigma^2)$, $d = 3$ in our case. Recall that given two PDFs f_i and f_k, the squared Hellinger distance between the two distributions is given by

$$d_H(f_i, f_k)^2 = \int \left(\sqrt{f_i(x)} - \sqrt{f_k(x)}\right)^2 dx$$

i.e., the Euclidean distance between the square-root of the PDFs. Note that the squared Hellinger distance can be computed using the following equivalent formula: $d_H(f_i, f_k)^2 = 2 - 2\int \sqrt{f_i(x) f_k(x)} dx$. For computational simplicity, we consider the following equivalent alternative:

$$d_H(f_i, f_k)^2 = 2 - 2(E_{f_i}[\sqrt{T(x)(1 - T(x))}] + E_{f_k}[\sqrt{T(x)(1 - T(x))}])$$

where $T(x) = \frac{f_i(x)}{f_i(x) + f_k(x)}$ and $E_h[\cdot] = \int \cdot h(x) dx$. A sample-based version of this expression can be computed by replacing the expectations with their sample averages and the distributions with their kernel estimates,

$$E_{f_i}[\sqrt{T(x)(1 - T(x))}] \approx \frac{1}{n_i} \sum_{j=1}^{n_i} \sqrt{T(x_{ij})(1 - T(x_{ij}))}$$

Naturally, the distance calculation can be directly applied to a K-NN classifier. This approach can be considered an alternative to a set distance between two collections instances.

Moreover, this approach allows for a feature vector construction. Consider a new example X associated with PDF f. The feature vector for this example can be constructed as $\phi(X) = [d_H(f, f_1), d_H(f, f_2), \ldots, d_H(f, f_N)]^T$ where N is the number of training examples. Note that this feature vector has a fixed size, independent of the number of instances (pixels) in its bag-of-words representations. This representation can be applied to a variety of classifiers. For example, in SVM [15] the classifier can be of the form $\text{sgn}\langle w, \phi(X)\rangle$. In many cases, the SVM solution results in a sparse vector w for which the non-zero entries correspond to support vectors. In our setup, the Hellinger distance to key multi-instance examples will determine the output of the classifier.

3. METHODS AND RESULTS

Despite its simplicity, K-NN is an effective classification technique [15] which works as follows. When testing an unknown data point, the Euclidean distances for all known points are calculated. The classes of the closest K points are then identified and the unknown point is classified using majority voting of these known points.

		Dye rank		
Class	Method	1st	2nd	3rd
Acids	Mean	**1.2**	**2.4**	4.3
Acids	GMode	2.4	**2.4**	3.6
Acids	Hellinger	1.6	**2.4**	**2.8**
Alcohols	Mean	**7.5**	**8.3**	**8.3**
Alcohols	GMode	8.3	8.7	8.7
Alcohols	Hellinger	7.9	**8.3**	8.7
Amines	Mean	7.1	7.1	7.1
Amines	GMode	7.1	7.1	7.5
Amines	Hellinger	**6.3**	**6.7**	**6.7**
Explosives	Mean	2.8	3.2	4.3
Explosives	GMode	3.2	4.7	5.9
Explosives	Hellinger	**1.2**	**2.0**	**2.8**
Thiol	Mean	0.8	5.1	5.1
Thiol	GMode	0.8	3.6	4.7
Thiol	Hellinger	**0.4**	**3.2**	**4.0**

Table 1. The error rate of the 3 best performing dyes for each feature extraction method. The numbers are reported as % leave–one–out classification error.

We apply a K-NN classifier to each dye for each feature extraction technique in a 1 vs all setting. From earlier work [12] it was shown that the sensor is proficient in detecting acids, alcohols, amines, explosives and thiols so these are the classes for which we train classifiers. In order to carry out both model selection and estimation of the generalization error, double-cross validation using *leave–one–out* is performed. Our scheme result in a total of 155 classifiers per feature extraction method (31 dyes $\times$ 5 classes).

To establish if the Hellinger method produces greater or smaller classification error rate relative to the mean and global mode we examine wins, ties, and losses. To determine ties we use significance testing following McNemar significance test [16] using $\alpha = 0.01$ due to the amount of hypotheses we test. For Hellinger vs mean we find that Hellinger has eight wins, 146 ties and one loss. For Hellinger vs global mode we find Hellinger better nine times and global mode two times and 144 ties. Of out the twenty significant results we have a positive false discovery rate (pFDR) of 0.10, that is, we expect that two of the significant results where erroneously declared significant [17]. Table 1 shows how the feature extraction methods compare against each other when we choose the three best dyes for each combination of chemical/feature.

We also apply K-NN classifiers in a multi-class setting resulting in a total of 31 classifiers per feature extraction method, one classifier per dye. Fig. 2 shows the classification error for each of the method ordered by classification error using the Hellinger method. Performing the same hypothesis test idiom as before, we find that the Hellinger method was significantly better in 14 cases out of 62 (better than the mean and global mode in seven cases respectively, not always for

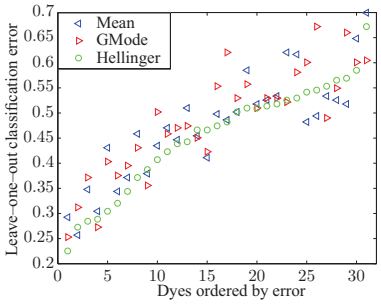

Fig. 2. Classification error for the feature extraction methods when k-NN is used to quantify the errors.

the same dyes) and worse in zero cases. The pFDR is 0.02 in the multi-class setting.

4. CONCLUSION

Despite the variability in the color reading of a given compound using one sensor, traditional methods consider representing the entire reading using a single value. To account for this variability, we proposed a complete distribution representation. To classify using the distribution representation, we adopted the Hellinger distance-based K-NN algorithm. To evaluate the potential benefit of using the complete distribution as opposed to the mean only for example, we compared single feature vector representation with the full distribution representation. We showed that the distribution representation with a Hellinger K-NN approach is either equal or better than the single vector representation with a Euclidean K-NN approach. The evidence for Hellinger being the better method is especially strong in the multi-class setting where it was significantly better in 23% of the cases.

References

[1] M. S. Schmidt, N. Kostesha, F. Bosco, J. K. Olsen, C. Johnsen, K. A. Nielsen, J. O. Jeppesen, T. S. Alstrøm, J. Larsen, T. Thundat, M. H. Jakobsen, and A. Boisen, "Xsense - a miniaturised multi-sensor platform for explosives detection," in *Proceedings of SPIE*, 2011.

[2] K. S. Suslick, N. A. Rakow, and A. Sen, "Colorimetric sensor arrays for molecular recognition," *Tetrahedron*, vol. 60, no. 49, pp. 11133–38, Nov. 2004.

[3] N. Rakow, A. Sen, M. C. Janzen, J. B. Ponder, and K. S. Suslick, "Molecular recognition and discrimination of amines with a colorimetric array.," *Angewandte Chemie (International ed. in English)*, vol. 44, no. 29, pp. 4528–32, July 2005.

[4] C. Zhang and K. S. Suslick, "A colorimetric sensor array for organics in water.," *Journal of the American Chemical Society*, vol. 127, no. 33, pp. 11548–9, Aug. 2005.

[5] C. Zhang, D. P. Bailey, and K. S. Suslick, "Colorimetric sensor arrays for the analysis of beers: a feasibility study.," *Journal of agricultural and food chemistry*, vol. 54, no. 14, pp. 4925–31, July 2006.

[6] N. V. Kostesha, T. S. Alstrøm, C. Johnsen, K. A. Nielsen, J. O. Jeppesen, J. Larsen, M. H. Jakobsen, and A. Boisen, "Development of the colorimetric sensor array for detection of explosives and volatile organic compounds in air," in *Proceedings of SPIE*, Apr. 2010, vol. 7673, pp. 76730I–76730I–9.

[7] N. V. Kostesha, T. S. Alstrøm, C. Johnsen, K. A. Nielsen, J. O. Jeppesen, J. Larsen, A. Boisen, and M. H. Jakobsen, "Multi-colorimetric sensor array for detection of explosives in gas and liquid phase," in *Proceedings of SPIE*, 2011.

[8] S. H. Lim, L. Feng, J. W. Kemling, C. J. Musto, and K. S. Suslick, "An Optoelectronic Nose for Detection of Toxic Gases.," *Nature chemistry*, vol. 1, pp. 562–567, Sept. 2009.

[9] C. Zhang and K. S. Suslick, "Colorimetric sensor array for soft drink analysis.," *Journal of agricultural and food chemistry*, vol. 55, no. 2, pp. 237–42, Jan. 2007.

[10] D. Kim, V. M. Lynch, K. Nielsen, C. Johnsen, J. O. Jeppesen, and J. L. Sessler, "A chloride-anion insensitive colorimetric chemosensor for trinitrobenzene and picric acid," *Analytical and bioanalytical chemistry*, vol. 395, no. 2, pp. 393–400, Sept. 2009.

[11] J. S. Park, F. Le Derf, C. M. Bejger, V. M. Lynch, J. L. Sessler, K. Nielsen, C. Johnsen, and J. O. Jeppesen, "Positive Homotropic Allosteric Receptors for Neutral Guests," *A European Journal*, vol. 16, no. 3, pp. 848–54, Jan. 2010.

[12] T. S. Alstrøm, J. Larsen, N. V. Kostesha, M. H. Jakobsen, and A. Boisen, "Data representation and feature selection for colorimetric sensor arrays used as explosives detectors," in *IEEE International Workshop on Machine Learning for Signal Processing*, Sept. 2011.

[13] K. M. Carter, R. Raich, W. G. Finn, and A. O. Hero, "Information preserving component analysis: Data projections for flow cytometry analysis," *Selected Topics in Signal Processing, IEEE Journal of*, vol. 3, no. 1, pp. 148–158, 2009.

[14] K. M. Carter, R. Raich, W. G. Finn, and A. O. Hero, "Fine: Fisher information nonparametric embedding," *IEEE transactions on pattern analysis and machine intelligence*, pp. 2093–2098, 2009.

[15] C. M. Bishop, *Pattern Recognition and Machine Learning*, Springer, 2006.

[16] Quinn McNemar, "Note on the sampling error of the difference between correlated proportions or percentages," *Psychometrika*, vol. 12, pp. 153–157, 1947.

[17] John D. Storey, "A direct approach to false discovery rates," *Journal of the Royal Statistical Society: Series B*, vol. 64, no. 3, pp. 479–498, 2002.

We acknowledge the support from the Danish Agency for Science and Technology's, Program Commission on Nanoscience Biotechnology and IT (NABIIT). Case number: 2106-07-0031 - Miniaturized sensors for explosives detection in air. Further we acknowledge Mikkel Schmidt, Dept. of Informatics and Mathematical Modeling, Technical University of Denmark and Ryota Tomioka, Dept. of Mathematical Informatics, University of Tokyo for invaluable and insightfull discussions.

FEATURE EXTRACTION USING DISTRIBUTION REPRESENTATION FOR COLORIMETRIC SENSOR ARRAYS USED AS EXPLOSIVES DETECTORS

Tommy S. Alstrøm[a], *Raviv Raich*[b], *Natalie V. Kostesha*[c], *Jan Larsen*[a]

[a]Dept. of Informatics and Mathematical Modeling,
Technical University of Denmark
Richard Petersens Plads 321, 2800 Kgs. Lyngby, Denmark
{tsal,jl}@imm.dtu.dk

[b]School of Electrical Engineering and Computer Science
Oregon State University, Corvallis, OR 97331-5501
raich@eecs.oregonstate.edu

[c]Dept. of Micro- and Nanotechnology,
Technical University of Denmark
ørsteds Plads 345 East, DK-2800, Kgs. Lyngby, Denmark
natalie.kostesha@nanotech.dtu.dk

ABSTRACT

We present a colorimetric sensor array which is able to detect explosives such as DNT, TNT, HMX, RDX and TATP and identifying volatile organic compounds in the presence of water vapor in air. To analyze colorimetric sensors with statistical methods, a suitable representation of sensory readings is required. We present a new approach of extracting features from a colorimetric sensor array based on a color distribution representation. For each sensor in the array, we construct a K–nearest neighbor classifier based on the Hellinger distances between color distribution of a test compound and the color distribution of all the training compounds. The performance of this set of classifiers are benchmarked against a set of K–nearest neighbor classifiers that is based on traditional feature representation (e.g., mean or global mode). The suggested approach of using the entire distribution outperforms the traditional approaches which use a single feature.

Index Terms— Hellinger distance, chemo–selective compounds, explosives detection, feature extraction, K–nearest neighbor classification

D.1 INTRODUCTION

Over the past decade, explosives have been a preferred tool for terrorists, yet there is no satisfactory mobile and portable solution to detect explosives. To detect a variety of military and industrial explosives easily, new technologies must be developed. There are several application areas for explosives sensors, such as anti-terrorism (screening luggage and mail packages, checking suspects and mass transit systems), demining and environmental monitoring of hazardous compounds.

Sensors must not only easily detect a variety of hidden explosives, they must also be able to detect illegal chemicals and products of the explosives industry. Further requirements are that the sensing device should be portable, rapid, highly sensitive, specific (minimize false alarms), and inexpensive [1].

Over the past years a number of detection methods have been developed and successfully applied in explosives detectors. These include, but are not limited to, gas chromatography, Raman spectrometry, mass spectrometry, ion mobility spectrometry and colorimetric sensors. Suslick *et al.* described the application of the colorimetric sensor array for detecting volatile organic compounds in the gas phase [2, 3] as well as for identifying different organic compounds in the liquid phase [4, 5]. In our project we develop a colorimetric sensor array that can be useful in detecting and identifying explosives such as TNT, DNT, HMX, RDX and TATP [6, 7]. The colorimetric sensor is a fascinating technique for distinguishing different chemical compounds belonging to various classes, like amines, cyanides, alcohols, arenes, ketones, aldehydes and acids in the parts-per-million (ppm) and parts-per-billion (ppb) ranges [3, 8, 9]. In our research we use a completely different class of chemo–selective compound, which has already shown excellent results for detecting TNT. This type of colorimetric sensor could be successfully applied in national security and defense [10, 11].

A colorimetric sensor array consists of a number of chemo–selective compounds of various colors that will undergo a color change when subjected to an environment or a target substance, hereafter denoted an *analyte*. These chemo–selective compounds, which are typically called *dyes* are digitalized. Currently we use a flatbed scanner. One dye consists of several hundred pixels, but classically a dye is considered to have only one color, which is commonly found by calculating the mean or global mode pixel value [12]. We hypothesize that the complete distribution of color pixel value may contain additional information that can

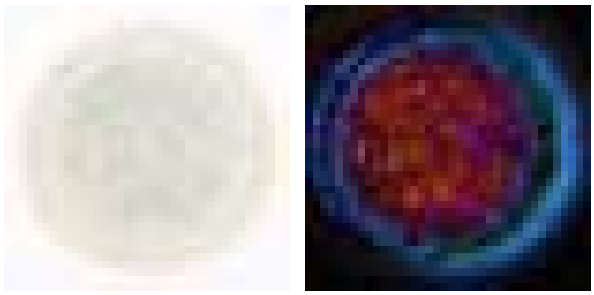

Figure D.1: An example of a specific dye of colorimetric sensor array exposed to the explosive analyte RDX. A: the sensor before exposure. B: the enhanced difference image.

improve classification accuracy relative the information associated with a single pixel value such as the mean.

In this paper, we present a new method for representation and analyzing of the output of a colorimetric sensor array using the complete color distribution. To classify a given analyte, we propose a K-NN approach which uses the Hellinger distance between color distributions as a metric. By comparing this with a K-NN that use of a single feature such as the mean or global mode we are able to demonstrate significant improvement in accuracy.

D.2 COLORIMETRIC SENSORS

The colorimetric sensor array consists of a number of chemo–selective compounds immobilized onto silica gel resulting in circular spots (Fig. D.1A). Each individual spot was approximately 3 mm in diameter with the total size of the sensor array of approximately 2.5 cm $\times$ 4.0 cm.

The dataset used in this paper has been discussed in detail in earlier work [12] but is summarized here for completeness. The sensor array has been exposed to analytes belonging to the various chemical families – 9 families in total, making it a multi-class dataset. The chemical families are: acids (45), alcohols (27), amines (42), arenes (14), environment (28), explosives (56), inorganic explosives (14), ketones (13) and thiols (14). The number in the parenthesis denotes the number of examples measured for the class in question, bringing to total number of examples to 253.

Data acquisition

Once the images of the sensor arrays have been digitalized, feature extraction is employed, typically using the mean pixel value. In order for the mean to be a robust measure of color change, the pixels of a dye have to be normally distributed (or at least have a symmetric distribution with one mode) and relatively free from outliers. As can be seen in Fig. D.1 this may not always be the case. From a chemical point of view we know that a dye should only have one color, as the dye is homogeneous and exposed to a homogeneous vapor. However, noise is induced from: the scanner, the enhanced temperature for explosive detection, external light, and roughness of the surface. Some of these effects can be handled easily. The high temperature often results in a ring near the perimeter of the dyes (the coffee stain effect) and this area of the dyes is unreliable. In order to accommodate this effect, a smaller area of a dye is used for feature extraction, corresponding to 2/3 of the dye radius. To handle the other noise effects that cause pixel outliers, we have in earlier work suggested that the global mode is the most robust single value statistic compared to the mean, mode or median [12]. The global mode finds the most frequent pixel value occurring in a dye and as such is guaranteed to calculate a pixel value that exist in the given dye.

Histogram features

In addition to the mean and global mode features used to characterize the color change response, we consider in this context the bag-of-words representation for multiple instance examples. The i'th example (dye) is represented by $X_i = \{x_{i1}, \ldots, x_{in_i}\}$, where x_{ij} is the j'th three–dimensional difference RGB pixel value between control and exposed, and n_i is the number of pixels considered for the representation of the i'th example. For several classifiers a notion of distance between examples is a key component. To construct a distance between two examples in the bag-of-words representation, we propose to represent each multi-instance example with a distribution and use the Hellinger distance as a metric between two examples. The motivation behind this approach is that differences between distributions, which are not directly measurable through the mean (or other moments), can still be detected. This approach was demonstrated to be effective in several application areas, e.g., disease classification using flow cytometry [13] and document classification [14].

Assuming an underlying probability density function f_i such that $x_{ij} \sim f_i$ for

$j = 1, 2, \ldots, n_i$, one can associate X_i with the following kernel density estimate

$$f_i(x) = \frac{1}{n_i} \sum_{j=1}^{n_i} K(x - x_{ij})$$

where $K(x) = 1/(2\pi\sigma^2)^{d/2} \exp(-||x||^2/2\sigma^2)$, $d = 3$ in our case. Recall that given two PDFs f_i and f_k, the squared Hellinger distance between the two distributions is given by

$$d_H(f_i, f_k)^2 = \int \left(\sqrt{f_i(x)} - \sqrt{f_k(x)}\right)^2 dx$$

i.e., the Euclidean distance between the square-root of the PDFs. Note that the squared Hellinger distance can be computed using the following equivalent formula: $d_H(f_i, f_k)^2 = 2 - 2\int \sqrt{f_i(x) f_k(x)} dx$. For computational simplicity, we consider the following equivalent alternative:

$$d_H(f_i, f_k)^2 = 2 - 2(E_{f_i}[\sqrt{T(x)(1 - T(x))}] + E_{f_k}[\sqrt{T(x)(1 - T(x))}])$$

where $T(x) = \frac{f_i(x)}{f_i(x)+f_k(x)}$ and $E_h[\cdot] = \int \cdot h(x) dx$. A sample-based version of this expression can be computed by replacing the expectations with their sample averages and the distributions with their kernel estimates,

$$E_{f_i}[\sqrt{T(x)(1 - T(x))}] \approx \frac{1}{n_i} \sum_{j=1}^{n_i} \sqrt{T(x_{ij})(1 - T(x_{ij}))}$$

Naturally, the distance calculation can be directly applied to a K-NN classifier. This approach can be considered an alternative to a set distance between two collections instances.

Moreover, this approach allows for a feature vector construction. Consider a new example X associated with PDF f. The feature vector for this example can be constructed as $\phi(X) = [d_H(f, f_1), d_H(f, f_2), \ldots, d_H(f, f_N)]^T$ where N is the number of training examples. Note that this feature vector has a fixed size, independent of the number of instances (pixels) in its bag-of-words representations. This representation can be applied to a variety of classifiers. For example, in SVM [15] the classifier can be of the form $\text{sgn}\langle w, \phi(X)\rangle$. In many cases, the SVM solution results in a sparse vector w for which the non-zero entries correspond to support vectors. In our setup, the Hellinger distance to key multi-instance examples will determine the output of the classifier.

D.3 METHODS AND RESULTS

Despite its simplicity, K-NN is an effective classification technique [15] which works as follows. When testing an unknown data point, the Euclidean distances

		Dye rank		
Class	Method	1st	2nd	3rd
Acids	Mean	**1.2**	**2.4**	4.3
Acids	GMode	2.4	**2.4**	3.6
Acids	Hellinger	1.6	**2.4**	**2.8**
Alcohols	Mean	**7.5**	**8.3**	**8.3**
Alcohols	GMode	8.3	8.7	8.7
Alcohols	Hellinger	7.9	**8.3**	8.7
Amines	Mean	7.1	7.1	7.1
Amines	GMode	7.1	7.1	7.5
Amines	Hellinger	**6.3**	**6.7**	**6.7**
Explosives	Mean	2.8	3.2	4.3
Explosives	GMode	3.2	4.7	5.9
Explosives	Hellinger	**1.2**	**2.0**	**2.8**
Thiol	Mean	0.8	5.1	5.1
Thiol	GMode	0.8	3.6	4.7
Thiol	Hellinger	**0.4**	**3.2**	**4.0**

Table D.1: The error rate of the 3 best performing dyes for each feature extraction method. The numbers are reported as % leave–one–out classification error.

for all known points are calculated. The classes of the closest K points are then identified and the unknown point is classified using majority voting of these known points.

We apply a K-NN classifier to each dye for each feature extraction technique in a 1 vs all setting. From earlier work [12] it was shown that the sensor is proficient in detecting acids, alcohols, amines, explosives and thiols so these are the classes for which we train classifiers. In order to carry out both model selection and estimation of the generalization error, double-cross validation using *leave–one–out* is performed. Our scheme result in a total of 155 classifiers per feature extraction method (31 dyes $\times$ 5 classes).

To establish if the Hellinger method produces greater or smaller classification error rate relative to the mean and global mode we examine wins, ties, and losses. To determine ties we use significance testing following McNemar significance test [16] using $\alpha = 0.01$ due to the amount of hypotheses we test.

For Hellinger vs mean we find that Hellinger has eight wins, 146 ties and one loss. For Hellinger vs global mode we find Hellinger better nine times and global mode two times and 144 ties. Of out the twenty significant results we have a

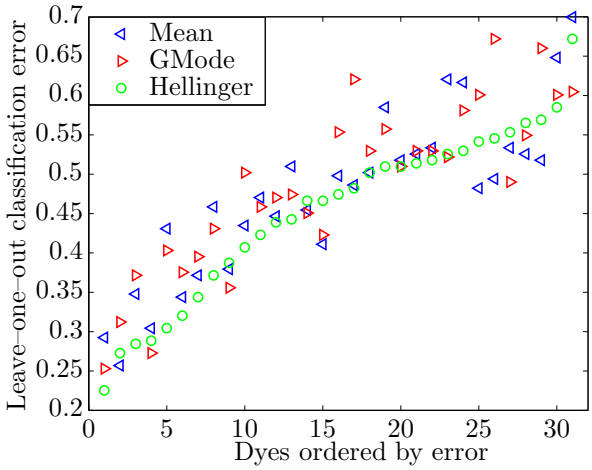

Figure D.2: Classification error for the feature extraction methods when k-NN is used to quantify the errors.

positive false discovery rate (pFDR) of 0.10, that is, we expect that two of the significant results where erroneously declared significant [17]. Table D.1 shows how the feature extraction methods compare against each other when we choose the three best dyes for each combination of chemical/feature.

We also apply K-NN classifiers in a multi-class setting resulting in a total of 31 classifiers per feature extraction method, one classifier per dye. Fig. D.2 shows the classification error for each of the method ordered by classification error using the Hellinger method. Performing the same hypothesis test idiom as before, we find that the Hellinger method was significantly better in 14 cases out of 62 (better than the mean and global mode in seven cases respectively, not always for the same dyes) and worse in zero cases. The pFDR is 0.02 in the multi-class setting.

D.4 CONCLUSION

Despite the variability in the color reading of a given compound using one sensor, traditional methods consider representing the entire reading using a single value. To account for this variability, we proposed a complete distribution representation. To classify using the distribution representation, we adopted the Hellinger distance-based K-NN algorithm. To evaluate the potential benefit

of using the complete distribution as opposed to the mean only for example, we compared single feature vector representation with the full distribution representation. We showed that the distribution representation with a Hellinger K-NN approach is either equal or better than the single vector representation with a Euclidean K-NN approach. The evidence for Hellinger being the better method is especially strong in the multi-class setting where it was significantly better in 23% of the cases.

References

[1] Michael S. Schmidt, Natalie V. Kostesha, Filippo G. Bosco, Jesper K. Olsen, Carsten Johnsen, Kent A. Nielsen, Jan O. Jeppesen, Tommy S. Alstrøm, Jan Larsen, Thomas Thundat, Mogens H. Jacobsen, and Anja Boisen. Xsense - a miniaturised multi-sensor platform for explosives detection. In *Proceedings of SPIE*, volume 8031, pages 803123–803123–7, 2011. doi: 10.1117/12.884050.

[2] Kenneth S. Suslick, Neal A. Rakow, and Avijit Sen. Colorimetric sensor arrays for molecular recognition. *Tetrahedron*, 60(49):11133–11138, November 2004. ISSN 00404020. doi: 10.1016/j.tet.2004.09.007.

[3] Neal A. Rakow, Avijit Sen, Michael C. Janzen, Jennifer B. Ponder, and Kenneth S. Suslick. Molecular recognition and discrimination of amines with a colorimetric array. *Angewandte Chemie (International ed. in English)*, 44(29):4528–32, July 2005. ISSN 1433-7851. doi: 10.1002/anie.200500939.

[4] Chen Zhang and Kenneth S. Suslick. A colorimetric sensor array for organics in water. *Journal of the American Chemical Society*, 127(33):11548–9, August 2005. ISSN 0002-7863. doi: 10.1021/ja052606z.

[5] Chen Zhang, Daniel P. Bailey, and Kenneth S. Suslick. Colorimetric sensor arrays for the analysis of beers: a feasibility study. *Journal of agricultural and food chemistry*, 54(14):4925–31, July 2006. ISSN 0021-8561. doi: 10.1021/jf060110a.

[6] Natalie V. Kostesha, Tommy S. Alstrøm, Carsten Johnsen, Kent A. Nielsen, Jan O. Jeppesen, Jan Larsen, Mogens H. Jakobsen, and Anja Boisen. Development of the colorimetric sensor array for detection of explosives and volatile organic compounds in air. In *Proceedings of SPIE*, volume 7673, pages 76730I–76730I–9, 2010. doi: 10.1117/12.850310.

[7] Natalie V. Kostesha, Tommy S. Alstrøm, Carsten Johnsen, Kent A. Nielsen, Jan O. Jeppesen, Jan Larsen, Anja Boisen, and Mogens H. Jakobsen. Multicolorimetric sensor array for detection of explosives in gas and liquid phase.

In *Proceedings of SPIE*, volume 8018, pages 80181H–80181H–12, 2011. doi: 10.1117/12.883895.

[8] Sung H. Lim, Liang Feng, Jonathan W. Kemling, Christopher J. Musto, and Kenneth S. Suslick. An Optoelectronic Nose for Detection of Toxic Gases. *Nature chemistry*, 1:562–567, September 2009. ISSN 1755-4349. doi: 10.1038/nchem.360.

[9] Chen Zhang and Kenneth S. Suslick. Colorimetric sensor array for soft drink analysis. *Journal of agricultural and food chemistry*, 55(2):237–42, January 2007. ISSN 0021-8561. doi: 10.1021/jf0624695.

[10] Dae-Sik Kim, Vincent M. Lynch, Kent A. Nielsen, Carsten Johnsen, Jan O. Jeppesen, and Jonathan L. Sessler. A chloride-anion insensitive colorimetric chemosensor for trinitrobenzene and picric acid. *Analytical and bioanalytical chemistry*, 395(2):393–400, 2009. doi: 10.1007/s00216-009-2819-4.

[11] Jung S. Park, Franck Le Derf, Christopher M. Bejger, Vincent M. Lynch, Jonathan L. Sessler, Kent A. Nielsen, Carsten Johnsen, and Jan O. Jeppesen. Positive Homotropic Allosteric Receptors for Neutral Guests: Annulated Tetrathiafulvalene–Calix[4]pyrroles as Colorimetric Chemosensors for Nitroaromatic Explosives. *Chemistry - A European Journal*, 16(3):848–54, January 2010. ISSN 1521-3765. doi: 10.1002/chem.200902924.

[12] Tommy S. Alstrøm, Jan Larsen, Natalie V. Kostesha, Mogens H. Jakobsen, and Anja Boisen. Data representation and feature selection for colorimetric sensor arrays used as explosives detectors. In *IEEE International Workshop on Machine Learning for Signal Processing (MLSP)*, pages 1–6, 2011. doi: 10.1109/MLSP.2011.6064615.

[13] Kevin M. Carter, Raviv Raich, William G. Finn, and Alfred O. Hero. Information Preserving Component Analysis: Data Projections for Flow Cytometry Analysis. *IEEE Journal of Selected Topics in Signal Processing*, 3 (1):148–158, February 2009. ISSN 1932-4553. doi: 10.1109/JSTSP.2008.2011112.

[14] Kevin M. Carter, Raviv Raich, William G. Finn, and Alfred O. Hero. FINE: fisher information nonparametric embedding. *IEEE transactions on pattern analysis and machine intelligence*, 31(11):2093–8, November 2009. ISSN 1939-3539. doi: 10.1109/TPAMI.2009.67.

[15] Christopher M. Bishop. *Pattern Recognition and Machine Learning*. Springer, Secaucus, NJ, USA, 2006. ISBN 0387310738.

[16] Quinn McNemar. Note on the sampling error of the difference between correlated proportions or percentages. *Psychometrika*, 12(2):153–157, June 1947. ISSN 0033-3123. doi: 10.1007/BF02295996.

[17] John D. Storey. A direct approach to false discovery rates. *Journal of the Royal Statistical Society: Series B (Statistical Methodology)*, 64(3):479–498, August 2002. ISSN 13697412. doi: 10.1111/1467-9868.00346. URL http://doi.wiley.com/10.1111/1467-9868.00346.

Appendix E

Hausdorff and Hellinger for Colorimetric Sensor Array Classification

Tommy S. Alstrøm, Bjørn S. Jensen, Mikkel N. Schmidt, Natalie V. Kostesha, and Jan Larsen. Hausdorff and Hellinger for Colorimetric Sensor Array Classification. In *IEEE International Workshop on Machine Learning for Signal Processing (MLSP)*, pages 1–6, 2012. doi: 10.1109/MLSP.2012.6349724.

The layout of the paper has been revised.

HAUSDORFF AND HELLINGER FOR COLORIMETRIC SENSOR ARRAY CLASSIFICATION

Tommy S. Alstrøm[a], *Bjørn S. Jensen*[a], *Mikkel N. Schmidt*[a], *Natalie V. Kostesha*[b], *Jan Larsen*[a]

[a]Dept. of Informatics and Mathematical Modeling,
Technical University of Denmark
Asmussens Allé 321, 2800 Kgs. Lyngby, Denmark
{tsal,bjje,mns,jl}@imm.dtu.dk

[b]Dept. of Micro- and Nanotechnology,
Technical University of Denmark
Ørsteds Plads 345 East, DK-2800, Kgs. Lyngby, Denmark
natalie.kostesha@nanotech.dtu.dk

ABSTRACT

Development of sensors and systems for detection of chemical compounds is an important challenge with applications in areas such as anti-terrorism, demining, and environmental monitoring. A newly developed colorimetric sensor array is able to detect explosives and volatile organic compounds; however, each sensor reading consists of hundreds of pixel values, and methods for combining these readings from multiple sensors must be developed to make a classification system. In this work we examine two distance based classification methods, K-Nearest Neighbor (KNN) and Gaussian process (GP) classification, which both rely on a suitable distance metric. We evaluate a range of different distance measures and propose a method for sensor fusion in the GP classifier. Our results indicate that the best choice of distance measure depends on the sensor and the chemical of interest.

We acknowledge the support from the Danish Agency for Science and Technology's, Program Commission on Nanoscience Biotechnology and IT (NABIIT). Case number: 2106-07-0031 - Miniaturized sensors for explosives detection in air. Further we acknowledge assistant professor Raviv Raich, Oregon State University, for lending his code for distance calculation based on Hellinger distances using Parzen windows [1, 2].

Index Terms— Hausdorff distance, Hellinger distance, chemo–selective compounds, feature extraction, K–nearest neighbor classification, Gaussian Process Classification

E.1. INTRODUCTION

The development of rapid, reliable, and portable solutions for detection of chemical compounds is an important challenge with many possible applications including screening luggage and packages for explosives, detecting land mines, and monitoring the environment for hazardous compounds. In recent years a number of methods has been developed based on different technologies such as gas chromatography, Raman spectrometry, mass spectrometry, ion mobility spectrometry and colorimetric sensors.

Colorimetric sensors can be used to detect a wide range of organic compounds in gas as well liquid phase [3–8]. In previous work a novel colorimetric sensor array developed by Kostesha et al. has been described [9, 10]. The sensor array proved useful for identifying a wide range of explosives as well as other compounds such as amines, cyanides, alcohols, arenes, ketones, aldehydes and acids. A colorimetric sensor contains a chemo-selective compound: A so-called dye which changes color when exposed to a target chemical compound denoted as analyte. The sensor is read by capturing a digital image of the dye before and after exposure to an analyte. Typically, the mean color change is used for detection; however, in earlier work it has been shown that accuracy can be improved by considering the complete distribution of color change for different image pixels [11]. An example of a colorimetric sensor is shown on Fig. E.1. In this example the mean value is a particular bad choice as the mean color value is scarcely present in the sensor as shown on Fig. E.1C. Furthermore, the sensor array comprises several colorimetric sensors, and detection could likely be improved further by combining information from multiple sensors.

In this paper, we present new methods for analyzing the output of a colorimetric sensor array using the complete distribution of color changes. We hypothesize that using the entire distribution of a sensor one will get an equal or better classification accuracy compared to a single feature representation such as the mean value. To classify a given analyte, we compare the de-facto method K-Nearest Neighbor (KNN) with a Gaussian process (GP) classifier. Both of these approaches rely on a measure of similarity between sensor readings—the KNN through a suitable distance measure and the GP through a covariance function. We motivate and compare several measures of similarity, demonstrating that a proper choice of similarity measure can significantly improve classification accuracy using a single dye. Finally, we propose a multi kernel method using

GP for fusing information from several sensors leading to superior performance compared to using a single sensor.

E.2. MATERIALS AND METHODS

In this section we describe the colorimetric sensor data and the proposed classification approach.

E.2.1. Notation

$N = 253$	Number of observations
$L = 3$	Number of channels (RGB)
$M = 31$	Number of dyes/sensors
$N_{\text{pix}} = [49; 1009]$	Pixels per dye/sensor
$\boldsymbol{x}_{l,n}$	$1 \times N_{\text{pix}}$ vector of pixel values
$\boldsymbol{X}_n = [\boldsymbol{x}_{1,n}^\top \boldsymbol{x}_{2,n}^\top \boldsymbol{x}_{3,n}^\top]^\top$	$3 \times N_{\text{pix}}$ matrix with RGB pixel values
$\mathcal{X} = \{x_n \| n = 1 : N\}$	a set of inputs
$\mathcal{Y} = \{y_n; x_n | n = 1 : N\}$	a set of labels for the given inputs

E.2.2. Colorimetric sensor data

The colorimetric sensor array consists of a number of chemo–selective compounds immobilized onto silica gel resulting in circular spots (Fig. E.1A). Each individual sensor was approximately 3 mm in diameter with the total size of the sensor array of approximately 2.5 cm × 4.0 cm.

The dataset used in this paper has been discussed in detail in earlier work [12] but is summarized here for completeness. The sensor array has been exposed to analytes belonging to various chemical families; acids (45), alcohols (27), amines (42), explosives (56) and other (83). The number in the parenthesis denotes the number of examples measured for the class in question. The group denoted other is not one chemical family but comprises various molecules that is used as reference measurements.

E.2.2.1. Data acquisition

The sensors were scanned using an ordinary flatbed scanner immediately after immobilization of dyes and then again after exposure of target analytes. The images are then pixel aligned, the dye locations are identified and finally pixel

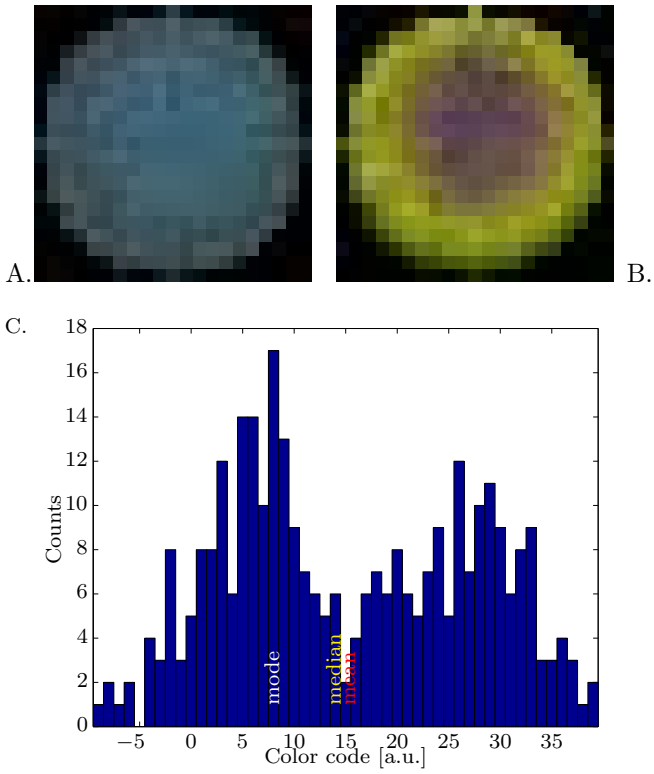

Figure E.1: An example of a specific dye of colorimetric sensor array exposed to the explosive analyte HMX. A: the sensor before exposure. B: the enhanced difference image. C: histogram of difference of the blue channel.

extraction is performed [12, 13]. The pixels are extracted by fitting a circular disc to the entire dye. Due to the chemistry of the sensor array often a distinct ring near the perimeter of the dyes appears (the coffee stain effect) and this area of the dyes is deemed unreliable. In order to accommodate for this effect a smaller area of a dye is used for feature extraction, corresponding to 2/3 of radius of the fitted circular disc [13]. Based on the pixel values features can be calculated, e.g. using the mean value, or distances between measurements.

E.2.3. Classification Methods

E.2.3.1. K-Nearest Neighbor

The KNN is a simple yet effective classification technique [14] which works as follows. When testing a data point belonging to an unknown class, the distances to all points with known class labels are calculated. The classes of the closest K points are then identified and the unknown point is classified using majority voting. In order to carry out both model selection and estimation of the generalization error, double-cross validation using *leave-one-out* is performed. The inner loop is used to determine the value of K and the outer loop is used to estimate the generalization error.

E.2.3.2. Gaussian Process Classification

We now turn to a different but equally powerful classification framework based on a non-parametric Bayesian approach. The core of any probabilistic classification methods is a likelihood function modeling the likelihood of observing a specific outcome. Here we consider the cumulative Gaussian (known as a probit model) defined as

$$p\left(y_n|f\left(\boldsymbol{X}_n\right)\right) = \int_{-\infty}^{y_n \cdot f(\boldsymbol{X}_n)} \mathcal{N}\left(t|0,1\right) dt = \Phi\left(y_n \cdot f\left(\boldsymbol{X}_n\right)\right) \tag{E.1}$$

parameterized by a given a functional value, $f(\boldsymbol{X}_n)$. Hence, the model or free parameter is the functional value, $f(\boldsymbol{X}_n)$, and by taking a Bayesian approach, we can directly consider the posterior over the function defined by the finite set of random variables, $\mathbf{f} = [f(\boldsymbol{X}_1), f(\boldsymbol{X}_2), ..., f(\boldsymbol{X}_N)]^\top$, i.e.,

$$p\left(\mathbf{f}|\mathcal{Y},\mathcal{X}\right) = \frac{p\left(\mathcal{Y}|\mathbf{f}\right)p\left(\mathbf{f}|\mathcal{X}\right)}{\int p\left(\mathcal{Y}|\mathbf{f}\right)p\left(\mathbf{f}|\mathcal{X}\right)d\mathbf{f}} = \frac{p\left(\mathcal{Y}|\mathbf{f}\right)p\left(\mathbf{f}|\mathcal{X}\right)}{p\left(\mathcal{Y}|\mathcal{X}\right)} \tag{E.2}$$

The natural prior for, $f(\cdot)$, is a Gaussian Process (GP) and we denote a function drawn from a GP as $f\left(\boldsymbol{X}\right) \sim \mathcal{GP}\left(\mathbf{0}, k(\cdot,\cdot)_{\boldsymbol{\theta}_c}\right)$ with a zero mean function, and $k(\cdot,\cdot)_{\boldsymbol{\theta}_c}$ referring to the covariance function with hyper-parameters $\boldsymbol{\theta}_c$, defining the covariance between the random variables $\boldsymbol{f}$. The GP can thus be considered a distribution over functions, i.e., $p\left(\mathbf{f}|\mathcal{X},\boldsymbol{\theta}_c\right)$.

Given the probit likelihood model, the posterior over $\boldsymbol{f}$ needs to be approximated and we resort to Expectation Propagation (EP) which provides a Gaussian approximation to the posterior [15]. The hyper parameters are approximated by point-estimates found by considering the marginal likelihood/evidence which can be optimized in regards to the hyper parameters by gradient methods. This possibility is a clear advantage over non-Bayesian methods.

The prediction for a new input $\boldsymbol{X}^*$ is obtained by first computing the predictive distribution, $p(f^*|\mathcal{Y}, \mathcal{X}, \boldsymbol{X}^*)$, which is Gaussian due to the EP approximation. The probability of a given outcome y^* is computed by $P(y|\mathcal{Y}, \mathcal{X}, \boldsymbol{X}^*) = \int p(y|f^*)\, p(f^*|\mathcal{Y}, \mathcal{X}, \boldsymbol{X}^*) df^*$.

E.2.4. Distances and Covariance Functions

The two classification methods outlined above both require some notion of similarity either in the form of a distance function/metric or in the form of a covariance function. In the following we present and motivate a number of distance measures that can be used for measuring similarities between dyes.

E.2.4.1. Mean and "inner mean"

The traditional approach when using colorimetric sensors is to calculate the mean value of the response by averaging the color change over all pixels.

Since we have observed that pixel values in the outer edge of the dyes are less reliable, we propose to estimate an optimal radius instead of a fixed radius (typically r=2/3) and compute the mean in the central region within this radius. Assuming that each dye should have a unique color change and such that any variation is due to noise, a reasonable assumption is to choose the radius that estimates the mean most accurately. This is done by choosing

$$\hat{r} = \arg\min_r \frac{1}{\sqrt{N_{\text{pix}}(r)}} \sigma(r), \tag{E.3}$$

where $N_{\text{pix}}(r)$ and $\sigma(r)$ denote the number of pixels and the standard deviation of pixel values within the central region with radius r. We denote this method "Inner Mean".

E.2.4.2. Hellinger Distance

As an alternative to computing the average color change, we can consider the distribution of color change over the dye. The Hellinger distance measures similarity between two probability measures $f_i(\mathbf{x})$ and $f_j(\mathbf{x})$ and is given by

$$d_{\text{He}}(f_i, f_j)^2 = \int \left(\sqrt{f_i(\mathbf{x})} - \sqrt{f_j(\mathbf{x})} \right)^2 d\mathbf{x} \tag{E.4}$$

Using the Hellinger distance require us to choose how to represent the probability measures. We consider a nonparametric and a parametric approach: The first is a Parzen window Kernel density estimator which have been discussed in earlier

work [11]:

$$f_i(\mathbf{x}) = \frac{1}{n_i}\sum_{k=1}^{n_i} K(\mathbf{x} - \mathbf{x}_{ik}) \tag{E.5}$$

where $K(\mathbf{x}) = 1/(2\pi\sigma^2)^{d/2}\exp(-||\mathbf{x}||^2/2\sigma^2)$ and the kernel width is set to $\sigma = 1$. The second approach is a multivariate normal distribution using a full covariance matrix

$$f_i(\mathbf{x}) = \frac{1}{(2\pi)^{d/2}|\boldsymbol{\Sigma}_i|^{d/2}}\exp\left(-\frac{1}{2}(\boldsymbol{\mu}_i - \mathbf{x})^\top {\boldsymbol{\Sigma}_i}^{-1}(\boldsymbol{\mu}_i - \mathbf{x})\right) \tag{E.6}$$

where $\boldsymbol{\mu}_i$ is the mean and $\boldsymbol{\Sigma}_i$ the covariance matrix which is estimated by maximum likelihood.

E.2.4.3. The Hausdorff Distance

The Hausdorff distance measures distance between two point sets, and it is small if all points in each set are close to some point in the other set. This could be useful for comparing dye color changes that are not uniform over the dye. First define the distance between two points $\mathbf{x}_i$ and $\mathbf{x}_j$ as the Euclidean distance $d(\mathbf{x}_i, \mathbf{x}_j) = \|\mathbf{x}_i - \mathbf{x}_j\|_2$. The distance between a point $\mathbf{x}_i$ and a set $\boldsymbol{X}_j$ is then $d(\mathbf{x}_i, \boldsymbol{X}_j) = \min_{\mathbf{x}_j \in \boldsymbol{X}_j} d(\mathbf{x}_i, \mathbf{x}_j)$. The Hausdorff distance is defined as

$$d_{\mathrm{Ha}}(\boldsymbol{X}_i, \boldsymbol{X}_j) = \max\left\{\max_{\mathbf{x}_i \in \boldsymbol{X}_i} d(\mathbf{x}_i, \boldsymbol{X}_j), \max_{\mathbf{x}_j \in \boldsymbol{X}_j} d(\mathbf{x}_j, \boldsymbol{X}_i)\right\} \tag{E.7}$$

As an alternative approach one can use the modified Hausdorff distance which is more robust in the presence of noise and outliers

$$d_{\mathrm{MH}}(\boldsymbol{X}_i, \boldsymbol{X}_j) = \max\left\{\frac{1}{N_{\boldsymbol{X}_i}}\sum_{\mathbf{x}_i \in \boldsymbol{X}_i} d(\mathbf{x}_i, \boldsymbol{X}_j), \frac{1}{N_{\boldsymbol{X}_j}}\sum_{\mathbf{x}_j \in \boldsymbol{X}_j} d(\mathbf{x}_j, \boldsymbol{X}_i)\right\} \tag{E.8}$$

It should be noted that this distance is not a metric as the triangle inequality is not fulfilled [16].

E.2.4.4. From Distances to Covariance Functions

Given a distance metric $d(\boldsymbol{X}_i, \boldsymbol{X}_j)$ we use the distance substitution approach [17] based on a squared exponential kernel, $k(\boldsymbol{X}_i, \boldsymbol{X}_j) = \exp\left(-\frac{1}{\sigma_l}d(\boldsymbol{X}_i, \boldsymbol{X}_j)\right)$. We note that a valid covariance function may be constructed directly for the Hellinger distance by considering the inner product given by the integral which

is known as the Probability Product Kernel [18]; however, to make a fair comparisons we treat the Hellinger distance like the other distance measures. Note also, that since the modified Hellinger distance is not a metric, the distance substitution kernel is not positive definite [17].

The use of kernels provides a convenient way of integrating information from different sensors by combining different kernels in a weighted sum. Thus, different dyes can be combined by constructing the following kernel

$$k\left(\boldsymbol{X}_i, \boldsymbol{X}_j\right) = \sigma^2 \mathbf{I} + \sum_{m=1}^{M} \alpha_m k\left(\boldsymbol{X}_i^m, \boldsymbol{X}_j^m\right) \tag{E.9}$$

where each kernel function is the distance substitution kernel with one of the respective metrics.

To fuse the difference dyes we employ a forward selection method using the following steps. 1) For a given dye, perform a grid search of hyper parameters σ^2, α_m and σ_l. 2) Find the hyper parameters by optimizing the evidence in GP using the optimal point found in the grid as initial guess. 3) Perform *leave-one-out* cross validation to get classification error. 4) Choose the dye that yields the lowest classification error.

E.2.5. Evaluation

We apply nearest neighbor classifiers to each dye for each feature extraction technique in a one vs all setting. From earlier work [12] it was shown that the sensor is proficient in detecting among others acids, alcohols, amines and explosives so these are the classes we evaluate. The generalization error is estimated using LOOCV [19]. This scheme result in a total of 124 classifiers of each type per feature extraction method (31 dyes $\times$ 4 classes).

To judge the differences in classification performance we use the McNemar significance test [20]. The McNemar is a paired test which uses the the number of cases where two classifiers disagree about a decision. From this test we calculate p–values for each comparison and use the multiple hypothesis framework proposed by Storey [21]. Based on the p–values we can calculate the expected positive false discoveries (E[pFD]) for our significant differences, that is, the expected quantity of wrongly significant results amount all found significant results.

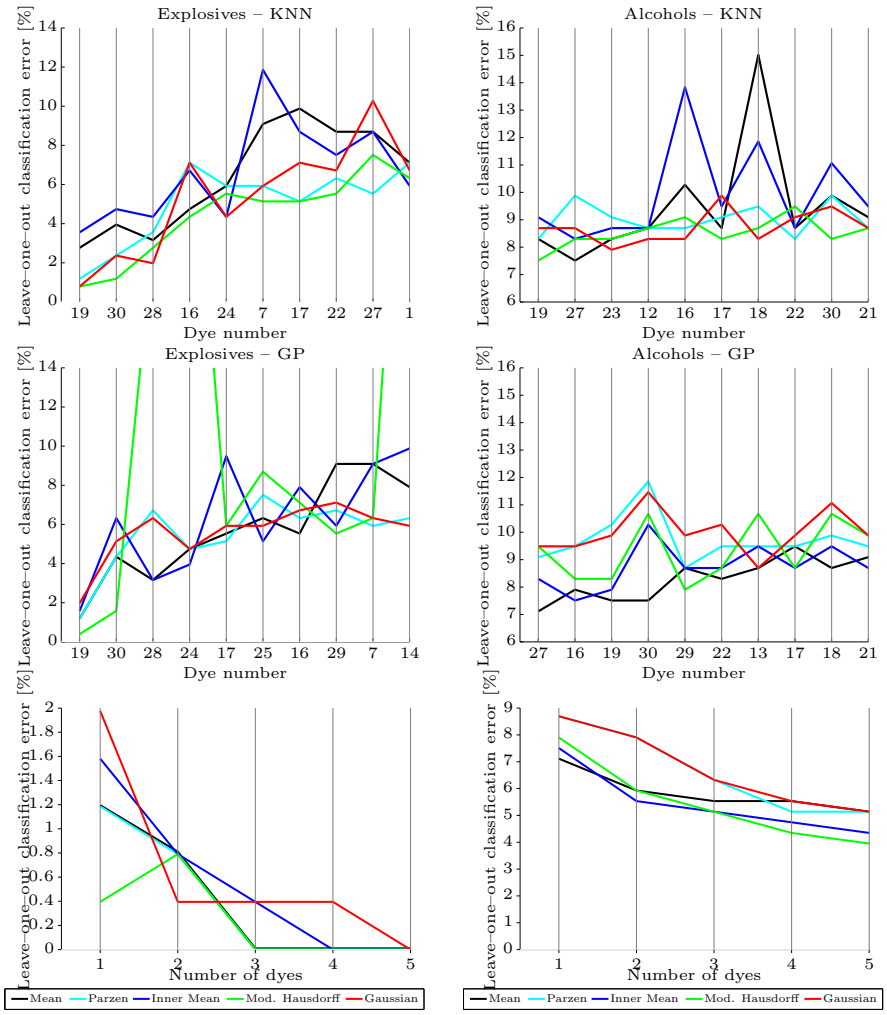

Figure E.2: Classification error for the different measures of similarity for GP and KNN. The top panels show the best performing dyes for explosives and alcohols using KNN. The middle panels show the best performing dyes using GP. The bottom panels shows the result of fusing the dyes together using GP. Bottom left is explosives and bottom right is alcohols.

Chemical	M	P	IM	MH	G	E[pFD]	n
Acids	1	2	2	6	0	0.89	11
Alcohols	0	0	0	0	3	0.15	3
Amines	1	0	1	0	0	1.02	2
Explosives	0	3	0	7	1	0.98	11

Table E.1: Number of instances the best performing method is significantly better than another method. The methods are Mean, Parzen, Inner Mean, Mod. Hausdorff and Gaussian. E[pFD] is the expected positive false discoveries and n is the number of significant results.

E.3. RESULTS AND DISCUSSION

Initially we employ KNN and rank the dyes according to their best performance. Fig. E.2 top panels show the dye ranking for KNN. The modified Hausdorff is the best performer for dyes 19 and 30 where it is significantly better than the single feature methods. Further the distribution methods are generally better or on par compared to the single feature methods.

Table E.1 shows a summery of the McNemar significance tests. The overall best distance is the modified Hausdorff method although it is noteworthy that this method is not best even once for alcohols whereas is is best for numerous occasions for acids and explosives. Looking into the dyes reveal that the top dyes for acids largely overlap with the top dyes for explosives whereas for alcohols one of the top dyes is dye number 5. For this dye the Inner Mean is significantly better than any of the other methods. It should be noted that the majority of the differences is between one of the distribution methods and the single feature method, i.e. of the 52 significant results, only on 3 instances was the Parzen window worst and only 4 times where the Mod. Hausdorff method worst. Considering we have a total of 6 false discoveries we can only conclude that the distribution methods are significantly better than the single feature methods. To explore the effect of the methods deeper we fuse the dyes using GP.

Initially we want to establish the performance of GP in the same setting as KNN. Fig. E.2 show the classification performance for GP when classifying explosives. Again the modified Hausdorff is the top performer for the first two dyes, which is again dye 19 and 30. However for dye 28 and 24 the modified Hausdorff coupled with GP yields an error of 21% and 30% respectively. This might very well be an effect of the fact that the modified Hausdorff is not a valid metric and as such the corresponding kernel might not be psd [16, 17]. But as the case of KNN, the figure does not show a clear indication of which method is superior

although it seems that modified Hausdorff is able to capture more information about dye 19 and 30 than the the methods.

When fusing the dyes one by one using forward selection we find no significant results between the methods (Fig. E.2). To get a significant result the performance must at least differ 2.4 percent points but already with one dye we are below that margin.

E.4. CONCLUSIONS

We have proposed three new methods for representation of sensory data in colorimetric sensor arrays, namely the Inner Mean, Hellinger distance using a Gaussian distribution and the Modified Hausdorff. Each method have it's merits. The Inner Mean seem to be particularly proficient for dye number 5 and 22 whereas the modified Hausdorff is especially strong for dye number 19 and 30. This suggests that none of the methods are capable of representing all the dye measurements optimally, although the methods that use the entire histogram are more often superior.

The modified Hausdorff method is the overall best performing method. It is particularly strong for classifying explosives, and since the distance calculation is based on sets of pixels and is parameter-free it can potentially work a lot better for high dimensional data where the Hellinger distance method might be inappropriate.

Finally, we have demonstrated that fusing the sensors can improve the classification error. GP classification effectively identifies which dyes should be included and generally including more dyes reduces the LOOCV error rate. In the fusing scheme the modified Hausdorff method also works well and is the overall best performer. Future work could be to combine all distance methods and learn the combination using Multiple Kernel Learning or evidence optimization instead of minimizing the classification error.

E.5. REFERENCES

[1] Kevin M. Carter, Raviv Raich, William G. Finn, and Alfred O. Hero. Information Preserving Component Analysis: Data Projections for Flow Cytometry Analysis. *IEEE Journal of Selected Topics in Signal Processing*, 3 (1):148–158, February 2009. ISSN 1932-4553. doi: 10.1109/JSTSP.2008.2011112.

[2] Kevin M. Carter, Raviv Raich, William G. Finn, and Alfred O. Hero. FINE: fisher information nonparametric embedding. *IEEE transactions on pattern analysis and machine intelligence*, 31(11):2093–8, November 2009. ISSN 1939-3539. doi: 10.1109/TPAMI.2009.67.

[3] Chen Zhang and Kenneth S. Suslick. A colorimetric sensor array for organics in water. *Journal of the American Chemical Society*, 127(33):11548–9, August 2005. ISSN 0002-7863. doi: 10.1021/ja052606z.

[4] Kenneth S. Suslick, Neal A. Rakow, and Avijit Sen. Colorimetric sensor arrays for molecular recognition. *Tetrahedron*, 60(49):11133–11138, November 2004. ISSN 00404020. doi: 10.1016/j.tet.2004.09.007.

[5] Neal A. Rakow, Avijit Sen, Michael C. Janzen, Jennifer B. Ponder, and Kenneth S. Suslick. Molecular recognition and discrimination of amines with a colorimetric array. *Angewandte Chemie (International ed. in English)*, 44(29):4528–32, July 2005. ISSN 1433-7851. doi: 10.1002/anie.200500939.

[6] Chen Zhang, Daniel P. Bailey, and Kenneth S. Suslick. Colorimetric sensor arrays for the analysis of beers: a feasibility study. *Journal of agricultural and food chemistry*, 54(14):4925–31, July 2006. ISSN 0021-8561. doi: 10.1021/jf060110a.

[7] Sung H. Lim, Liang Feng, Jonathan W. Kemling, Christopher J. Musto, and Kenneth S. Suslick. An Optoelectronic Nose for Detection of Toxic Gases. *Nature chemistry*, 1:562–567, September 2009. ISSN 1755-4349. doi: 10.1038/nchem.360.

[8] Chen Zhang and Kenneth S. Suslick. Colorimetric sensor array for soft drink analysis. *Journal of agricultural and food chemistry*, 55(2):237–42, January 2007. ISSN 0021-8561. doi: 10.1021/jf0624695.

[9] Natalie V. Kostesha, Tommy S. Alstrøm, Carsten Johnsen, Kent A. Nielsen, Jan O. Jeppesen, Jan Larsen, Mogens H. Jakobsen, and Anja Boisen. Development of the colorimetric sensor array for detection of explosives and volatile organic compounds in air. In *Proceedings of SPIE*, volume 7673, pages 76730I–76730I–9, 2010. doi: 10.1117/12.850310.

[10] Natalie V. Kostesha, Tommy S. Alstrøm, Carsten Johnsen, Kent A. Nielsen, Jan O. Jeppesen, Jan Larsen, Anja Boisen, and Mogens H. Jakobsen. Multicolorimetric sensor array for detection of explosives in gas and liquid phase. In *Proceedings of SPIE*, volume 8018, pages 80181H–80181H–12, 2011. doi: 10.1117/12.883895.

[11] Tommy S. Alstrøm, Raviv Raich, Natalie V. Kostesha, and Jan Larsen. Feature extraction using distribution representation for colorimetric sensor

arrays used as explosives detectors. In *IEEE International Conference on Acoustics, Speech, and Signal Processing (ICASSP)*, pages 2125–2128, 2012. doi: 10.1109/ICASSP.2012.6288331.

[12] Tommy S. Alstrøm, Jan Larsen, Natalie V. Kostesha, Mogens H. Jakobsen, and Anja Boisen. Data representation and feature selection for colorimetric sensor arrays used as explosives detectors. In *IEEE International Workshop on Machine Learning for Signal Processing (MLSP)*, pages 1–6, 2011. doi: 10.1109/MLSP.2011.6064615.

[13] Tommy S. Alstrøm and Jan Larsen. Feature Extraction and Signal Representation for Colorimetric Sensor Arrays. Technical report, DTU Informatics, 2011. URL http://www.imm.dtu.dk/pubdb/p.php?5845.

[14] Christopher M. Bishop. *Pattern Recognition and Machine Learning*. Springer, Secaucus, NJ, USA, 2006. ISBN 0387310738.

[15] Carl E. Rasmussen and Christopher K. I. Williams. *Gaussian Processes for Machine Learning*. MIT Press, April 2006. URL http://www.gaussianprocess.org/gpmlhttp://www.ncbi.nlm.nih.gov/pubmed/15112367.

[16] Marie-Pierre Dubuisson and Anil K. Jain. A modified Hausdorff distance for object matching. In *Proceedings of 12th International Conference on Pattern Recognition*, pages 566–568, 1994. ISBN 0-8186-6265-4. doi: 10.1109/ICPR.1994.576361.

[17] Bernard Haasdonk and Claus Bahlmann. Learning with Distance Substitution Kernels. *Pattern Recognition*, 3175:220–227, 2004. doi: 10.1007/978-3-540-28649-3_27.

[18] Tony Jebara, Risi Kondor, and Andrew Howard. Probability Product Kernels. *Journal of Machine Learning Research*, 5:819–844, 2004. URL http://jmlr.csail.mit.edu/papers/v5/jebara04a.html.

[19] Lars K. Hansen and Jan Larsen. Linear unlearning for cross-validation. *Advances in Computational Mathematics*, 5(1):269–280, 1996. doi: 10.1007/BF02124747.

[20] Quinn McNemar. Note on the sampling error of the difference between correlated proportions or percentages. *Psychometrika*, 12(2):153–157, June 1947. ISSN 0033-3123. doi: 10.1007/BF02295996.

[21] John D. Storey. A direct approach to false discovery rates. *Journal of the Royal Statistical Society: Series B (Statistical Methodology)*, 64(3):479–498, August 2002. ISSN 13697412. doi: 10.1111/1467-9868.00346. URL http://doi.wiley.com/10.1111/1467-9868.00346.

Appendix F

Advanced detection of explosives using colorimetric sensor array

---

Natalie V. Kostesha, Tommy S. Alstrøm, Olga V. Mednova, Carsten Johnsen, Kent A. Nielsen, Jan O. Jeppesen, Mogens H. Jakobsen, Jan Larsen, and Anja Boisen. Advanced detection of explosives using multi-colorimetric sensor array. *Will be submitted to Journal of American Chemical Society (JACS)*, 2013.

This manuscript is yet to be submitted as should be considered work in progress. Some details still needs to be ironed out, but the manuscript is included as it explains a lot of details about colorimetric sensor arrays.

Advanced detection of explosives using colorimetric sensor array

Natalie V. Kostesha[a], Tommy S. Alstrøm[b], Olga V. Mednova[a], Carsten Johnsen[c], Kent A. Nielsen[c], Jan O. Jeppesen[c], Mogens H. Jakobsen[a], Jan Larsen[b], and Anja Boisen[a]

[a]*Department of Micro and Nanotechnology, Technical University of Denmark, Ørsteds Plads 345 East, DK-2800, Kgs. Lyngby, Denmark*

[b]*Department of Applied Mathematics and Computer Science, Technical University of Denmark, Richard Petersens Plads 305, 2800 Kgs. Lyngby, Denmark*

[c]*Department of Physics, Chemistry and Pharmacy, University of Southern Denmark, Campusvej 55, DK-5230, Odense M, Denmark*

Abstract

Through the combination of chemically selective compounds with colour changing properties we developed a colorimetric sensor array for the detection of explosives like DNT, HMX, RDX and TATP. The colorimetric sensing technology was based on an array of chemo-selective compounds belonging to different chemical families immobilized on a solid support. Upon exposure to an analyte in suspicion the colorimetric array changes colour. Almost each chosen compound reacted chemo-selectively with the analyte of interest. Colour changes indicated the presence of unknown explosives and volatile organic compounds. The colorimetric sensor was sensitive to DNT in the concentration from 1 ppm and higher. Such sensing technology can be used to screen for relevant explosives in a complex background as well as to distinguish mixtures of volatile organic compounds distributed in gas phase.

Keywords: colorimetric sensor array, DNT, HMX, RDX, TATP, chemo-selective compounds, tetrathiafulvalene, RGB, principal component analysis, the K–nearest neighbor analysis.

* Corresponding Author: Natalie Kostesha, natalie.kostesha@nanotech.dtu.dk; Tel: + 45 45 258142;
Fax: + 45 45 88 77 62; www.dtu.dk; http://www.xsense.dk/

Introduction

The production and utilization of explosives and explosive-related compounds have a great concern on public security and environment. New technology must be developed to detect easily a variety of explosives, illegal chemicals and drugs, drug precursors carried by suspects as well as hidden in mails, luggage and conveyance. Colorimetric sensing technique is a promising analytical method which can be used for detection and identification of explosives with high probability. This method is an easy-to-use on-site method similar to the well-known pH paper stick which shows a prominent response based on colour changes in the presence of explosives. The colorimetric sensor array (31 dyes) is based on the application of four successive dye classes: Tetrathiafulvalene derivatives (TTF), Lewis acid/base dyes (i.e. metal ion containing dyes), Brønsted acidic or basic dyes (i.e. pH indicators), and dyes with large permanent dipoles (i.e. zwitterionic solvatochromic dyes).

Suslick et al. demonstrated the capability of the colorimetric sensor array to sense different analytes, even a mixture of analytes by applying three classes of chemo-selective compounds: 1). Lewis acid or base dyes, 2). Brønsted acidic or basic dyes and 3). Dyes with large permanent dipoles. The colorimetric response is based on specific interactions between molecules e.g. dipolar and multipolar interactions, acid-based interaction, van der Waals interaction and physical adsorption.[1,2] The colorimetric array was able to change the colour upon exposure to an analyte of interest. Digital imaging of the colorimetric array before and after exposure to analytes, like for example amine molecules, gave the possibility to create a colour difference map which was presented as a unique fingerprint for each molecule of interest.[3] The colorimetric sensing technology has already been successfully applied for the visualization of the presence of relevant molecules in a complex background[4,5] as well as for the distinction of volatile organic compound mixtures distributed in a liquid phase.[6]

The colorimetric sensor has shown promising results in the detection of molecules at low concentration rates, e.g. in detection of formaldehyde with detection limit of 20 ppm,[7] mercury in aqueous environments demonstrating a detection limit of 2 ppm,[8] in selective detection of closely related amines with a detection limit of 600 ppb,[3] even in detection of an explosive, like triacetone triperoxide – TATP.[9] The sensor has been exposed to the liquids testing an ethanol rate and organic compounds in the beer[10] and a CO_2 content in soft drink samples.[11]

For the first time a new colorimetric sensor array containing 31 chemo-selective compounds was applied and examined in the prospect of detecting explosive molecules e.g. 2,4-dinitrotoluene (DNT); 1,3,5-trinitroperhydro-1,3,5-triazine (RDX); 1,3,5,7-tetranitro-1,3,5,7-tetraazacyclooctane (HMX); 3,3,6,6,9,9-hexamethyl-1,2,4,5,7,8-hexaoxacyclononane (TATP). The colorimetric sensor array presented in this paper was designed by using derivatives of tetrathiafulvalene (TTF) molecules (1-15 dye) with their ability to change colour combined with additional three classes of chemo-selective compounds described above (16-31 dye).[1]

In general, the TTF molecular unit presented in Figure 1A was the core unit for synthesis of 13 TTF molecules. TTF molecules containing various incorporated electron withdrawing and accepting groups represented in Figure 1B; TTF molecules were synthesized at the University of Southern Denmark (More information on synthesis presented in Supplementary Material). The conductive properties of TTF molecules[12] first are based on oxidation-reduction behaviour of the TTF molecular unit where the neutral non-aromatic 14 π-system turns to aromatic 6-π system converting from the radical-cation ($TTF^{\bullet+}$) to dication (TTF^{2+}) and vise-versa (Fig. 1A).[13,14] Also, the conductivity can be enhanced by modifying the TTF unit with electron withdrawing and accepting groups (Fig. 1B). Conductive properties and chemical stability of TTF have enabled TTF molecules to play a fundamental role in material science, macrocyclic and supramolecular chemistry; during the past two decades and being a key candidates for the construction of sensors,[15,16] switches,[17] for synthesis of conducting and semiconducting polymers and materials.[18] Tetrathiafulvalene and TTF derivatives are known as molecules which provide non-covalent interactions between molecules, where interactions such as hydrogen bonding, π- π interactions, ion-dipole etc. which also occurred and provide the formation of supramolecular complexes between molecules. [19] The formation of supramolecular complexes in TTF chemistry is a common effect; a TTF molecular originates as a host molecular, binding another molecular which occurred to be a guest molecular, thereby producing the supramolecular complex. A host is usually larger than a guest molecular containing groups to perform hydrogen bonding, whereas a guest molecular fitting a binding site, providing groups to complete the interaction. Supramolecular host-guest complexes exhibit good stability in both solutions and solid phases. The chemo-selective properties of TTF molecules have attracted considerable attention due to the electron donor-acceptor

properties, their capability of recognizing specific analytes and potential selective colour change after exposure to a specific analyte.[16] TetraTTF-calix[4]pyrrole is one of the promising molecules for the detection of explosives. A tetraTTF-calix[4]pyrrole-based sensor has been tested already in the identification of 3,5-dinitrobenzoate,[20] trinitrobenzene, picric acid,[21] towards anions such as Cl^-, Br^-, F^-.[15] TTF molecules can be used in detection of other chemical compounds belonging to various classes: amines, alcohols, arenes, ketones, aldehydes, and acids.[22] In this research the application of tetrathiafulvalene and TTF derivatives was expanded for sensing and identification of the most widely used military high-energetic explosives.

The main effort in efficient detection of explosives is based on the development of a method which will be successful in the detection of molecules in low concentrations in gas or vapour phase. Explosives in both solid and liquid form release some vapour denoted as a vapour pressure which depends exponentially on a temperature range. By knowing the heat of sublimation it is possible to perform a rough theoretical calculation of the vapour pressure of explosives based on the Antoine equation as a simplified from of the Clausius-Clapeyron equation.[23,24] Due to the low vapour pressure of explosives under the ambient conditions the detection of such materials as DNT or RDX usually fails. However, the temperature rise effects on the vapour pressure parameters thereby enhance the concentration of explosives from particles per billion (ppb) to particles per million (ppm), respectively and therefore increase a chance for explosives tracking. Terrorists and distributors of illegal materials always work towards the development of new compositions and substances with low vapour pressures which are not easy to detect.

New methods have been developed for sensing vapours emanating from explosives; these technologies are mainly based on the application of electrochemical approaches,[25] calorimetric [26–28] and optical[9] methods and etc. In this paper we present a simple chemical sensor, like an artificial nose, based on the application of a colorimetric sensor array for detecting explosives like DNT, RDX, HMX and TATP. The chemo-selective compounds in the array have been chosen due to their potential selectively change colour after exposure of the specific explosives.

To increase the colorimetric sensor probability we applied different statistical methods. To evaluate the colorimetric sensor features four independent classifiers were applied in this work: 1). 1–Nearest-neighbor (1-NN); 2). *k*– Nearest-neighbor (*k*–NN); 3). Sparse logistic regression (SLR) and 4). Artificial neural networks (ANN). We have found that the best statistic depends on both the experimental setup and the classifier employed. The goal of this work was to identify the optimal mathematical approach which can be applied in detection of explosives. By using multiple classifiers we were able to improve the detection accuracy of the sensor of 62.8%.

Materials and Methods

Reagents:

Analytes that have been exposed to the sensor: 1-methyl-2,4-dinitrobenzene (DNT), dimethyl sulfoxide (DMSO), 1,4-dichlorobenzene (DB) and 1-nitro-2-octyloxybenzene (NPOE) were acquired from Sigma-Aldrich (St. Louise, MO, USA); 1,3,5-trinitroperhydro-1,3,5-triazine (RDX), 1,3,5,7-tetranitro-1,3,5,7-tetraazacyclooctane (HMX), 3,3,6,6,9,9-hexamethyl-1,2,4,5,7,8-hexaoxacyclononane (TATP) were supplied from the Danish Emergency Management Agency (Beredskabstyrelsen).

For the colorimetric sensor array 31 dyes were applied. TTF compounds – dyes 1 to 15 in the array were synthesized at the department of Physics, Chemistry and Pharmacy, University of Southern Denmark. The information on TTF

compounds presented in the Supplementary Material part. Other dyes: Alizarin (16), bromocresol green (17), bromocresol purple (18), bromothymol blue sodium salt (19), bromphenol blue (20), xylenol blue (21), chlorphenol red (22), cresol red (23), crystal violet lactone (24), 2,6-dichloro-4-(2,4,6-triphenyl-1-pyridinio)-phenolate (25), Reichardt's dye (26), phenol red (27), rosolic acid (28), methyl red (29), nitrazine yellow (30), 4-brom-2,6-dimethylphenol (31) were provided from Sigma-Aldrich (St. Louise, MO, USA). Stock solutions of chemo-selective compounds (1% in NPOE, DMSO and DB) were freshly prepared and stored in a lightproof flask before use.

Colorimetric sensor array:

A colorimetric sensor array was designed by using 31 selected dyes. Dyes were immobilized onto silica gel Kieselgel $60F_{254}$ plates (Merck KGaA, Germany) in the working volume of 1 μL per spot. Since explosives have very low vapor pressure at room temperature and consequently low concentration, tested analytes were heated up. Explosives were detected at 25º C and the elevated temperature of 35°C, 50°C, 70°C and 100°. Samples of explosives in tightly closed vessels were heated up at defined temperature during 3 hours and removed from a heating system before the measurements.

Pictures of the colorimetric sensor array before and after the exposure of an analyte were scanned through an ordinary flatbed scanner (Epson V750-M Pro Perfection scanner). Pictures were obtained immediately after immobilization of dyes and after exposure of analytes. The colorimetric sensor was dipped into a vessel containing an analyte and remained there during 2 minutes. Images from the Epson scanner were obtained at 600 dots per inch in RGB color and saved in tiff format. Pictures were analyzed using the MatLab software.

Data extraction:

In order to extract the color code from each dye the position of each dye on the image was located. The exact procedure that was used is described in. Each dye was represented using the red, green, and blue color scheme. In this model every color is provided as red, green, and blue color (RGB); RGB values are given in the 0-255 integer range. The minimum intensity of the color gives black (0;0;0) and maximum white color (255;255;255). After the dye was located and converted to RGB values, we calculated the median value of each. We used the median instead of the mean in order to be more robust to noise and outliers.

A traditional difference map was obtained from the values of red, green or blue colors after exposure minus the value of red, green or blue color before the exposure. Since the RGB color scheme does not allow negative values the absolute difference was taken. In the detection of DNT part we used the real value obtained from the colorimetric sensor. In the detection of other explosives part in order to enhance the visibility of the colors difference maps the RGB values were first scaled with a factor 5 and then shifted by 10. The instances where the difference map (before scaling) resulted in a color value lower than 3 the pixel was rounded down to a color value of 0.

However, the elimination of negative values and the need for scaling in order to make the differences visible imply that color the difference map does not produce unique representations and further that sign-information is list. As an alternative we suggest to use bar plots where each bar represents the cumulative density function (CDF) of difference values.

Statistical visualization

Data obtained with the colorimetric sensor array has been evaluated by using the principal component analysis (PCA) method. PCA is a simple, non-parametric method which is often used to visualize high dimensional data. The original data obtained from the colorimetric sensor is of 93 dimensions (31 dyes, 3 colors per dye) which is not visualized in an informative figure unless data processing has been done[22,29]. PCA will transform the data matrix and identify the linear projections which have maximum variability often denoted principal components. Each successive linear projection is orthogonal to all previous projections. Assuming that the sensor has a high signal to noise ratio the first principal components will visually analyte dispersion nicely.

Data evaluation:

To assess the ability of the colorimetric sensor array to classify explosives we build a multi-nominal classifier which is called *K*-nearest-neighbor[30,31]. The K–nearest neighbor has been as an effective classification technique provided that measurements made on identical analytes make up clusters in the data space. The method works as follows; Data is separated into two sets, a training set and a test set. The test set corresponds of just a single measurement; however each measurement in the data set will become a test set exactly once. Thus *N* data sets are created. This procedure in called *leave-one-out crosses validation* (LOO-CV). When identifying the analyte in the test set the Euclidian distance between the point (one measurement corresponds to one point in 93 dimensional space) in the test set and every point in the training set is calculated. The *K* closest points and the corresponding analyte are then identified. The unknown measurement is now classified using majority voting among the identified analytes. In case of a tie the algorithm uses the nearest neighbor among the tied classes to break the tie selecting the closest point as the analyte. Possible values of K is set to [1;20]. To choose the value of *K* the training set is evaluated using LOO-CV and the value that maximizes classification accuracy is chosen. In case of more than one optimal *K* the smallest value is favored.

Results:

Detection of DNT

The colorimetric sensor array first was exposed to vapour emanating from the explosive 2,4-dinitrotoluene (DNT). Samples of DNT were heated up to 100° C to achieve the saturated condition. The response of the colorimetric sensor before and after exposure of DNT is presented in Figure 2. Experiments here were performed when CSCs were in the random order applied on the solid support.

The idea of the randomization of CSC in the array was based on the understanding of cross-reactivity effects if such exists between chemo-selective compounds after the immobilization. The cross-reactivity effect was analyzed before and after exposure of DNT.

From the obtained results we could conclude that chemo-selective compounds do not react with each other after the immobilization on the solid support, the randomization of CSC didn't effect on the colorimetric sensor response. The stability of CSC on the solid support were also evaluated; we couldn't observed dyes colour changes after the application on the solid support. Only, bromocresol purple (18) initiated the color changes from green to brown before the assay due to the reaction with molecules present in air. We recommend applying bromocresol purple in the end of the array to avoid the spontaneous reaction with molecules present in the air. In our previous work we have investigated the "the coffee stain effect" of dyes applied on the solid support[32].

Results on the detection of DNT were evaluated after 16 independent measurements which were performed during 8 days. The Figure 2 presents one of 16 experiments where the random immobilization of chemo-selective compounds on a solid support was applied. The position of CSCs was assessed and adjusted according to the positions of dyes presented in the Material and Methods part and Tab. 1S in the Supplementary Material.

After the exposure of DNT the chemo-selective compounds changed colour. Almost each chosen dye reacted chemo-selectively with the analyte of the interest. (Fig.2B, C). Chemo-selective compounds under the number of 8, 10, 12, 13, 14, 15 – TTF family and 16, 17, 18, 19, 20, 21, 22, 23, 24, 27, 28, 29 and 30 shown the response on presence of DNT. Chemo-selective compounds under the number of 2, 3, 4, 7, 8, 9, 13 – TTF family and 16, 17, 18, 19, 20, 21, 22, 23, 24, 25, 26, 27, 28, 29 and 30 shown the response on the elevated temperature - 100° C. An unspecific response on both DNT and 100° C has been shown by 19 dyes out of 31 dyes applied in the assay. Probability of the experiment is presented in the Supplementary Material part. It has been describe earlier in[22] that the elevated temperature was effected on the sensor response.

Data presented in this experiment was not enhanced by a mathematical method which allows increasing the visibility of the colours difference maps after the modification of RGB values, the unmodified signal was presented on Figure 2. Chemo-selective compounds under the number of 8, 10, 12, 14, 15, 19 and 24 demonstrated the specific response on the presence of DNT. By using difference map analysis was possible to distinguish the color difference after the RGB extraction (Fig. 2C). Moreover by a naked eye it was possible to observe the different between the analyte and the control: compound 3 became dark yellow in presence of DNT and at 100° C turned to yellow (Fig. 2B); compound 9 became light-yellow in presence of DNT and at 100° C turned to light brown, compound 10 became grey in presence of DNT, the same color appeared for the compound 12 in presence of DNT, compounds 14 and 15 turned brown in presence of DNT, compound 19 became yellow in presence of DNT and at 100° C turned to grey-yellow, compound 24 became light yellow in the presence of DNT and turned to blue at 100° C. Moreover, compound 25 became more brownish and compound 26 became dark grey at 100° C (Fig. 2A, B).

The different map analysis is a very common method in colorimetry for RGB values extraction[2]. A difference map is able to compose a unique fingerprint for each analyte and this can be a possibility to make a sensor response visible, therefore simplifies the interpretation of results if fast answer is needed. In our research we developed the sensor for detecting analytes with low vapor pressure like explosives and we can conclude that the different map analysis is relatively weak method for this purpose. Furthermore, sometime negative color change values were obtained during data analysis especially if a color of CSC became less intensive or disappeared from the solid support after the analyte exposure; during the different map analysis such values are usually eliminated, basically the calculation is taking the absolute value of a pixel value before and after exposure to an analyte.

Our goal was to evaluate the response of the colorimetric sensor from the statistical point of view. We employed the principal component analysis (PCA) and cumulative density function (CDF) analysis. The applied algorithm for data estimation was described in the supplementary material and in[22]. To evaluate the difference between DNT and 100° C statistically 16 independent measurements were preformed. Experiments were conducted during 8 days, 2 accomplished measurements were completed per day, and 2 measurements were failed due to the data lost. Figure 3 shows the PCA plot for DNT and 100° C for 1st to the 2th principal components (PC). According to the PCA plot the overlap in the response between DNT and 100° C is insignificant (Fig.3A). We could observe that 100 °C and DNT grouped into

clusters. The PCA plot supports the difference map analysis where we could observe specific responses on DNT and100° C.

Another alternative to difference map we suggest to use bar plots where each bar represents cumulative density function (CDF) of the color change for a given dye color (RGB) when exposed to a given analyte. The CDF plot presenting the sensor response on the presence of DNT displayed in Figure 3B. The analysis was performed after the mathematical evaluation of color changes similar to the difference map. Mathematical algorithms were applied in order to analyze both positive and negative values simultaneously during color changes with statistical methods; the sensory output was put into a numerical form. Bars on the graph represent colour changes in the numerical form similar to RGB after calculation of the median and probability values of the signal. Different colours of bars illustrate the statistics; 14 measurements were evaluated. Compete mathematical algorithms of data extraction from the colorimetric sensor is presented in the Supplementary Material part. The cumulative densities function analysis represents the response of 4 chemo-selective compounds which were defined as significant in detection of DNT and were different from a control: compound 12 in the blue and green spectra, compound 14 in the green spectra, compound 15 in the green spectra and compound 24 in the blue spectra.

Sensor kinetics

In this work we were trying to investigate the sensor response when different concentration of DNT were applied and understand the sensor sensitivity in relation to color changes. It is well know that DNT has low vapor pressure at room temperature; at 25° C corresponds to 0.34 ppm[23].

DNT samples were heated up to 25° C, 35° C, 50° C and 70° C to achieve DNT concentration of 0.33; 1.09; 6.05 and 47.4 ppm, respectively. The vapor pressure was calculated from the Antoine equation reported as the relation between vapor pressure of a pure compound and temperature. Our results correspond to the literature data[23].

All experiments were performed at room temperature, however to obtained different concentration of the explosive, DNT samples were heated up during 3 hours at the elevated temperature as described above. The colorimetric sensor was immersed into a vessel where the relevant concentration of DNT was achieved and remained there for 2 min; the "naked eye" response was observed as a color change of CSC already at the concentration of DNT of 6.05ppm, sample was heated up to 50° C.

To evaluate the sensor response four measurements on each concentration of DNT were performed. Data analysis has shown that compounds with number 8, 12 and 13 were able to detect DTN when samples were heated up from 25° C to 70° C (Fig. 4A), thereby the sensor response increased with the increscent of DNT concentrations. However, compound 13 has shown stable color response on different concentrations of DNT. Compounds have shown the color shift in the blue and green spectra, similar spectra for DNT as described above when DNT samples were heated up to 100° C.

It is evident that the color intensity of the sensor increased with concentration and slop of the colorimetric curve rose up (Fig. 4B); the response of the colorimetric sensor became more prominent because the concentration of DNT increased.

Figure 4B shows a concentration-response curve obtained from the colorimetric sensor when DNT samples were heated up to certain temperature.

Detection of other explosives

Simultaneously, with the detection of DNT we have applied the colorimetric sensor for detection of other explosives: HMX, RDX and TATP. HMX and RDX are chemically related explosives belonging to the nitramines; HMX has four carbon and four nitrogen atoms placed in the variable order in the eight-membered ring where one nitro-group attached to each nitrogen atom; RDX has similar structure to HMX with the difference in one carbon and nitrogen and one nitro-group group, respectively. TATP is a peroxide based explosive, which can be obtained by a reaction between acetone and hydrogen peroxide forming the cyclic trimer of acetone peroxide. DNT, HMX, RDX and TATP are belonging to different chemical classes.

The detection of explosives was performed under the same conditions as has been described in the detection of DNT section. Experiments were carried out under the saturated condition of analyte vapours; analytes were heated up to 100° C. The resulting colorimetric sensor was applied for 2 minutes for analysis of vapour emanating by HMX, RDX and TATP. Digital imaging of the colorimetric array before and after exposure to analytes was used for creating of difference map for each explosive of interest (Fig.6). In this experiment in order to enhance the visibility of the colours difference maps the RGB values were first scaled with a factor 5 and then shifted by 10. The instances where the difference map (before scaling) resulted in a colour value lower than 3 the pixel was rounded down to a colour value of 0. The analysis has shown that almost each chosen dye reacted chemo-selectively with the analyte of interest. A change in a colour signature indicates the presence of explosive molecules. By using the digital imaging analysis we could observe that obtained responses on all four analytes were unspecific, but different from a control. Only, compound 12 - TTF and compound 24 - Crystal violet lactone have shown the specific response on the present of DNT (Fig. 6).

To analyse acquired data statistically signal processing methods were applied such as CDF, PCA and confusion matrix (CM) analysis (Supplementary Material). Measurements have been taken during eight days performing sixteen measurements in total (N=8; n=2), two measurement were failed due to the data lost.

The colour distributions in the numeric form are presented in Figure 7 as a CDF plot after the data processing. CSCs under the number of 12 (TTF), Bromothymol blue sodium salt (19) and Crystal violet lactone (24) demonstrated the signal to DNT, HMX, RDX, TATP and Control-100º C. Compound 19 and 24 demonstrated the specific signal to 100º C. Compounds 12 and 24 demonstrated the specific signal to DNT. The response to HMX, RDX and TATP was unspecific.

Since the sensor application in the future will be adapted to the detection of explosives under the complex environment, like detection of dangerous materials in airports, marine ports and train stations. Additional analytes which are not related to explosive materials, but could be present in the air were tested by the colorimetric sensor. Our goal was to evaluate the colorimetric sensor on the presence of other molecules and estimate false positive and negative alarms. In this paper we didn't describe in details the sensor response non-explosive materials; the previous results were published in[22]. Non-explosive materials were described in the Supplementary Material part and here we combine tested analytes in one group and describe it as Other.

To establish the difference in detection of explosives in relation to other analytes the PCA analysis was applied (Fig.8). In the domains where colorimetric sensors have been investigated, PCA showed high precision and low false alarm rate. The closely related K-Nearest Neighbor (KNN) classifier which uses the Hellinger distance between colour distributions as a metric was able to demonstrate significant improvement in accuracy. Figure 8 shows the PCA plot for the 2nd to the 4th principal components (PC) for explosive and control - DNT, HMX, RDX, TATP and 100° C as selected analytes and Other as selected non-explosive analytes. PCA has shown the overlap in the response for DNT, HMX,

RDX and TATP. However, the overlap between explosives and 100° C was insignificant (Fig. 8). Similar results were achieved between explosives and non-explosive analytes – Other. Using principal components 2 and 4 we could observed that 100 °C and explosives grouped tightly into two separate clusters. PCA has shown similar response (no difference) on the detection of DNT, HMX, RDX and TATP. DNT, HMX, RDX and TATP grouped into one cluster. Non-explosive analytes were separate from explosives and control. Obtained results demonstrated that the colorimetric sensor can separate explosives and non-explosive materials.

Discussion

The colorimetric sensor technology relied on an array of 31 chemically selective compounds. In the array compounds from number 1 to 15 correspond to tetrathiafulvalene or TTF-like compounds with the common formula of $(H_2C_2S_2C)_2$. TTF compounds are unique class of molecules with hydrocarbon fulvalene - $(C_5H_4)_2$ in their structure where 4 CH groups replaced with sulfur atoms (Fig. 1). TTF compounds applied in this work were synthesized in SDU. Commercially available compounds from number 16 to 31 in the array were Lewis acid/base dyes (i.e. metal ion containing dyes), Brønsted acidic or basic dyes (i.e. pH indicators), and dyes with large permanent dipoles (i.e. zwitterionic solvatochromic dyes). Suslick et al. has already designed and patented several colorimetric sensor arrays based on the application of some compounds from numbers 16 to 31 in our array[1,2]. Application of four classes of compounds together in the colorimetric array and evaluation of their colorimetric behaviour from the statistical point of view is described for the first time in this paper.

The chemo-selective compounds described in this publication have capability selectively recognize specific analytes; this recognition is a function of intermolecular interactions, basically weak, non-covalent interactions, donor-acceptor and host-guest interactions. In host-guest interactions, the interaction specific for TTF-like compounds, we consider that a host molecular binding another molecule, a guest, and composes a supramolecular complex. In the supramolecular complex a large host molecular is usually a hydrogen bond donor and a small guest molecular is hydrogen bond acceptor. The binding of the explosives by TTF-like compounds, is primarily facilitated by the formation of hydrogen bonds between pyrrole and amino groups of TTF-like compounds and nitro-groups of DNT. The non-covalent binding can occur between TTF-like compounds and neutral target molecules like DNT, TNT or toluene forming stable measurable response, like colorimetric or electrochemical.

The TTF-unit alone (Fig. 1A) (compound 12 in Tab. 1S) also has the donor-accepting properties; the reversible oxidation is shown in Fig.1A. By the oxidation of the TTF-unit, the system is transformed from the neutral non-aromatic 14 π-system to the aromatic 6 π-system in the radical-cation ($TTF^{\bullet+}$) and dication (TTF^{2+}). The binding of analytes allows the transfer of electrons from the electron rich TTF-unit that creates a reflection on the oxidation potential. The investigation of the electrochemical properties of tetraTTF-calix[4]pyrrole (compound 14 in Tab. 1S) revealed two oxidation peaks at -0.04V to 0.53V. For several times TTF-like compounds were applied as a redox-responsive sensor for detection of chlorine, heavy metal ions[33].

TetraTTF-calix[4]pyrrole (compounds 14 and 15 in Tab. 1S) is one of the promising molecules that has good binding affinity towards anions. Apart from this tetraTTF-calix[4]pyrrole can form the reversible cone conformation suitable for detection of chloride ions[20,34] and 1,3-alternate conformation suitable for detection of different electron-deficient compounds, like chloride salt of tetraalkylammonium[16]. The colorimetric response was observed upon addition of nitro-aromatic explosives, e.g. deficient guests, trinitrobenzene and picric acid to tetraTTF-calix[4]pyrrole, the colour of a

solution turned from yellow to green[21]. The optically active tetraTTF-calix[4]pyrrole-based sensor has already been applied for the detection of 1,3,5-trinitrobenzene, tetrafluoro- p-benzoquinone, tetrachloro-p-benzoquinone, p-benzoquinone, and 1,3,5-trinitrophenole[35].

In this work the focus on tetraTTF-calix[4]pyrroles (number 14 and 15 in Tab. 1S) was due to their ability to form strong complex with pyrrole units forming the cone conformation of the molecular. Binding with the pyrrole group is the essential part in the detection of explosives, moreover the 1,3-alternate conformation is also suitable for this purpose while the interaction with electron-deficient guests. In order to increase sensing properties of TTF-like compounds, different functional groups (Fig. 1B) either electron withdrawing group (EWG) e.g. NO_2- (compound: 1, 3); COOMe- (compound: 2, 4, 7); CN- (compound: 2, 10); $CH_3C_6H_4SO_2$- (compound: 1, 5, 6, 7, 9); Br- (compound: 11) or electron donating group (EDG) e.g. NH_2- (compound: 3, 8); NH- (compound: 8, 14, 15) can be incorporated to the TTF-unit. The specific colorimetric response was observed when the charge transfer from the electron rich TTF unit (compound: 12), tetraselenofulvalene (TSeF) (compound: 13), the selenium analogue of TTF and TTF-modified with EDGs e.g. compounds 8, 14 and 15 were binding of electron-deficient compounds, like DNT containing 2 electron deficient nitro-groups.

The presence of DNT in the gas phase was also detected by other applied CSCs, from 16 to 31 in Table 1S e.g. Bromothymol blue sodium salt (number 19) and Crystal violet lactone (number 24). Where, the most significant and applicable compound in detection of DNT and other explosives was crystal violet lactone (number 24) (Fig 3A and 7). In the colorimetric array the original – transparent colour of the dye turned into yellow in the presence of DNT and remained transparent in the presence of HMX, RDX and TATP. At elevated temperature this dye turned to the blue colour.

According to the analyzed data, CSCs were not only being able to detect specific analytes, also they were able to change the colour pattern specifically at the high temperature. This effect has been described in previous publications we were able to observe the colour change of CSCs when the temperature was elevated[22]. CSCs under the number of 3, 9, 17, 24, 25 and 26 changed their colour at 100° C. The thermo-stability phenomenon of CSCs was investigated in this research; however the dipper analysis of this effect can be applied for the development of the thermo-sensor that can be used together with the chemo-selective sensor.

The sensor response was investigated under the presence of DNT at different concentrations. We could observe the dose response effect where the colour difference related to the concentration of the analyte.

The colorimetric sensor array demonstrated a high classification rate to explosives, especially to DNT. The colorimetric sensor can be tested and evaluated as a thermo-sensor due to the specific colour changes at 100° C. From the obtained results the presence of DNT could be determinate by the colorimetric sensor with high precision, with zero false negatives (See also confusion matrix in the Supplementary Material part). However, the colorimetric sensor was very unreliable for HMX, RDX and TATP; molecules were detected with a low precision rate: HMX was detected by sensor 4 times out of 14 measurements; RDX was detected 8 times out of 14 measurements; TATP only 3 times out of 14 measurements was classified correctly(See also confusion matrix in the Supplementary Material part).

HMX and RDX have very similar chemical structure. When RDX is manufactured in the large-scale over than 6% of HMX is available in the explosive mixture, and also various impurities and intermediate products are present. Also, RDX and HMX on the market are present as a mixture with other explosives like TNT, PETN and other.

It was observed that TATP is difficult to detect by using colorimetric molecules with donor-acceptor properties[9]. This is probably, why the colorimetric sensor was not able to detect the difference between RDX, HMX and TATP

The resulting colorimetric sensor was used for the analysis vapour of acetone, acetic acid, ethanol, formic acid, hydrochloric acid, methanol, propanol, and toluene[22]. To evaluate and expand the potential of the colorimetric sensor advanced signal processing and statistic methods such as principal component analysis and hierarchical cluster analysis will be applied to enhanced the sensor accuracy and reduce false alarm rate.

Conclusions:

The colorimetric sensor is a unique proprietary colour change-based sensor technology developed at DTU Nanotech and SDU with enormous potential to form the basis of a practical technological platform for the detection of traces of explosives like DNT, HMX, RDX and TATP. Using colorimetric sensors it is possible to observe colour changes due to particular molecules of interest that are indicative of explosives; be they amines, alcohols, phenols, ketones, aldehydes, or acids in the ppm and ppb range.

We are working towards the detection possibilities by the selection of new colorimetric molecules that undergo colour changes in the presence of explosives and illegal molecules, as well as improving immobilisation methods for anchoring dye molecules on the solid support.

This colorimetric sensor array is a rapid detection method. During of this work we could decrease the sensing time, it is possible to achieve accurate results within 2 minutes. The colorimetric sensing technology can be used as a platform for the rapid detection and analysis of potential illegal substances through detection of their vapour with high specificity and sensitivity. Prior and this research showed a low limit in detection, improvement in sensitivity, specificity, enhanced simplicity, advanced data processing and validation may be obtainable with the multi-colorimetric sensor as compared to currently used technologies.

Another advantage of this technique is that colorimetric sensor array is an inexpensive approach, and can potentially be produced as single use disposable units.

References:

(1) Suslick, K. S.; Rakow, N. A.; Sen, A. *Tetrahedron* **2004**, *60*, 11133–11138.

(2) Janzen, M. C.; Ponder, J. B.; Bailey, D. P.; Ingison, C. K.; Suslick, K. S. *Analytical Chemistry* **2006**, *78*, 3591–3600.

(3) Rakow, N. A.; Sen, A.; Janzen, M. C.; Ponder, J. B.; Suslick, K. S. *Angewandte Chemie-International Edition* **2005**, *44*, 4528–4532.

(4) Huang, X.; Xin, J.; Zhao, J. *Journal of Food Engineering* **2011**, *105*, 632–637.

(5) Suslick, B. a; Feng, L.; Suslick, K. S. *Analytical chemistry* **2010**, *82*, 2067–73.

(6) Zhang, C.; Suslick, K. S. *Journal of the American Chemical Society* **2005**, *127*, 11548–9.

(7) Feng, L.; Musto, C. J.; Suslick, K. S. *Journal of the American Chemical Society* **2010**, *132*, 4046–7.

(8) Shunmugam, R.; Gabriel, G. J.; Smith, C. E.; Aamer, K. a; Tew, G. N. *Chemistry (Weinheim an der Bergstrasse, Germany)* **2008**, *14*, 3904–7.

(9) Lin, H.; Suslick, K. S. *Journal of the American Chemical Society* **2010**, *132*, 15519–21.

(10) Zhang, C.; Bailey, D. P.; Suslick, K. S. *Journal of Agricultural and Food Chemistry* **2006**, *54*, 4925–4931.

(11) Zhang, C.; Suslick, K. S. *Journal of Agricultural and Food Chemistry* **2007**, *55*, 237–242.

(12) Demiralp, E.; Goddard, W. A. **1997**, *5639*, 8128–8131.

(13) Bendikov, M.; Wudl, F.; Perepichka, D. F. *Tetrathiafulvalenes, oligoacenenes, and their buckminsterfullerene derivatives: the brick and mortar of organic electronics.*; 2004; Vol. 104, pp. 4891–946.

(14) Nielsen, M. B.; Lomholt, C.; Becher, J. *Chemical Society Reviews* **2000**, *29*, 153–164.

(15) Nielsen, K. A.; Jeppesen, J. O.; Levillain, E.; Becher, J. **2003**, *3824*, 187–191.

(16) Nielsen, K. A.; Martin-Gomis, L.; Sarovac, G. H.; Sanguinet, L.; Gross, D. E.; Fernandez-Lazaro, F.; Stein, P. C.; Levillain, E.; Sessler, J. L.; Guldi, D. M.; Sastre-Santos, A.; Jeppesen, J. O. *Tetrahedron* **2008**, *64*, 8449–8463.

(17) Pease, a R.; Jeppesen, J. O.; Stoddart, J. F.; Luo, Y.; Collier, C. P.; Heath, J. R. *Accounts of chemical research* **2001**, *34*, 433–44.

(18) Kaminska, I.; Das, M. R.; Coffinier, Y.; Niedziolka-Jonsson, J.; Woisel, P.; Opallo, M.; Szunerits, S.; Boukherroub, R. *Chemical communications (Cambridge, England)* **2012**, *48*, 1221–3.

(19) Steed, J.W., Atwood, J. L. *Supramolecular Chemistry*; Sons, J. W. &, Ed.; 2 nd.; 2009; p. 990.

(20) Nielsen, K. a. *Tetrahedron Letters* **2012**, *53*, 5616–5618.

(21) Kim, D.-S.; Lynch, V. M.; Nielsen, K. a; Johnsen, C.; Jeppesen, J. O.; Sessler, J. L. *Analytical and bioanalytical chemistry* **2009**, *395*, 393–400.

(22) Kostesha, N. V.; Alstrøm, T. S.; Johnsen, C.; Nilesen, K. a.; Jeppesen, J. O.; Larsen, J.; Jakobsen, M. H.; Boisen, A. *SPIE Proc.* **2010**, *7673*, 76730I–76730I–9.

(23) Östmark, H.; Wallin, S.; Ang, H. G. *Propellants, Explosives, Pyrotechnics* **2012**, *37*, 12–23.

(24) Oxley, J. C.; Smith, J. L.; Luo, W.; Brady, J. *Propellants, Explosives, Pyrotechnics* **2009**, *34*, 539–543.

(25) Forzani, E. S.; Lu, D.; Leright, M. J.; Aguilar, A. D.; Tsow, F.; Iglesias, R. a; Zhang, Q.; Lu, J.; Li, J.; Tao, N. *Journal of the American Chemical Society* **2009**, *131*, 1390–1.

(26) Greve, a.; Olsen, J.; Privorotskaya, N.; Senesac, L.; Thundat, T.; King, W. P.; Boisen, a. *Microelectronic Engineering* **2010**, *87*, 696–698.

(27) Yi, D. C.; Greve, A.; Hales, J. H.; Senesac, L. R.; Davis, Z. J.; Nicholson, D. M.; Boisen, A.; Thundat, T. *Applied Physics Letters* **2008**, *93*, 3.

(28) Senesac, L. R.; Yi, D.; Greve, A.; Hales, J. H.; Davis, Z. J.; Nicholson, D. M.; Boisen, A.; Thundat, T. *Review of Scientific Instruments* **2009**, *80*, 9.

(29) Carey, J. R.; Suslick, K. S.; Hulkower, K. I.; Imlay, J. a; Imlay, K. R. C.; Ingison, C. K.; Ponder, J. B.; Sen, A.; Wittrig, A. E. *Journal of the American Chemical Society* **2011**, *133*, 7571–6.

(30) Alstrøm, T. S.; Larsen, J.; Kostesha, N. V; Jakobsen, M. H.; Boisen, A.; Plads, R. P.; Lyngby, K.; East, Ø. P. **2011**.

(31) Alstrøm, T. S.; Raich, R.; Kostesha, N. V; Larsen, J.; Plads, R. P.; Lyngby, K.; East, P. .

(32) Alstrøm, T. S.; Jensen, B. S.; Schmidt, M. N.; Kostesha, N. V; Larsen, J.; Allé, A.; Lyngby, K.; East, Ø. P. **2012**.

(33) Nielsen, K. a.; Martín-Gomis, L.; Sarova, G. H.; Sanguinet, L.; Gross, D. E.; Fernández-Lázaro, F.; Stein, P. C.; Levillain, E.; Sessler, J. L.; Guldi, D. M.; Sastre-Santos, Á.; Jeppesen, J. O. *Tetrahedron* **2008**, *64*, 8449–8463.

(34) Nielsen, K. A.; Cho, W. S.; Jeppesen, J. O.; Lynch, V. M.; Becher, J.; Sessler, J. L. *Journal of the American Chemical Society* **2004**, *126*, 16296–16297.

(35) JEPPESEN J.O.; NIELSEN K.A New porphyrinogen derivative useful for detection of explosive chemicals such as 2,4,6-trinitrotoluene, 1,3,5-trinitrobenzene or 1,3,5-trinitrophenole **2008**, 46.

Figures:

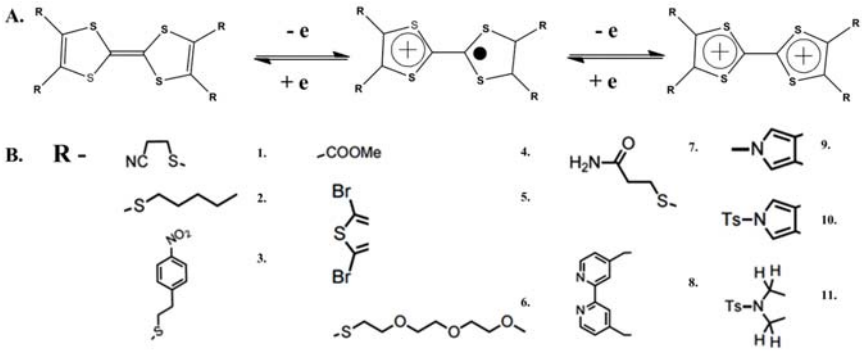

Fig.1. Simplified schematics of reversible two electron reduction-oxidation mechanism (**A.**) and schematic structure of the diversity of TTF molecules applied for the colorimetric sensor (**B.**). Common radicals: **1.** R- Cyanoethylthio; **2.** R-Pentylthio; **3.** R-(4-Nitrophenyl)ethylthio; **4.** R-Methoxycarbonyl; **5.** 2,5-Dibromo-[*c*]thieno; **6.** R-2-(2-(2-Methoxyethoxy)ethoxy)ethylthio; **7.** R-2-(Carboxamide)ethylthio; **8.** R- ????; **9.** R-[*c*]pyrrolo; **10.** R-*N*-Tos yl-[*c*]pyrrolo; **11.** R- *N*-Tosyl-2,5-Dihydro-[*c*]pyrrolo. Molecules with different radicals in TTF structure were synthesized in SDU. Complete structure and synthesis of the molecules described in the Supplementary Material and [Patent ,Ref].

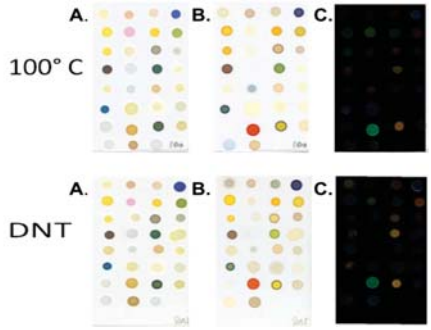

Fig. 2. Representation of the colorimetric sensor array before and after the exposure of DNT. Results were obtained in the presence of DNT in the gas phase at 100° C. The control experiment - 100° C. The images of the difference map was generated after the mathematical calculations of the colour changes; and presented as the difference map obtained from the absolute values of RGB values of each dye spot before and after the exposure of the target.

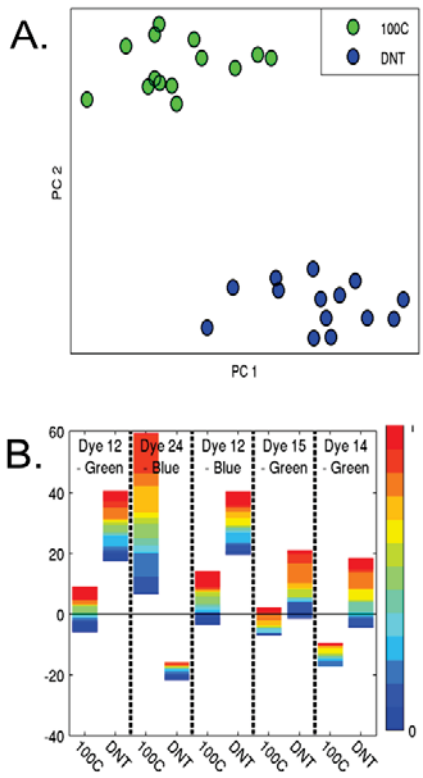

Fig 3.The PCA results (**A.**) and CDF plot (**B.**) of the colorimetric sensor array obtained from the response results of DNT (N=7; n=2). The DNT signal was compared with the signal obtained at the elevated temperature 100° C. **A.** The PCA plot demonstrates the position of DNT and 100° C replicates demonstrating the significant variables in relation to principal components (PC) to axis 1 and 2. **B.** The cumulative densities function analysis represents the response of chemo-selective compounds of 12, 12, 14, 15, and 24; molecules were defined as significant in detection of DNT. Up to 14 independent measurements (coloured right side of the plot **B.**) were performed to evaluate colour changes of in the array (the left side of the plot **B.** demonstrates the delimitation of RGB values). Bars on the scheme represent colour changes after calculation of the median and probability values of the signal.

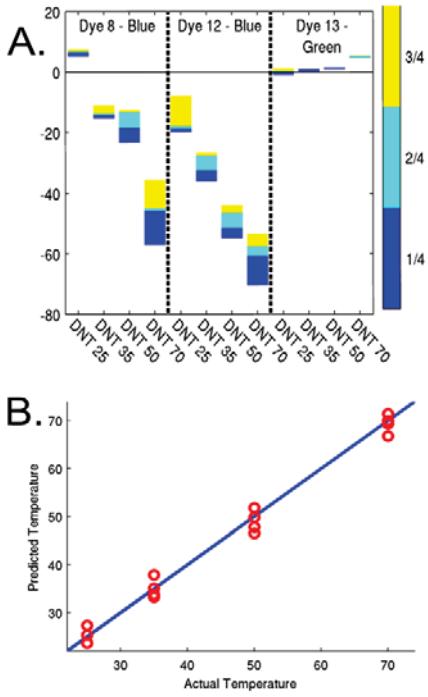

Fig 4. Representation of the sensor response at different concentrations of DNT obtained at temperatures – 25, 35, 50 and 70° C (N=1; n=4). **A.** The cumulative densities function analysis represents the response of chemo-selective compounds on DNT at different temperatures; 8, 12, 13 molecules were defined as significant in detection of DNT. Four independent measurements (coloured right side of the plot **A.**) were performed to evaluate colour changes of in the array (the left side of the plot **A.** demonstrates the delimitation of RGB values). Bars on the scheme represent colour changes after calculation of the median and probability values of the signal.

(**B.**) Calculation of the sensor correlations elevated temperatures – 25, 35, 50, 70 and 100° C (actual temperature) and predicted temperature (o-y) in relation to different concentration of DNT molecules.

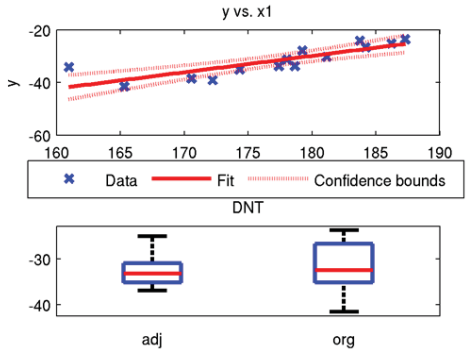

Fig. 5 Mathematical representation of the signal-noise ratio of the colorimetric sensor during DNT detection.

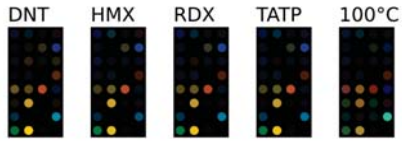

Figure 6. A difference map of the colorimetric sensor array obtained in the presence of DNT, HMX, RDX and TATP in the gas phase; saturated analyte vapour at 100° C - Control. The images of the difference map were generated after the mathematical calculations of the absolute values of RGB values.

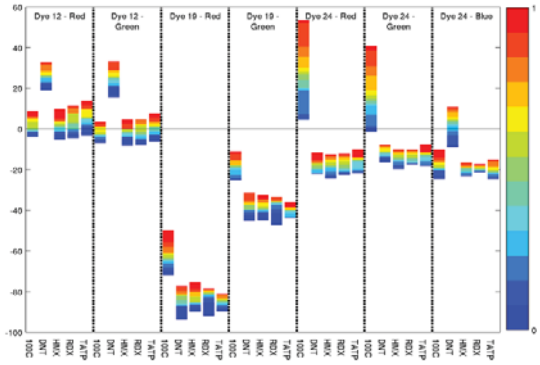

Fig. 7. The cumulative densities function analysis for DNT, RDX, HMX and TATP (N=7; n=2). The signals obtained from detection of explosives were compared with the signal obtained at the elevated temperature 100° C - Control. CSCs in the array – 12 (TTF), Bromothymol Blue sodium salt (19) and Chlorphenol Red (24) were defined as significant in detection of DNT and control. Coloured right side of the plot – number of performed detections (N=8; n=2). The left side of the plot demonstrates the result of RGB values. Bars on the scheme represent colour changes after calculation of the median and probability values of the signal.

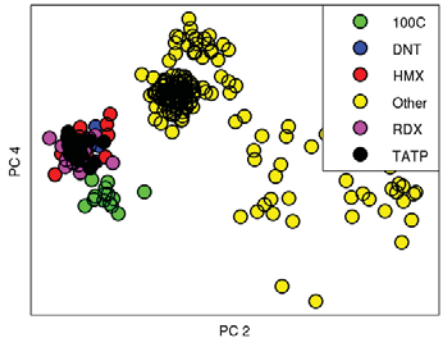

Figure 8. The PCA plot of the colorimetric sensor array obtained from the response results of DNT, HMX, RDX and TATP versus Other (Fig. 7) (N=7; n=2). The signals obtained from detection of explosives were compared with the signal obtained at the elevated temperature 100° C. The PCA plot demonstrates the position of DNT and 100° C replicates demonstrating the significant variables which were obtained after the mathematical analysis in relation to principal components (PC) to axis 2 and 4. The colorimetric sensor was demonstrated the independent response on the identification of explosives versus Other (environment).

Supplementary material

Advanced detection of explosives using colorimetric sensor array

Natalie V. Kostesha[a], Tommy S. Alstrøm[b], Olga V. Mednova[a], C. Johnsen[c], Kent A. Nielsen[c], Jan O. Jeppesen[c], Mogens H. Jakobsen[a], Jan Larsen[b] and Anja Boisen[a]

[a]*Department of Micro and Nanotechnology, Technical University of Denmark, Ørsteds Plads 345 East, DK-2800, Kgs. Lyngby, Denmark*

[b]*Department of Informatics and Mathematical Modelling, Technical University of Denmark, Richard Petersens Plads 321, 2800 Kgs. Lyngby, Denmark*

[c]*Department of Physics and Chemistry, University of Southern Denmark, Campusvej 55, DK-5230, Odense M, Denmark*

Our research is based on the selection of chemo-selective compounds (dyes) that undergo color changes in the presence of explosives and volatile organic compounds (VOCs). The list tested VOCs presented below (Table s2). The colorimetric sensor presented in this paper contains of 31 chemically selective dyes immobilized on a silica gel membrane (Table s1).

Table s1. List of chemo-selective compound tested and applied further in the colorimetric sensor array for detection of explosives and volatile organic compounds.

№	CAS-№.:	Formula	M_w	Structure and Name	Availability
1	NA	$C_{13}H_{25}N_3O_6S_7$	760.00	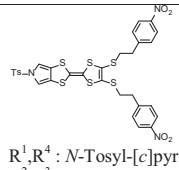 R^1,R^4 : *N*-Tosyl-[*c*]pyrrolo R^2,R^3 : 2-(4-Nitrophenyl)ethylthio	Synthetic procedure described in [1]
2	NA	$C_{38}H_{30}N_4O_8S_{12}$	1055.45	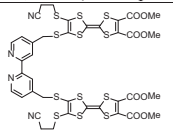 R^1 : (4'-{[7-(2-Cyanoethylthio)-2,3-Dimethoxy-carbonyl-6-thiomethylene]tetrathiafulvalene}-4-	Synthetic procedure described in [1]

				bipyridine)methylethio R^2,R^3 : Methoxycarbonyl R^4 : 2-Cyanoethylthio	
3	NA	$C_{28}H_{28}N_4O_6S_8$	773.07	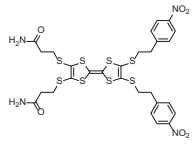 R^1,R^4 : 2-(Carboxamide)ethylthio R^2,R^3 : 2-(4-Nitrophenyl)ethylthio	Synthetic procedure described in [1]
4	26314-39-6	$C_{14}H_{12}O_8S_8$	436.50	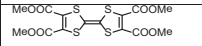 R^1,R^2,R^3,R^4 : Methoxycarbonyl	[2]
5	300766-19-2	$C_{25}H_{31}NO_2S_7$	601.97	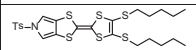 R^1,R^4 : *N*-Tos yl-[*c*]pyrrolo R^2,R^3 : Pentylthio	[3]
6	NA	$C_{25}H_{35}NO_2S_7$	606.01	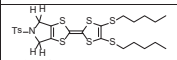 R^1,R^4 : *N*-Tosyl-2,5-Dihydro-[*c*]pyrrolo R^2,R^3 : Pentylthio	Synthetic procedure described in [1]
7	NA	$C_{19}H_{15}NO_6S_5$	516.65	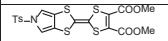 R^1,R^4 : *N*-Tosyl-[*c*]pyrrolo R^2,R^3: Methoxycarbonyl	Synthetic procedure described in [1]
8	NA	$C_{25}H_{31}N_3S_6$	565.92	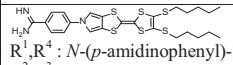 R^1,R^4 : *N*-(*p*-amidinophenyl)-[*c*]pyrrolo R^2,R^3 : Pentylthio	Synthetic procedure described in [1]
9	NA	$C_{23}H_{35}NO_6S_6$	613.92	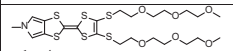 R^1,R^4 : *N*-Methyl-[*c*]pyrrolo R^2,R^3 : 2-(2-(2-Methoxyethoxy)ethoxy)ethylthio	Synthetic procedure described in [1]
10	132765-36-7	$C_{18}H_{16}N_4S_8$	544.87	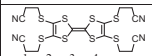 R^1,R^2,R^3,R^4 : 2-Cyanoethylthio	Synthetic procedure described in [4]

11	NA	$C_{14}H_{14}Br_2S_{12}$	566.52	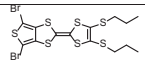 R^1,R^4 : 2,5-Dibromo-[*c*]thieno R^2,R^3 : Propylthio	Synthetic procedure described in [5]
12	31366-25-3	$C_6H_4S_4$	204.36		Sigma-Aldrich.Co.LLC.
13	55259-49-9	$C_{10}H_{12}Se_4$	448.04	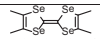 R^1,R^2,R^3,R^4 : Methyl	Sigma-Aldrich.Co.LLC.
14	NA	$C_{100}H_{148}N_4O_{24}S_{24}$	2559.82	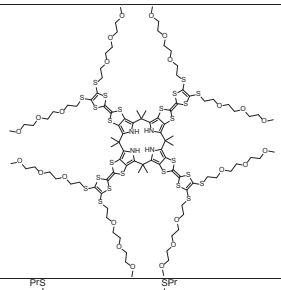	[6]
15	NA	$C_{68}H_{84}N_4S_{24}$	1727,01	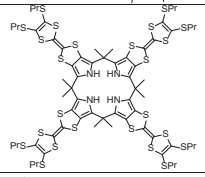	[7]
16	72-48-0	$C_{14}H_8O_4$	240.21	Alizarin	Sigma-Aldrich.Co.LLC.
17	76-60-8	$C_{21}H_{14}Br_4O_5S$	698.01	Bromocresol Green	Sigma-Aldrich.Co.LLC.
18	115-40-2	$C_{21}H_{16}Br_2O_5S$	540.22	Bromocresol Purple	Sigma-Aldrich.Co.LLC.
19	34722-90-2	$C_{27}H_{27}Br_2NaO_5S$	646.36	Bromothymol Blue sodium salt	Sigma-Aldrich.Co.LLC.
20	115-39-9	$C_{19}H_{10}Br_4O_5S$	669.96	Bromphenol Blue	Sigma-Aldrich.Co.LLC.
21	125-31-5	$C_{23}H_{22}O_5S$	410.48	Xylenol Blue	Sigma-Aldrich.Co.LLC.

22	4430-20-0	$C_{19}H_{12}Cl_2O_5S$	423.27	Chlorphenol Red	Sigma-Aldrich.Co.LLC.
23	1733-12-6	$C_{21}H_{18}O_5S$	382.43	Cresol Red	Sigma-Aldrich.Co.LLC.
24	1552-42-7	$C_{26}H_{29}N_3O_2$	415.53	Crystal Violet Lactone	Sigma-Aldrich.Co.LLC.
25	121792-58-3	$C_{29}H_{19}Cl_2NO$	468.37	2,6-Dichloro-4-(2,4,6-triphenyl-1-pyridinio)phenolate	Sigma-Aldrich.Co.LLC.
26	10081-39-7	$C_{41}H_{29}NO$	551.68	Reichardt's dye	Sigma-Aldrich.Co.LLC.
27	143-74-8	$C_{19}H_{14}O_5S$	354.38	Phenol Red	Sigma-Aldrich.Co.LLC.
28	603-45-2	$C_{19}H_{14}O_3$	290.31	Rosolic acid	Sigma-Aldrich.Co.LLC.
29	493-52-7	$(CH_3)_2NC_6H_4N=NC_6H_4CO_2H$	269.30	Methyl Red	Sigma-Aldrich.Co.LLC.
30	5423-07-4	$C_{16}H_8N_4Na_2O_{11}S_2$	542.36	Nitrazine yellow	Sigma-Aldrich.Co.LLC.
31	2374-05-2	$BrC_6H_2(CH_3)_2OH$	201.06	4-Bromo-2,6-Dimethylphenol	Sigma-Aldrich.Co.LLC.

Experimental design

Notation for experimental design section

B	Number of blocks; $B = 15$.
N_s	Number of sensors; $N_s = 31$. One dye / chemo-selective compound corresponds to one sensor.
L	Number of sensor responses; L= 3.
N_a	Number of analytes; $N_a = 18$.
N	Number of measurements; $N = N_a B -$ missing arrays $= 253$.

To conduct experiments correctly, we employ the randomized complete blocked design approach (RCBD). In this design the measurements are grouped into blocks, and within each block each analyte is exposed to the sensor array exactly once. The purpose of the design is to enable more precise estimation of effects since the variation from block to block can be removed; hence the RCBD is often referred to as a noise reducing design. Moreover, the order of the chemo-selective compounds (CSC) on the silica gel was randomized between 15 blocks. This is due to the fact that some of chemo-selective compounds used in this array were very reactive, the order those compounds on the silica gel support was randomized. We analyzed the sensor sensitivity to the

environment first since some CSCs were exposed to the environment before the sensor array was exposed to the target analyte. This behavior of CSCs was predictable due to a strong reactive environment of a chemical laboratory. However, the response of CSCs on the environment was neglected; pictures of the colorimetric sensor have been taken immediately after the immobilization of dyes and directly after the exposure of analytes and this response were evaluated.

The application of CSCs on the silica gel support was around of 20 minutes (6 applications were performed per 1 assay) thus the maximum time a compound was exposed to the surrounding environment was around 20 minutes.

The total experimental design is listed in Table s2. The experiment lasted for 8 days, with two days break between day 4 and 5. Every day one block was executed in the morning and another block in the afternoon; although on the 8th day only the morning block was executed. The room temperature (RT) was measured each day and was always in the range 21-25° C.

During performed measurements it was observed that CSCs could change colors due to their stability; a new batch of CSCs was prepared every 3rd day.

The design contained in total of $B = 15$, where each analyte was measured exactly once excluding mishaps. During the experiments some random mishaps occurred resulting in sensor array loss. The lost sensor arrays are listed in Table s3. Alternatively, we could have chosen to disregard incomplete blocks as whole, but we choose to use the entire collected data.

Table s2. The list of analytes tested by the colorimetric sensor array.

Tested analyte								
Acid	**Alcohol**	**Amine**	**Arene**	**Environment**	**Explosive**	**Inorganic Explosive**	**Ketone**	**Thiol**
Acetic acid	Ethanol	Ethylendiamine	Toluene	100° C	DNT	KNO_3	Acetone	Mercaptoethanol
Formic acid	Methanol	Propylamine		RT	HMX			
Hydrochloric acid		Triethanolamine			RDX			
					TATP			

Table s3. List of excluded sensor arrays.

Day 1 block1	**Day 1 block 2**	**Day 8 block 1**
Acetone	Acetone	RT
DNT	Ethylendiamine	100° C

Ethanol	Ethanol	KNO3
HMX	Mercaptoethanol	
Methanol	Propylamine	
RDX	Triethanolamine	
TATP	Toluene	

The careful experimental design allowed us to control nuisance factors that could influence the experiment performance and conclusions. Two factors were investigated, the first factor was a block effect (which coincides with the day effect) and the second factor we were taking in account was a spotting effect (which corresponds with dyes distribution on the solid support).

The spotting effect characterizes the different variability of the spotting procedure; factors such as the origin of the solid support, mechanical damage of the solid support, pH, solvents and humidity can effect on the spotting procedure. Moreover, the immobilization of compounds on the silica gel is likely to induce noise as this is manual labor.

Digital imaging of the dye's array before and after exposure to the analyte (Tab. s2) creates a color difference map which composes a unique fingerprint for each analyte.

Silica gel slides carrying colorimetric arrays were scanned before exposing dyes to an analyte, if the color of a dye before exposure affected the sensor response then that was estimated as a nuisance effect. That factor was undesired and can be minimized by refining and perfecting the sensor manufacturing procedure, thus the effect was not relevant for determining of the sensor performance.

Traditionally, the model that is implicitly assumed when working with colorimetric sensor arrays is

$$y_{ijkl} = \mu_{ikl} + \epsilon_{ijkl} \quad (1)$$

where, y_{ijkl} is the color difference sensor response. The i index refers to different treatments, $i = \{1,2,\dots,N_a\}$. A treatment consists of exposing the array to an analyte in 2 minutes using a fixed temperature of 100°C for organic explosives and room temperature for other analytes. The j index refers to repeated measurements, $j = \{1,2,\dots,N\}$. The index k and l are the sensor response index, i.e. we operate with $N_s = 31$ dyes with $L = 3$ channels for each dye (RGB); $k = \{1,2,\dots,N_s\}$, $l = \{1,2,3\}$. Thus we have $N_s L = 93$ systems that must be analysed as each sensor array yields a total of 93 readouts per measurement. The noise term ϵ_{ijkl} is assumed to be independent and normally distributed. The significant term in the equation is the treatment term μ_{ikl} which is the mean sensor response (k, l) of the i^{th} treatment. The colorimetric sensor was measured against controls (100°C and RT), so to verify statistically the sensor measurement is significant to the target analyte and we have the null hypothesis (H_0 and H_1):

$$\begin{aligned} H_0&: \mu_{ikl} = \mu_{ckl} \\ H_1&: \mu_{ikl} \neq \mu_{ckl} \end{aligned} \quad (2)$$

where, μ_{ckl} refers to the mean of the control treatment. Since our experimental design was a blocked noise reducing design we can augment the Equation 1 and test for a block effect in the Equation 3:

$$y_{ijkl} = \mu_{ikl} + \beta_{jkl} + \epsilon_{ijkl} \tag{3}$$

where β_{jkl} is the effect of the jth block. As the experiment was designed according to the scheme where each repetition was in a distinct block, j can be replaced as the block index instead of the repetition index j (β_{jkl} instead of i). For each of our N_sL system there will be B block effect variables. All of these variables must be zero; otherwise there is an effect from the blocking. Thus the null hypothesis that can be applied is

$$\begin{aligned} &H_0: \beta_{1kl} = \beta_{2kl} = \cdots = \beta_{Bkl} = 0 \\ &H_1: \beta_{jkl} \neq 0 \quad \text{for at least one } j \end{aligned} \tag{4}$$

We can choose to augment the equation further by considering if the difference color contains all possible information, i.e. the color of a dye before exposure to analyte might influence on a response in general. This corresponds to conducting analysis of covariance (ancova) originally proposed by Fisher[8]. Formally, the color before exposure to analyte is a possible covariate (or concomitant variable) of the sensor response:

$$y_{ijkl} = \mu_{ikl} + \beta_{jkl} + \alpha_{ikl}\left(x_{ijkl} - \bar{x}_{i\cdot kl}\right) + \epsilon_{ijkl} \tag{5}$$

where α_{ikl} is a linear regression coefficient. If α_{ikl} is different than zero, then the color response before exposure has influence on sensor response (k, l) for treatment i. The null hypothesis when testing for significant covariates is

$$\begin{aligned} &H_0: \alpha_{ikl} = 0 \\ &H_1: \alpha_{ikl} \neq 0 \end{aligned} \tag{6}$$

The model specified in eq. (5) is considered the complete model and is applied to the data. Using that model, adjusted responses that averages out the effects from blocks and covariates have been calculated. This is done by using the estimated means μ_{ikl} and then adding the residuals. The adjusted values were used to create the PCA and CDF plots as well as calculate confusion matrices in the main paper.

Hypothesis testing

Since we are performing multiple hypothesis tests we applied a low significance acceptance level of $\alpha = 0.01$ during the analysis.

The hypotheses are tested using two different tests. The treatment effects specified in eq. (2) are most likely not normally distributed with constant variance. In order to make the results as convincing as possible we choose a test that only put mild assumptions on the distribution of the treatment effects. Hence we test using the Mann–Whitney–Wilcoxon (MWW) test[9,10]. The MWW test is a nonparametric test with the only assumptions that treated data is ordinal and independently (randomly) collected. The null hypothesis of the MWW test is that two variables (in this case, the

treatment versus the control) are stochastically equal. The alternative hypothesis is that one of the variables is stochastically greater than the other.

To perform the hypothesis tests specified in eq. (4) and (6), we use the traditional student[1] t-test[11]. The t-test tests if the mean of a normally distributed variable is significantly different than zero. For testing the block effects it is reasonable assumptions, since each block is containing (almost) identical treatments. Hence, the variation for the blocks should be only due to measurement noise and a block offset. The same can be said for the regression coefficients α. Here, it is the same treatment that is always applied, since the regression coefficients are estimated for each treatment. Further, given the amount of samples the t-test should be approximately correct.

To summarize the outcomes of the hypothesis tests requires more work. The p-value from a hypothesis test is the probability of rejecting a true H_0. Hence, when performing many hypothesis tests it is likely that some of these are wrongfully found significant. E.g. from an average point of few, given 20 tests with p=0.05 one of them is wrong even though all of them is found significant.

Table s4 summarizes the gathered variables when multiple hypothesis tests are performed.

Table s4**.** Possible outcomes of multiple hypothesis tests. $\boldsymbol{W}$ and $\boldsymbol{R}$ are results from the significance tests, $\boldsymbol{W}$ is the number of times $\boldsymbol{H_0}$ was not rejected and $\boldsymbol{R}$ is the number of times $\boldsymbol{H_0}$ was rejected. $\boldsymbol{U}$ is the number of times $\boldsymbol{H_0}$ was true and also found true by the test. $\boldsymbol{T}$ is the number of times the test found $\boldsymbol{H_0}$ true even though it was false. Likewise $\boldsymbol{V}$ is the number of times $\boldsymbol{H_0}$ was true but was found false by the test. So $\boldsymbol{T}+\boldsymbol{V}$ is the total amount of false findings and $\boldsymbol{U}+\boldsymbol{S}$ is the total amount of true findings.

	Not Significant	Significant
Null H_0 true	U	V
Alternative H_1 true	T	S
Totals	W	R

The issue here is that we are only able to observe W and R as these are totals from the significant test. The other variables U, V, T, S are unobserved variables and unknown. To handle this issue the framework of controlling the false discovery rate is applied[12]. In this framework the ratio of falsely significant results is estimated:

$$\text{FDR} = E[V/R] \tag{7}$$

The FDR is used to inform about the strength of the findings, e.g. if $\text{FDR} = 0.5$ it means that half of the significant results are expected to be wrongfully found significant. The FDR controlled such that $\text{FDR} < 0.01$, that is at most 1% of the significant results are wrongfully found significant.

For each dye/coefficient we report the number of significant results and the highest significant p-value. Table(s5-s9 in other document).

[1] Student was an alias used by William Sealy Gosset.

To further summarize the results we can estimate the q-value, which is the expected FDR given that significant results was found, often written as positive false discovery rate[13]

$$q = E[\frac{V}{R}|R > 0] \quad (8)$$

The q-value is estimated according to the framework proposed by Storey[14] with the accompanying software QVALUE. The approach allows for weak block dependences in p-values which is likely the case for colorimetric sensor arrays.

Kinetics plot
To evaluate how able the sensor is to estimate the temperature / analyte density an experiment is conduction. Four repetitions was made each temperature was measured each day.

A linear regression is performed selecting dye 8,12,13,18,29 (REF: MLSP2012 paper) as these are dyes that are particular proficient at detecting explosives. Since we are an ill-posed problem we employ forward selection using Bayesian Information Criterion to select which dyes should be used as regressors. The model is build using LOO-CV. (This needs updating, discuss at meeting at the 5th)

Supporting Information
All hypothesis testing, linear regression and PCA was made using MATLAB R2012b ModelLinear class. The k-nearest neighbor classification was made using custom MATLAB script. All code and data can be downloaded at http://www.imm.dtu.dk/pubdb/p.php?6504

Confusion matrix here

As additional evidence that the model specified in eq. (5) is reducing the noise of the experiment, a k-nn classifier was applied to the data, i.e. we are comparing the results if we are using the model specified in eq. (1) versus the model in eq. (5). A significant improvement is observed and it must be said that if the model in eq. (5) is used when analyzing data from colorimetric array, a significant increase in accuracy may be obtained.

Figure s1: The confusion matrix when using the model in eq. (1)

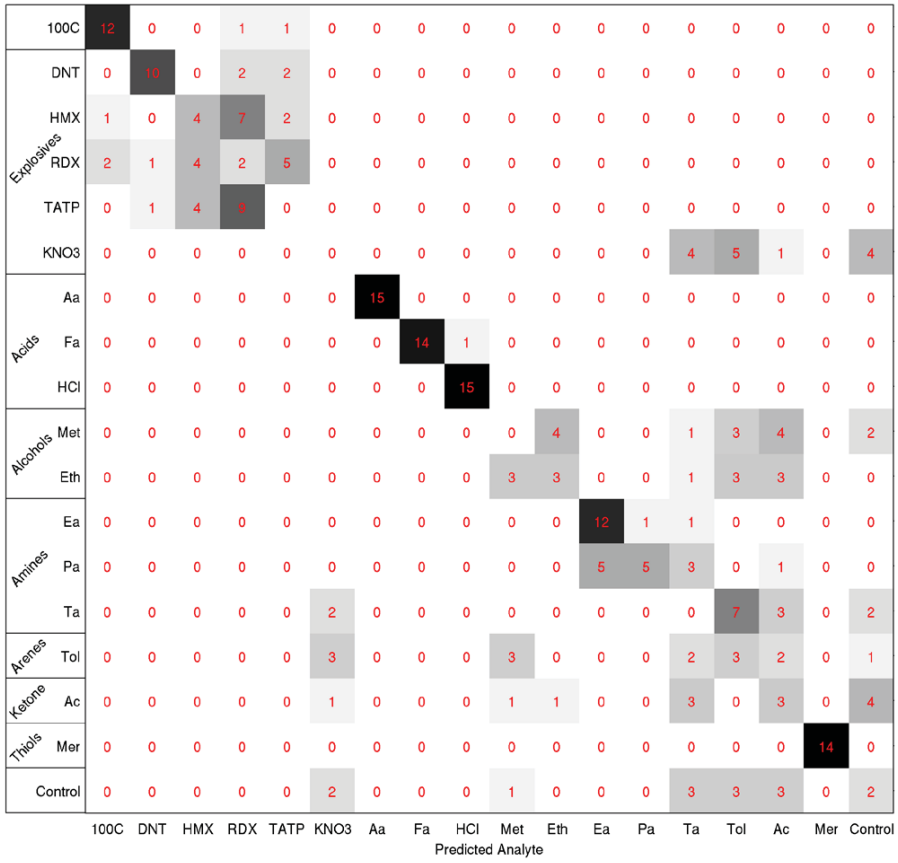

Figure s2: The confusion matrix when using the model in eq. (5).

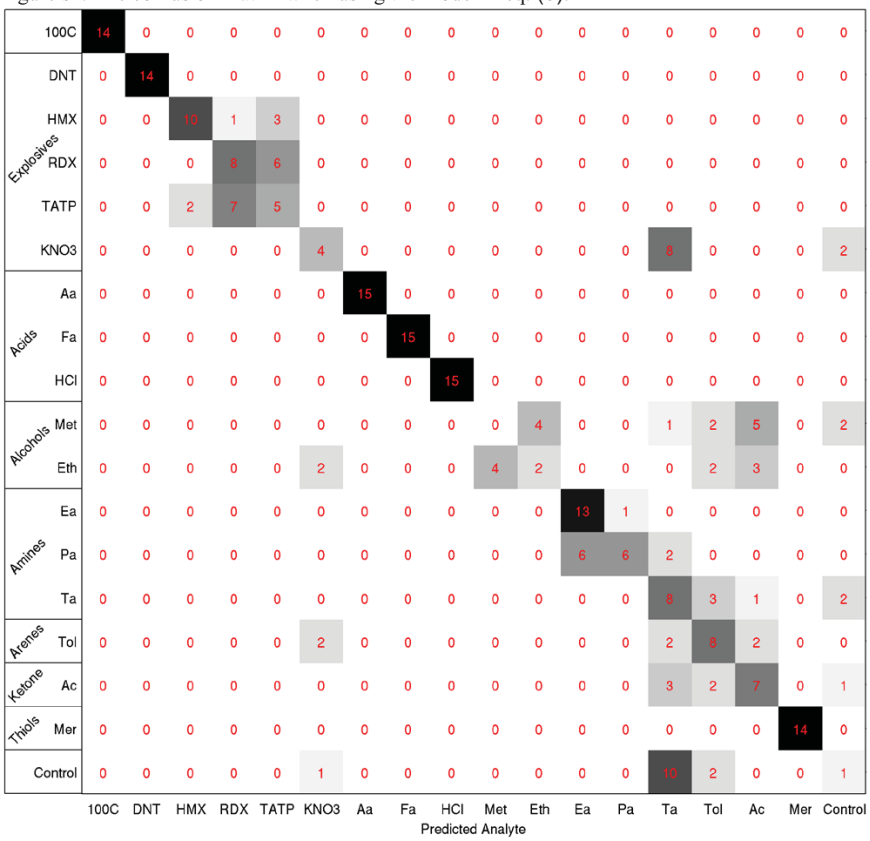

References

(1) Jeppesen, J. O.; Kostesha, N. V.; Johnsen, C.; Nielsen, K. A.; Boisen, A.; Jakobsen, M. H. Multisensor array useful for detection and/or identification of an analyte (e.g. amines, alcohols, ketones and thiols) in the gas phase or in the liquid phase, comprises at least two different chemo-selective heteroaryl compounds **2011**.

(2) Le Coustumer, G.; Mollier, Y. *Journal of the Chemical Society, Chemical Communications* **1980**, 38.

(3) Rice, J. E.; Okamoto, Y. *The Journal of Organic Chemistry* **1981**, *46*, 446–447.

(4) Svenstrup, N.; Rasmussen, K. M.; Hansen, T. K.; Becher, J. *Synthesis* **1994**, 809–812.

(5) Kim, D.-S.; Lynch, V. M.; Nielsen, K. A.; Johnsen, C.; Jeppesen, J. O.; Sessler, J. L. *Analytical and bioanalytical chemistry* **2009**, *395*, 393–400.

(6) Larsen, J.; Lenoir, C. *Synthesis* **1989**, 134–134.

(7) Nielsen, K. A.; Cho, W.-S.; Lyskawa, J.; Levillain, E.; Lynch, V. M.; Sessler, J. L.; Jeppesen, J. O. *Journal of the American Chemical Society* **2006**, *128*, 2444–51.

(8) Fisher, R. A. *Annals of Human Genetics* **1938**, *8*, 376–386.

(9) Wilcoxon, F. *Biometrics Bulletin* **1945**, *1*, 80–83.

(10) Mann, H. B.; Whitney, D. R. *The annals of mathematical statistics* **1947**, *18*, 50–60.

(11) Student *Biometrika* **1908**, *6*, 1–25.

(12) Benjamini, Y.; Hochberg, Y. *Journal of the Royal Statistical Society. Series B ...* **1995**, *57*, 289–300.

(13) Storey, J. D. *Journal of the Royal Statistical Society: Series B (Statistical Methodology)* **2002**, *64*, 479–498.

(14) Storey, J. D.; Taylor, J. E.; Siegmund, D. *Journal of the Royal Statistical Society. Series B (Statistical Methodology)* **2004**, *66*, 187–205.

Table 5: Summary of the hypothesis test $H_0 : a_{ikl}\ 1 = 0$ for TTF dyes when organic and inorganic explosives were measured. R is the number of rejected H_0 for a given dye. The listed p-value is the highest value of the significant results.

Dye	100° C	DNT	HMX	KNO_3	RDX	TATP
1	$R = 3$ $p < 0.001$	$R = 2$ $p = 0.001$	$R = 3$ $p < 0.001$	$R = 0$	$R = 3$ $p < 0.001$	$R = 3$ $p < 0.001$
2	$R = 3$ $p < 0.001$	$R = 3$ $p < 0.001$	$R = 3$ $p < 0.001$	$R = 0$	$R = 3$ $p < 0.001$	$R = 3$ $p < 0.001$
3	$R = 3$ $p < 0.001$	$R = 3$ $p < 0.001$	$R = 3$ $p < 0.001$	$R = 2$ $p < 0.001$	$R = 3$ $p < 0.001$	$R = 3$ $p < 0.001$
4	$R = 3$ $p < 0.001$	$R = 3$ $p < 0.001$	$R = 3$ $p < 0.001$	$R = 0$	$R = 3$ $p < 0.001$	$R = 3$ $p < 0.001$
5	$R = 3$ $p < 0.001$	$R = 3$ $p < 0.001$	$R = 2$ $p = 0.002$	$R = 0$	$R = 3$ $p < 0.001$	$R = 3$ $p < 0.001$
6	$R = 2$ $p < 0.001$	$R = 2$ $p < 0.001$	$R = 2$ $p < 0.001$	$R = 1$ $p = 0.001$	$R = 2$ $p < 0.001$	$R = 2$ $p < 0.001$
7	$R = 3$ $p < 0.001$	$R = 3$ $p < 0.001$	$R = 3$ $p < 0.001$	$R = 0$	$R = 3$ $p < 0.001$	$R = 3$ $p < 0.001$
8	$R = 2$ $p < 0.001$	$R = 3$ $p < 0.001$	$R = 3$ $p = 0.001$	$R = 1$ $p < 0.001$	$R = 2$ $p < 0.001$	$R = 2$ $p < 0.001$
9	$R = 3$ $p < 0.001$	$R = 3$ $p < 0.001$	$R = 3$ $p < 0.001$	$R = 0$	$R = 3$ $p < 0.001$	$R = 3$ $p < 0.001$
10	$R = 2$ $p < 0.001$	$R = 2$ $p = 0.003$	$R = 3$ $p = 0.001$	$R = 0$	$R = 3$ $p = 0.002$	$R = 2$ $p < 0.001$
11	$R = 2$ $p < 0.001$	$R = 3$ $p = 0.005$	$R = 3$ $p < 0.001$	$R = 3$ $p < 0.001$	$R = 3$ $p < 0.001$	$R = 3$ $p = 0.005$
12	$R = 3$ $p < 0.001$	$R = 3$ $p < 0.001$	$R = 2$ $p = 0.001$	$R = 0$	$R = 1$ $p < 0.001$	$R = 3$ $p < 0.001$
13	$R = 3$ $p < 0.001$	$R = 3$ $p = 0.006$	$R = 3$ $p = 0.002$	$R = 2$ $p = 0.003$	$R = 2$ $p = 0.003$	$R = 3$ $p = 0.002$
14	$R = 3$ $p < 0.001$	$R = 3$ $p < 0.001$	$R = 3$ $p < 0.001$	$R = 0$	$R = 3$ $p < 0.001$	$R = 3$ $p < 0.001$
15	$R = 3$ $p = 0.002$	$R = 3$ $p < 0.001$	$R = 3$ $p = 0.002$	$R = 0$	$R = 3$ $p < 0.001$	$R = 3$ $p < 0.001$

Table 6: Summary of the hypothesis test $H_0 : a_{ikl}\ 1 = 0$ for non-TTF dyes when organic and inorganic explosives were measured. R is the number of rejected H_0 for a given dye. The listed p-value is the highest value of the significant results.

Dye	100° C	DNT	HMX	KNO_3	RDX	TATP
16	$R = 0$	$R = 3$ $p = 0.003$	$R = 2$ $p = 0.004$	$R = 0$	$R = 3$ $p < 0.001$	$R = 3$ $p < 0.001$
17	$R = 1$ $p < 0.001$	$R = 2$ $p = 0.002$	$R = 2$ $p < 0.001$	$R = 0$	$R = 2$ $p < 0.001$	$R = 2$ $p = 0.001$
18	$R = 2$ $p < 0.001$	$R = 2$ $p < 0.001$	$R = 2$ $p < 0.001$	$R = 0$	$R = 2$ $p < 0.001$	$R = 2$ $p < 0.001$
19	$R = 2$ $p < 0.001$	$R = 2$ $p < 0.001$	$R = 3$ $p = 0.004$	$R = 0$	$R = 3$ $p = 0.004$	$R = 2$ $p < 0.001$
20	$R = 1$ $p < 0.001$	$R = 1$ $p < 0.001$	$R = 2$ $p = 0.001$	$R = 0$	$R = 2$ $p = 0.004$	$R = 2$ $p = 0.005$
21	$R = 0$	$R = 0$	$R = 2$ $p = 0.007$	$R = 0$	$R = 0$	$R = 0$
22	$R = 2$ $p < 0.001$	$R = 2$ $p < 0.001$	$R = 2$ $p < 0.001$	$R = 0$	$R = 2$ $p < 0.001$	$R = 2$ $p < 0.001$
23	$R = 0$	$R = 0$	$R = 1$ $p < 0.001$	$R = 0$	$R = 1$ $p = 0.001$	$R = 1$ $p < 0.001$
24	$R = 1$ $p < 0.001$	$R = 1$ $p < 0.001$	$R = 1$ $p < 0.001$	$R = 1$ $p = 0.002$	$R = 1$ $p < 0.001$	$R = 1$ $p < 0.001$
25	$R = 3$ $p < 0.001$	$R = 3$ $p < 0.001$	$R = 3$ $p < 0.001$	$R = 0$	$R = 3$ $p < 0.001$	$R = 3$ $p < 0.001$
26	$R = 2$ $p = 0.006$	$R = 0$	$R = 0$	$R = 0$	$R = 0$	$R = 0$
27	$R = 0$	$R = 1$ $p = 0.003$	$R = 0$	$R = 0$	$R = 0$	$R = 1$ $p < 0.001$
28	$R = 2$ $p = 0.003$	$R = 3$ $p < 0.001$	$R = 2$ $p = 0.001$	$R = 0$	$R = 3$ $p = 0.002$	$R = 3$ $p = 0.001$
29	$R = 3$ $p < 0.001$	$R = 2$ $p = 0.002$	$R = 1$ $p < 0.001$	$R = 1$ $p < 0.001$	$R = 2$ $p = 0.005$	$R = 2$ $p = 0.006$
30	$R = 1$ $p = 0.001$	$R = 0$	$R = 1$ $p < 0.001$	$R = 0$	$R = 3$ $p = 0.006$	$R = 0$
31	$R = 3$ $p < 0.001$	$R = 3$ $p < 0.001$	$R = 3$ $p < 0.001$	$R = 0$	$R = 3$ $p < 0.001$	$R = 3$ $p < 0.001$

Table 7: Treatment effect different from control H_0 : $_{ijk} = {}_{cjk}$, TTF dyes. R is the number of rejected H_0 for a given dye. The listed p-value is the highest value of the significant results

Dye	DNT	HMX	KNO_3	RDX	TATP
1	$R=1$ $p=0.002$	$R=0$	$R=3$ $p<0.001$	$R=3$ $p=0.009$	$R=0$
2	$R=2$ $p=0.003$	$R=0$	$R=3$ $p<0.001$	$R=0$	$R=0$
3	$R=2$ $p<0.001$	$R=0$	$R=3$ $p=0.004$	$R=0$	$R=0$
4	$R=1$ $p=0.002$	$R=2$ $p=0.006$	$R=2$ $p<0.001$	$R=1$ $p=0.002$	$R=2$ $p<0.001$
5	$R=0$	$R=0$	$R=2$ $p=0.001$	$R=3$ $p=0.004$	$R=1$ $p=0.001$
6	$R=3$ $p<0.001$	$R=0$	$R=3$ $p=0.002$	$R=0$	$R=0$
7	$R=0$	$R=2$ $p<0.001$	$R=2$ $p<0.001$	$R=3$ $p<0.001$	$R=2$ $p=0.003$
8	$R=2$ $p<0.001$	$R=2$ $p<0.001$	$R=0$	$R=2$ $p<0.001$	$R=2$ $p<0.001$
9	$R=3$ $p=0.005$	$R=3$ $p<0.001$	$R=3$ $p=0.005$	$R=0$	$R=0$
10	$R=2$ $p<0.001$	$R=3$ $p=0.002$	$R=3$ $p<0.001$	$R=0$	$R=0$
11	$R=3$ $p=0.006$	$R=0$	$R=2$ $p<0.001$	$R=1$ $p=0.001$	$R=0$
12	$R=3$ $p<0.001$	$R=0$	$R=3$ $p<0.001$	$R=1$ $p<0.001$	$R=0$
13	$R=2$ $p<0.001$	$R=1$ $p<0.001$	$R=1$ $p<0.001$	$R=2$ $p=0.005$	$R=3$ $p=0.003$
14	$R=2$ $p<0.001$	$R=3$ $p=0.002$	$R=3$ $p<0.001$	$R=3$ $p<0.001$	$R=3$ $p<0.001$
15	$R=3$ $p<0.001$	$R=0$	$R=3$ $p<0.001$	$R=3$ $p=0.009$	$R=1$ $p=0.002$

Table 8. Treatment effect different from control $H_0: {}_{ijk} = {}_{cjk}$, Non-TTF dyes. R is the number of rejected H_0 for a given dye. The listed p-value is the highest value of the significant results

Dye	DNT	HMX	KNO3	RDX	TATP
16	$R=3$ $p=0.002$	$R=0$	$R=3$ $p=0.007$	$R=1$ $p=0.002$	$R=1$ $p<0.001$
17	$R=2$ $p<0.001$	$R=2$ $p<0.001$	$R=3$ $p=0.001$	$R=1$ $p<0.001$	$R=2$ $p<0.001$
18	$R=1$ $p<0.001$	$R=1$ $p<0.001$	$R=3$ $p<0.001$	$R=1$ $p<0.001$	$R=1$ $p<0.001$
19	$R=3$ $p<0.001$	$R=3$ $p<0.001$	$R=2$ $p<0.001$	$R=3$ $p<0.001$	$R=3$ $p<0.001$
20	$R=2$ $p=0.001$	$R=2$ $p<0.001$	$R=3$ $p=0.004$	$R=1$ $p<0.001$	$R=2$ $p<0.001$
21	$R=2$ $p<0.001$	$R=2$ $p<0.001$	$R=2$ $p<0.001$	$R=2$ $p<0.001$	$R=2$ $p<0.001$
22	$R=3$ $p=0.006$	$R=3$ $p<0.001$	$R=3$ $p<0.001$	$R=3$ $p=0.001$	$R=3$ $p<0.001$
23	$R=3$ $p<0.001$	$R=3$ $p<0.001$	$R=2$ $p<0.001$	$R=3$ $p<0.001$	$R=3$ $p<0.001$
24	$R=3$ $p<0.001$	$R=2$ $p<0.001$	$R=3$ $p<0.001$	$R=2$ $p<0.001$	$R=2$ $p<0.001$
25	$R=1$ $p<0.001$	$R=1$ $p<0.001$	$R=1$ $p<0.001$	$R=3$ $p=0.003$	$R=3$ $p=0.007$
26	$R=3$ $p<0.001$	$R=3$ $p=0.002$	$R=3$ $p<0.001$	$R=3$ $p<0.001$	$R=3$ $p<0.001$
27	$R=2$ $p<0.001$	$R=2$ $p<0.001$	$R=2$ $p<0.001$	$R=2$ $p<0.001$	$R=2$ $p<0.001$
28	$R=2$ $p<0.001$	$R=3$ $p<0.001$	$R=3$ $p=0.001$	$R=2$ $p<0.001$	$R=2$ $p<0.001$
29	$R=0$	$R=2$ $p<0.001$	$R=3$ $p=0.001$	$R=2$ $p<0.001$	$R=2$ $p<0.001$
30	$R=2$ $p<0.001$	$R=2$ $p<0.001$	$R=3$ $p<0.001$	$R=2$ $p<0.001$	$R=2$ $p<0.001$
31	$R=0$	$R=0$	$R=3$ $p<0.001$	$R=3$ $p=0.004$	$R=0$
	$R=65$ $q=0.000$	$R=51$ $q=0.004$	$R=79$ $q=0.000$	$R=58$ $q=0.004$	$R=53$ $q=0.002$

Table 9: Summary of the hypothesis test H_0 : $_{ikl} = 0$, $i = \{1,2,\ldots,B\}$. R is the number of rejected H_0 for a given dye. The listed p-value is the highest value of the significant results.

Dye	Block
1	$R = 2$ $p = 0.004$
2	$R = 3$ $p < 0.001$
3	$R = 3$ $p < 0.001$
4	$R = 3$ $p < 0.001$
5	$R = 0$
6	$R = 1$ $p < 0.001$
7	$R = 3$ $p < 0.001$
8	$R = 2$ $p < 0.001$
9	$R = 3$ $p < 0.001$
10	$R = 3$ $p < 0.001$

Dye	Block
11	$R = 1$ $p < 0.001$
12	$R = 3$ $p < 0.001$
13	$R = 3$ $p = 0.002$
14	$R = 3$ $p = 0.006$
15	$R = 0$
16	$R = 1$ $p = 0.002$
17	$R = 3$ $p = 0.002$
18	$R = 1$ $p < 0.001$
19	$R = 0$
20	$R = 3$ $p < 0.001$

Dye	Block
21	$R = 3$ $p < 0.001$
22	$R = 1$ $p < 0.001$
23	$R = 1$ $p < 0.001$
24	$R = 0$
25	$R = 3$ $p < 0.001$
26	$R = 2$ $p = 0.002$
27	$R = 0$
28	$R = 1$ $p < 0.001$
29	$R = 3$ $p = 0.003$
30	$R = 3$ $p = 0.004$

Dye	Block
31	$R = 0$

Appendix G

Analytes

In this appendix the compounds that has been handled during this ph.d. is described in detail. There is also a table that shows which chemical family the various compounds belong to.

Compound	Possible application
Acetic acid	A raw material in production of acetic anhydride, acetates, dyes (salts of acetic acid (Fe, Al, Cr, etc.). Acetic acid is used as a solvent in production of varnish, latex coagulant, acetylating agent in the organic synthesis. In medicine for production of aspirin. In the manufacture of condiments, pickles, canned foods in the form of vinegar - 3-15% aqueous solution and vinegar - 80% aqueous solution food acetic acid.
Acetone	Commonly used solvent of many organic chemicals: nitrocellulose and cellulose acetate (synthetic fiber). Due to the relatively low toxicity it is used in chemical and pharmaceutical industry for the synthesis of acetic anhydride, diacetone alcohol, methyl methacrylate, diphenylolpropane, isophorone and many other compounds.

Compound	Possible application
Ammonium Nitrate	Nitrogen fertilizer. It is also used in the production of explosives (e.g. ammonites – amatol), in the reprocessing of irradiated nuclear fuel.
Benzodioxol	A precursor for perfumes, insecticide and pharmaceuticals. In production of safrole and ecstacy.
Diesel	Diesel fuel
2,4-Dinitrotoluene	manufacture of explosives, dyes, in organic synthesis, as a plasticizer. Precursor in the production of trinitrotoluene (TNT)
Ethanol	A solvent of many organic chemicals: diethylether, chloroform, acetaldehyde, acetic acid, ethylacetate, ethylamine, ethylacrylate, ethylsilicates, etc. Ethanol is component of antifreeze, jet fuel, can be used as a biofuel. Used in electronics, as household chemical, in production of explosives.
Ethylendiamine	Used as a plasticizers for phenol-formaldehyde resins, polyurethane fibers, used to stabilize the lubricants and rubber latex in the production of polyurethanes and thermoplastic adhesives, in production of fungicides and additives to motor oils, in pharmaceutical industry.
Formic acid	Used in dyeing of textiles and paper, leather processing, and as a preservative in silage of green mass, fruit juices, as well as for disinfection of barrels of beer and wine. In production of pesticides, solvents (e.g. dimethylformamide - DMF), salts and esters. Used as a solvent - nitrates and cellulose acetate; as a perfume - soap, used in he production of vitamins B1, A, E.
Heptane	Added to motor fuels to increase high-octane components, n-heptane is used as a solvent.
HMX	Octahydro-1,3,5,7-tetranitro-1,3,5,7-tetrazocine - is a military class explosives. HMX is the highest-energy solid explosive.

Compound	Possible application
Hydrochloric acid	Used in production in organic synthesis – production of vinyl chloride and rubber; production of chlorides (Mn, Fe, Zn), sodium glutamate, as a catalyst (e.g. alkylation of benzene).
Isosafrole	Synthesis of illegal drugs.
Mercaptoethanol	Research: electrophoresis, biological antioxidant.
Methanol	In production of formaldehyde, methyl methacrylate, methylamines, dimethyl, methylformate, acetic acid, methyl alcohol, acetic anhydride, vinyl acetate, ethanol, acetaldehyde, ethylene glycol. As an additive to gasoline (methyl alcohol has a high octane number) and as a part of biofuel. In pharmaceutical industry.
Pentanol	
Potassium nitrate	Used as a basic fertilizer containing 44% K2O and 13% Nitrogen); production of explosives
Propanol	Used as a solvent for waxes, polyamide containing inks, synthetic resins, polyacrylonitrile, co-solvent of PVC adhesives, gelling and plasticizing agent. It is also used for the synthesis of propionic acid, propionaldehyde, propylamine, detergents, pesticides, drugs.
Propylamine	Used as cellulose modifiers, corrosion inhibitors and stabilizers. In pharmaceutical industry, in production of lubricates, dyes, resins, for the treatment of textile and leather products, crude oil emulsion breakers, etc. As cleaning, flotation agents, emulsion floor wax, antioxidants and rubber accelerators.
RDX	Hexahydro-1,3,5-trinitro-1,3,5-triazine - cyclonite or hexogen is currently the most important military high explosive.
TATP	Triacetone triperoxide is peroxide based type explosive.
Toluene	Used in production of TNT.

Compound	Possible application
Triethanolamine	Used in the cement industry as a binder between synthetic and natural ingredients of cement, in the production of corrosion inhibitors, synthetic fibers. Used as an absorbent of "acid" gases (H2S, CO2, SO2, etc.) during purification of process gases at oil refineries, gas production and chemical industries. In pharmaceutical industry and cosmetics as a emulsifying, dispersing, stabilizing foams agent, detergents, shampoos, detergents.
TNT	Trinitrotoluene, used the manufacturing of dyes, explosives; used as a solvent in production of polymers, printing inks, in rubber and pharmaceutical industry.
Water	Purified water, commonly used solvent.

Categorization of analytes

Chemical family	Analyte	Abbreviation
Acid	Acetic acid	AA
	Formic acid	FA
	Hydrogen chloride	HCl
Alcohol	Ethanol	EtOH
	Methanol	MeOH
	Pentanol	PeOH
	Propanol	PrOH
Aldehyde	Nonanal	NA
	Octonal	OA
Amine	Ethylendiamine	EDA
	Propylamine	PA
	Triethanolamine	TEA
Arene	Diaminotoluene	DAT
	Toluene	Tol
Drug	Benzodioxole	BDO
	Isosafrole	IA
	Lysergic acid diethylamide	LSD
	Phenylacetone	PhA
Explosive	Dinitrotoluene	DNT
	Octogen	HMX
	Cyclotrimethylenetrinitramine	RDX
	Triacetone Triperoxide	TATP
	Trinitrotoluene	TNT
Ketone	Acetone	Ac
Other	Diesel	Diesel
	Heptane	Hep
Salt	Potassium chloride	KCl
	Potassium nitrate	KNO3
	Ammonium chloride	NH4Cl
	Ammonium nitrate	AN
	Sodium chloride	NaCL
Thiol	Mercaptoethanol	ME

Bibliography

David A. Wernick and Mary Ann Von Glinow. Reflections on the Evolving Terrorist Threat to Luxury Hotels: A Case Study on Marriott International. *Thunderbird International Business Review*, 54(5):729–746, September 2012. ISSN 10964762. doi: 10.1002/tie.21496.

John Rollings and Liana S. Wyler. Terrorism and Transnational Crime: Foreign Policy Issues for Congress. *Report for Congress*, R41004, 2012.

Maki K. Habib. Humanitarian Demining: Reality and the Challenge of Technology - The State of the Arts. *International Journal of Advanced Robotic Systems*, page 1, 2007. ISSN 1729-8806. doi: 10.5772/5699.

International Campaign to Ban Landmines, Landmine Monitor 2012 (Ottawa: Mines Action Canada: December 2012). Landmine and Cluster Munition Monitor, 2012. ISBN 978-2-8399-1102-3. URL www.the-monitor.org.

Antonio Maria Costa, Fabio Valencia Cossio, and Franco Frattini, editors. *Digest of Terrorist Cases*. United Nations Office on Drugs and Crime, v.09-86635 edition, 2010.

Kenneth G. Furton and Myers J. Lawrence. The scientific foundation and efficacy of the use of canines as chemical detectors for explosives. *Talanta*, 54 (3):487–500, May 2001. ISSN 00399140.

Suman Singh. Sensors–an effective approach for the detection of explosives. *Journal of hazardous materials*, 144(1-2):15–28, June 2007. ISSN 0304-3894. doi: 10.1016/j.jhazmat.2007.02.018.

Jehuda Yinon. Detection of Explosives by Electronic Noses. *Analytical Chemistry*, 75(5):98 A–105 A, March 2003. ISSN 0003-2700. doi: 10.1021/ac0312460.

Yanghai Gui, Changsheng Xie, Jiaqiang Xu, and Guoqing Wang. Detection and discrimination of low concentration explosives using MOS nanoparticle sensors. *Journal of hazardous materials*, 164(2-3):1030–5, May 2009. ISSN 1873-3336. doi: 10.1016/j.jhazmat.2008.09.011.

Michael J. Fitch, Megan R. Leahy-Hoppa, Edward W. Ott, and Robert Osiander. Molecular absorption cross-section and absolute absorptivity in the THz frequency range for the explosives TNT, RDX, HMX, and PETN. *Chemical Physics Letters*, 443(4–6):284–288, August 2007. ISSN 0009-2614. URL http://www.sciencedirect.com/science/article/pii/S0009261407008676.

Jeffrey Barber, Daniel E. Hooks, David J. Funk, Richard D. Averitt, Antoinette J. Taylor, and Dmitri Babikov. Temperature-Dependent Far-Infrared Spectra of Single Crystals of High Explosives Using Terahertz Time-Domain Spectroscopy. *The Journal of Physical Chemistry A*, 109(15):3501–3505, March 2005. ISSN 1089-5639. doi: 10.1021/jp044384h. URL http://dx.doi.org/10.1021/jp044384h.

Stacy-Ann Barshick and Wayne H. Griest. Trace Analysis of Explosives in Seawater Using Solid-Phase Microextraction and Gas Chromatography/Ion Trap Mass Spectrometry. *Analytical Chemistry*, 70(14):3015–3020, May 1998. ISSN 0003-2700. doi: 10.1021/ac980060b. URL http://dx.doi.org/10.1021/ac980060b.

J. Chance Carter, S. Michael Angel, Marion Lawrence-Snyder, Jon Scaffidi, Richard E. Whipple, and John G. Reynolds. Standoff Detection of High Explosive Materials at 50 Meters in Ambient Light Conditions Using a Small Raman Instrument. *Applied spectroscopy*, 59(6):769–775, June 2005. URL http://as.osa.org/abstract.cfm?URI=as-59-6-769.

Dana A. Shea and Daniel Morgan. Detection of explosives on airline passengers: Recommendation of the 9/11 Commission and related issues. *CRS Report for Congress*, April(RS21920):1–6, 2007. URL http://oai.dtic.mil/oai/oai?verb=getRecord&metadataPrefix=html&identifier=ADA453711.

Danminar, 2012. URL http://www.danminar.dk.

APOCO, 2012. URL http://www.apopo.org.

AIRSENSE Analytics, 2012. URL http://www.airsense.com/en.

RKI Instruments, Inc., 2012. URL http://www.rkiinstruments.com.

Industrial Scientific, 2012. URL http://www.indsci.com.

Joseph R. Stetter, S. Strathmann, Carol McEntegart, Maylin Decastro, and William R. Penrose. New sensor arrays and sampling systems for a modular electronic nose. *Sensors and Actuators B: Chemical*, 69(3):410–419, October 2000. ISSN 0925-4005. URL http://www.sciencedirect.com/science/article/pii/S0925400500005037.

Kenneth S. Suslick, Keren I. Hulkower, Avijit Sen, Mitchell A. Sroka, and William B. McNamara III. Method and apparatus for detecting ammonia from exhaled breath, August 2004a.

Natalie V. Kostesha, Tommy S. Alstrøm, Carsten Johnsen, Kent A. Nielsen, Jan O. Jeppesen, Jan Larsen, Mogens H. Jakobsen, and Anja Boisen. Development of the colorimetric sensor array for detection of explosives and volatile organic compounds in air. In *Proceedings of SPIE*, volume 7673, pages 76730I–76730I–9, 2010. doi: 10.1117/12.850310.

Xsense. Xsense - Miniaturized Sensors for Explosives Detection in Air, 2012. URL http://www.xsense.dk.

Baranidharan Raman, Douglas C. Meier, Jon K. Evju, and Steve Semancik. Designing and optimizing microsensor arrays for recognizing chemical hazards in complex environments. *Sensors and Actuators B: Chemical*, 137(2):617–629, April 2009. ISSN 0925-4005. URL http://www.sciencedirect.com/science/article/pii/S0925400508008125.

Benny Kimberg, editor. *Report of the The International Conference on Mine Clearance Technology*. United Nations, 1996.

Global Terrorism Index, Capturing the Impact of Terrorism from 2002 - 2011. Institute for Economics & Peace, 2012.

National Consortium for the Study of Terrorism and Responses to Terrorism (START). (2012). Global Terrorism Database [Data file]. Retrieved from http://www.start.umd.edu/gtd.

David Hoffman. *The Oklahoma City Bombing and the Politics of Terror*. 1998. ISBN 0922915490. URL http://www.constitution.org/ocbpt/ocbpt.htm.

Danske regler tjekkes efter Oslo-bombe. *Politiken*, 25:1, July 2011a.

Etbenet bombemand skal forklare sig i byretten. *Politiken*, 16:3, May 2011b.

Udvist terrordømt fra Gasvejsag anker sin dom. *Politiken*, 23:4, October 2008.

International campaign to ban landmines, 2012. URL http://www.icbl.org.

Michael S. Schmidt, Natalie V. Kostesha, Filippo G. Bosco, Jesper K. Olsen, Carsten Johnsen, Kent A. Nielsen, Jan O. Jeppesen, Tommy S. Alstrøm, Jan Larsen, Thomas Thundat, Mogens H. Jacobsen, and Anja Boisen. Xsense - a miniaturised multi-sensor platform for explosives detection. In *Proceedings of SPIE*, volume 8031, pages 803123–803123–7, 2011a. doi: 10.1117/12.884050.

Kneipp Kneipp, Yang Wang, Harald Kneipp, Lev T. Perelman, Irving Itzkan, Ramachandra R. Dasari, and Michael S. Feld. Single molecule detection using surface-enhanced Raman scattering (SERS). *Physical Review Letters*, pages 1667–1670, 1997. URL http://link.aps.org/doi/10.1103/PhysRevLett.78.1667.

Ivan Talian, Klaus B. Mogensen, Andrej Oriňák, Dušan Kaniansky, and Jörg Hübner. Surface-enhanced Raman spectroscopy on novel black silicon-based nanostructured surfaces. *Journal of Raman Spectroscopy*, 40(8):982–986, 2009. ISSN 1097-4555. URL http://dx.doi.org/10.1002/jrs.2213.

Dechang Yi, Anders Greve, Jan H. Hales, Larry R. Senesac, Zachary J. Davis, Don M. Nicholson, Anja Boisen, and Thomas Thundat. Detection of adsorbed explosive molecules using thermal response of suspended microfabricated bridges. *Applied Physics Letters*, 93(15):154102, October 2008a. ISSN 00036951. doi: DOI:10.1063/1.3002285. URL http://dx.doi.org/doi/10.1063/1.3002285http://link.aip.org/link/?APPLAB/93/154102/1.

Dechang Yi, Larry Senesac, and Thomas Thundat. Speciation of Energetic Materials on a Microcantilever Using Surface Reduction. *Scanning*, 30(2):208–212, 2008b. ISSN 1932-8745. doi: 10.1002/sca.20096. URL http://dx.doi.org/10.1002/sca.20096http://www.ncbi.nlm.nih.gov/pubmed/18288710.

Larry R. Senesac, Dechang Yi, Anders Greve, Jan H. Hales, Zachary J. Davis, Don M. Nicholson, Anja Boisen, and Thomas Thundat. Micro-differential thermal analysis detection of adsorbed explosive molecules using microfabricated bridges. *Review of Scientific Instruments*, 80 (3):35102, March 2009. ISSN 1089-7623. doi: 10.1063/1.3090881. URL http://link.aip.org/link/?RSI/80/035102/1http://link.aip.org/link/?RSINAK/80/035102/1.

Anders Greve, Jesper K. Olsen, Natalya L. Privorotskaya, Larry R. Senesac, Thomas Thundat, William P. King, and Anja Boisen. Micro-calorimetric sensor for vapor phase explosive detection with optimized heat profile. *Microelectronic Engineering*, 87(5-8):696–698, May 2010. ISSN 0167-9317. doi: 10.1016/j.mee.2009.12.069. URL http://www.sciencedirect.com/science/article/pii/S0167931709009125http://dx.doi.org/10.1016/j.mee.2009.12.069.

Roberto Raiteri, Massimo Grattarola, Hans-Jürgen Butt, and Petr Skládal. Micromechanical cantilever-based biosensors. *Sensors and Actuators B: Chemical*, 79(2–3):115–126, October 2001. ISSN 0925-4005. URL http://www.sciencedirect.com/science/article/pii/S0925400501008565.

Jurgen Fritz. Cantilever biosensors. *Analyst*, 133(7):855–863, 2008. ISSN 0003-2654. URL http://dx.doi.org/10.1039/B718174D.

Anja Boisen, Søren Dohn, Stephan S. Keller, Silvan Schmid, and Maria Tenje. Cantilever-like micromechanical sensors. *Reports on Progress in Physics*, 74(3):36101, 2011. ISSN 0034-4885. URL http://stacks.iop.org/0034-4885/74/i=3/a=036101.

Jurgen Fritz, Marko K. Baller, Hans P. Lang, Hugo E. Rothuizen, Peter Vettiger, Ernst Meyer, Hans-Joachim Güntherodt, Christoph Gerber, and James K. Gimzewski. Translating Biomolecular Recognition into Nanomechanics. *Science*, 288(5464):316–318, 2000. doi: 10.1126/science.288.5464.316. URL http://www.sciencemag.org/content/288/5464/316.abstract.

Maria L. Sushko, John H. Harding, Alexander L. Shluger, Rachel A. McKendry, and Moyu Watari. Physics of Nanomechanical Biosensing on Cantilever Arrays. *Advanced Materials*, 20(20):3848–3853, 2008. ISSN 1521-4095. doi: 10.1002/adma.200801344. URL http://dx.doi.org/10.1002/adma.200801344.

James K. Gimzewski, Christoph Gerber, Ernst Meyer, and Reto R. Schlittler. Observation of a chemical reaction using a micromechanical sensor. *Chemical Physics Letters*, 217(5–6):589–594, 1994. ISSN 0009-2614. doi: 10.1016/0009-2614(93)E1419-H. URL http://www.sciencedirect.com/science/article/pii/0009261493E1419H.

Natalie V. Kostesha, Tommy S. Alstrøm, Carsten Johnsen, Kent A. Nielsen, Jan O. Jeppesen, Jan Larsen, Anja Boisen, and Mogens H. Jakobsen. Multicolorimetric sensor array for detection of explosives in gas and liquid phase. In *Proceedings of SPIE*, volume 8018, pages 80181H–80181H–12, 2011. doi: 10.1117/12.883895.

Chen Zhang and Kenneth S. Suslick. A colorimetric sensor array for organics in water. *Journal of the American Chemical Society*, 127(33):11548–9, August 2005. ISSN 0002-7863. doi: 10.1021/ja052606z.

Kent A. Nielsen, Luis Martín-Gomis, Ginka H. Sarova, Lionel Sanguinet, Dustin E. Gross, Fernando Fernández-Lázaro, Paul C. Stein, Eric Levillain, Jonathan L. Sessler, Dirk M. Guldi, Ángela Sastre-Santos, and Jan O. Jeppesen. Binding studies of tetrathiafulvalene-calix[4]pyrroles with electron-deficient guests. *Tetrahedron*, 64(36):8449–8463, September 2008. ISSN

0040-4020. URL http://www.sciencedirect.com/science/article/pii/S0040402008010740.

Quinn McNemar. Note on the sampling error of the difference between correlated proportions or percentages. *Psychometrika*, 12(2):153–157, June 1947. ISSN 0033-3123. doi: 10.1007/BF02295996.

John D. Storey. A direct approach to false discovery rates. *Journal of the Royal Statistical Society: Series B (Statistical Methodology)*, 64(3):479–498, August 2002. ISSN 13697412. doi: 10.1111/1467-9868.00346. URL http://doi.wiley.com/10.1111/1467-9868.00346.

Claude E. Shannon. Programming a computer for playing chess. *Philosophical Magazine Series 7*, 41(314):256–275, 1950a.

Claude E. Shannon. Theseus, an electrically controlled mouse, 1950b. URL http://techchannel.att.com/play-video.cfm/2010/3/16/In-Their-Own-Words-Claude-Shannon-Demonstrates-Machine-Learning.

MIT Museum Collections. Theseus, 2007. URL http://webmuseum.mit.edu/detail.php?type=related&kv=76066&t=objects.

Alan M. Turing. Computing Machinery and Intelligene. *Mind Association*, 59 (236):433–460, 1950.

Jonathan Skillings. Getting machines to think like us, 2006. URL http://news.cnet.com/Getting-machines-to-think-like-us/2008-11394_3-6090207.html.

John McCarthy. What is artificial intelligence. Technical report, Stanford University, 2007. URL http://www-formal.stanford.edu/jmc/whatisai.pdf.

Tom M. Mitchell. *Machine Learning*. McGraw Hull, 1997. ISBN 0070428077.

Neal D. Lawrence. Machine learning for cognitive science 1: What is machine learning? In *Cognitive Science and Machine Learning Summer School (MLSS), Sardinia*. PASCAL - Pattern Analysis, Statistical Modelling and Computational Learning, 2010. URL http://videolectures.net/mlss2010_lawrence_mlfcs.

Karl Pearson. On Lines and Planes of Closest Fit to Systems of Points in Space. *Philosophical Magazine*, 2(6):559–572, 1901. doi: 10.1080/14786440109462720.

Lars Eldén. *Matrix Methods in Data Mining and Pattern Recognition*. Society for Industrial and Applied Mathematics, Philadelphia, PA, USA, 2007. ISBN 9780898716269.

Jonathon Shlens. A Tutorial on Principal Component Analysis. Technical report, Center for Neural Science, New York University, 2009. URL http://www.snl.salk.edu/~shlens/pca.pdf.

Daniel D. Lee and H. Sebastian Seung. Learning the parts of objects by non-negative matrix factorization. *Nature*, 401(6755):788–791, October 1999. doi: 10.1038/44565.

Pentti Paatero and Unto Tapper. Positive matrix factorization: A non-negative factor model with optimal utilization of error estimates of data values. *Environmetrics*, 5(2):111–126, 1994. doi: 10.1002/env.3170050203.

James O. Berger. *Statistical Decision Theory and Bayesian Analysis*. Springer Verlag New York, Inc., 2nd edition, 1985. ISBN 0387960988.

Christopher M. Bishop. *Pattern Recognition and Machine Learning*. Springer, Secaucus, NJ, USA, 2006. ISBN 0387310738.

Trevor Hastie, Robert Tibshirani, and Jerome Friedman. *The Elements of Statistical Learning: Data Mining, Inference, and Prediction*. Springer, 2nd editio edition, June 2008. doi: 10.1198/jasa.2004.s339. URL http://pubs.amstat.org/doi/abs/10.1198/jasa.2004.s339.

Ming-Hui Chen, Peter Müller, Dongchu Sun, Keying Ye, and Dipak K. Dey, editors. *Frontiers of Statistical Decision Making and Bayesian Analysis*. Springer, 1st edition, 2010. ISBN 978-1-4419-6943-9.

Lars K. Hansen and Jan Larsen. Linear unlearning for cross-validation. *Advances in Computational Mathematics*, 5(1):269–280, 1996. doi: 10.1007/BF02124747.

Pierre-Simon Laplace. *Théorie analytique des probabilités*. Paris, Ve. Courcier, 1812.

David J. C. MacKay. Bayesian Interpolation. *Neural Computation*, 4(3):415–447, May 1992a. ISSN 0899-7667. doi: 10.1162/neco.1992.4.3.415.

Stephen M. Stigler. Gauss and the Invention of Least Squares. *The Annals of Statistics*, 9(3):465–474, 1981. ISSN 0090-5364. doi: 10.1214/aos/1176345451.

Warren S. McCulloch and Walter Pitts. A logical calculus of the ideas immanent in nervous activity. *The Bulletin of Mathematical Biophysics*, 5(4):115–133, December 1943. ISSN 0007-4985. doi: 10.1007/BF02478259.

F Rosenblatt. *Principles of Neurodynamics*. Spartan Book, 1962.

Kurt Hornik, Maxwell Stinchcombe, and Halbert White. Multilayer feedforward networks are universal approximators. *Neural Networks*, 2(5):359–366, January 1989. ISSN 08936080. doi: 10.1016/0893-6080(89)90020-8.

Kurt Hornik. Approximation capabilities of multilayer feedforward networks. *Neural Networks*, 4(2):251–257, January 1991. ISSN 08936080. doi: 10.1016/0893-6080(91)90009-T.

Kurt Hornik. Some new results on neural network approximation. *Neural Networks*, 6(8):1069–1072, January 1993. ISSN 08936080. doi: 10.1016/S0893-6080(09)80018-X.

Sigurdur Sigurdsson, Peter A. Philipsen, Lars K. Hansen, Jan Larsen, Monika Gniadecka, and Hans C. Wulf. Detection of skin cancer by classification of Raman spectra. *IEEE transactions on bio-medical engineering*, 51(10):1784–93, October 2004. ISSN 0018-9294. doi: 10.1109/TBME.2004.831538.

Steffen L. Lauritzen. Time Series Analysis in 1880: A Discussion of Contributions Made by T.N. Thiele. *International Statistical Review*, 49(3):319–331, 1981. doi: 10.1093/acprof:oso/9780198509721.003.0003.

Christopher K. I. Williams and Carl E. Rasmussen. Gaussian Processes for Regression. In *Advances in Neural Information Processing Systems*, volume 8, 1996.

Carl E. Rasmussen and Christopher K. I. Williams. *Gaussian Processes for Machine Learning*. MIT Press, April 2006a. URL http://www.gaussianprocess.org/gpmlhttp://www.ncbi.nlm.nih.gov/pubmed/15112367.

Carl E. Rasmussen and Hannes Nickisch. Gaussian Processes for Machine Learning (GPML) Toolbox. *Journal of Machine Learning Research*, 11:3011–3015, 2010. URL http://jmlr.csail.mit.edu/papers/v11/rasmussen10a.html.

Mark Schmidt, Glenn Fung, and Rómer Rosales. Fast Optimization Methods for L1 Regularization: A Comparative Study and Two New Approaches. In Joost Kok, Jacek Koronacki, Raomon Mantaras, Stan Matwin, Dunja Mladenic, and Andrzej Skowron, editors, *Machine Learning: ECML 2007*, volume 4701 of *Lecture Notes in Computer Science*, pages 286–297. Springer Berlin / Heidelberg, 2007. doi: 10.1007/978-3-540-74958-5_28.

Günter Sauerbrey. Verwendung von Schwingquarzen zur Wägung dünner Schichten und zur Mikrowägung. *Zeitschrift für Physik*, 155(2):206–222, April 1959. ISSN 1434-6001. doi: 10.1007/BF01337937.

Hsin-Hsien Lu, Yerra Koteswara Rao, Tzong-Zeng Wu, and Yew-Min Tzeng. Direct characterization and quantification of volatile organic compounds by

piezoelectric module chips sensor. *Sensors and Actuators B: Chemical*, 137 (2):741–746, April 2009. ISSN 09254005. doi: 10.1016/j.snb.2009.01.060.

Annika M. Rosengren, Kerstin Golker, Jesper G. Karlsson, and Ian A. Nicholls. Dielectric constants are not enough: principal component analysis of the influence of solvent properties on molecularly imprinted polymer-ligand rebinding. *Biosensors & bioelectronics*, 25(3):553–7, November 2009. ISSN 1873-4235. doi: 10.1016/j.bios.2009.06.042.

Pengchao Si, John Mortensen, Alexei Komolov, Jens Denborg, and Preben J. Møller. Polymer coated quartz crystal microbalance sensors for detection of volatile organic compounds in gas mixtures. *Analytica chimica acta*, 597(2): 223–30, August 2007. ISSN 1873-4324. doi: 10.1016/j.aca.2007.06.050. URL http://www.ncbi.nlm.nih.gov/pubmed/17683733.

Zhihua Ying, Yadong Jiang, Xiaosong Du, Guangzhong Xie, Junsheng Yu, and Huiling Tai. Polymer coated sensor array based on quartz crystal microbalance for chemical agent analysis. *European Polymer Journal*, 44(4):1157–1164, April 2008. ISSN 00143057. doi: 10.1016/j.eurpolymj.2008.01.015.

Kelly Sepcic, Mira Josowicz, Jiri Janata, and Ted Selby. Diagnosis of used engine oil based on gas phase analysis. *The Analyst*, 129(11):1070, 2004. ISSN 0003-2654. doi: 10.1039/b406619g.

Ali Gulbag, Feyzullah Temurtas, and Ismihan Yusubov. Quantitative discrimination of the binary gas mixtures using a combinational structure of the probabilistic and multilayer neural networks. *Sensors and Actuators B: Chemical*, 131(1):196–204, April 2008. doi: 10.1016/j.snb.2007.11.008.

Hamdi M. Saraoglu and Mehmet Kocan. Determination of Blood Glucose Level-Based Breath Analysis by a Quartz Crystal Microbalance Sensor Array. *IEEE Sensors Journal*, 10(1):104–109, January 2010. ISSN 1530-437X. doi: 10.1109/JSEN.2009.2035769. URL http://ieeexplore.ieee.org/lpdocs/epic03/wrapper.htm?arnumber=5352205.

Bekir Mumyakmaz, Ahmet Özmen, Mehmet A. Ebeoğlu, and Cihat Taşaltın. Predicting gas concentrations of ternary gas mixtures for a predefined 3D sample space. *Sensors and Actuators B: Chemical*, 128(2):594–602, January 2008. ISSN 09254005. doi: 10.1016/j.snb.2007.07.062.

Ahmet Özmen, F. Tekce, Mehmet A. Ebeoğlu, Cihat Taşaltın, and Zafer Z. Öztürk. Finding the composition of gas mixtures by a phthalocyanine-coated QCM sensor array and an artificial neural network. *Sensors and Actuators B: Chemical*, 115(1):450–454, May 2006. ISSN 09254005. doi: 10.1016/j.snb.2005.10.007.

Ya-Ling Wang and Jeng-Shong Shih. Multi-channel piezoelectric crystal gas sensor with principal component analysis for organic solvent pollutants from polymer plants. *Journal of the Chinese Chemical Society*, 53(6):1427–1437, December 2006. ISSN 0009-4536.

Grace Wahba. *Spline Models for Observational Data*. Society for Industrial and Applied Mathematics, January 1990. ISBN 978-0-89871-244-5. doi: 10.1137/1.9781611970128.

Alex J. Smola and Peter Bartlett. Sparse Greedy Gaussian Process Regression. In *Advances in Neural Information Processing Systems*, 2000.

Tommy S. Alstrøm and Jan Larsen. Feature Extraction and Signal Representation for Colorimetric Sensor Arrays. Technical report, DTU Informatics, 2011. URL http://www.imm.dtu.dk/pubdb/p.php?5845.

Robert Bemis. DNA MicroArray Image Processing Case Study, 2004. URL http://www.mathworks.com/matlabcentral/fileexchange/2573.

Abraham Savitzky and Marcel E. J. Golay. Smoothing and Differentiation of Data by Simplified Least Squares Procedures. *Analytical Chemistry*, 36(8): 1627–1639, July 1964. ISSN 0003-2700. doi: 10.1021/ac60214a047. URL http://dx.doi.org/10.1021/ac60214a047.

Hans B. Nielsen. UCMINF - an Algorithm for Unconstrained, Nonlinear Optimization. Technical Report IMM-TEC-0019, IMM, Technical University of Denmark, 2001.

Hans B. Nielsen. A MATLAB toolbox for optimization and data fitting 2.2, 2010. URL http://www2.imm.dtu.dk/~hbni/immoptibox/.

Kent A. Nielsen. A colorimetric tetrathiafulvalene-calix[4]pyrrole anion sensor. *Tetrahedron Letters*, 53(42):5616–5618, October 2012. ISSN 00404039. doi: 10.1016/j.tetlet.2012.08.011.

Frank Wilcoxon. Individual Comparison by Ranking Methods. *Biometrics Bulletin*, 1(6):80–83, 1945.

Henry B. Mann and Donald R. Whitney. On a test of whether one of two random variables is stochastically larger than the other. *The annals of mathematical statistics*, 18(1):50–60, 1947. URL http://projecteuclid.org/euclid.aoms/1177730491.

Douglas C. Montgomery. *Design and Analysis of Experiments*. John Wiley & Sons Inc., 7th edition, 2009. ISBN 978-0-470-39882-1.

Ronald A. Fisher. The statistical utilization of multiple measurements. *Annals of Human Genetics*, 8(4):376–386, 1938. URL http://onlinelibrary.wiley.com/doi/10.1111/j.1469-1809.1938.tb02189.x/abstract.

Kevin M. Carter, Raviv Raich, William G. Finn, and Alfred O. Hero. Information Preserving Component Analysis: Data Projections for Flow Cytometry Analysis. *IEEE Journal of Selected Topics in Signal Processing*, 3(1):148–158, February 2009a. ISSN 1932-4553. doi: 10.1109/JSTSP.2008.2011112.

Kevin M. Carter, Raviv Raich, William G. Finn, and Alfred O. Hero. FINE: fisher information nonparametric embedding. *IEEE transactions on pattern analysis and machine intelligence*, 31(11):2093–8, November 2009b. ISSN 1939-3539. doi: 10.1109/TPAMI.2009.67.

Tony Jebara, Risi Kondor, and Andrew Howard. Probability Product Kernels. *Journal of Machine Learning Research*, 5:819–844, 2004. URL http://jmlr.csail.mit.edu/papers/v5/jebara04a.html.

Marie-Pierre Dubuisson and Anil K. Jain. A modified Hausdorff distance for object matching. In *Proceedings of 12th International Conference on Pattern Recognition*, pages 566–568, 1994. ISBN 0-8186-6265-4. doi: 10.1109/ICPR.1994.576361.

Bernard Haasdonk and Claus Bahlmann. Learning with Distance Substitution Kernels. *Pattern Recognition*, 3175:220–227, 2004. doi: 10.1007/978-3-540-28649-3_27.

Neal A. Rakow and Kenneth S. Suslick. A colorimetric sensor array for odour visualization. *Nature*, 406(6797):710–3, August 2000. ISSN 0028-0836. doi: 10.1038/35021028.

Kenneth S. Suslick, Neal A. Rakow, and Avijit Sen. Colorimetric sensor arrays for molecular recognition. *Tetrahedron*, 60(49):11133–11138, November 2004b. ISSN 00404020. doi: 10.1016/j.tet.2004.09.007.

Neal A. Rakow, Avijit Sen, Michael C. Janzen, Jennifer B. Ponder, and Kenneth S. Suslick. Molecular recognition and discrimination of amines with a colorimetric array. *Angewandte Chemie (International ed. in English)*, 44(29):4528–32, July 2005. ISSN 1433-7851. doi: 10.1002/anie.200500939.

Chen Zhang, Daniel P. Bailey, and Kenneth S. Suslick. Colorimetric sensor arrays for the analysis of beers: a feasibility study. *Journal of agricultural and food chemistry*, 54(14):4925–31, July 2006. ISSN 0021-8561. doi: 10.1021/jf060110a.

Sung H. Lim, Liang Feng, Jonathan W. Kemling, Christopher J. Musto, and Kenneth S. Suslick. An Optoelectronic Nose for Detection of Toxic Gases. *Nature chemistry*, 1:562–567, September 2009. ISSN 1755-4349. doi: 10.1038/nchem.360.

Chen Zhang and Kenneth S. Suslick. Colorimetric sensor array for soft drink analysis. *Journal of agricultural and food chemistry*, 55(2):237–42, January 2007. ISSN 0021-8561. doi: 10.1021/jf0624695.

Michael C. Janzen, Jennifer B. Ponder, Daniel P. Bailey, Crystal K. Ingison, and Kenneth S. Suslick. Colorimetric sensor arrays for volatile organic compounds. *Analytical chemistry*, 78(11):3591–600, June 2006. ISSN 0003-2700. doi: 10.1021/ac052111s.

Benjamin A. Suslick, Liang Feng, and Kenneth S. Suslick. Discrimination of complex mixtures by a colorimetric sensor array: coffee aromas. *Analytical chemistry*, 82(5):2067–73, March 2010. ISSN 1520-6882. doi: 10.1021/ac902823w.

Xiao-gang Luo, Ping Liu, Chang-jun Hou, Dan-qun Huo, Jia-le Dong, Huanbao Fa, and Mei Yang. A novel chemical detector using colorimetric sensor array and pattern recognition methods for the concentration analysis of NH3. *The Review of scientific instruments*, 81(10):105113, October 2010. ISSN 1089-7623. doi: 10.1063/1.3501965.

Jesper K. Olsen, Anders Greve, Larry R. Senesac, Thomas Thundat, and Anja Boisen. Differential thermal analysis microsystem for explosive detection. In Thomas George, M Saif Islam, and Achyut K Dutta, editors, *Micro- and Nanotechnology Sensors, Systems, and Applications III*, volume 8031, page 80312P. SPIE, 2011a. doi: 10.1117/12.883960. URL http://link.aip.org/link/?PSI/8031/80312P/1.

Jesper K. Olsen, Larry R. Senesac, Thomas Thundat, and Anja Boisen. Trace explosives detection by micro differential thermal analysis. In *Micro Electro Mechanical Systems (MEMS), 2011 IEEE 24th International Conference on*, pages 984–987, 2011b. ISBN 1084-6999 VO -.

Filippo G. Bosco, En-Te Hwu, and Anja Boisen. High-throughput readout system for cantilever-based sensing of explosive compounds. In Thomas George, M Saif Islam, and Achyut K Dutta, editors, *Micro- and Nanotechnology Sensors, Systems, and Applications II*, volume 7679, page 767925. SPIE, 2010. doi: 10.1117/12.850008. URL http://link.aip.org/link/?PSI/7679/767925/1.

Kent A. Nielsen, Won-Seob Cho, Jan O. Jeppesen, Vincent M. Lynch, Jan Becher, and Jonathan L. Sessler. Tetra-TTF Calix[4]pyrrole: A Rationally Designed Receptor for Electron-Deficient Neutral Guests. *Journal of the American Chemical Society*, 126(50):16296–16297, November 2004. ISSN 0002-7863. doi: 10.1021/ja044664a.

Jung S. Park, Franck Le Derf, Christopher M. Bejger, Vincent M. Lynch, Jonathan L. Sessler, Kent A. Nielsen, Carsten Johnsen, and Jan O. Jeppesen. Positive Homotropic Allosteric Receptors for Neutral Guests: Annulated Tetrathiafulvalene–Calix[4]pyrroles as Colorimetric Chemosensors for Nitroaromatic Explosives. *Chemistry - A European Journal*, 16(3):848–54, January 2010. ISSN 1521-3765. doi: 10.1002/chem.200902924.

Tommy S. Alstrøm, Jan Larsen, Natalie V. Kostesha, Mogens H. Jakobsen, and Anja Boisen. Data representation and feature selection for colorimetric sensor arrays used as explosives detectors. In *IEEE International Workshop on Machine Learning for Signal Processing (MLSP)*, pages 1–6, 2011. doi: 10.1109/MLSP.2011.6064615.

Klarite. Klarite, 2012. URL http://www.d3technologies.co.uk.

Jessica L. Arlett, Edward B. Myers, and Michael L. Roukes. Comparative advantages of mechanical biosensors. *Nature Nanotechnology*, 6(4):203–215, April 2011. ISSN 1748-3387. URL http://dx.doi.org/10.1038/nnano.2011.44.

Desiree S. Grubisha, Robert J. Lipert, Hye-Young Park, Jeremy Driskell, and Marc D. Porter. Femtomolar Detection of Prostate-Specific Antigen: An Immunoassay Based on Surface-Enhanced Raman Scattering and Immunogold Labels. *Analytical Chemistry*, 75(21):5936–5943, September 2003. ISSN 0003-2700. doi: 10.1021/ac034356f. URL http://dx.doi.org/10.1021/ac034356f.

Jesper Kenneth Olsen. *Micro Calorimetric Sensors for Explosives Detection*. PhD thesis, Technical University of Denmark (DTU), 2011.

Filippo G. Bosco, En-Te Hwu, Ching-Hsiu Chen, Stephan Keller, Michael Bache, Mogens H. Jakobsen, Ing-Shouh Hwang, and Anja Boisen. High throughput label-free platform for statistical bio-molecular sensing. *Lab Chip*, 11(14):2411–2416, 2011. doi: 10.1039/C1LC20116F. URL http://dx.doi.org/10.1039/C1LC20116F.

Dae-Sik Kim, Vincent M. Lynch, Kent A. Nielsen, Carsten Johnsen, Jan O. Jeppesen, and Jonathan L. Sessler. A chloride-anion insensitive colorimetric chemosensor for trinitrobenzene and picric acid. *Analytical and bioanalytical chemistry*, 395(2):393–400, 2009. doi: 10.1007/s00216-009-2819-4.

Javier Tamayo, Daniel Ramos, Johan Mertens, and Montserrat Calleja. Effect of the adsorbate stiffness on the resonance response of microcantilever sensors. *Applied Physics Letters*, 89(22):224104, 2006. doi: 10.1063/1.2388925. URL http://link.aip.org/link/?APL/89/224104/1.

Alejandro Blanco, Nairmen Mina, Miguel E. Castro, Jairo Castillo-Chara, and Samuel P. Hernandez-Rivera. Spectroscopic investigation of the spectroscopic signatures of 2,4-DNT and 2,6-DNT: their interactions with sand particles. In Russell S Harmon, J Thomas Broach, John H Holloway, and Jr., editors, *Detection and Remediation Technologies for Mines and Minelike Targets IX*, volume 5415, pages 1357–1366. SPIE, 2004. doi: 10.1117/12.542870. URL http://link.aip.org/link/?PSI/5415/1357/1.

Esam M. A. Ali, Howell G. M. Edwards, and Ian J. Scowen. In-situ detection of single particles of explosive on clothing with confocal Raman microscopy. *Talanta*, 78(3):1201–1203, May 2009. ISSN 0039-9140. URL http://www.sciencedirect.com/science/article/pii/S0039914008009211.

Michael J. Kleeman, James J. Schauer, and Glen R. Cass. Size and Composition Distribution of Fine Particulate Matter Emitted from Motor Vehicles. *Environmental Science & Technology*, 34(7):1132–1142, February 2000. ISSN 0013-936X. doi: 10.1021/es981276y. URL http://dx.doi.org/10.1021/es981276y.

John W. Haas III, James M. Sylvia, Kevin M. Spencer, Thomas M. Johnston, and Susan L. Clauson. Surface-enhanced Raman sensor for nitroexplosive vapors. In Abinash C Dubey, James F Harvey, and J Thomas Broach, editors, *Detection and Remediation Technologies for Mines and Minelike Targets III*, volume 3392, pages 469–476. SPIE, 1998. doi: 10.1117/12.324179. URL http://link.aip.org/link/?PSI/3392/469/1.

Jan O. Jeppesen, Natalie V. Kostesha, Carsten Johnsen, Kent A. Nielsen, Anja Boisen, and Mogens H. Jakobsen. Multisensor array useful for detection and/or identification of an analyte (e.g. amines, alcohols, ketones and thiols) in the gas phase or in the liquid phase, comprises at least two different chemo-selective heteroaryl compounds, 2011.

Michael S. Schmidt, Jörg Hübner, and Anja Boisen. Large Area Fabrication of Leaning Silicon Nanopillars for Surface Enhanced Raman Spectroscopy. *Advanced Materials*, pages OP11–OP18, November 2011b. ISSN 09359648. doi: 10.1002/adma.201103496. URL http://www.ncbi.nlm.nih.gov/pubmed/22105972.

Hamdi M. Saraoğlu and Burçak Edin. E-Nose System for Anesthetic Dose Level Detection using Artificial Neural Network. *Journal of Medical Systems*, 31(6):475–482, August 2007. ISSN 0148-5598. doi: 10.1007/s10916-007-9087-7.

J.O. O. Mahony, K. Nolan, M.R. R. Smyth, and B. Mizaikoff. Molecularly imprinted polymers—potential and challenges in analytical chemistry. *Analytica Chimica Acta*, 534(1):31–39, April 2005. ISSN 00032670. doi: 10.1016/j.aca.2004.07.043.

József Szejtli. Introduction and General Overview of Cyclodextrin Chemistry. *Chemical Reviews*, 98(5):1743–1754, July 1998. ISSN 0009-2665. doi: 10.1021/cr970022c.

Abdul R. Khan, Peter Forgo, Keith J. Stine, and Valerian T. D'Souza. Methods for Selective Modifications of Cyclodextrins. *Chemical Reviews*, 98(5):1977–1996, July 1998. ISSN 0009-2665. doi: 10.1021/cr970012b.

Shigeru Kurosawa, Tomoya Hirokawa, Kazuya Kashima, Hidenobu Aizawa, Dae-Sang Han, Yasuo Yoshimi, Yuji Okada, Kiyoshi Yase, Jun Miyake, Minoru Yoshimoto, and Jöns Hilborn. Detection of deposition rate of plasma-polymerized films by quartz crystal microbalance. *Thin Solid Films*, 374(2):262–267, October 2000. ISSN 00406090. doi: 10.1016/S0040-6090(00)01161-5.

Jay W. Grate and Michael H. Abraham. Solubility interactions and the design of chemically selective sorbent coatings for chemical sensors and arrays. *Sensors and Actuators B: Chemical*, 3(2):85–111, February 1991. ISSN 09254005. doi: 10.1016/0925-4005(91)80202-U.

Bjørn Winther-Jensen and Kristian Glejbøl. Method and apparatus for the excitation of a plasma, 2003.

DTUInformatics. DTU:Toolbox. URL http://cogsys.imm.dtu.dk/toolbox/.

Chih-Jen Lin. Projected gradient methods for nonnegative matrix factorization. *Neural computation*, 19(10):2756–79, October 2007. ISSN 0899-7667. doi: 10.1162/neco.2007.19.10.2756.

Carl E. Rasmussen and Christopher K. I. Williams. GPML code, 2006b. URL http://www.gaussianprocess.org/gpml.

Radford M. Neal. *Bayesian Learning for Neural Networks*. Springer-Verlag New York, lecture no edition, 1996. ISBN 0-387-94724-8.

Sigurdur Sigurdsson, Jan Larsen, Lars K. Hansen, Peter A. Philipsen, and Hans C. Wulf. Outlier estimation and detection application to skin lesion classification. In *IEEE International Conference on Acoustics Speech and Signal Processing*, volume 1, pages I–1049–I–1052. IEEE, May 2002. ISBN 0-7803-7402-9. doi: 10.1109/ICASSP.2002.5743975.

David J. C. MacKay. A Practical Bayesian Framework for Backpropagation Networks. *Neural Computation*, 4(3):448–472, May 1992b. ISSN 0899-7667. doi: 10.1162/neco.1992.4.3.448.

David J. C. MacKay. The Evidence Framework Applied to Classification Networks. *Neural Computation*, 4(5):720–736, September 1992c. ISSN 0899-7667. doi: 10.1162/neco.1992.4.5.720.

Thomas Kolenda, Lars K. Hansen, Jan Larsen, and Ole Winther. Independent component analysis for understanding multimedia content. In H Bourlard, T Adali, S Bengio, J Larsen, and S Douglas, editors, *Proceedings of the 12th IEEE Workshop on Neural Networks for Signal Processing*, pages 757–766, Piscataway, New Jersey, 2002. IEEE. ISBN 0-7803-7616-1. doi: 10.1109/NNSP.2002.1030096.

Ian T. Nabney. Netlab 3.3: Algorithms for Pattern Recognition, 2004. URL http://www1.aston.ac.uk/eas/research/groups/ncrg/resources/netlab/.

Isabelle Guyon and André Elisseeff. An introduction to variable and feature selection. *The Journal of Machine Learning Research*, 3:1157–1182, March 2003. ISSN 1532-4435. URL http://jmlr.csail.mit.edu/papers/v3/guyon03a.html.

Tommy S. Alstrøm, Raviv Raich, Natalie V. Kostesha, and Jan Larsen. Feature extraction using distribution representation for colorimetric sensor arrays used as explosives detectors. In *IEEE International Conference on Acoustics, Speech, and Signal Processing (ICASSP)*, pages 2125–2128, 2012. doi: 10.1109/ICASSP.2012.6288331.